

You can jump to the first article of the beamline by clicking titles.

VI. EXPERIMENTAL PROGRAMS

During the period from April 1982 to March 1983, most of the beam times have been assigned to members of working groups, which are described in §V.1, for commissioning and testing optics of beam lines, experimental apparatuses, and for doing preliminary experiments. From June 1983, 9 X-ray stations and 3 VUV stations have been made open for general users.

Following reports are submitted by the representative of each experimental proposal as progress reports. These reports are presented

without any editorial work and reviewing by referees.

These reports are arranged according to the number of beam lines at which the experiment has been performed. A report describing a summary of activities of a working group is indicated by letters 'WG' in the column of proposal number. The letters 'WGP' in the column of the proposal number shows that the work is performed using a priority beam time of the working group members. The reports given a sign CT are contributed by users allotted with charged beam-time.

Table of Contents for Experimental Progress Reports

<u>Title</u>	<u>Authors</u>	<u>Proposal Number</u>	<u>Page</u>
<u>BL-2</u>			
Angular-Distribution Measurements of Photoelectrons Ejected from Atoms and Molecules Using Undulator Radiation	Y. Suzuki, H. Maezawa, A. Yagishita, T. Sasaki	WGP	VI-1
<u>BL-4A</u>			
X-Ray Fluorescence Analysis by Synchrotron Radiation	A. Iida, Y. Gohshi, T. Matsushita, et al.	42 WG	VI-2
Development of a Dispersive X-ray Absorption Spectrometer for Time Resolved EXAFS Experiment	T. Matsushita, H. Oyanagi, and U. Kaminaga	53	VI-4
Macromolecular Crystallography with SR	N. Sakabe and N. Kamiya	33	VI-5
<u>BL-4B</u>			
Study of Phase Transition in Potassium-Graphite Intercalation Compounds by Synchrotron Radiation X-Rays	H. Suematsu, R. Nishitani, Y. Uno, Y. Fujii and T. Matsushita	34	VI-6
Monochromatized X-Ray Experiments by the Diffractometer for Liquid and Melt	The Test-Run Group for Liquid and Melt Diffraction	43 WG	VI-7
An Energy Dispersive-Experiment of X-Ray Diffraction by Glasses: Silica Glass	The Test-Run Group for Liquid and Melt Diffraction	43 WG	VI-8
An Energy-Dispersive Experiment of X-Ray Diffraction by Liquids: Carbon Tetrachloride	The Test-Run Group for Liquid and Melt Diffraction	43 WG	VI-9
An Energy-Dispersive Experiment of X-Ray Diffraction by Gases: Sulfur Hexafluoride	The Test-Run Group for Liquid, Melt and Gas Diffraction	46 WG	VI-10

<u>Title</u>	<u>Authors</u>	<u>Proposal Number</u>	<u>Page</u>
<u>BL-4C</u>			
Structural Study by X-Ray Diffraction at Low Temperature	S. Kagoshima, J. Harada, M. Sakata, K. Tsuji and T. Nakajima	31 WG	VI-11
X-Ray Diffraction Measurements Under Low Temperature and High Pressure at the Photon Factory	K. Tsuji, T. Ishidate, K. Yamamoto, H. Takahashi, M. Sakata, J. Harada, S. Kagoshima and T. Nakajima	31 WGP	VI-13
A Temperature Factor Measurement of Amorphous Cu ₆₀ Ti ₄₀	M. Sakata, S. Hashida, J. Harada, K. Tsuji, S. Kagoshima, T. Ishikawa and T. Nakajima	31 WGP	VI-14
High Pressure Experiments Using MAX80	S. Shimomura, N. Yamaoka, T. Yagi, M. Wakatsuki, K. Tsuji, O. Fukushima, H. Kawamura, K. Aoki, S. Akimoto	37 WGP	VI-15
Direct Observation of the Conversion Reaction from Graphite to Diamond	S. Yamaoka, O. Shimomura, T. Yagi, T. Akai, H. Fujiwara, H. Kanda, T. Kikegawa, K. Kuroda, N. Mori, T. Nagashima, T. Suzuki, et al.	37 WGP	VI-16
Compressibility Measurements of Gold at Room Temperature and 600°C	T. Yagi, S. Shimomura, N. Yamaoka, T. Fujimura, N. Hamaya, M. Nomura, J. Suzaki, T. Suzuki, K. Tabata, et al.	37 WGP	VI-17
Time-Resolved X-Ray Diffraction on the Pressure-Induced Phase Transition in BaS	N. Hamaya, T. Yagi, S. Yamaoka, O. Shimomura, K. Tabata, J. Susaki, K. Tsuji, K. Murata, T. Kikegawa, H. Kawamura and S. Akimoto	37 WGP	VI-18
<u>BL-10A</u>			
Four-Circle Diffractometer of Vertical type on BL-10A	T. Tagai, M. Tokonami, T. Sakamaki, Y. Sato, K. Ohsumi, H. Nakazawa, Y. Abe, T. Hirai, et al.	35 WG	VI-19
Diffuse Scattering from β -PbF ₂	K. Koto and Y. Ito	35 WGP	VI-20
Cation Ordering in the Structure of Cu ₉ As ₄ Se ₁₃	Y. Takeuchi, N. Haga, F. Nishi, K. Ohsumi and M. Tokonami	35 WGP	VI-21
The Absolute Orientation of Hemimorphite	Y. Takeuchi, K. Ohsumi, N. Haga, F. Nishi and M. Tokonami	35 WGP	VI-22
Reinvestigation of the Lilliant Structure	K. Ohsumi, K. Tsutsui, Y. Takeuchi and M. Tokonami	35 WGP	VI-23
Preliminary Experiment to Use the X-Ray Guide Tube as a "Low- Pass" Filter of Polychromatic X-Rays	H. Nakazawa, T. Tagai, and Y. Satow	35 WGP	VI-24

<u>Title</u>	<u>Authors</u>	<u>Proposal Number</u>	<u>Page</u>
Examination of Single Crystal Diffraction Data Collection from Micro-Size Specimens Using Four-Circle Diffractometer	S. Sueno, K. Ohsumi, M. Kimata, H. Yurimoto, K. Kakehuda and M. Ohmasa	35 WGP	VI-25
X-Ray Topography of a Cube-Shaped Diamond	H. Nakazawa, T. Tagai, H. Hirai, A. Nuiki and Y. Satow	35 WGP	VI-26
On the Sites of Off-Stoichiometric Ni and Al Atoms in Cu-Al-Ni Alloy	Y. Abe, K. Ohsumi, T. Tagai and M. Tokonami	35 WGP	VI-27
RDF Study Empolying Anomalous Dispersion Effect	A. Nuiki, N. Nakazawa, Y. Hasegawa, M. Isobe, T. Tagai and S. Sasaki	35 WGP	VI-28
Measurements of Diffuse Streaks Scattered by Fine Segregates of B-MnO ₂	M. Ohmasa, N. Yamada, H. Nakazawa, Y. Satow, T. Tagai and S. Sueno	35 WGP	VI-29
Radiation Biology Studies with Monochromatic X-Rays	T. Ito,	27 WG	VI-30
Chromosome Aberrations Induced in Chinese Hamster Ovary (CHO) Cells by Synchrotron Radiation	H. Ohara, T. Yamada, H. Majima, K. Shinohara, K. Kobayashi, K. Hieda, and H. Maezawa	27	VI-32
Irradiation of Cultured Mammalian Cells Containing Bromine in the DNA by Monochromatic Synchrotron Radiation at 0.09 and 0.1 nm	K. Shinohara, H. Ohara, H. Majima, S. Okada, H. Maezawa, K. Kobayashi, K. Hieda, A. Ito, T. Yamada and T. Ito	27	VI-33
<u>BL-10B</u>			
EXAFS Study of Behavior of Rh ₆ (CO) ₁₆ on Al ₂ O ₃	H. Kuroda, N. Kosugi, K. Asakura and H. Ishii	WGP	VI-34
EXAFS and XANES of FeCl ₃ Aqueous Solutions	H. Kuroda, N. Kosugi, K. Asakura, H. Ishii and M. Nomura	WGP	VI-35
EXAFS and XANES of FeCl ₃ Dissolved in Organic Solvents	H. Kuroda, N. Kosugi, K. Asakura, H. Ishii and M. Nomura	WGP	VI-36
Polarized XANES Studies of Transition Metal Complexs I. Square Planar CuCl ₄ ²⁻ Complex	H. Kuroda, N. Kosugi, T. Yokoyama, K. Asakura and H. Ishii	WGP	VI-37
Short Range Order in Amorphous GeTe Studied by Means of EXAFS	H. Oyanagi, K. Tanaka, T. Matsushita and M. Ito	WGP	VI-38
EXAFS Study of Bromine-doped Polyacetylene	M. Tokumoto, H. Oyanagi, T. Ishiguro, H. Shirakawa, H. Nemoto, T. Matsushita, M. Ito, H. Kuroda and K. Kohra	WGP	VI-39
Polarized EXAFS Studies of Polyacetylene: Evidence for Structural Ordering of Bromine Polyions	H. Oyanagi, M. Tokumoto, T. Ishiguro, H. Shirakawa, H. Nemoto, T. Matsushita, M. Ito, and H. Kuroda	WGP	VI-40

<u>Title</u>	<u>Authors</u>	<u>Proposal Number</u>	<u>Page</u>
Polarization Dependent Near Edge Structure of Polyacetylene Doped with Bromine and Iodine	H. Oyanagi, M. Tokumoto, T. Ishiguro, H. Shirakawa, H. Nemoto, T. Matsushita, M. Ito and H. Kuroda	WGP	VI-41
Fluorescence EXAFS Studies of Hemoprotein: Thermal Spin Equilibrium	H. Oyanagi, T. Izuka, R. Makino, T. Matsushita and M. Ito	WGP	VI-42
Structural Studies of the Superionic Conductor $Rb_4Cu_{16}Cl_{13}I_7$ by X-Ray Absorption Spectroscopy	H. Oyanagi, M. Tokumoto, T. Ishiguro, T. Matsushita, and M. Ito	WGP	VI-43
Near Edge Structure Studies of Tetrahedrally Bonded Compounds: Ge, GeO_2 , GaAs, and ZnSe	H. Oyanagi, T. Fujikawa, T. Matsushita, M. Okuno, and M. Ito	WGP	VI-44
EXAFS Study on Premelting Phenomenon of Gallium	M. Hida, H. Maeda, Y. Ysu, S. Iida, H. Terauchi, N. Kamijo, T. Murata and C. Watanabe	2	VI-45
EXAFS Study on Lattice Relaxation of Ultra Fine Nickel Particles	M. Hida, H. Maeda, N. Wada, K. Kimura, T. Morimoto, Y. Kuroda, S. Iida, H. Terauchi, N. Kamijo, Y. Tsu and T. Murata	4	VI-46
Local Lattice Structure in Solid Solutions of Alkali Halides	T. Murata, H. Maeda, H. Hida, H. Terauchi and N. Kamijo	5	VI-48
EXAFS Study on the Local Structure Near the Martensitic Phase Transition of $AuCuZn_2$	H. Terauchi, S. Iida, K. Tanabe, K. Kikukawa, Y. Nishihata, H. Maeda, M. Hida, N. Kamijo and T. Murata	6	VI-49
XANES Study on the Local Structure of a Quasi-1D Mixed Valance Crystal Wolfram's Red Salt	H. Terauchi, S. Iida, K. Tanabe, K. Kikukawa, Y. Nishihata, H. Maeda, M. Hida, N. Kamijo, and T. Murata	6	VI-50
EXAFS Study on Local Structure of Amorphous and Liquid Ge - Se System	H. Maeda, A. Terauchi, S. Iida, M. Hida, T. Murata and N. Kamijo	7	VI-51
Studies on the Local Structure of the Phase Transition in Invar Alloys	O. Yamada, H. Maeda, I. Nakai, K. Kamon, Lui Wan Li, H. Tokuhara and M. Mimura	9	VI-52
EXAFS Study on the Premelting Phenomenon of Rubidium	Y. Tsu, M. Hida, H. Maeda and S. Watanabe	10	VI-53
EXAFS and XANES Studies of Chemically Fixed Mo and Cr Catalysts I. Mo_2/SiO_2 Catalyst	H. Kuroda, N. Kosugi, H. Ishii, K. Asakura and T. Yokoyama	15	VI-54
XANES of Metal Carbonyl Molecules I. GAS- and Liquide-Phase $Fe(CO)_5$	H. Kuroda, N. Kosugi, T. Yokoyama, K. Asakura and H. Ishii	16	VI-55

<u>Title</u>	<u>Authors</u>	<u>Proposal Number</u>	<u>Page</u>
EXAFS and XANES Studies of Metal-Halide-Doped Polyacetylenes I. FeCl ₃ -Doped Polyacetylene	H. Kuroda, I. Ikemoto, N. Kosugi, K. Asakura, H. Ishii, H. Shirakawa, T. Kobayashi, H. Oyanagi, and T. Matsushita	17	VI-56
EXAFS and XANES Studies of Metal- Halide-Doped Polyacetylenes II. MoCl ₅ - and WCl ₆ -Doped Polyacetylenes	H. Kuroda, I. Ikemoto, N. Kosugi, K. Asakura, H. Ishii, T. Yokoyama, H. Shirakawa, T. Kobayashi, H. Oyanagi, M. Nomura and T. Matsushita	17	VI-57
XANES of Highly-Conductive Mixed- Valence Organic Charge Transfer Salts I. (TMTSF) ₂ X and Related Materials	H. Kuroda, I. Ikemoto, K. Kikuchi N. Kosugi, K. Asakura, H. Ishii and T. Yokoyama	18	VI-58
Surface Structure of SMSI Catalyst I. Rh/TiO ₂ Catalyst	H. Kuroda, N. Kosugi, K. Asakura, H. Ishii and T. Yokoyama	19	VI-59
Study on the Structure of the Active Sites for the Formation of Oxy- Geneted Compounds from CO-H ₂ Under Mild Conditions	S. Naito, N. Kosugi, K. Asakura, H. Ishii, T. Yokoyama, K. Tamaru and H. Kuroda	20	VI-60
EXAFS Study of Catalysts for Photo- decomposition of H ₂ O	K. Domen, A. Kudo, T. Onishi N. Kosugi, K. Asakura, H. Ishii, T. Yokoyama and K. Kuroda	21	VI-61
XANES Studies on Mixed-Valency and Abnormal Valency in the Complexes of Ferrocene Derivative	K. Sato, M. Iwai, Y. Watanabe, S. Nakashima, H. Sano, I. Ikemoto, N. Kosugi, K. Asakura, H. Ishii, T. Yokoyama and H. Kuroda	22	VI-62
XAS Studies on Bimetallic Rh-Co Carbonyl-Derived Catalysts I. Preliminary Experiments on Rh/SiO ₂ Catalyst	H. Kuroda, N. Kosugi, T. Yokoyama, H. Ishii, K. Asakura, M. Ichikawa and T. Fukushima	24	VI-63
EXAFS Study on the Structure of Heteropolymolybdates in Solution	Y. Sasaki, A. Kobayashi, T. Ozeki, H. Kuroda, N. Kosugi, K. Asakura, H. Ishii and T. Yokoyama	25	VI-64
Influences of Various Ligands on Jahn-Teller Effect of Complexes in Solution	N. Matsubayashi, I. Watanabe, K. Murata and S. Ikeda	57	VI-66
EXAFS Study of Fluorites	N. Kamiyo, K. Koto, Y. Ito, K. Tanabe, K. Kikukawa, H. Maeda, M. Hida, T. Murata and H. Terauchi	60	VI-67
<u>BL-10C</u>			
Anomalous Scattering Phenomena Applied to the Study of Short- Range Order in Ternary Alloys	S. Hashimoto, H. Iwasaki, Y. Watanabe, K. Ohshima, J. Harada, M. Sakata, H. Terauchi, T. Matsushita, T. Nakajima and T. Ishikawa	41 WGP	VI-68

<u>Title</u>	<u>Authors</u>	<u>Proposal Number</u>	<u>Page</u>
Dynamic Behaviour of Biopolymers Studied by Small-Angle Scattering (I)	T. Ueki, Y. Hiragi, Y. Izumi, H. Tagawa, M. Katoka, Y. Muroga, T. Matsushita and Y. Amemiya	12 WGP	VI-70
Performance of Multi-Detector System for Fluorescence EXAFS Experiment	H. Oyanagi, T. Ishiguro, T. Matsushita, and K. Kohra		VI-72
<u>BL-11A</u>			
Fine Structure of Ti $L_{2,3}$ Edges in Ti, TiS and TiS ₂	S. Nakai, M. Ohashi, K. Ogata, M. Yanagihara and H. Maezawa	WG	VI-73
Sensitive Z Dependence of $M_{4,5}$ Giant Resonance Absorption Spectra of Z=49-57 Elements	Y. Iguchi, H. Maezawa, M. Yanagihara, Y. Suzuki and T. Sasaki	56	VI-74
Collapse of the f-Symmetric Final State Wavefunction in the 3d-Excitation Spectra of Atomic X_e , C_s and B_a	B. Sonntag, T. Nagata, U. Sato, Y. Satow, A. Yagishita, M. Yanagihara and T. Sasaki	72	VI-75
X-Ray Lithography: Soft X-Ray Spectral Characterization of Resist Polymer	K. Mochiji, T. Kimura, H. Obayashi, M. Yanagihara and T. Sasaki	CT	VI-76
Photoefficiency Evaluation of Photocathodes for Soft X-Ray Experiments	A. Sawaki, T. T. Yamashita, Y. Iguchi, H. Maezawa, Y. Yanagihara, Y. Suzuki and T. Sasaki	CT	VI-77
Reflection of VUV Light from Mirror Surfaces	M. Yanagihara, T. Koide, M. Niwano, T. Miyahara, S. Sato, Y. Iguchi, T. Sasaki	61	VI-78
$K^{+}L_{2,3}$ Absorption Spectra of Potassium Halides	M. Yanagihara, Y. Iguchi, H. Maezawa, T. Sasaki	WGP	VI-79
<u>BL-11B</u>			
Contact Microscopy with Synchrotron Radiation X-Rays Using Transmission Grating	S. Aoki, T. Ohta, M. Nomura and S. Kikuta	WGP	VI-80
S- $L_{2,3}$ Emission Spectra of Sulfure Compounds Excited by Synchrotron Radiation	K. Taniguchi, T. Ohta and M. Nomura	WGP	VI-81
<u>BL11C</u>			
Extreme Ultraviolet Absorption Spectra of K-Na Alloys	I. Fukui, S. Suzuki, T. Hanyu, H. Fukutani, H. Kato, H. Sugawara, I. Nagakura, S. Nakai, T. Hirokawa, T. Ishii and T. Miyahara	WGP	VI-82
Inner Core Excitation Spectra of Alkaline Earth and Rare Earth Metals	T. Hanyu, T. Miyahara, T. Kamada, K. Asada, H. Ohkuma, H. Ishii,	67	VI-84

<u>Title</u>	<u>Authors</u>	<u>Proposal Number</u>	<u>Page</u>
<u>BL-12A</u>			
Electron Correlations in Photoionization of Atoms	Y. Ichikawa, Y. Sato, J. Murakami, T. Nagata, B. Sonntag, A. Yagishita, M. Yoshino	26	VI-85
Dynamic Measurement of Photoionization Processes of Gases	M. Nakamura, M. Watanabe, Y. Morioka, Y. Kageyama, T. Hayashi, K. Naito, H. Kato and S. Yamaguchi	55	VI-86
Ionization and Dissociation of Highly Excited Molecules	Y. Hatano, K. Shinsaka, H. Koizumi, T. Yoshimi, M. Toriumi, M. Ukai, S. Arai, E. Suzuki, Y. Tanaka, M. Morita, A. Yagishita, K. Ito	69	VI-87
<u>BL-15A</u>			
Performances of the Muscle Diffractometer	K. Wakabayashi, T. Hamanaka, Y. Amemiya, H. Tanaka, T. Wakabayashi and H. Hashizume	WG	VI-88
Time-Resolved X-Ray Diffraction of Contracting Skeletal Muscle	H. Tanaka, T. Kobayashi, H. Hashizume, Y. Amemiya and H. Sugi	11	VI-91
X-Ray Diffraction Studies of Structural Change of Muscle Filaments in Connection with Muscle Contraction	K. Wakabayashi, T. Hayashi, A. Fujishima, T. Hamanaka, M. Konishi, S. Kurihara, Y. Umazume and Y. Amemiya	30	VI-92
Test of Integral Type Position- Sensitive Detector and Its Appli- cation to Small Angle Scattering Experiments	K. Hasegawa and K. Mochiki	71	VI-93
Time-Resolved X-Ray Diffraction Studies of TMV and Their Protein Assemblies	M. Taniguchi, Y. Amemiya, K. Wakabayashi, T. Taniguchi, Y. Satow and Y. Kamiya	48	VI-95
Localization of Physiologically Active Tyrosines in Purple Membrane and Their Localization Change on Absorption of Light	F. Tokunaga, M. Kataoka, N. Sato, K. Takeda, O. Hisatomi, M. Hirai and Y. Amemiya	45	VI-96
<u>BL-15B</u>			
Photographic Investigation of a Human Tooth (15 B 1, Dec. 1982)	P. Spieker	36 WGP	VI-97
Test of an X-Ray Interferometer (15 B 1, Jun. 1982)	P. Spieker	36 WGP	VI-98
Test of a "Monolithic Fixed Exit Beam Monochromator" (15 B 1, Jun./Jul. 1983)	P. Spieker	36 WGP	VI-99
High Speed X-Ray Topography	M. Ando, J. Chikawa, H. Hashizume, K. Hayakawa, T. Imura, T. Ishikawa, S. Kishino, S. Nagakura, O. Nittono, and S. Suzuki	70 WG	VI-100

<u>Title</u>	<u>Authors</u>	<u>Proposal Number</u>	<u>Page</u>
Studies on Dynamical Behavior of Lattice Defects in Ice by Rapid X-ray Topography	Ice Topography Group	54	VI-101
An Examination of the X-Ray Magnetic Bragg Reflection and Its Application to the Fundamental Magnetism	K. Namikawa M. Ando, T. Nakajima, P. Spieker and S. Hosoya	65	VI-102
Real Time X-Ray Topographic Study of Phase Transition of Fe_3O_4 and $TbVO_4$ Crystals	S. Suzuki, H. Unoki, S. Chikazumi, S. Todo, T. Nakajima and M. Ando	70 WGP	VI-103
Real Time X-Ray Topography Camera Using Fluorescence Film and Image Intensifier	S. Suzuki, H. Kawata and M. Ando	70 WGP	VI-104
X-Ray Topography of GaAs Crystal	H. Takaoka, K. Ikeda, Y. Homma, Y. Ishii and M. Ando	70 WGP	VI-105
Synchrotron X-Ray Section Topography	Y. Sugita and H. Kawata	70 WGP	VI-106
A Study on Defects in CaF_2 Single Crystals	Cui Cheng-Jia and Tomoya Ogawa	70 WGP	VI-107
Study on the Melting Mechanism of Forsterite Mg_2SiO_4 by means of X-Ray Topography	Y. Takeuchi, T. Yamanaka and K. Ogata	70 WGP	VI-108
Synchrotron Radiation Topographs of As-Grown Tin Single Crystal Plates	O. Nittono, T. Ogawa and S. Nagakura	70 WGP	VI-109
<u>BL-15C</u>			
Magnetic Diffraction of X-Rays from a Fe -3%Si Crystal	S. Nakatani, Y. Ushigami, T. Ishikawa, S. Kikuta, H. Saka and T. Imura	36 WGP	VI-110
Structure Analysis of the $NiSi_2/(111)Si$ Interface by the X-Ray Standing Wave Method	K. Akimoto, T. Ishikawa, T. Takahashi and S. Kikuta	36 WGP	VI-111
Polarization Ratio and Rotation of the Electric Vector of Synchrotron Radiation	T. Ishikawa, S. Annaka and K. Kohra	36 WGP	VI-112
Measurement of X-Ray Refractive Index by Multiple Reflection Diffractometer	H. Kato, T. Ogawa, S. Hattori, M. Kawata, Y. Kobayashi, K. Umezawa, T. Ishikawa and K. Ishida	36 WGP	VI-114
Precision Lattice Parameter Measurement System on the Basis of the Triple-Crystal Arrangement Applied to the Bond Method	K. Sugii, T. Ishikawa, K. Nakayama, H. Takaoka, and S. Kikuta	36	VI-115
<u>LINAC (0.5 GeV ELECTRON BEAM EXTRACTION PORT)</u>			
A new type of undulator making use of standing microwaves	T. Shintake, K. Huke, J. Tanaka, I. Sato and I. Kumabe		VI-116

Angular Distribution Measurements of Photoelectrons Ejected from Atoms and Molecules Using Undulator Radiation

Y. Suzuki, A. Yagishita, H. Maezawa, H. Kitamura and T. Sasaki

Photon Factory, National Laboratory for High Energy Physics
Oho-machi, Tsukuba-gun, Ibaraki-ken, 305 Japan

Introduction

The angular distribution of photoelectrons ejected from target atoms and molecules by a linear-polarized light impact is given by, in the dipole approximation,

$$I(\epsilon, \theta) = \frac{\sigma(\epsilon)}{4\pi} \left(1 + \frac{\beta(\epsilon)}{2} (3\cos^2\theta - 1)\right),$$

where ϵ is the kinetic energy of the photoelectrons, $\sigma(\epsilon)$ is the partial photoionization cross section, θ is the angle between the electric vector of the incident radiation and the direction of the photoelectron, and $\beta(\epsilon)$ is the asymmetric parameter that characterizes the angular distribution.

We have measured the $\beta(\epsilon)$ for the 3d electrons of Kr and Xe, the 3p of Kr, and the 1s of N₂ and O₂ in photon energies from 400 to 900 eV.

Experiment

The quasi-monochromatic radiation from the undulator, which was installed PF storage ring, was employed as a light source without monochromator. The number of period in the undulator is 60. The length of each period is 6 cm. The maximum K value is 1.7. The energy of the first harmonic of the undulator radiation is continuously varied from 400 to 900 eV by changing the K value.

The polarization of the radiation has been checked through measurement of the angular distribution of He 1s photoelectrons. The degree of polarization was found to be 99.9 ± 0.01%, and $\beta_{1s}(\epsilon)$ of He was 1.995 ± 0.007 at $h\nu = 400$ eV. The instrument is schematically shown in Fig. 1. The energy of electron is measured by an electrostatic hemispherical analyzer (mean radius 50 mm) that is mounted on the rotatable table perpendicular to the photon beam axis.

Results

The measured values of $\beta_{3d}(\epsilon)$ for Xe are shown in Fig. 2 where the solid line is the theoretical value given by Kennedy and Manson¹. The present data agree with the theoretical value except the deviation near the threshold.

The measured values of $\beta_{1s}(\epsilon)$ for N₂ are shown in Fig. 3. For diatomic molecule, Dehmer and coworkers² have predicted the f-type shape resonance for N_{1s} photoionization, and also calculated the values of β parameter in the reso-

nance region. According to their calculation, near the threshold the $\beta_{1s}(\epsilon)$ of core 1s-electron shows the oscillation and its minima at about 10 eV above threshold, and in the high energy region $\beta(\epsilon)$ approaches the constant value $\beta = 2$ which corresponds to the value of β for 1s-shell of the free atom. The calculated $\beta_{1s}(\epsilon)$ is shown in Fig. 4 by the solid line. Our data agree with Dehmer's theory, but appreciable deviation from the theoretical $\beta(\epsilon)$ still remains.

References

- 1) D. J. Kennedy and S. T. Manson, Phys. Rev. A5 227 (1972).
- 2) D. Dill, S. Wallace, J. Siegel and J. L. Dehmer, Phys. Rev. Lett. 41 1230 (1978), Phys. Rev. Lett. 42 411 (1979).

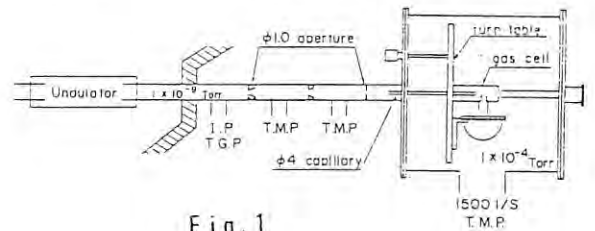


Fig. 1

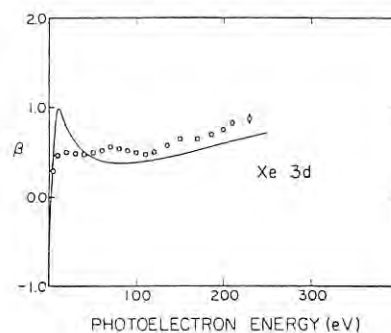


Fig. 2

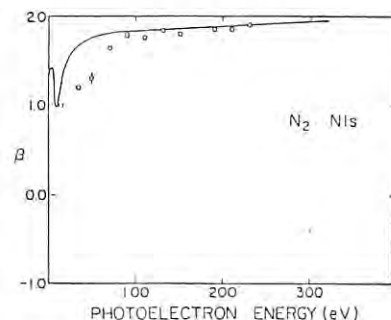


Fig. 3

X-RAY FLUORESCENCE ANALYSIS BY SYNCHROTRON RADIATION

Y. Gohshi*, A. Iida*, T. Matsushita**
and

Ultra Trace Element Analysis Working Group

Introduction

X-ray fluorescence trace and micro analysis using a synchrotron radiation (SR) source are of value in both research and technology. The outstanding properties of X-ray spectrochemical analysis are : tunability of the energy spectrum, high brightness, and polarization for reduced background scattering.¹⁾ In this report the preliminary results of our energy dispersive X-ray fluorescence analysis (XFA) are presented. The minimum detection limits (MDL) obtainable with SR excitation are studied in detail, including both white and monochromatic excitation. Taking advantage of the continuous spectrum of SR, various monochromatization methods are examined.

Results

BL-15A2 (Jun. '82), BL-15C (Feb. '83) and BL-4A (Jun. '83) were used for energy dispersive XFA measurements. A preliminary experiment at BL-15A2 was done using conventional instruments. The results to be reported here were obtained from the experiments at BL-15C and BL-4A using a specially designed spectrometer (see Instrumentation section). The samples measured were Standard Reference Material, metal adsorbed chelate resins, semiconductors, and several kinds of environmental and biomedical samples.

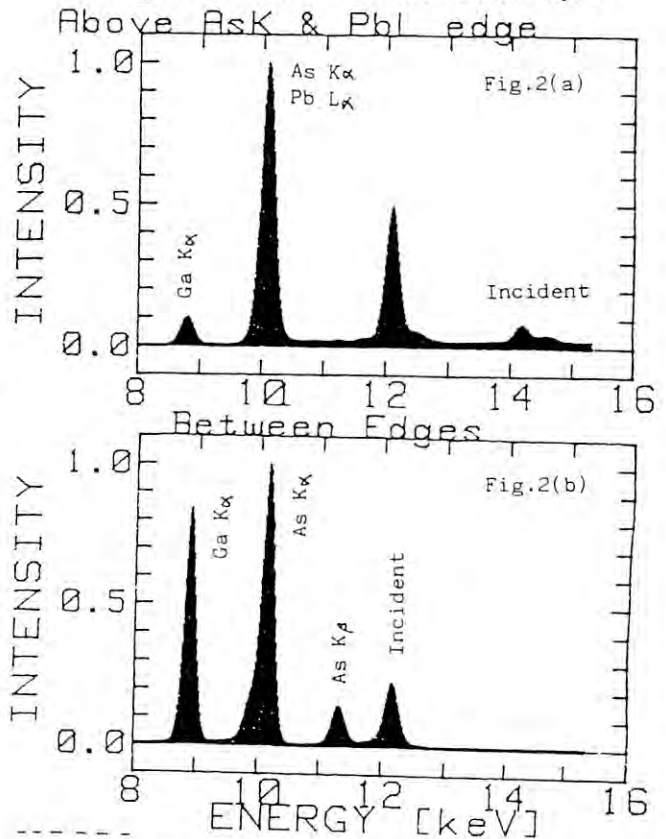
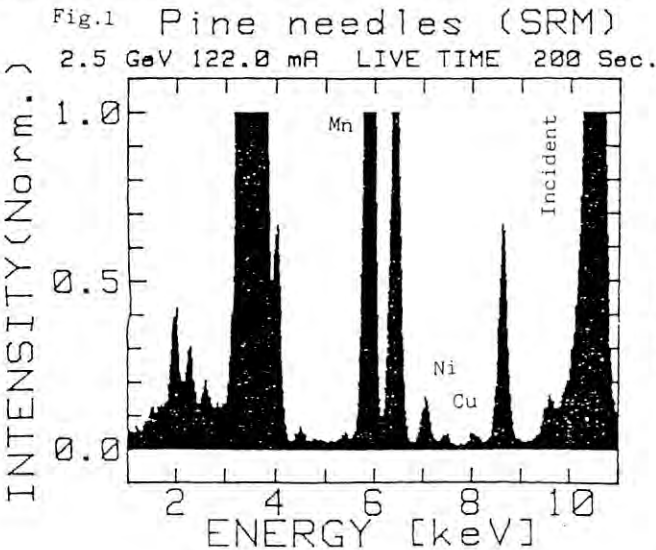
We first examined the difference between the white and the monochromatic excitation modes. With direct white excitation, the fluorescence radiation was very strong but the signal to noise ratio was low due to the strong background, which may have originated from the vertical polarization component of the SR and the finite detector solid angle. When the excitation beam was monochromatized by a crystal monochromator, the continuous background was reduced drastically and a high signal to noise ratio was attained.

Reduction in background scattering due to polarization, and effects of the excitation energy

on quantitative analysis were both demonstrated experimentally. The spectrum obtained from the pine needles (Standard Reference Material) is shown in Fig.1. A Si monochromator was used. The 3×10^{-6} g/g copper peak and 3.5×10^{-6} g/g nickel peak were clearly observed. In a series of measurements using metal adsorbed chelate resins with different concentrations, which is used trace element analysis in solution, the MDL was at the 0.1 ppm level, which is 10^{-1} lower than the MDL of the conventional method. Due to the high brightness and collimation of SR, the absolute detectability was $10^{-11} \sim 10^{-10}$ g, which is lower by a factor of $10^{-1} \sim 10^{-2}$ than that of the conventional method.

Furthermore, the energy tunability of SR was effectively used to remove overlapping peaks. To cite one example, if the excitation energy was higher than both the As K and Pb L edges, the As K and Pb L peaks overlapped completely due to the poor resolution of SSD (Fig.2(a)). When the excitation energy was set between the As K and Pb L edges, the Pb L peak was completely suppressed (Fig.2(b)). Thus we can separate the As K peak from the Pb L contribution experimentally. This example clearly shows the advantage of the energy tunability of SR to remove overlapping peaks and to avoid interference effects.

During the monochromatic excitation experi-



* Univ. of Tokyo, Hongo, Tokyo
** KEK, Oho-machi, Tsukubagun, Ibaraki

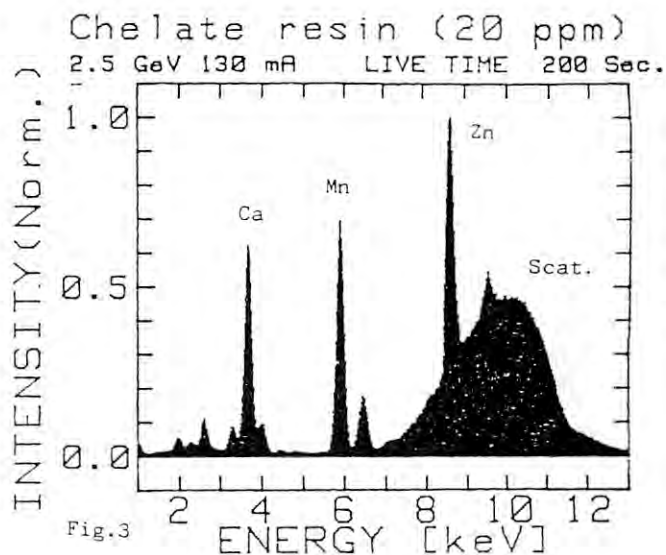
ments, we observed considerable contribution from second order reflection by the graphite monochromator, but the effect of the higher harmonics was negligible with the Si monochromator, which does not have second order reflection. Since the energy spectrum from the storage ring extends up to 25 keV or more, we must pay careful attention to the higher harmonics effects. These higher harmonics were effectively rejected by the use of a mirror in combination with the crystal monochromator.

Various other samples, including semiconductors, environmental and biomedical samples were measured, the results of which will be reported elsewhere.

In energy dispersive XFA, one of the difficulties which limit the improvement of the MDL is the saturation of the SSD at a high counting rate. The ratio of the scattered to the fluorescence radiation depends strongly on the type of sample and the excitation mode. In order to get a wide variety of excitation parameters (i.e. energy band width and flux), a monochromator system alternative to the crystal monochromator (which has rather narrow band width) was desired. For that purpose, we tested the combination of a total reflection mirror and an absorber, which has attained an energy band width of more than 10 %²⁾. Fig.3 shows the spectrum of a metal adsorbed chelate resins containing 20 ppm Zn and Mn obtained by this method. This result shows that the wide band pass monochromator is very effective both in the detection of light elements and in the adjustments of the excitation intensity. We are also planning to develop the wide band pass monochromator consisting of transmission plus reflection mirrors.

Conclusions

The preliminary results reported here are quite promising. Minimum detection limits were improved remarkably, especially in respect to the absolute amount detectable. When line interference was absent, the minimum detection limits obtained was about 0.1 ppm and $10^{-11} \sim 10^{-10}$ g.



To facilitate the future use of the wavelength dispersive crystal spectrometer and the application to various types of samples, we are developing monochromator systems which can attain desirable energy band pass and intensities.

The authors gratefully acknowledge the support given by the PF staff and members of Ultra Trace Element Analysis Working Group.

References

- 1) C. J. Sparks, Jr., in Synchrotron Radiation Research, H. Winick and S. Doniach, eds., p.491 (Plenum Press, N.Y. 1980)
- 2) D. H. Bilderback. Nucl. Instr. and Meth. 195 (1982)67

DEVELOPMENT OF A DISPERSIVE X-RAY ABSORPTION SPECTROMETER FOR TIME-RESOLVED EXAFS EXPERIMENT

T. Matsushita, H. Oyanagi* and U. Kaminaga**

Photon Factory, National Laboratory for High Energy Physics
Oho-machi, Tsukuba-gun, Ibaraki 305

* Electrotechnical Laboratory, Umezono, Sakura-mura, Niihari-gun, Ibaraki 305

** Rigaku Corp. Matsubara-cho, Akishima, Tokyo 196

A dispersive X-ray absorption spectrometer, schematically shown in Fig. 1, was constructed in order to obtain EXAFS/XANES spectrum in 1.0 - 0.01sec. The spectrometer is in principle of the same design as the one reported earlier.^{1,2} A bent triangular-shaped crystal (silicon 111 or 400) is used to disperse and focus the synchrotron X-ray beam. X-ray beams of different energies as a function of the converging angle is focused at F which is located inside of the Rowland circle. The sample is placed at F. A flat platinum-coated fused quartz mirror is placed between the sample and a detector. By aligning the glancing angle of the beam to the mirror surface, the harmonics from the crystal are rejected.

As a detector, a photodiode array sensor (RETICON RL1024SF) with a fiber optic face plate is used. On the surface of the face plate, a fine-powder phosphor (GdO₂S:Tb) screen is formed with a thickness of ~50² μm. The diode array consists of 1024 diodes separated by 25.4 μm to each other. The signal from each diode is successively digitized by a 12-bit A/D converter and store into a memory. With a system schematically shown in Fig. 2, a minimum exposure time of 5 msec has been attained. Data for 16 successive exposures with a time interval of 5 msec - 999 sec can be stored with this system and later transferred to a computer.

Figure 3 shows results of Fourier transform of EXAFS spectrum from a copper metal foil. The upper curve is obtained from the data taken in a conventional point-by-point mode at BL-10B station of the Photon Factory. The lower curve is for the dispersive method. The EXAFS spectrum was taken in 50 msec with the dispersive spectrometer when the storage ring operates at 2.5 GeV and 100 mA. The agreement in peak positions between two curves in Fig. 3 is fairly good. The difference in peak height is probably due to the non-linearity of the photodiode array detector. A further improvement of the system is under way.

The authors would like to thank Dr. S. Suzuki for providing them fine-powder GdO₂S:Tb phosphor and for advices for preparing a thin phosphor layer on the detector.

References

- 1) T. Matsushita and R. P. Phizackerley, Jpn. J. Appl. Phys. 20 (1981) 2223-2228.
- 2) R. P. Phizackerley, Z. U. Rek, G. B. Stephenson, S. D. Conradson, K. O. Hodgson, T. Matsushita and H. Oyanagi, J. Appl. Cryst. 16 (1983) 220-232.

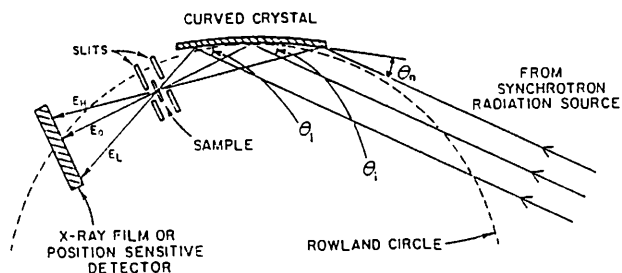


Fig. 1

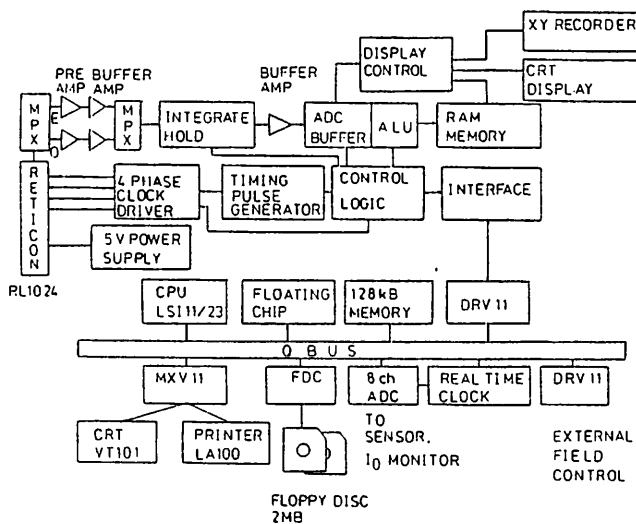


Fig. 2

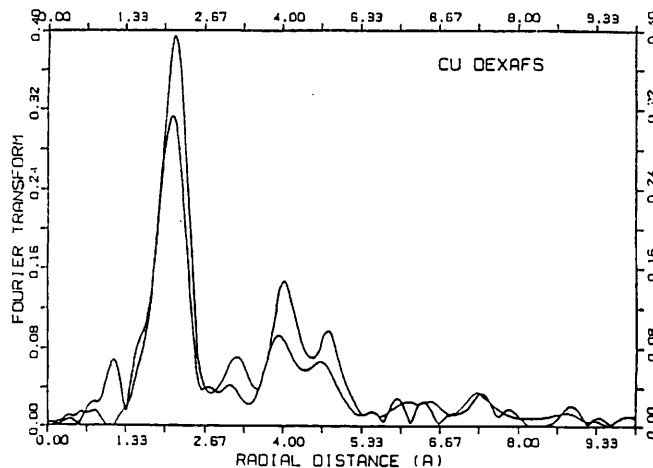


Fig. 3

MACROMOLECULAR CRYSTALLOGRAPHY WITH SR

Preliminary experiments using a Weissenberg
Camera with multi-layer-line screens for
macromolecular crystallography

Research group 33 : N. Sakabe, N. Kamiya
Department of Chemistry, Faculty of Science
Nagoya University, Chikusa, Nagoya 464

Introduction

Synchrotron X-radiation sources are having a considerable impact on protein crystallography, giving intense tunable collimated X-ray beams for single crystal diffraction experiments. A Weissenberg camera with multi-layer-line screens was constructed for the collection of many reflections up to high resolution with high signal-to-background ratio from a crystal with large unit-cell dimensions without losing any diffracted beams by screens (1). We will give a brief description of the selection of X-rays with definite wavelength and the alignment of the instrument, and discuss the comparison between SR and rotating anode sources.

Experimental and results

Beam line 4A was used for 23 hours on July 22, 1983. A flat type Si (111) monochromator was provided by PF. The beam of the wavelength 1.542 \AA was selected by referring absorption edge of Ni foil (1.488 \AA).

It is a time consuming step to adjust the orientation of such a heavy camera to the SR beam pass directly because we cannot enter the hutch while beam shutter is open. To solve this problem the SR beam pass was visualized using laser beam as shown in Fig. 1.

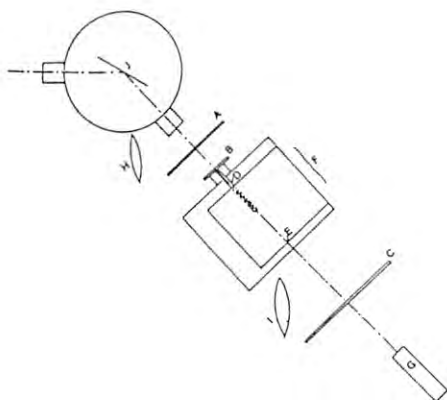


Fig. 1 Schematic representation of the alignment of the camera.

A, B & C: stainless steel plates whose size are 50×50 , 20×20 and $100 \times 100 \text{ mm}^2$ respectively. The plate is covered with fluorescent paint, and has a hole of $r = 0.5 \text{ mm}$ at the centre.

D: collimator.

E: a hole of $r = 0.2 \text{ mm}$ for the alignment.

G: laser source.

H & I: magnifying glasses.

The procedure of alignment is as follows;

1. Set the A and C plates so that the SR beam passes through the pin holes of A and C.

2. Set laser source (G) so that the laser beam passes through the two pin holes of C and A.

3. Set the Weissenberg camera (F) without collimator (D) so that the laser beam passes through the two pin holes of B and E.

A Weissenberg photograph (Fig. 2) was taken with monochromatized SR beam. According to the comparison of photographs, brilliance on this condition may be 3-4 times higher than that of $\text{CuK}\alpha 1$ radiation generated by a Rigaku 200H rotating-anode tube with a doubly bent LiF monochromator (0.1 mm focusing cusp, run at 50 kV and 24 mA, divergence of the beam - 2 mrad). The most prominent feature of this photograph is that the Bragg spots are very sharp.

In order to get more brilliant source, an asymmetric cut curved Si (111) monochromator is going to be constructed and will be used at the next beam time.

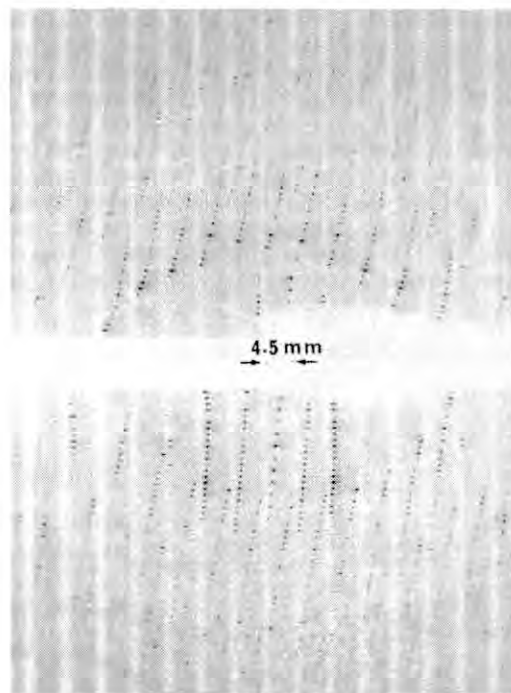


Fig. 2 Weissenberg photograph of the multi-layer-line screen of a crystal (G-actin DNase I complex, space group $P2_12_12_1$, $a = 42.0$, $b = 224.8$, $c = 77.3 \text{ \AA}$, with a-axis rotation and c-axis along SR beam, rotation angle = 9° and exposure time = 9 h).

Reference

- 1) N. Sakabe: J. Appl. Cryst. 16 (1983) in press.

STUDY OF PHASE TRANSITIONS IN POTASSIUM-GRAPHITE INTERCALATION COMPOUNDS BY SYNCHROTRON RADIATION X-RAY.

H.Suematsu, R.Nishitani, Y.Uno, Y.Fujii*, and T.Matsushita**

Institute of Materials Science, University of Tsukuba, Sakura, Ibaraki 305.

*Faculty of Engineering Science, Osaka University, Toyonaka, Osaka 560.

**KEK. National Laboratory for High Energy Physics, Oho-machi, Ibaraki 305.

The graphite intercalation compounds(GIC) have a unique crystal structure so-called as "stage structure", which is characterized by the alternation of n graphite(G) layers and one intercalant(I) layer. The stage n can be controlled by vapor pressure of I. Inserted I-atoms between G-layers are loosely bound to G-lattice, so that in high stage potassium(K)-GICs K-atoms behave as a two dimensional(2D) liquid even at low temperature below room temperature. The liquid structure depends on the inplane density of I, which can be also controlled by K pressure p_K .

In the present study we have investigated the insitu observation of inplane liquid structure in the stage transition region and of the liquid-solid transition in 1st stage K-GIC.

X-ray diffraction measurements were carried out by using synchrotron radiation white X-ray source(BL-4B) at KEK-PF, and the energy dispersive detection system. The graphite sample was sealed in a glass ampoule and was held at $T_G=390^\circ\text{C}$, while p_K in the ampoule was accurately controlled. The correction of X-ray source profile, absorption of the ampoule and others were made by comparing the diffuse scattering of air and the diffraction intensity of SnI_4 powder in a similar ampoule.

The (hk0) spectra for 2nd and 1st stages are shown in Fig.1. At $p_K < 0.18$ Tor we can see liquid haloes of K and also the Bragg reflection(100) of G, in which the compound is 2nd stage. With increasing p_K the halo peak q_0 increases gradually, which implies that the inplane density is dependent on p_K (Fig.2). At the critical p_K the compound changes to 1st stage and q_0 increases simultaneously(i.e. a dense liquid phase). In the 1st stage

region we can see a similar p_K -dependence of q_0 to 2nd stage. These results are the first evident observation of non-stoichiometry of inplane composition; it has been believed so far that they are stoichiometric compounds such as $\text{C}_8\text{K}(n=1)$ or $\text{C}_{12}\text{K}(n=2)$. The non-stoichiometry may give some crucial effects on the inplane structure such as the discommensuration modulation especially in 2nd stage, which is one of the most up-to-date controversy.

The next important result is the liquid-solid transition in 1st stage. For a low p_K i.e. a low inplane concentration($q_0 \lesssim 1.42 \text{ \AA}^{-1}$) K-atoms are in liquid phase. However with increasing p_K consequently inplane K density, K-atoms become to correlate to each other in either direction of the a- and also c-axes; the liquid halo q_0 shifts to a larger value along q_a and at the same time the line width Δq_a becomes narrower, while the correlation in the c-axis stacking also grows up. Finally the solidification begins when q_0 reaches the value of the K-superlattice 2×2 (relative to G unit cell). These results show that the "melting" of K-layer is nearly of the 2nd order phase transition, although it is in practice of the 1st order. Thus we can see first that the 1st stage K-GIC is a very unique system in which the precursor effect of solidification can be observed in liquid phase at a fairly lower μ (chemical potential) than the critical μ_m .

The present authors gratefully acknowledge stimulating discussions of Prof.Y.Yamada and experimental assistances of Messrs. Mukaida and Onishi.

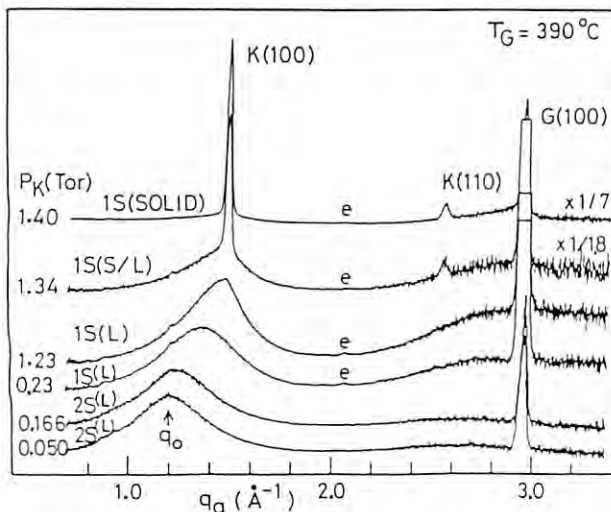


Fig.1 X-ray (hk0) diffraction spectra in K-GIC as a function of K pressure p_K . 1S: 1st stage, 2S: 2nd stage, S:solid, L:liquid, e: escape peak, K(100): Bragg reflection of K-superlattice 2×2 .

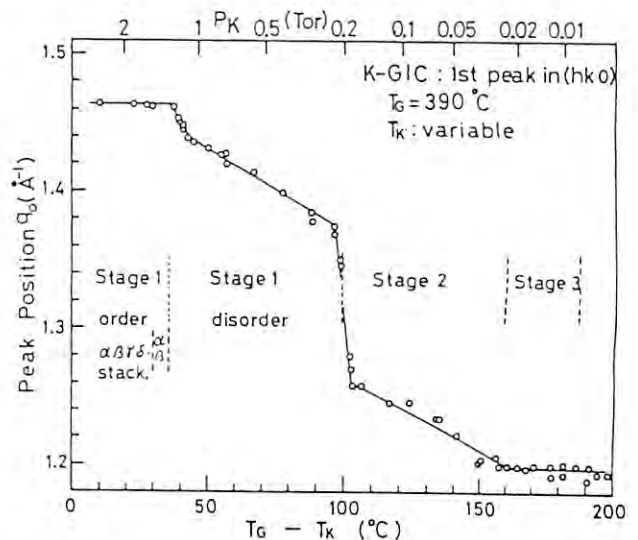


Fig.2 K-pressure p_K -dependence of inplane liquid halo peak q_0 .

MONOCHROMATIZED X-RAY EXPERIMENTS BY THE DIFFRACTOMETER FOR LIQUID AND MELT

The Test-Run Group for Liquid and Melt Diffraction*

Introduction

Synchrotron radiation offers strong and parallel X-rays for diffraction experiments. It is useful for planning of synchrotron experiments to know the intensities of monochromatized X-ray beams. However, there are no reports concerning the quantitative comparison of the intensities for monochromatized synchrotron radiation with those for characteristic X-rays from conventional generators. For this purpose, measurements of diffraction intensities were carried out at the experimental station No. 4B, utilizing the diffractometer for liquids and melts.

The diffractometer for liquids and melts has an attached analyzer to obtain a better resolution in comparison with a pure-Ge SSD. Tests of the analyzer were also carried out, utilizing the diffractometer in the monochromatized X-ray mode.

Measurements of Intensities

To obtain characteristic X-rays, a rotating Cu anode tube generator(Rigaku RU200) with 50 μm focus was used. The X-rays passed through a divergence slit of 3° were monochromatized to Cu K α radiation($\lambda=1.54 \text{ \AA}$) by a curved LiF(220) crystal with $r=320 \text{ mm}$, and then, focussed on a receiving slit of 200 μm . Intensity of the beam passed through the receiving slit was measured with an ionic chamber with Ar gas. To obtain monochromatized synchrotron X-rays with $\lambda=1.54 \text{ \AA}$, a Si(111) plate was mounted on the sample holder of the diffractometer. The white synchrotron radiations passed through an incident slit of 2 mm were monochromatized by the Si plate, and then received with a slit of 1 mm to be measured the intensity of the monochromatized X-rays by the ionic chamber on the detector arm. The EXAFS of copper was also measured to estimate a resolution of the Si(111) monochromator used.

Tests for the analyzer which was mounted on the detector arm in place of the SSD were carried out by using the characteristic Cu K α radiations. The analyzer consists of a Ge(220) crystal analyzer, a scintillation counter, a pre-analyzer slit of 1 mm and a post-analyzer slit of 150 μm . The white synchrotron radiation beams were monochromatized to $\lambda=0.9 \text{ \AA}$ by a Si(111) plate and passed through an incident slit of 1 mm to irradiate copper foil at the sample holder. The fluorescent X-rays generated were analyzed by a symmetrical scanning of the analyzer and the detector.

Results

Intensities of the monochromatized X-rays from synchrotron radiation were compared with those of the characteristic X-rays in Table 1. It was concluded that even if the simplest set-up the monochromatized synchrotron X-rays were several times stronger than the characteristic X-rays from conventional generators. An absorption spectrum obtained by this set-up was shown in Fig. 1 and the resolution(FWHM) of the Si(111) monochromator was estimated to be about 10 eV.

The Cu K α spectrum obtained by the analyzer

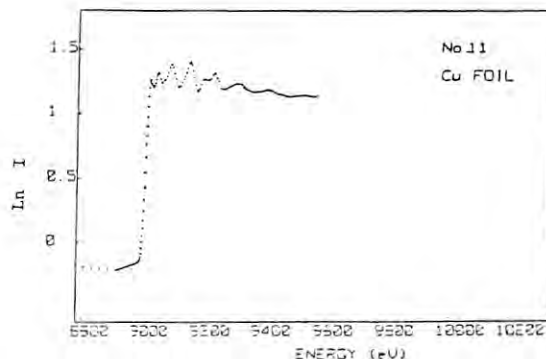


Fig. 1 EXAFS data for copper foil.

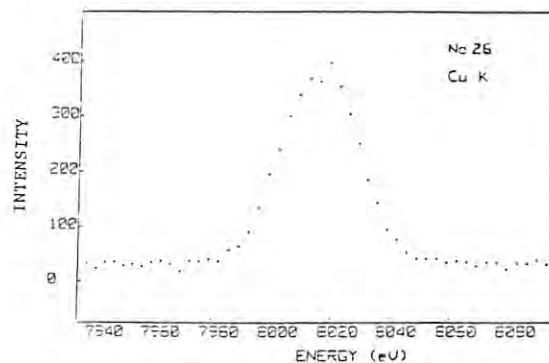


Fig. 2 Cu K α spectrum obtained by a Ge(220) analyzer.

Table 1 Intensities of monochromatized synchrotron X-rays($\lambda=1.54 \text{ \AA}$) and Cu K α radiations by a conventional X-ray source.

Condition	Total number of photons	Number of photons per unit area(mm^2) of monochromator
<u>Conventional Source</u>		
20 kV 10 mA	1.5×10^7 cps	4.5×10^4 cps
20 kV 100 mA	1.5×10^8 cps	4.5×10^5 cps
30 kV 100 mA	4.4×10^8 cps	1.3×10^6 cps
40 kV 100 mA	7.6×10^8 cps	2.3×10^6 cps
<u>Synchrotron Source</u>		
2.5GeV 52 mA	1.8×10^9 cps	4.3×10^8 cps

was shown in Fig. 2, and the resolution of the analyzer was estimated to be about 40 eV and insufficient to anomalous dispersion and Compton profile measurements which required at least a resolution of about 10 eV. However, the pre-analyzer slit can be replaced by the smaller opening one, since the monochromatized synchrotron radiation beams are strong enough to reduce the scattering area, and improvement of resolution may be easily attainable.

* F.Marumo, K.Tothji, K.Suzui, Y.Udagawa, M.Ando, S.Sasaki, M.Yoshizawa, T.Yamanaka, K.Arakawa, N.Nakagawa and M.Miyake

AN ENERGY DISPERSIVE-EXPERIMENTS OF X-RAY DIFFRACTION BY GLASSES: SILICA GLASS

The Test-Run Group for Liquid and Melt Diffraction*

Introduction

The energy-dispersive method of X-ray diffraction was successfully applied to the structural study of molecular liquids by Nishikawa and Murata.¹⁾ One of the advantages of this method in comparison with the angular dispersive method lies at the point that the obtainable data cover a wide range of $S = 4\pi \sin\theta/\lambda$. The angular dispersive method with Mo K α ²⁾ and Rh K α ³⁾ radiations gave diffraction data up to 16.0 and 20.0 in S, respectively in their experiments. However, intensity curves of glasses in the region of the larger S-values than 20.0 show still some structures, due to the existence of correlations in atomic pairs.⁴⁾ This fact causes the truncation effects on the Fourier integrals in the calculations of radial distribution functions which are used for the structural analyses of amorphous materials.

The present work aims to show that energy-dispersive experiments on glasses with synchrotron radiation can give data of high quality comparable to those of angular dispersive experiments, and also to clarify the maximum S-value of the diffraction data available with the diffractometer constructed. Silica glass was chosen for the test sample, since it had been most extensively studied so far among glasses.^{2,3,4)}

Measurements of diffraction intensities were carried out at the experimental station No. 15A2, using the diffractometer for liquids and melts in the white-radiation mode.

Experimental

A silica glass was polished to a plate of 0.27 mm in thickness. The plate was fixed to the sample holder for powder specimens and attached on the θ -axis of the goniometer. Intensity measurements were carried out in the transmission geometry with the symmetrical θ - 2θ setting. An Al-foil of 0.3 mm in thickness was placed at the first slit of the diffractometer to cut off the low energy photons.

Scattered X-rays were detected by a pure Ge SSD backed up by a multi-channel analyzer. The region of the photon energy of 0-35 keV was

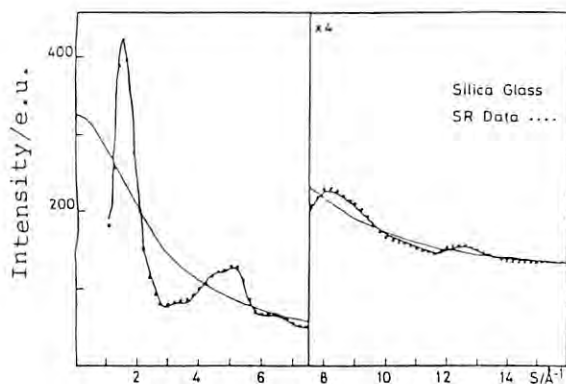


Fig. 1. Intensity curves for silica glass.

divided into 1024 channels. The scattering angles 2θ were selected at 7, 12, 20, 35, 50, 70 and 100° . Beyond the scattering angle of 90° , liquid nitrogen begins to pour out of the dewar of the SSD. Scattered photons were accumulated for 1500-4000 seconds at the respective scattering angles. An incident beam spectrum was experimentally determined by using the diffraction data of gaseous SF₆ at the scattering angle of $2\theta=55^\circ$.

Results

The observed energy-spectra of scattered X-rays were analyzed according to the method described in Ref. 1. The reduced intensity curve was plotted in Fig. 1 in comparison with that obtained with the angular dispersive method with Mo K α radiations.²⁾ The result of the present work is in a good agreement with that of the conventional experiments. The use of the synchrotron radiation should be very effective in shortening the running time, for the angular dispersive measurements need several days to complete data collection on one sample. Moreover, the synchrotron radiation can afford intensity data with S-values in a wide range, which can not be obtained by the angular dispersive experiments. Experimental conditions were summarized in Table 1.

Table 1. Diffraction data for silica glass

Scattering angle(2θ)	Accumulated time(sec.)	Data recorded(S)	Data available(S)
7	1500	0.8- 2.7	1.1- 2.0
12	2000	1.3- 4.7	1.9- 3.5
20	2000	2.1- 7.9	3.3- 5.9
35	3000	3.6-13.7	5.7-10.3
50	3000	5.0-19.2	8.1-14.4
70	4000	6.8-26.1	10.9-19.6
100	4000	9.1-34.9	14.6-26.2

References

- 1) K. Nishikawa and Y. Murata, Bull. Chem. Soc. Jpn., 52 (1979) 293.
- 2) H. Morikawa, S. Miwa, M. Miyake, F. Marumo and T. Sata, J. Amer. Ceram. Soc., 65 (1982) 78.
- 3) R. L. Mozzi and B. E. Warren, J. Appl. Cryst., 2 (1969) 164.
- 4) M. Misawa, D. L. Price and K. Suzuki, J. Non-Cryst. Solids, 37 (1980) 85.

* F. Marumo, H. Morikawa, H. Otaki, T. Yamaguchi, K. K. Lee, Y. Tamura, K. Ozutsumi, Y. Takeuchi, Y. Kudo, K. Sugiyama, T. Iijima, T. Mitsuhashi and M. Ando

AN ENERGY-DISPERSIVE EXPERIMENT OF X-RAY DIFFRACTION BY LIQUIDS. CARBON TETRACHLORIDE.

The Test-Run Group for Liquid and Melt Diffraction*

Introduction

The energy-dispersive method of X-ray diffraction was first applied to the study of the structure of molecular liquids by Murata and Nishikawa.^{1,2)} Among several advantages of this method discussed by them is that changes of the incident beam lead to no serious error in the measurement of relative intensities. Thus this method is suitable for experiments with the use of synchrotron radiation, in which the intensity of the incident beam changes rather rapidly.

The purpose of the present work is to show that energy-dispersive experiments of synchrotron X-ray diffraction can produce data of high quality comparable to that of laboratory-scale experiments. Carbon tetrachloride was chosen as the sample, for it had been most extensively studied so far.^{1,2)}

Measurements of diffraction intensities, i.e., the energy-spectra of diffracted photons, were performed at the experimental station No. 15A2, utilizing the diffractometer for liquids and melts in the white-radiation mode.

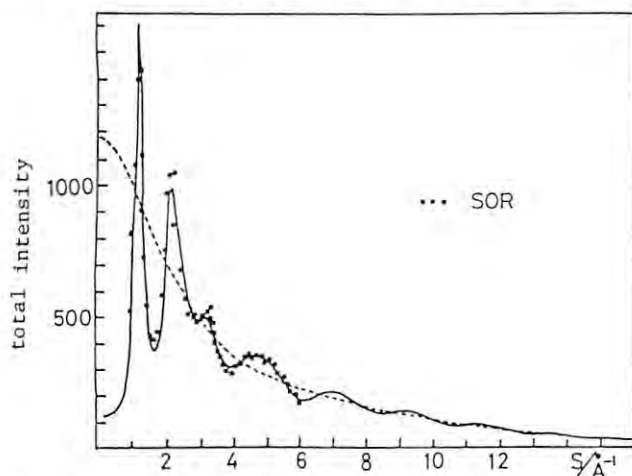
Measurements of CCl_4

A sample holder for liquids was available as an attachment to the diffractometer. It is a combination of stainless steel rings. A liquid sample poured in by the use of a hypodermic syringe is held between two Mylar films of 25 μm thickness as a thin layer. The thickness of the sample was 0.75 mm in the present experiment.

The sample holder is fixed on the θ -axis of the goniometer, and measurements were made in the transmission geometry with the θ - 2θ arrangement.

Scattered X-rays were detected by a pure Ge SSD backed up by a multi-channel pulse-height analyzer system. The region of the photon energy of 0 - 35 keV was divided into 1024 channels. The scattering angles 2θ were selected at 6, 12 and 20°. Scattered photons were accumulated for 1000 sec for each scattering angle.

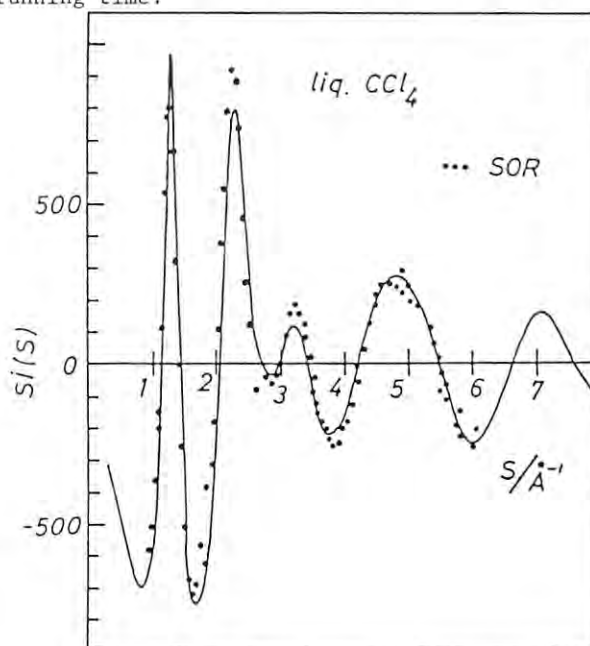
The energy-spectrum of the incident radiation was determined from the scattering intensities of gaseous SF_6 at a high scattering angle.³⁾

Fig. 1 Total intensity for liquid CCl_4 .

Results

The observed energy-spectra of scattered X-rays were analyzed according to the method described in Ref. 1, with revision and improvement developed recently. The derived total coherent intensity is plotted in Fig. 1 in comparison with the best result of the laboratory-scale experiments shown by the solid curve. Also shown in Fig. 2 are the weighted structure functions $s_i(s)$ which are reduced from the total coherent intensities of Fig. 1 by subtraction of the atomic background intensity and multiplication of s . In both Fig. 1 and 2 the results of the present work are in good agreement with the best results of the laboratory-scale experiments.

The increase of count rates, or the shortening of the running time, by the use of synchrotron radiation is not astounding for such a heavy molecule as CCl_4 , because the count rates were largely determined by the time constants of detector electronics. However, for lighter molecules which need hours of accumulation time in laboratory-scale experiments, use of synchrotron radiation should be very effective in shortening the running time.

Fig. 2 Weighted structure function $s_i(s)$ for liquid CCl_4 .

References

- 1) Y. Murata and K. Nishikawa, Bull. Chem. Soc. Jpn., 51 (1978) 411.
- 2) K. Nishikawa and Y. Murata, Bull. Chem. Soc. Jpn., 52 (1979) 293.
- 3) The preceding paper in this Activity Report.

*F. Marumo, H. Morikawa, T. Iijima, K. Nishikawa, T. Mitsuhashi, K. Arakawa, M. Miyake, T. Yamaguchi, M. Ando, H. Ohtaki, M. Yoshizawa, and T. Fukamachi

AN ENERGY-DISPERSIVE EXPERIMENT OF X-RAY DIFFRACTION BY GASES. SULFUR HEXAFLUORIDE.

The Test-Run Group for Liquid, Melt and Gas Diffraction*

Introduction

An energy-dispersive experiment of synchrotron X-ray diffraction by gaseous SF₆ was performed at the experimental station No. 15A2 by the use of the diffractometer for liquids and melts. The white radiation was used as the incident beam. Scattered X-rays were detected by an SSD backed up by a multi-channel pulse-height analyzer system.

The energy-dispersive method makes the best use of the continuous energy-distribution of synchrotron radiation and especially useful for samples with weak scattering power as gases.¹⁾ Moreover changes of the intensity of the incident beam lead to no serious error in the energy-dispersive method. Thus it is suitable for the experiments of synchrotron radiation in which the beam intensity varies rather rapidly.

The Energy-Spectrum of the Incident Beam

The energy-spectrum of the synchrotron radiation is greatly modified inevitably by the absorption by air in the hutch and windows, and intentionally by the absorber inserted by experimenters. Figure 1 shows such modification of the energy-spectrum. Curve A is the theoretical

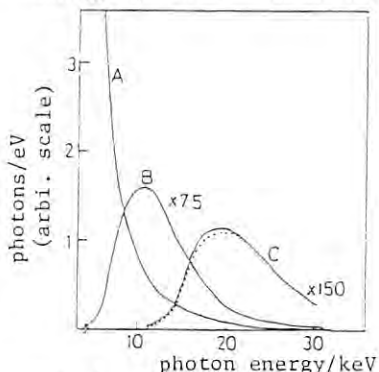


Fig. 1 Energy-spectrum of synchrotron radiation.

prediction for the radiation from the ring at 2.5 GeV electron energy and with 8.33 m orbital radius,²⁾ in a constant-energy bandwidth. B is the result of absorption by a Be window (0.4 mm), He gas in the beam line (1 atm, 25 m) and air in the hutch (1 atm, 2m). C is the result of further absorption by Al-foil (1.6 mm)

placed at the first slit of the diffractometer. The broken curve shows further modification due to the detection efficiency of the pure-Ge SSD.

In the present work the incident spectrum was determined experimentally by the scattering intensities from the sample at large s-values ($s=4\pi E \sin\theta/hc$, E: photon energy, 2θ : scattering angle).

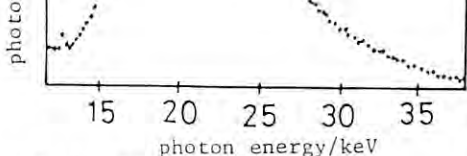


Fig. 2 Incident beam spectrum determined experimentally.

The determined spectrum is shown in Fig. 2. Agreement of Fig. 2 with the broken curve in Fig. 1 is only qualitative.

Measurements of Scattering Intensities

A cylindrical sample cell with an inner diameter of 100 mm was filled with gaseous SF₆ at 3 atm. Thin Mylar film (0.1 mm thick) were used for windows of the cell. Scattered photons were accumulated for 1000 - 2000 sec at the scattering angles 12, 20, 35, and 55°. The data set at $2\theta=55^\circ$ was used for determining the incident spectrum by an assumption that the observed intensities are in agreement with the theoretical predictions based on the Hartree-Fock independent atom model, in the region of large s-values.

In order to confirm the reproducibility of the incident spectrum before and after an injection, the energy-spectra of scattered photons were observed at the same scattering angle before and after every injection. The reproducibility was found satisfactory.

Analysis and Results

The observed energy-spectra were analyzed by a routine procedure of the energy-dispersive method, which includes normalization by the incident spectrum, the absorption correction, and other corrections.¹⁾

The obtained total intensities (coherent

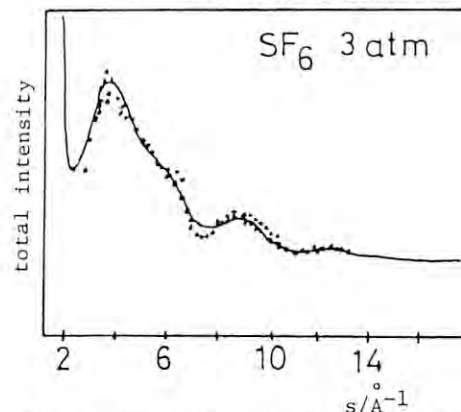


Fig. 3 Total intensity for gaseous SF₆.

plus incoherent) were plotted in Fig. 3 in comparison with the theoretical values shown by the solid curve. The theoretical values were computed by the use of Hartree-Fock atomic scattering factors, the structure parameters determined by gas electron diffraction, and the spectroscopic values of mean amplitudes of vibration. The agreement between theory and experiment is satisfactory.

References

- 1) T. Iijima and T. Mitsuhashi, X-ray Instrumentation for Photon Factory, ed. by S. Hosoya (KTK Publishing Co. Tokyo, to be published).
- 2) S. Kikuta, J. Cryst. Soc. Jpn., 18 (1976) 65.

*T. Iijima, T. Mitsuhashi, K. Arakawa, K. Nishikawa, M. Taguchi, H. Morikawa, M. Ando, T. Matsushita and F. Marumo

STRUCTURAL STUDY BY X-RAY DIFFRACTION AT LOW TEMPERATURE

Working Group for Low Temperature X-Ray Diffraction

S. Kagoshima,^a J. Harada,^b M. Sakata,^b K. Tsuji,^c and T. Nakajima^d
 College of Arts and Sciences, University of Tokyo, Komaba, Meguro,
 Tokyo 153,^a Faculty of Engineering, Nagoya University, Chikusa, Nagoya
 464,^b Institute for Solid State Physics, University of Tokyo,
 Roppongi, Minato, Tokyo 106,^c and KEK, National Laboratory for High
 Energy Physics, Oho-machi, Tsukuba-gun, Ibaraki 305^d

Introduction

The working group has been preparing a set of apparatuses for x-ray diffraction at low temperature. The system is composed of a goniometer, a computer, a cryostat, and an electromagnet. The first two have already been completed by the end of August, 1983 although only the design has been finished of the remaining apparatuses. Several preliminary experiments were done during the process of the preparation. Results of them are independently reported on other pages of this volume. Present report is mainly concerned with the preparation of the goniometer and the computer system.

Goniometer system

It is needless to say that low temperature measurements play important roles in structural studies. Many materials undergo structural changes at low temperature. However, conventional goniometers are usually inadequate to low temperature x-ray diffraction. When the temperature range to be realized is lower than -100 K, some kind of cryostat must be used and, therefore, a special design is required for the goniometer. Large and heavy metal-dewars are needed when experiments are to be done below -4 K. The goniometer should have a capacity of load as large as 20-50 kg.

Furthermore, structural changes taking place at very low temperatures where real phonons are already frozen are usually driven by the electronic degree of freedom, the spin degree of freedom etc. Therefore perturbations like high magnetic field, high electric field, laser radiation etc. may play important roles in order to clarify properties of those structural changes. Also from this point of view a goniometer designed specially is useful, which has a large capacity of load and a wide flexibility for various types of experiments.

The working group has designed a goniometer which satisfy the requirement mentioned above. Its capacity of load is 50 kg for the standard combination and reaches 500 kg when some parts are replaced with others although the diffraction angle

is limited to a narrow range in this case. The goniometer is essentially a horizontal, two-axis one. However, the detector stage can slide along the vertical χ -arc. This makes it possible to use this goniometer like a four-axis one. Figure 1 shows the schematic view of the goniometer thus prepared. Details of the specification of the goniometer are described on other pages of this volume.

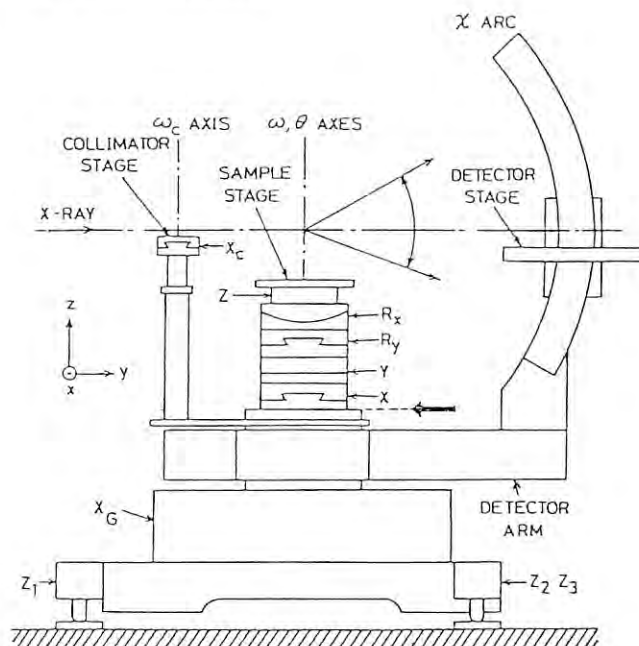


Fig. 1 Schematic view of the goniometer for low temperature x-ray diffraction.

The goniometer for low temperature measurements has no permanent location in PF. It can be set at any experimental station.

The working group has done several test workings of the goniometer system. A few minor defects have already been removed: (1) The receiving slit was improved in order to reject the scattering from air. (2) The height adjusting mechanism of the sample stage was more adjusted. Its motion was initially not smooth.

Computer system

Until June of 1983, our group had no computer system. Test runs were done by using computers prepared by

working groups for x-ray measurements of liquid and for precision x-ray diffraction. The computer system for low temperature measurements was introduced in June. Figure 2 shows its block diagram. The computer can automatically control all driving motors of the goniometer except the dc-motors for the height adjustment of the basal plane. Also MCA, and SCA/SCALER are directly connected to the computer.

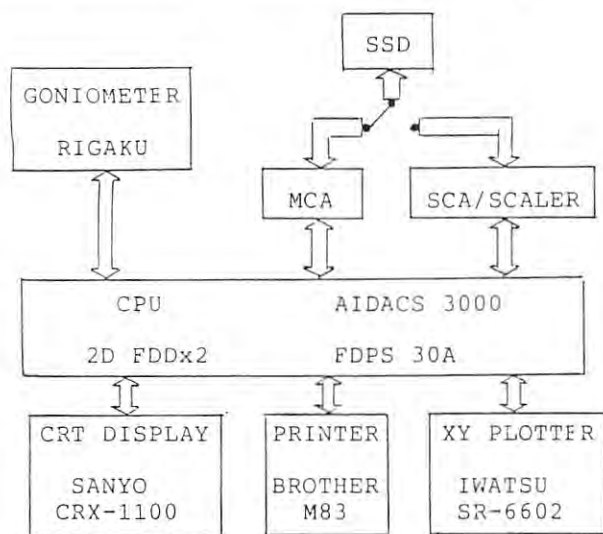


Fig. 2 Block diagram of the computer system for low temperature x-ray diffraction.

Experimental data to be brought back to users' institution are either stored in floppy disks or copied on outputs from the printer or the plotter. When the direct connection becomes possible between our computer and the main computer of PF, standard magnetic tapes can be used to store the data.

Preliminary experiments

We have tried to do several experiments. One of them is x-ray diffraction measurements at low temperature under high pressure. Pressure induced phase transition of Cs was studied by using a diamond anvil attached in a metal dewar. A white x-ray beam and a solid-state detector were used. Definite results were not obtained because of some troubles related to pressure control system. Concerning x-ray measurements themselves, however, hopeful results were obtained; the integrated intensity of main Bragg reflection was higher than 10000 counts/1000 sec when a collimator with 0.1 mm dia. was used. This is a result much better than usual for this kind of measurements.

Also the compressibility of $c\text{-Si}_{1-x}\text{Ge}_x$ was measured at room temperature. Experimental results give a conclusion that this material has a randomly mixed structure having a fluctuation in the interatomic distance.

Another experiment was the diffuse scattering study of metallic alloys. This work was done in collaboration with the working group for diffuse scattering measurements in order to check the computer system which controls both the goniometer and the MCA. It was verified that the whole measuring system works as expected.

Remaining works to be done

During the preliminary experiments described above, several points were found to be more refined. (1) Various types of collimators and receiving slits must be prepared. (2) Softwares must be completed for, at least, a few standard experiments. The most important problem remaining is the preparation of a cryostat system for general purposes. Two types of cryostats have already been equipped; a metal dewar which produces very low temperature by using ^3He , and a small type cryostat which is cooled down by a continuous flow of liquid helium or liquid nitrogen. In addition, the working group has a plan of introducing another type of cryostat. It is a small-type cryostat whose principle of operation is based on a thermodynamic closed-cycle of He gas. The lowest temperature to be reached is about 15K. The cryostat can be operated by an electric switch only.

The authors are grateful to Dr. T. Ishikawa of KEK for advice and help in preparation of the software for the computer.

X-RAY DIFFRACTION MEASUREMENTS UNDER LOW TEMPERATURE AND HIGH PRESSURE AT THE PHOTON FACTORY

K.Tsuji^a, T.Ishidate^b, K.Yamamoto^b, H.Takahashi^c, M.Sakata^d, J.Harada^d, S.Kagoshima^e and T.Nakajima^f
^aInstitute for Solid State Physics, University of Tokyo, Tokyo 106, ^bFaculty of Science, Shizuoka University, Shizuoka 422, ^cFaculty of Science, Hokkaido University, Sapporo 060, ^dFaculty of Engineering, Nagoya University, Nagoya 464, ^eCollege of General Education, University of Tokyo, Tokyo 153, ^fKEK, National Laboratory for High Energy Physics, Tsukuba 305

Introduction

Diamond anvil cell is a most convenient and useful apparatus for high pressure research. It, however, needs a large cryostat and a long measuring time to perform the x-ray diffraction measurements under low temperature and high pressure. X-rays from synchrotron radiation are suitable for high pressure experiments because of high brightness and continuous spectrum in energy. We have measured the x-ray diffraction under low temperature and high pressure by using a diamond anvil cell driven by helium gas, a large cryostat and a goniometer for low temperature experiments.

Diamond anvil cell for measurements under low temperature and high pressure

Fig. 1 illustrates a cross sectional view of the diamond anvil cell which has been used in the present study under low temperature and high pressure^{1,2}. All parts of the cell are machined from Be-Cu alloy except for the diamond mounting plates, which are of SKD-11 steel. The injected helium gas extends the bellows driving the piston. The double-walled doughnut type bellows have an effective area of 6.3 cm² and a maximum gas pressure of 80 bar. The cell is attached to a cryostat. Stainless-steel pipe with an outer diameter of 1 mm and an inner diameter of 0.5 mm is used for helium gas feed. The gas pressure in the bellows chamber can be continuously changed and is measured with a precision Bourdon tube gauge with an accuracy of 0.1 bar.

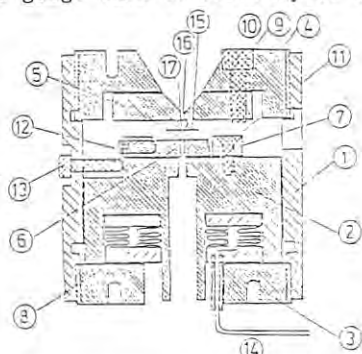


Fig. 1

The window of cryostat for x-ray is made of Be sheet with a thickness of 0.5 mm. Beryllium is cemented to the flange by epoxy resin.

After the sample is pressurized by rotating the screw, helium gas is introduced to the bellows chamber. The relation between the pressure at sample and the gas pressure is shown in Fig. 2. After the force of bellows to push the piston is greater than the initial pressing force, the pressure at sample increases with gas pressure. With decreasing gas pressure, the pressure at sample decreases showing a slight hysteresis.

X-ray diffraction measurements under low temperature and high pressure

X-ray diffraction was measured by energy dispersive method. Incident x-rays impinge on the sample in the diamond anvil cell through incident slit of 0.1 mm diameter. Diffracted x-rays are detected by a handy type Ge SSD through receiving slit. Energy calibration of SSD system is performed by measuring the fluorescence x-rays from Cu and Mo foils. When the temperature is lowered, the sample position moves due to the thermal contraction of the cryostat. X-ray diffraction from Cu powder attached on the face of diamond is used for detecting the movement of the sample position. A typical total counts of diffraction peak is more than 10,000 counts for 1,000 seconds measurements.

To measure the temperature dependence of volume change of Cs on the pressure-induced phase transition, x-ray diffraction has been measured as functions of temperature and pressure. When the pressure increased, the diffraction pattern from cesium oxide appeared. Fig. 3 shows the relative volume change of cesium oxide as a function of gas pressure at 90 K and 290 K. With decreasing gas pressure at 90 K, the volume change is small and it shows a large hysteresis. With elevating temperature, the volume increases. At 290 K the relative volume change is almost proportional to the gas pressure. The large hysteresis at 90 K may be due to the frozen silicone oil, which is used as pressure-transmitting medium. The detailed analysis of the results is in progress.

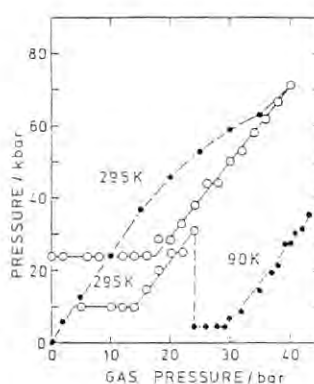


Fig. 2

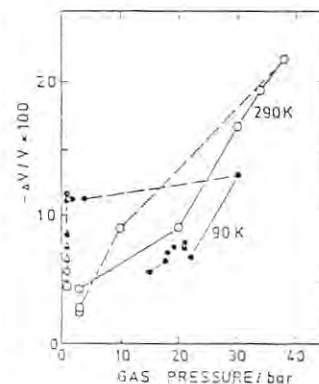


Fig. 3

References

- 1) N.Sakai, T.Kajiwara, K.Tsuji and S.Minomura: Rev. Sci. Instrum. 53 (1982) 499.
- 2) N.Sakai, T.Takemura and K.Tsuji: J. Phys. Soc. Jpn. 51 (1982) 1811.

A TEMPERATURE FACTOR MEASUREMENT OF AMORPHOUS $\text{Cu}_{60}\text{Ti}_{40}$

M. Sakata¹⁾, S. Hashiba¹⁾, J. Harada¹⁾, K. Tsuji²⁾,
 S. Kagoshima³⁾, T. Ishikawa⁴⁾ and T. Nakajima⁴⁾

- 1) Dept. of Applied Physics, Univ. of Nagoya, Chikusa-ku, Nagoya, Japan
- 2) Institute for Solid State Physics, Univ. of Tokyo, Roppongi, Minato-ku, Tokyo, Japan
- 3) Dept. of General Education, Univ. of Tokyo, Komaba, Meguro-ku, Tokyo, Japan
- 4) KEK, National Laboratory for High Energy Physics, Oho-machi, Tsukuba-gun, Ibaraki, Japan

Introduction

Temperature factor of the crystalline materials for which three dimensional atomic configuration is known is normally determined so as to interpret the decrease of integrated Bragg intensities (coherent scattering) with the magnitude of scattering vector Q . This method can not be applied to the amorphous materials. For this reason, there have been very few studies about thermal vibrations of the amorphous materials.

In this study we have tried to obtain average temperature factor of amorphous $\text{Cu}_{60}\text{Ti}_{40}$ alloy, \bar{B} , from the measurement of temperature dependence of coherent scattering. \bar{B} is given

$$G(r) = (2/\pi) \int Q(S_0(Q)-1) \exp(-\bar{B}(\sin \theta/\lambda)^2) \sin(Qr) dQ$$

where $S_0(Q)$ is the interference function without thermal vibrations and other notations are ordinary meanings.

It is one of the purpose of this study to investigate how accurately incident X-ray photons can be monitored in white X-ray experiment when incident beam decrease continuously after injection of electrons to SOR ring.

EXPERIMENT

The measurements of the total scattering of amorphous $\text{Cu}_{60}\text{Ti}_{40}$ alloy were done by the energy dispersive X-ray diffraction at 5 different temperatures, i.e. 98.5, 143.5, 182.5, 217.0, 250.0 and 296.2 K, using LTG (Low Temperature Group) 3 axis goniometer. The goniometer was set up at BL-4C when this experiment was carried out. The description of the goniometer is given elsewhere in this issues.

The thin Co filter (0.012 mm) was used in

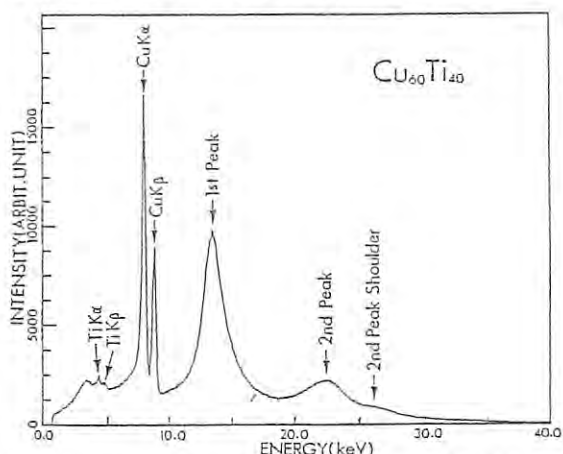


Fig. 1 The observed pattern at $2\theta=25^\circ$

order to reduce extremely intense CuK fluorescence to the comparable order with the first peak intensity of the specimen. After this treatment, intensity of $\text{CuK}\alpha$ was used to monitor the incident beam. The observed pattern at 98.5 K is given in Fig. 1. Because of high counting statistics, fluctuation of the line is small.

Some background measurements were performed with the counter collimation about 0.7° . It was found out that air scattering is still fairly strong with this collimation and it is necessary to evacuate around the specimen to have virtually zero background. It would be interesting to mention that air scattering is practically zero with this counter collimation at HIX (High Intensity X-ray) Laboratory, University of Nagoya.

Analysis and Results

The observed patterns were normalized using $\text{CuK}\alpha$ fluorescence. The normalized intensities of first maximum ($Q=2.96 \text{ \AA}^{-1}$) and minimum ($Q=4.11 \text{ \AA}^{-1}$) are shown in Fig. 2. It is noticeable that they oscillate in the same manner showing strong correlation between them, while their ratio is more or less constant. This strong correlation is seen in some other experiments done at the same period. Nothing certain can not be said at the moment what is the cause of this but the present method of monitoring incident profile should be re-examined.

Ignoring this oscillation, the temperature factor \bar{B} was obtained after converting the normalized first peak intensity to interference function $S(Q)$. As a preliminary result, \bar{B} at room temperature is obtained as 0.85 \AA^2 .

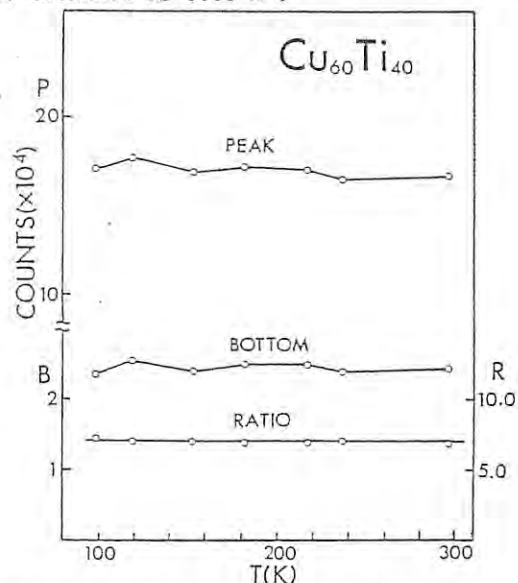


Fig. 2 Intensity vs Temperature

HIGH PRESSURE EXPERIMENTS USING MAX80

O.Shimomura¹, S.Yamaoka¹, T.Yagi², M.Wakatsuki³, K.Tsuji²
 O.Fukunaga¹, H.Kawamura⁴, K.Aoki⁵ and S.Akimoto²

- 1)National Institute for Research in Inorganic Materials,
 2)Institute of Solid State Physics, University of Tokyo,
 3)Institute for Material Science, University of Tsukuba,
 4)National Research Institute for Metals,
 5)National Chemical Laboratory for Industry.

High Pressure X-ray Group (HPX) carried out experiments to check the abilities of high pressure X-ray measurement system named MAX80 (Multi-Anvil type X-ray system designed in 1980) during the assigned beam time of three weeks (7/4 through 7/23) at BL-4C.

MAX80 was designed in order to perform following themes under high pressure and high temperature utilizing the characteristics of Synchrotron Radiation(SR).

1. Use of high brightness and small divergence
 - a) Precise determination of lattice constant
 - b) Dynamical observation of phase transition
 - c) Measurement in extended pressure and temperature region
2. Use of continuous spectrum distribution
 - a) EXAFS, XANES
 - b) Anomalous diffraction

At present, because we are not in a position to use a monochromator, we selected themes corresponding to 1. a), b) and c). They are a) Precise measurement of compressibility of Au at room and high temperature, b) Time resolved measurement of B1-B2 transition of BaS and c) In situ observation of transformation to diamond from graphite. Details of MAX80 and each experiments are described separately.

Figure 1 shows a comparison of diffraction profiles of Au and NaCl at high pressure and high temperature using conventional X-ray source and SR. The brightness of SR is so high that a slit system with smaller divergence can be used. Then the half widths of diffraction peaks are quite sharper compared to those with conventional source and are almost the same as those of the characteristic X-rays. By use of small divergence slit system, we can eliminate the diffracted X-rays from the pressure transmitting medium which surrounds the sample, so that the background level becomes lower. Therefore, the quality of data under pressure is comparable to that at normal pressure, and the accuracy in determination of lattice constant becomes better by 3 to 10 times. It was found that the accuracy does not change when the measuring time was shortened to 30 sec.

The incident beam profiles of conventional source and SR after the absorption correction due to pressure transmitting medium are illustrated in Fig. 1 by generous solid curves with operating conditions. In high pressure X-ray measurements, it is usual to use transmitting geometry. So, the diffracted intensity is proportional to transmittance, $\exp(-t)$, where μ is absorption coefficient and t is thickness of sample. Dashed curve in Fig. 1 shows the transmittance of Au and NaCl with $t = 1$ mm. Intensity of X-ray from bending magnet with 2.5 GeV operation shows maximum at about 12 keV and decreases monotonically with energy, then becomes negligible at around 25 keV.

On the other hand, the transmittance increases gradually above 15 keV. Therefore, the characteristic of high brightness is not fully utilized for high pressure X-ray experiments with 2.5 GeV operation. The situation becomes better with 3.0 GeV operation, and becomes excellent with a wiggler.

We added a function of TSS terminal to the microcomputer which is originally used for data acquisition so that the obtained data are immediately transferred to PF main computer and analyzed then the results are returned back to the microcomputer. The average time for the analysis is about 1 min, so that the obtained results are effectively used to determine the next experimental parameters, and overall feature of the experiments is easily understood in real time. More than 700 patterns were taken during three weeks, and most of data were analyzed by means of TSS before the end of machine time.

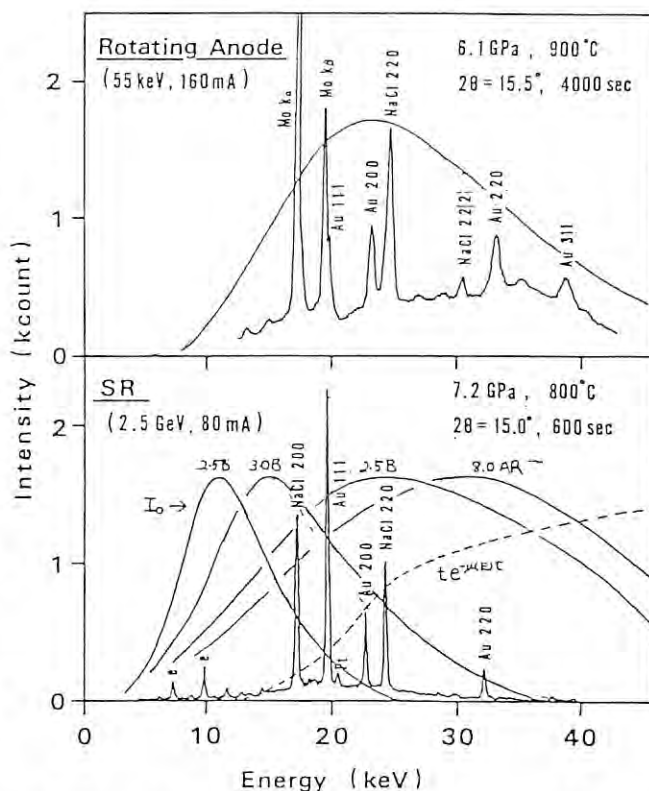


Figure 1. Comparison of diffraction profiles of Au and NaCl at high pressure and high temperature using conventional X-ray source and SR. See the text for generous solid curves and dashed curve.

DIRECT OBSERVATION OF THE CONVERSION REACTION FROM GRAPHITE TO DIAMOND

S.Yamaoka(1), O.Shimomura(1), T.Yagi(2), T.Akai(3), H.Fujiwara(4), H.Kanda(1), T.Kikegawa(5), K.Kuroda(4), N.Mori(6), T.Nagashima(1), T.Suzuki(2), K.Tabata(7), K.Takemura(2), S.Yamamoto(8) and S.Akimoto(2)

(1)Nat.Inst.Res.Inorg.Mater.

(3)Fac.Eng.Sci.,Osaka Univ.

(5)Res.Inst.Iron,Steel,Other Met.,Tohoku Univ. (6)Fac.Sci.,Hokkaido Univ.

(7)Dept.Mater.Sci.,Tsukuba Univ.

(2)Inst.Solid State Phys.,Univ.Tokyo

(4)Fac.Sci.,Hiroshima Univ.

(6)Fac.Sci.,Hokkaido Univ.

(8)Dept.Earth Sci.,Nagoya Univ.

Introduction

Diamond synthesis is one of symbolic themes in high pressure research. The 'in situ' observation of the conversion reaction from graphite to diamond at very high temperature and pressure is quite an exciting problem and has long been a dream for high pressure researchers. By using MAX80, we could performed preliminary experiments on this problem.

Experimental

In the present experiment, direct heating method was adopted for diamond synthesis because its sample configuration is simple. In the center of the pressure transmitting medium of boron-epoxy resin for 4 mm size anvil, rods of graphite and solvent metal (nickel and iron were used) with the diameter of 0.6mm were stacked, through which direct electric current was conducted for heating themselves at high pressure.

X-ray experiments were done by energy dispersive method with the diffraction angle of 15° or 20°. First, press load was increased to 54 tons (which corresponds to about 6 GPa in this system) and then temperature increased to about 1600° C. X-ray diffraction patterns were taken on increasing pressure and temperature, and on and after the conversion reaction from time to time. The measuring time was 60 to 300 seconds.

Result

Fig.1 shows a typical example of the X-ray diffraction patterns taken during heating at high pressure. Diamond peaks appeared by replacing graphite ones at about 140 watts of heating power (which corresponds to about 1400°C). Additional peaks also appeared, which possibly correspond to the metal carbides.

In some runs, however, no diamond peaks appeared although graphite peaks disappeared and those of metal carbides appeared. This is because of the large crystal size of the grown diamond, which was found to be 20 to 30 μm in Fe and 60 to 80 μm in Ni solvent by SEM photograph taken after the run as shown in Fig.2. This shows that large diamond crystals were grown being covered with metal carbides.

Because metal carbides always co-

exist with the converted diamond crystals, and X-ray absorption coefficient differs largely in carbon and metal, we could directly see the conversion area from graphite to diamond by taking photographs of the transmitted X-rays from a sample. Fig.3(B) and (C) show ones before and after diamond formation, and (A) shows the X-ray beam position in the present X-ray run, which can be changed at will.

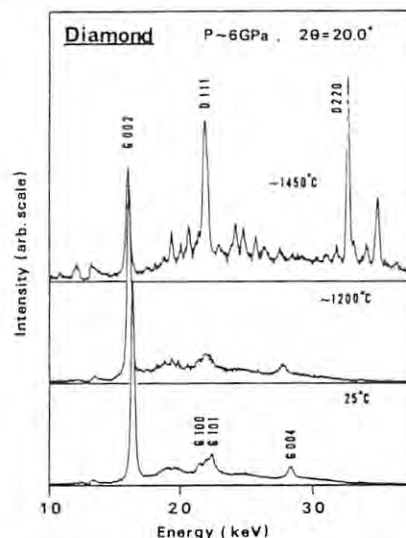


Fig.1 Change of diffraction patterns from graphite to diamond (Fe solvent metal)



Fig.2 Diamond grown in the present run (Ni solvent) x80

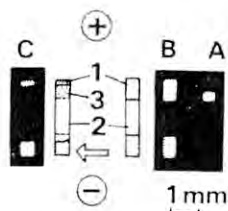


Fig.3 Transmitted X-ray photograph through the sample before (B) and after (C) diamond formation. 1:graphite,2:metal, 3:diamond+carbides

COMPRESSIBILITY MEASUREMENTS OF GOLD AT ROOM TEMPERATURE AND 600°C

T.Yagi¹, S.Shimomura², N.Yamaoka², T.Fujimura³, N.Hamaya⁴, M.Nomura⁵, J.Suzaki¹
 T.Suzuki¹, K.Tabata⁶, K.Takemura¹, A.Tomizuka³, S.Yamamoto⁷, W.Utsumi⁴, and S.Akimoto¹

- 1) Inst. Solid State Phys., Univ. Tokyo, Roppongi, Minato-ku, Tokyo 106, Japan
- 2) Nat. Inst. Res. Inorg. Mat., Namiki, Sakura-mura, Niihari-gun, Ibaraki 305, Japan
- 3) Res. Inst. Iron, Steel and Other Metals, Univ. Tohoku, Katahira, Sendai 980, Japan
- 4) Fac. Eng. Sci., Univ. Osaka, Machikaneyama, Toyonaka, Osaka 560, Japan
- 5) Fac. Sci., Univ. Hiroshima, Naka-ku, Hiroshima 730, Japan
- 6) Dept. Mat. Sci., Univ. Tsukuba, Sakura-mura, Niihari-gun, Ibaraki 305, Japan
- 7) Fac. Sci., Univ. Nagoya, Chigusa-ku, Nagoya 464, Japan

Introduction

Gold is often used as an internal pressure marker in x-ray diffraction experimental under high pressure(1). Its equations of state (P-V-T relations) are, however, not well established yet. The purpose of the present study is to determine the isothermal compression curves of gold very accurately at room temperature and at 600°C using NaCl as an internal pressure standard.

Experimental

A mixture of Au and NaCl was placed between two disk-shaped graphite heater and then imbedded in cube shaped pressure transmitting medium which is made of a mixture of amorphous boron and epoxy resin. Pressure was applied by squeezing the cube by six tungsten carbide anvils. X-ray measurements were made through gaps between anvils. The incident beam was 0.3 mm × gap width (-0.5 mm) and the exposure time was 600 sec. Temperature was measured by a thermocouple placed at the center of the specimen and pressure was calculated from the lattice parameter of NaCl using its equations of state(2).

Results

An example of the diffraction pattern of Au and NaCl obtained at elevated pressure and temperature is shown in Fig.1 together with the data obtained by conventional x-ray tube. It is clear that the use of SR greatly contributed not only to shorten the exposure time but also to make the diffraction peaks much sharper. At room temperature the lattice parameter calculated from different diffraction lines coincides well within the precision of 0.01% which is about 10 times more precise than conventional x-ray measurements under pressure. At high temperature, however, grain growth of the specimen has reduced the precision to 0.03%.

Resultant compression curves are shown in Fig.2. Reliable equations of state for gold can be deduced using these data.

References

- 1) J.C.Jamieson, J.N.Fritz and M.H.Manghnani, "High Pressure Research in Geophysics" edited by S.Akimoto and M.H.Manghnani, Adv. Earth and Planetary Sciences 12, P.12 (1982)
- 2) D.L.Decker, J. Appl. Phys., 42, 3239 (1971)

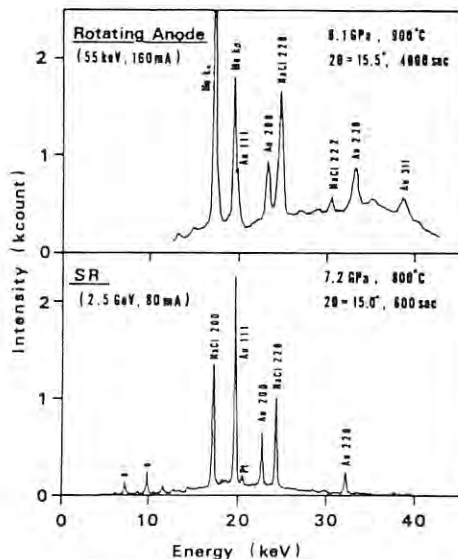


Fig.1. Diffraction profiles of Au+NaCl obtained by conventional source (above) and by SR (below) under high pressure and temperature.

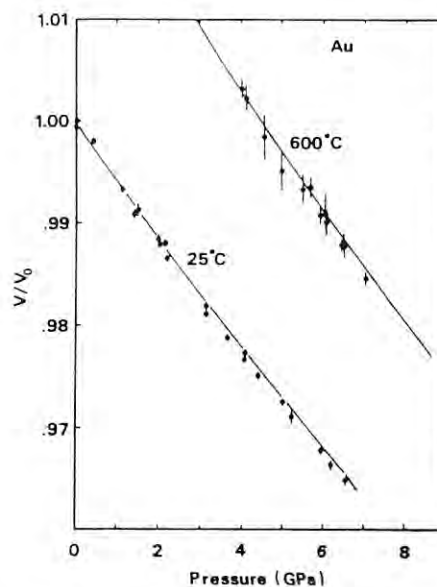


Fig.2. Isothermal compression curves of gold. Solid circles are from present study and solid lines are calculated curves deduced from shock compression data(1).

TIME-RESOLVED X-RAY DIFFRACTION ON THE PRESSURE-INDUCED PHASE TRANSITION IN BaS

N. Hamaya¹, T. Yagi², S. Yamaoka³, O. Shimomura³, K. Tabata⁴, J. Susaki²,
K. Tsuji², K. Murata¹, T. Kikegawa⁵, H. Kawamura⁶, and S. Akimoto²

¹Faculty of Engineering Science, Osaka University, Toyonaka, Osaka 560

²Institute for Solid State Physics, University of Tokyo, Minato-ku, Tokyo 106

³National Institute for Research in Inorganic Materials, Sakura-mura, Ibaraki 300-31

⁴Institute of Materials Science, University of Tsukuba, Sakura-mura, Ibaraki 305

⁵The Research Institute for Iron, Steel and Other Metals, Tohoku University, sendai 980

⁶National Research Institute for Metals, Sakura-mura, Ibaraki 305

Barium sulfide is known to undergo the B1-B2 phase transition at ≈ 7 GPa and room temperature¹. The primary purpose of this work is to determine the phase equilibrium relation between the two phases from kinetic behavior of the transition at high pressure and high temperature. Also we aim at checking the ability of the present system, SR x-ray and the high-pressure apparatus MAX80, to investigate the kinetics by a time-resolved x-ray diffraction method.

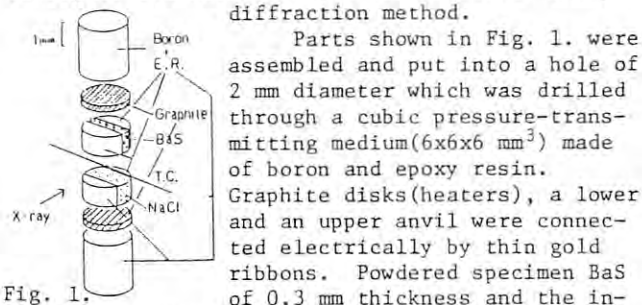


Fig. 1. Parts shown in Fig. 1. were assembled and put into a hole of 2 mm diameter which was drilled through a cubic pressure-transmitting medium (6x6x6 mm³) made of boron and epoxy resin. Graphite disks (heaters), a lower and an upper anvil were connected electrically by thin gold ribbons. Powdered specimen BaS of 0.3 mm thickness and the internal pressure calibrant NaCl were placed separately above and below a thermocouple, respectively, in order to avoid overlapping of diffraction peaks. We adopted an energy-dispersive x-ray diffraction method using SSD. Details of the system is described in other report.

Kinetic behavior of the transition was observed in such a way that a series of several measurements, one of which consists of 100 sec-exposure to x-ray and 2 sec-data-out, was started as soon as the pressure was set at a value by a quick increase or decrease of oil pressure at a constant temperature. After finishing a series of measurements, the press was raised to make x-ray beam hit NaCl. Then the press was moved down again, and following a pressure jump a next series was carried out at a new pressure value.

A typical series of profiles of BaS in Fig.1

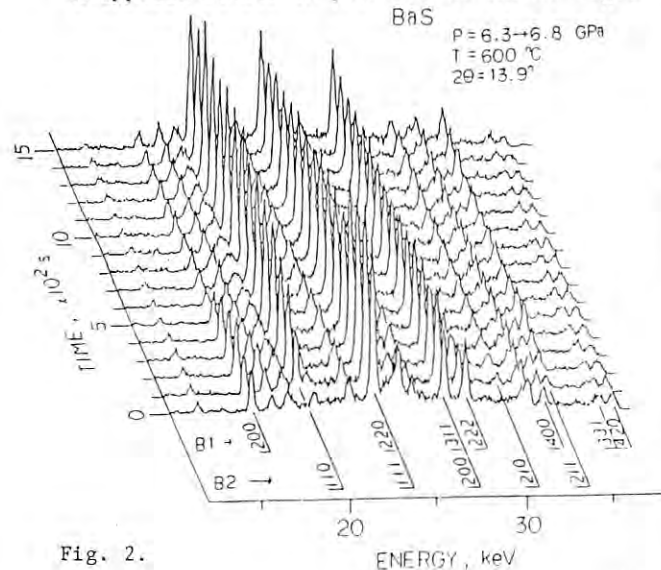


Fig. 2.

illustrates a process of the transition from the B1 to the B2 structure at 6.8 GPa and 600°C. We notice in this figure that the resolution of peak width and the S/N ratio are greatly improved in the present system in comparison with ordinary systems equipped with conventional x-ray sources. Indeed, the angular dispersion due to collimators and slits was reduced by less than tenth of SSD's instrumental resolution even at a small scattering angle of 13.9°.

We intended to study evolution of intensities of diffraction peaks quantitatively as a function of time at first. Data so far analyzed show that the transition begins to proceed very slowly after a few measurements and does not complete within several hours. This fact seems to be unusual, suggesting that the pressure was not kept constant throughout measurements. We infer that a large volume change associated with the transition seriously affects the internal pressure in a small sample chamber. It is necessary to detect pressure continuously and to compensate for change of it quickly.

Despite the above difficulty, we were able to determine the P-T phase diagram. Since a transformation rate was very small in BaS, we saw a metastable coexisting state of the two phases for several hours. It was not difficult to know which phase was stable in a certain P-T condition. Varying the pressure stepwise, we observed changes in intensities of diffraction peaks in a few measurements and compared them with those taken before the pressure jump. Thus determined phase diagram is presented in Fig. 3. Open and solid circles denote conditions at which the B1 and the B2 phase is respectively stable. Conditions where no change was detected within 700 sec are denoted by half-solid circles. An estimated phase boundary (solid line) has a negative slope as found in some alkali halides such as KBr, KI².

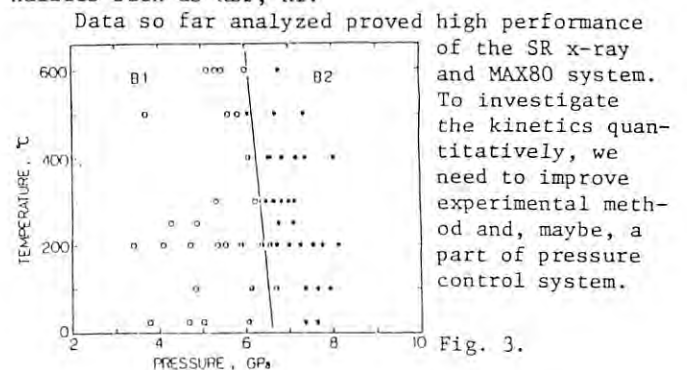


Fig. 3.

References

- 1) S. Yamaoka, O. Shimomura, H. Nakazawa and O. Fukunaga; Solid State Commun. 33(1980)87.
- 2) A. J. Darnell and W. McCollum; J. Phys. Chem. Solids 31(1970)805.

FOUR-CIRCLE DIFFRACTOMETER OF VERTICAL TYPE ON BL-10A

T.Tagai¹, M.Tokonami¹, T.Sakamaki², Y.Sato³, K.Ohsumi¹, H.Nakazawa⁴, Y.Abel¹, T.Hirai⁵, M.Ohmasa⁶, S.Sueno⁵, N.Haga¹, Y.Kudoh¹, F.Nishi¹, K.Tsukimura⁷, Y.Kanazawa⁷, N.Yamada⁶, S.Saito⁶, K.Kakefuda⁵, M.Watanabe⁴, A.Nukui⁴, I.Kawada⁴, F.Okamura⁴, I.Nakai⁸, M.Kimata⁹, K.Sugiyama¹, K.Ogata¹, K.Nakanishi¹, S.Sasaki³ and Y.Takeuchi¹

(Members of "MINERALS AND INORGANIC MATERIALS GROUP")

- 1 :Mineralogical Institute, University of Tokyo,
- 2 :Institute for Solid State Physics, University of Tokyo
- 3 :National Laboratory for High Energy Physics
- 4 :National Institute for Researches in Inorganic Materials
- 5 :Institute of Geoscience, Tsukuba University
- 6 :Institute of Material Science, Tsukuba University
- 7 :Geological Survey of Japan
- 8 :Institute of Chemistry, Tsukuba University

The vertical type four circle diffractometer, which is set on the beam line BL-10A, is designed specially for the structure analysis of very small crystal (ex. 10 micron) using strong X-ray from synchrotron and also for the anomalous scattering studies with monochromatic X-ray whose wave length is tunable over wide range.

The diffractometer system mainly consists of monochromator, guide path, adjustment carriage four circle diffractometer of vertical type, control system, detector system and mini-computer (see Figures).

In the optical system, the single type monochromator and guide path are adopted so as to minimize the loss of X-ray intensity. The monochromator crystals which are specially designed to have an adequate mosaic spread are introduced, because the "integrated intensity" of the Bragg reflections are necessary in the case of the structure analysis (ex. Si(111) with mosaic spread of 2.5 mrad). Two crystals are simultaneously set on the water-cooled goniometer of the monochromator. The one is perfect Si(111) crystal and the other is a mosaic one.

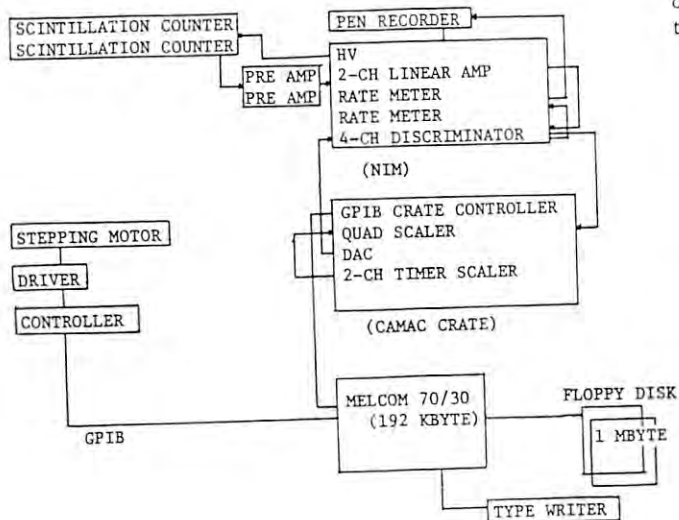
Then users can determine the orientation of the crystal by the perfect crystal and measure intensities with the mosaic one.

The distance between the monochromator and the diffractometer is about 2.5 m and the mechanism to align rapidly the diffractometer to the monochromatized X-ray beam is equipped.

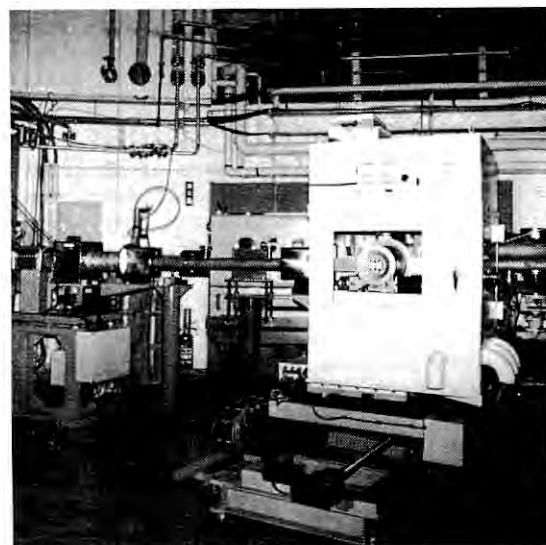
Using this diffractometer, the diffraction data of the following samples are collected ; GaAs, MgAl₂O₄ (spinel), Ca₃Ge₂O₉, Pb₃Bi₂S₆ (lillinite), (Ni,Fe)₉S₈ (pentlandite), Cu-As-Se, Cu-Al-Ni alloy, Zn₄Si₂O₇(OH)₂H₂O (hemimorphite), (Ni,Fe) (tetrataenite) and NaGeO₄ (amorphous).

Using this optical system, two other works have been carried out. The one is film method by precession/oscillation camera and the other is the radiation damage experiment by "RADIATION BIOLOGY GROUP" (align optical system by the members of our group).

With camera, the following experiments were carried out : Taka-amylase, ZnS (sphalerite), diffuse scattering of β-MnO₂, Satellite reflections of plagioclase, diffuse scattering and transition of PbF₂ (high temperature), topograph of cube diamond, diaspore (high temperature), FeS (high pressure), diffraction experiment from very small region, test of X-ray guide tube and mirror.



The construction of the controller- and detector-system



The four circle diffractometer of vertical type

DIFFUSE SCATTERING FROM β -PbF₂

K. Koto and Y. Ito

Institute of Scientific and Industrial Research, Osaka University
 Suita, Osaka 565 (JAPAN)

Introduction

Fluorites show intrinsic superionic conductivity above the temperature of a higher order phase transition accompanied with broad anomaly of specific heat. Of them, β -PbF₂ has the lowest transition temperature (\sim 700 K) and highest ionic conductivity. Diffusion mechanism of mobile ions in the lattice, based on the structure investigation by the Bragg reflections under from room temperature to just below the melting point has been studied on β -PbF₂ by neutrons(1,2) and X-rays(3,4).

In the results of the structure analysis by single crystal X-ray diffraction method, fluorine ions show strong anharmonicity of electron density distribution below the transition temperature, and above it, they are statistically distributed at four sites, xxx, displaced from the normal tetrahedral site, 0.25,0.25,0.25.(Fig.1)(3,4)

The deviation from the averaged structure determined based on the Bragg reflections, is one of the origins of diffuse scattering. The study of X-ray and neutron diffuse scattering from fast ion conductors such as fluorites, provide information about short range order of mobile ions and thermal motion. Coherent quasielastic diffuse scattering from fluorites has been observed by neutrons, which has been interpreted by cluster of mobile ions and vacancies.(5)

In this work, the X-ray diffuse scattering from β -PbF₂ has been observed at various temperature below and above the transition temperature to elucidate the deviations from the long range structure or the averaged structure, and behavior of mobile ions in the diffusion process.

Experimental

X-ray experiment was executed with precession camera furnished with oscillation mechanism on Beam Line 10-B at the KEK, Synchrotron Radiation

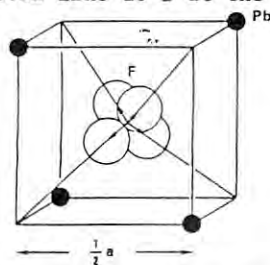


Fig.1. Statistical distribution of fluorine ion in the Pb tetrahedron, is displaced along the $\langle 111 \rangle$ direction.

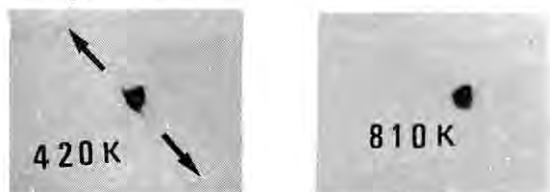


Fig.2. Diffuse scattering from β -PbF₂ at the temperature of 420 and 810 K. Arrows indicate the $\langle 111 \rangle$ direction.

Laboratory. Monochromatized radiation, $\lambda = 0.64 \text{ \AA}$, by Si monochromator crystal was used. Single crystal of β -PbF₂ with $0.1 \times 0.1 \times 0.1 \text{ mm}^3$ in size, was sealed in quartz capillary tubes with nitrogen gas to prevent from oxidation. The beam current usually decreased from 150 mA to 50 mA in 3 hours. Observation of diffuse scattering was concentrated on around 111 and 200 Bragg reflections. To save the exposing time, the oscillation was set to the above two Bragg reflections within 5° . To investigate the dependence of the features of diffuse scattering on temperature in β -PbF₂, X-ray photographs were taken at 295, 420, 580, 670, 720 and 810 K with 30-40 min. exposure time for each run.

Results

Figure 2 shows the spike-like diffuse scattering observed along the $\langle 111 \rangle$ direction around the Bragg reflection 111 in β -PbF₂. The features of the diffuse scattering around the reflection remains almost unchanged from room temperature to just below the transition temperature, 670 K. The intensity becomes weak in the region of the transition temperature, 720 K. Above the transition temperature, the diffuse scattering could not be observed around the 111 reflection. The observations of the diffuse scattering from β -PbF₂ may be attributed to strong anharmonic thermal motions in β -PbF₂ or to short range order of fluorine ions which can be suggested by statistically distributed fluorine ions.

Further quantitative investigation will be desired for the characteristics of features on the diffuse scattering, that is, the temperature dependence of the profile and intensity by counter method rather than photographic method.

Acknowledgement

Thanks are to Dr. Y. Satow, KEK, National Laboratory for High Energy Physics, for help in experiment and Dr. H. Nakazawa, National Institute for Research in Inorganic Materials, for facility of high temperature furnace for precession camera and help in experiment. Thanks are also to Prof. M. Tokonami, University of Tokyo, for useful discussions.

References

- 1) S.M. Shapiro and F. Reidinger, in, Physics of superionic conductors, ed. M.B. Salamon (Springer Berlin, 1979) P.45
- 2) M.H. Dickens, W. Hayes, C. Smith and M.T. Hutchings, in, Fast ion transport in solids, eds. F. Vashishta, J.N. Mundy and G.K. Shency (North-Holland, Amsterdam, 1979) P.225
- 3) K. Koto, H. Schulz and R.A. Huggins, Solid State Ionics 1 (1980) 355
- 4) K. Koto, H. Schulz and R.A. Huggins, Solid State Ionics 3/4(1981) 381
- 5) K. Clausen, W. Hayes, M.T. M.T. Hutchings, J.K. Kjems, P. Schnabel and C. Smith, Solid State Ionics 5 (1981) 589

CATION ORDERING IN THE STRUCTURE OF $Cu_9As_4Se_{13}$

Y. Takéuchi, N. Haga, F. Nishi, K. Ohsumi and M. Tokonami
 Mineralogical Institute, Faculty of Science, University of Tokyo
 Hongo, Tokyo 113 (Japan)

Introduction

For the crystalline phase, which was synthesized with starting chemical composition of $CuAsSe_2$, a chemical formula $Cu_7As_6Se_{13}$ was previously assumed¹ based on a bulk chemical analysis and the crystallographic data ($a = 14.025 \text{ \AA}$, $c = 9.61 \text{ \AA}$, $R3$, $Z = 3$). The structure was found to have a 13-fold superstructure based on the sphalerite type¹.

Electron microprobe analyses of the crystal which were later performed, however, revealed that the chemical composition was in fact close to $Cu_9As_4Se_{13}$, total number of the cations for 13 Se atoms being the same as that for the above formula. Such a confusion was arisen basically from the difficulty in distinguishing between Cu and As in this particular structure by diffraction method. We have thus undertaken re-investigation of the crystal structure with the use of the anomalous dispersion effects of the Cu atoms. This report covers the result obtained from our experiment performed in February 1983.

Preliminary analysis

A piece of crystal was ground to the shape of an ellipsoide with the dimensions of $0.1 \times 0.1 \times 0.08 \text{ mm}$ and used for the present study. As a preliminary study, we collected a set of 2152 graphite-monochromatized $MoK\alpha$ diffraction intensities. Least-squares refinement of the reported structure with LINUS² converged to give an $R = 8.9\%$, when an average of the form factors of As and Cu was used for these atoms. The reported structure has thus been confirmed to be essentially correct so far its atomic positions are concerned.

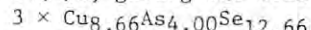
Use of the anomalous dispersion effects

Nothing that $\lambda k = 1.380 \text{ \AA}$ for Cu, we used

graphite monochromatized synchrotron radiation having the wave length of 1.40 \AA ; under this condition, f' for the Cu atom has the value of -4.49 . Then the diffraction intensities of a total of 266 superstructure reflections were measured with the four-circle diffractometer at the BL-10A beam line.

Based on the atomic parameters obtained by the preliminary analysis, structure factors were calculated using an average of the form factors for Cu and As for these atoms. The $z = 0$ section of the difference Fourier map then calculated is given in Fig. 1 (a). Note that the positive peaks in the map should correspond to the As-rich atomic sites and the negative peaks to Cu-rich sites. The map has thus successfully brought out the locations of the As atoms without ambiguity.

Least-squares refinement including the occupancy parameters converged to give an $R = 5.1\%$ for 248 reflections used. The Se positions on the threefold axes are found to be vacant by 34(2)%, giving the cell contents of



From this result, we may deduce a statistical model in which the As atoms have threefold pyramidal coordination. The structure now essentially satisfies the valence rule for tetrahedral structures³.

Further refinement is in progress based on a set of about 400 diffraction intensities collected during the July machine time.

References

- 1) Y. Takéuchi and H. Horiuchi: *Z. Krist.* 135 (1972) 93.
- 2) P. Coppens and W.C. Hamilton: *Acta Cryst.* A26 (1970) 71.
- 3) E. Parthe: Crystal Chemistry of Tetrahedral Structures. Gordon & Breach, N.Y.-London (1964).

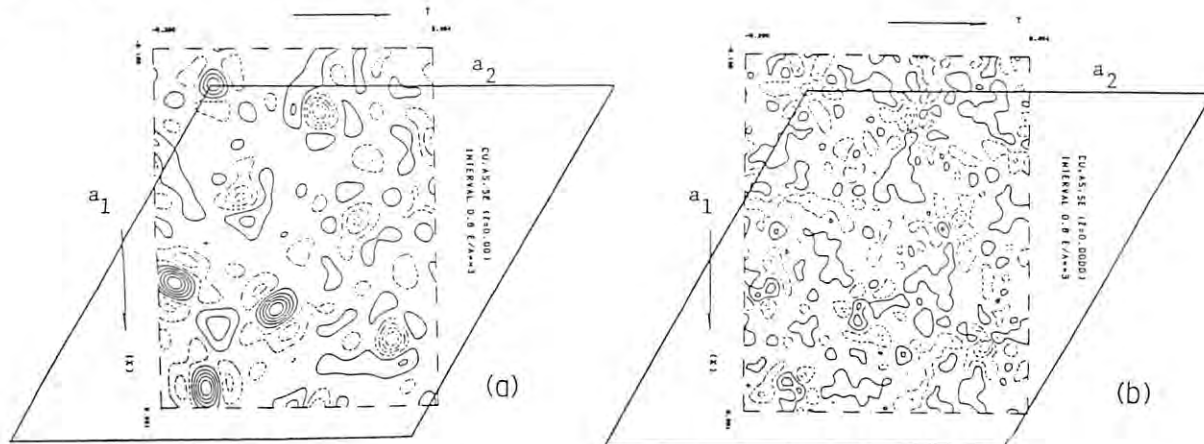


Fig. 1. The difference Fourier map, showing the $z=0$ section. (a) Based on synchrotron diffraction intensities, $\lambda=1.40 \text{ \AA}$. (b) Based on $MoK\alpha$ diffraction intensities, negative contours being broken.

The absolute orientation of hemimorphite

Y. Takéuchi, K. Ohsumi, N. Haga, F. Nishi and M. Tokonami
 Mineralogical Institute, Faculty of Science, University of Tokyo
 Hongo, Tokyo 113 (Japan)

Introduction

The absolute orientation of crystal structures that are noncentric and polar has been studied for sphalerite ZnS^1 , zincite ZnO^2 , and buergerite (Fe^{3+} tourmaline)³. In the first two cases, the anomalous dispersion effects of the Zn atoms were used under $AuL\alpha$ radiation, and in the buergerite under $CuK\alpha$.

With the use of synchrotron radiation at the Photon Factory, we may now select any desired wave length at will in the range of wave lengths covered by the now available optical system for the four-circle diffractometer at the BL-10A station. It is anticipated that the above sort of studies can be readily carried out for crystals having complex structures with results of high reliability. We have therefore undertaken the determination of the absolute orientation of the hemimorphite structure⁴ ($H_2Zn_2SiO_5$, $a = 8.38$, $b = 10.70$, $c = 5.11 \text{ \AA}$, $Imm2$, $Z = 4$). The structure of hemimorphite, which exhibits a well known polar habit, is built up of a framework consisting of Si_2O_7 groups and tetrahedra formed by the oxygen atoms about the Zn atoms. All tetrahedra point in nearly the same c direction, each having a face nearly parallel to (001). Hydrogen bonding in the structure has been studied by Takéuchi et al⁵.

Experimental

A crystal specimen from Santa Eulalia, Mexico was kindly supplied by Dr. R. V. Gaines for the present study. It is a group of large single crystals, about 20mm long along c . Morphological examination revealed that all crystals occur singly terminated at the analogous pole. The orthorhombic cell has dimensions $a = 8.366(1)$, $b = 10.714(1)$, $c = 5.113(1) \text{ \AA}$ (Takéuchi et al⁵). One of the crystals was ground to a thin plate, parallel to (010), with approximate dimensions $4.8 \times 3.7 \times 0.1 \text{ mm}$.

Table 1

h	k	l	$F_o(hkl)$		$F_o(\bar{h}\bar{k}\bar{l})$	$F_c(hkl)^*$		$F_c(\bar{h}\bar{k}\bar{l})^*$
-4	1	1	19.01	<	59.70	6.33	>	2.55
-3	2	1	196.86	>	167.26	22.88	<	27.72
-7	-3	2	202.09	>	178.76	22.33	<	25.46
-1	0	3	135.51	>	83.26	11.37	<	16.38
5	0	3	225.04	>	183.31	24.68	<	31.97
-5	-4	3	73.28	<	97.50	12.24	>	9.87
-2	3	1	196.58	>	189.46	44.83	<	51.23
-4	3	1	128.53	<	162.79	24.14	>	20.57
-1	1	2	87.02	<	109.10	15.13	>	12.90
-3	1	2	125.00	>	104.97	12.72	<	15.46
-2	2	2	128.81	<	146.21	22.99	>	20.04
-4	2	2	86.77	>	68.03	8.05	<	11.08
-3	3	2	176.08	<	211.76	37.65	>	33.09

* After Sakamaki et al.⁶

The direction of the analogous pole was recorded on it.

Preliminary measurements with $MoK\alpha$ of the intensities of reflexions transmitted through the crystal plate showed that the effect on intensities of a possible difference in path length was negligible for the reflexion pairs, hkl and $\bar{h}\bar{k}\bar{l}$.

Synchrotron radiation was then monochromatized with a Si plate parallel to (111) to provide an X-ray beam having the wave length of 1.27 \AA . As the value of λ_K/λ for Zn is 1.283 \AA , we have $\lambda_K/\lambda = 1.0087$ for the above wave length. Taking the analogous pole as the positive end of the c axis, the intensities of a set of 40 reflexion pairs were measured in the ω - 2θ scan mode.

Result

The sense of the inequalities for the observed intensity pairs was found to be opposite to that for calculated pairs of F values (Sakamaki et al⁶); in these calculations ($\lambda = 1.26 \text{ \AA}$), the direction in which the tetrahedra point was taken as minus c . It has thus been established that the tetrahedra point toward the analogous pole. Some of the structure-factor pairs are listed in Table 1.

References

- 1) S. Nishikawa and K. Matsukawa: Proc. Imp. Acad. Japan 4 (1928) 96.
- 2) J. C. Monier and R. Kern: Bull. Soc. franc. Miner. Crist. LXXIX (1956) 495.
- 3) R. Barton and G. Donnay: Acta Cryst. B25 (1967) 1524
- 4) T. Ito and J. West: Z. Krist. 83 (1932) 1.
- 5) Y. Takéuchi, S. Sasaki, W. Joswig and H. Fuess. Proc. Japan Acad. 54 (1978) 577.
- 6) T. Sakamaki, S. Hosoya and T. Fukamachi: Acta Cryst. A36 (1980) 183.

REINVESTIGATION OF THE LILLIANITE STRUCTURE

K. Ohsumi, K. Tsutsui, Y. Takéuchi and M. Tokomami
 Mineralogical Institute, Faculty of Science, University of Tokyo
 Hongo, Tokyo 113 (Japan)

Introduction

The lillianite structure is well known to be composed of polysynthetic cell twinning, across (311) of the galena structure, of galena slab.¹ The chemical composition of the material is well represented as $3\text{PbS} \cdot \text{Bi}_2\text{S}_3$. The lattice constants are: $a = 13.535 \pm 0.003$, $b = 20.451 \pm 0.005$, $c = 4.104 \pm 0.001 \text{ \AA}$. The space group is Bbmm. The unit cell contains four formula units.²

According to the structure already determined by means of equi-inclination Weissenberg method with $\text{Mok}\alpha$ radiation, there are three kinds of metal sites named M(1), M(2) and M(3) as shown in Fig.1. M(1) and M(2) sites are located in inner part of galena slab and occupied by Pb and Bi atoms at random, while M(3) site is just on the mirror plane and occupied by only Pb atom. As is the usual case, the determination of the site occupancy was performed on account of the geometry around metal site, since the characteristic X-ray generated by usual target materials like Mo, Cu, Fe etc. cannot distinguish between Pb and Bi atom. In consequence, the accurate occupancy in each metal site has been left unknown.

Among the pseudo-binary system of PbS and Bi_2S_3 , twelve mineral species have been reported before³ and all the structures already determined are composed of galena structure as a structure unit. The detailed structure, especially as for the site occupancy, should be revealed for the well understanding of the structural relationship among already known structures.

In order to attain the purpose mentioned above, making use of synchrotron radiation is now possible with four-circle diffractometer set up at the BL-10A station of Photon Factory.

Experimental

For the present study, the same crystal specimen as used for the previous structure determination was employed and mounted on the four-circle diffractometer at the BL-10A of Photon Factory. The chemical composition of the specimen contains a small amount of Ag by electron microprobe analysis. The specimen is almost cubic in form with dimension of approximately 0.09mm in edge.

Synchrotron radiation was monochromated by pyrolytic graphite(002) to provide X-ray beam

with the wave length of 0.96 \AA . The value of wave length was selected just longer than both L-absorption edges of Pb($\lambda_L = 0.95029 \text{ \AA}$) and Bi($\lambda_L = 0.92336 \text{ \AA}$) atoms. It results in the fact that a linear absorption coefficient can be made into small value of 339 cm^{-1} (cf. 866 cm^{-1} for $\text{Mok}\alpha$). Under the condition, the anomalous dispersion terms of both Pb and Bi atoms were estimated as $\Delta f'_{\text{Pb}} = -14.5$ and $\Delta f'_{\text{Bi}} = -12.3$ respectively, but imaginary terms ($\Delta f''$) were neglected at this stage of analysis compared with large values of real term ($f' + \Delta f'$). The difference between scattering factor of Pb and Bi atom at $\sin\theta/\lambda = 0.0$ is enlarged to 3.2.

A set of 237 intensity data (including 37 standard reflections) of $(hk0)$ was collected with the ω -2 θ step scan mode. After correction of dead time of detector system, Lorentz factor and absorption, all the intensities were normalized by those of standard reflections measured every ten reflections during data collection. It took about twelve hours for the data collection including three times of electron injection into the storage ring.

Result

Several cycles of least-square refinement using the program LINUS⁴ gave R-factor 0.06 under the condition of referring to the already determined structure as the starting model and employing the same scattering factors for metal atoms. The difference among weights of metal sites in d-Fourier map (Fig.2) seems to reveal features on the site occupancy of each metal site. A more quantitative study of the site occupancy is now in progress using three dimensional intensity data gathered under the same condition at BL-10A.

References

- 1) Y. Takéuchi and J. Takagi: Proc. Japan Acad. 10 (1974) 843.
- 2) J. Takagi and Y. Takéuchi: Acta Cryst. B28 (1972) 649.
- 3) B. Salanci and G.H. Moh: N. Jb. Miner. Abh. 112 (1969) 63.
- 4) P. Coppens and W.C. Hamilton: Acta Cryst. A26 (1970) 71.

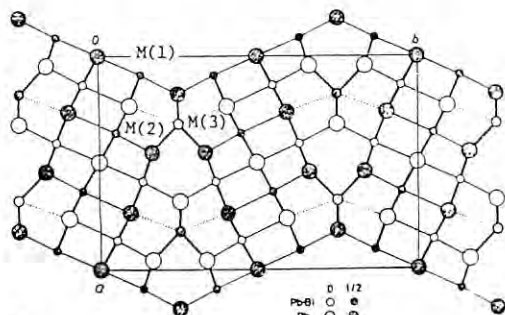


Fig.1 courtesy of Dr. J. Takagi

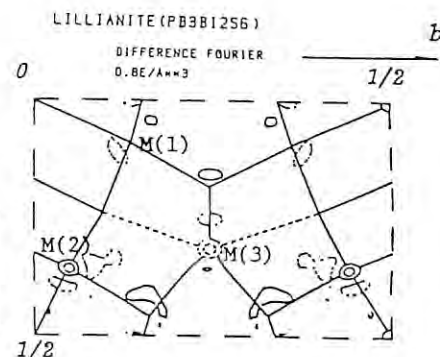


Fig.2

PRELIMINARY EXPERIMENT TO USE THE X-RAY GUIDE TUBE
AS A "LOW-PASS" FILTER OF POLYCHROMATIC X-RAYS

H. Nakazawa*, Tagai, T.** and Satow, Y.***

*National Institute for Research in Inorganic Materials, **Mineralogical Institute, University of Tokyo, ***National Laboratory for High Energy Physics.

Introduction

A laboratory glass-tube has recently been utilized as an X-ray guide tube (XGT) for transmitting X-rays in the distance (Nakazawa, 1983). The X-ray total external reflection (XTER) at the inside wall of the glass-tube was the principle of its use. Because the critical angle of XTER is a function of X-ray wavelength, it may also be probable that the XGT of a glass tube can be used as a "low-pass" filter of polychromatic X-rays, i.e. a filter to eliminate preferably X-rays of higher energy, when the tube is slightly bent or inclined from the direction of incidence.

Such a filter is demanded for the diffraction experiments by the film method using "monochromatized" synchrotron radiations (SR). Because of the polychromaticity of SR, the X-rays "monochromatized" by a conventional monochromator involve considerably components of those of higher harmonics. Hence a recorded diffraction pattern on a film is complicated by the presence of additional spots (or lines) due to such higher harmonics.

This report describes some preliminary results on the utilization of XGT as a low-pass filter of X-rays.

Experimental

A pyrex-glass tube of 1.0 mm inside and 6.0 mm outside diameters was tested as an XGT. The experimental setup is schematically shown in Fig. 1. The start of the tube (A, Fig.1) was fixed by a tool, and the other end of the tube (B, Fig.1) was pushed horizontally by a micrometer-head for the control of the inclination of the tube. Incident X-rays were "monochromatized" ones by a graphite monochromator placed in a housing at a distance of about 5 m from the start of the XGT. A wafer of Si(111) was used as a sample. With an appropriate screen, the 111 reflections of $\lambda_1 = 1.5$ and $\lambda_2 = 0.75$ Å were only recorded on a photographic film for an oscillation angle of ± 10 deg. The intensity distribution in the incident beam was also recorded simultaneously by using suitable absorbers of metal foils.

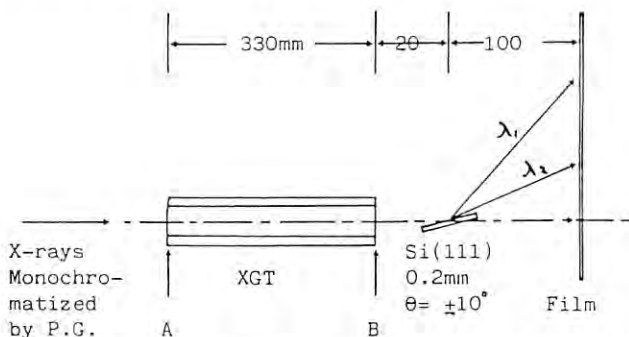


Fig. 1. Schematic illustration of the present setup.

Results and Discussion

A series of seven oscillation photographs is shown in Fig.1, where a set of three spots, which are the 111 reflection of λ_1 (top), that of λ_2 (middle) and the direct beam (bottom), is a part of an oscillation photograph. The series from left to right corresponds to step-wise increases of the inclination of the XGT being controlled by pushing the tube-end (B, Fig.1) at every 0.25 mm (7.6×10^{-3} rad.).

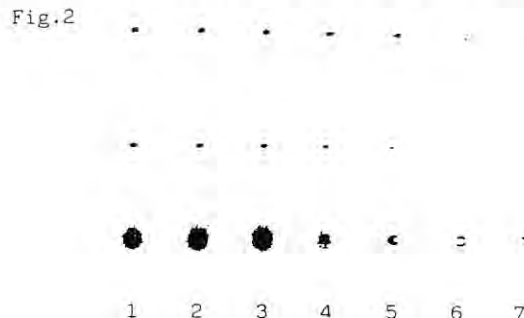
The first set was recorded at the original straight setting of the XGT for incident X-rays. It may be seen that the intensity of the 111 reflection of λ_1 and that of λ_2 are comparable.

When the tube is inclined, the intensity ratio of these two spots is decreased (2, 3, and 4, Fig.2). Assuming that the tube is ideally straight, the transmitted X-rays through the XGT are entirely reflected ones when the tube-end is pushed more than 1.0mm away from the original straight setting. The inclination angle of this case, 3.0×10^{-3} rad., satisfies the requirement that the X-rays of λ_1 pass through the XGT and those of λ_2 do not. The inclined XGT may act as the low-pass filter for X-rays. The 5-th set in Fig.2 is the resultant oscillation photograph of this case. The spot of λ_2 almost vanishes successfully.

There are, however, some disadvantages for its use: (1) The profile of the spots is complicated by the inhomogeneous distribution of X-rays which are reflected at the inside wall of the tube. (2) The intensity of λ_1 is also decreased when the inclination of the XGT is larger than the inside diameter of the tube (5, 6, and 7, Fig.2). Hence the alignment of the XGT at an optimum position is quite delicate.

The former disadvantage is essential for using the glass-tube of the cylindrical form. A simple flat mirror may be an easy solution for this difficulty, if an appropriate box-type collimator would be designed. The second point is a technical and not unsolvable difficulty.

At present, it is concluded that the XGT of a glass tube is really utilizable as a low-pass filter for a limited X-ray diffraction experiment which is not concerned about the profile of the diffraction spot, although more general use is not established for the reasons described above.



EXAMINATION OF SINGLE CRYSTAL DIFFRACTION DATA COLLECTION FROM MICRO-SIZE SPECIMENS USING FOUR-CIRCLE DIFFRACTOMETER

S. Sueno*, K. Ohsumi**, M. Kimata*, H. Yurimoto*, K. Kakehuda*, and M. Ohmasa***

* Institute of Geoscience, The University of Tsukuba, Ibaraki, 305 (Japan)

** Mineralogical Institute, The University of Tokyo, Hongo, Tokyo, 113 (Japan)

*** Institute of Materials Science, The University of Tsukuba, Ibaraki, 305 (Japan)

INTRODUCTION

There are many academically and/or industrially important inorganic materials of which crystal structures have never be refined or even unsolved by means of modern crystallographical techniques because of the difficulty for obtaining a single crystal whose optimum size is about 100 μm cubic for the conventional X-ray. One of the important characters of SOR beam is its strong beam intensity on hard X-ray region (0.5-2.0 \AA wave length) and this may be useful for collecting the X-ray diffraction data of micro-size single crystal specimens. We have examined the possibility of the data collection for several micro crystals using the four-circle diffractometer on BL10 beam line of Photon Factory, KEK.

SPECIMENS

Two orthoferrosilite single crystals (FeSiO_3) of 0.018 x 0.019 x 0.035 mm, and 0.01 x 0.012 x 0.03 mm in size were selected for the testing specimens. The reasons why orthoferrosilite has be chosen for this study are as follows:

(1) The diffraction intensity data measured on a conventional X-ray system for the same sample are available from Sueno and Kimata.

(2) Orthorhombic system is easy to find the crystal axes on a polarizing microscope, which simplifies the specimen selection and axis alignment.

(3) Many prismatic euhedral crystals with suitable sizes were available for this sample.

The specimens were mounted parallel to c axis on very fine glass fibers (10 μm in diameter). The crystals were then aligned on X-ray goniometer-heads by precession camera method using 50kV, 150mA $\text{Mok}\alpha$ radiation. The exposure time of an orientation photograph for the smaller specimen was about five hours.

TESTING PROCEDURES

The larger crystal was first tested on the four-circle diffractometer. The X-ray used was monochromatized by Si(111) platy crystal, 0.964 \AA in wave length. Two sets of slit combinations for the incident and the diffracted X-ray were tested, which are (#4 & #3) and (#3 & #3). The orientation matrix was obtained by means of manual peak search and then the diffraction peaks of fifteen selected reflections were examined for each set of slit combination. Figure 1a is a peak plotting of 12 0 0 reflection ($F_c=88.44$) measured using (#3 & #3) slit combination, and Figures 1b and 1c are those of 6 0 0 ($F_c=10.69$) which were measured using the (#4 & #3) and (#3 & #3) slit combinations respectively. It is clear that the slit combination (#3 & #3) shows better results although it gives weaker diffraction. However, on the test for the smaller crystal, we could not detect any diffraction peak even on the trial of longer measurement time.

DISCUSSION

On this examination, we used a platy silicon monochromator, but the energy distribution of the resulted X-ray was so narrow as to make the peak search difficult, and the incident beam intensity was not strong enough for the micro-crystal data collection. Therefore, it may be necessary to develop both a new monochromator system with the combination of a focusing monochromator system and a new optical system for insident beam including an X-ray guide tube. On the conventional X-ray system, the optimum size of specimen for the single crystal data collection is around 100 μm cubic, but on the SOR beam, it may still be possible to collect the available data from a micro-size specimen (1/100 in volume ratio) even on the present setup.

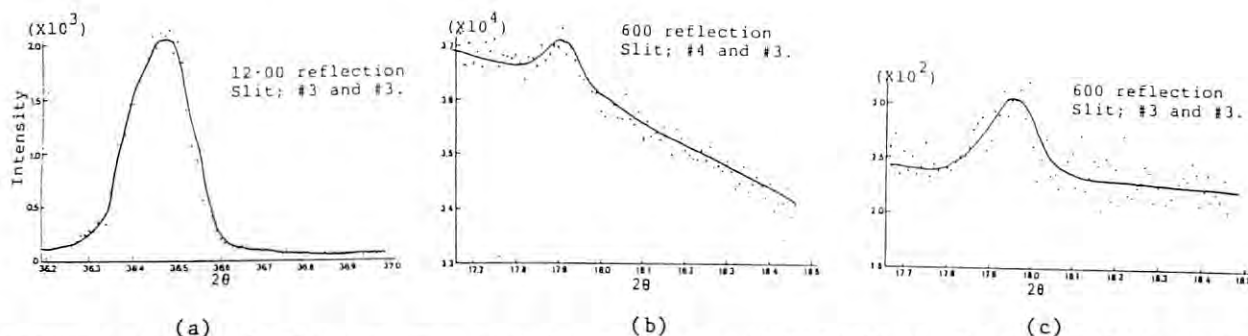


Figure 1. (a) The diffraction peak of 12 0 0 reflection ($F_c=88.44$). (b) The 6 0 0 diffraction peak ($F_c=10.69$) measured with (#4 & #3) slits. (c) The 6 0 0 diffraction peak measured with (#3 & #3) slit combination.

X-RAY TOPOGRAPHY OF A CUBE-SHAPED DIAMOND

H. Nakazawa*, Tagai, T.**, Hirai, H.***, Nukui, A.* and Satow, Y.****

*National Institute for Research in Inorganic Materials, **Mineralogical Institute, University of Tokyo, ***Institute of Geoscience, Tsukuba University, ****National Laboratory for High Energy Phys.

Introduction

The primary objectives of this experiment are (1) to observe the fine texture of a natural diamond being in cubic habit which is rare in the occurrence by using an easy method, and from more technical point of view, (2) to open another use of the four-circle diffractometer constructed for synchrotron radiation, of which the first principle of designing is the "tunability" of X-ray wavelength for a limited purpose such as the structure analysis employing the X-ray anomalous dispersion effect.

As seen in the report by MI working group (Tagai et al.) in the same issue, the system of the four-circle diffractometer has been constructed in such a way that the whole housing of the diffractometer moves and rotates to adjust to the incident X-rays which are reflected by a flat monochromator placed about 5 m apart from the diffractometer.

When a camera, or simply a photographic plate, is once placed in the housing normal to the direction of the incident beam, the oscillation photographs can easily be taken conveniently by using many diffraction spots, when the X-ray wavelengths are chosen to satisfy the Bragg condition of given reflections at the fixed angle of 45 deg. in 2θ . The "tunability" for X-ray wavelength, which is the most obvious advantage of this optical system may afford a rapid and easy method of observing the fine texture in the "slice" of a crystal.

Experimental

The overall scheme of the optical system used is described in other report of this issue (Tagai et al.). The X-ray topographic technique employed was similar to that applied in some recently reported studies (e.g. Moor & Lang, 1972). A slit made by two micrometer-heads equipped molybdenum edges (2 mm in thickness) was placed in the diffractometer housing before a sample crystal to make an incident ribbon-beam of X-rays (Fig. 1). A photographic plate was placed behind the sample normal to the incident beam. The sample crystal was oriented with a cube axis vertical. When X-rays of the wavelength of $\lambda = 0.9651 \text{ \AA}$ was used for the 220 reflection, the reflection angle, 2θ , was 45 deg., and hence the pattern recorded on the photographic plate was an undistorted map of the fine texture of the crystal "sliced" by the incident ribbon-beam. When the reflection was wanted to be changed, e.g., from 220 to 400, the diffractometer housing involving the entire setup for X-ray topography was moved to the position where the wavelength of the incident X-rays was changed from $\lambda = 0.9651$ to 0.6824 \AA to keep the reflection angle as 45 deg.

Results and Discussion

The cube-shaped diamond examined was colorless and was about 7 mm in edge length. Its surface was deeply pitted.

Two typical section topographs using 220

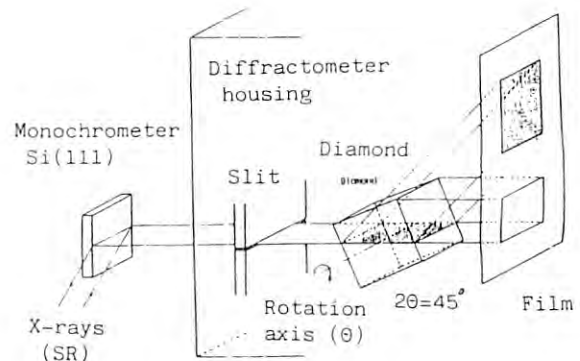


Fig. 1.

reflection are shown in the end of this report. They are a part of a series of six photographs which were taken at every angle $\Delta\theta = 0.05$ around the rotation axis of θ , while the X-ray wavelength was fixed at 0.9651 \AA .

Interesting seen in these photographs is that the inner part having a sector texture is covered by the outer part of highly mosaic crystal. The orientation mismatch of two adjacent sectors is about 0.03 deg. around the cube axis which is the rotation axis in the present setting. The angular range of the orientations of mosaic crystallites is about 0.3 deg. suggesting that the part is rather composed of the oriented crystallites than some imperfect crystals.

Similar internal texture has previously been reported by, e.g., Moor and Lang (1972), Lang (1974) and Orlov et al. (1982). The present photographs are much informative to understand the angular relations between sectors and also crystallites. One of the reason of this is the rapid and easy method of present experiment, e.g., the exposure time is only two minutes for one section topograph, and hence a series of photographs can be taken for successive change in crystal orientation, even if the angular difference is small as 0.01 degree.

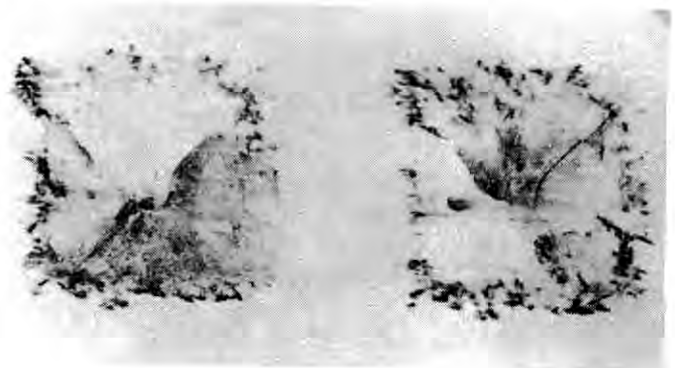


Fig.2.

ON THE SITES OF OFF-STOICHIOMETRIC Ni AND Al ATOMS IN Cu-Al-Ni ALLOY

Y.Abe,K.Ohsumi,T.Tagai and M.Tokomami
 Mineralogical Institute, Faculty of Science, University of Tokyo
 Hongo, Tokyo 113(Japan)

and
 K.Otsuka
 Institute of Materials Science, University of Tsukuba
 Sakura, Ibaraki 305(Japan)

Introduction

Cu-Al-Ni alloy system is well known for its pseudoelasticity and shape memory effect[1]. These two characteristics due to martensitic transformation are explained minutely in the review[2]. The single crystal used in the present study was synthesized by one of the authors (K.Otsuka) using modified Bridgeman technique[3]. The structure of the alloy is a DO₃ type ordered structure called β₁ matrix phase, where D represents Bi atom and O F respectively. The alloy shows multistage stress-induced martensitic transformation and the structure in each stage has already been made clear[4],[5],[6]. The purpose of the present study is to determine the sites of off-stoichiometric Al and Ni atoms. Taking account of the difference in atomic number between Cu(Z=29) and Ni(28), the wave length of X-ray have to be selected just close to Ni and Cu k-absorption edges in order to utilize an anomalous dispersion effect. Therefore, it has long been looked forward to the time when an arbitrary wave length can be used for the four-circle diffractometer set up at BL-10A.

The crystal data, composition and structure concerning to Cu-14.2Al-4.0Ni(wt%) used in the present study are shown in Tables 1, 2 and Figure 1.

Experimental

The nature of synchrotron radiation is quite different from that of conventional X-ray in following points especially in view of crystal structure analysis; parallelness, occasional spacial fluctuation, declining with time and polarization. These differences seem disadvantage in measuring the integrated intensities of Bragg reflections. Serious attention should be paid to the optical system using SR so as to simulate the usual case. In general, a pyrolytic graphite is used as a monochromator, since it has the character that monochromated X-ray has large dispersion in angle and width of the wave length. On the other hand, if a dispersion in wave length becomes smaller, the wave length just close to the absorption edge can be available. Accordingly, Si(111) plane was employed as a monochromator in the present study. In course, almost perfect parallelness of incident beam from Si(111) decreases a number of mosaic domains contributing to a Bragg reflection. For compensating it, the aperture with big size in diameter was selected as the slit just before the detector. In order to correct the decline of intensities of incident X-ray, standard reflections were measured at an interval of 6 or 12 reflections.

Data collection was carried out with two wave lengths using the four-circle diffractometer at BL-10A station with ω-2θ step scan mode (Δω=0.02°, scan range=1.0+0.8tanθ°). The step scan mode was employed for the careful examination of the profiles of reflections in early stage of experiment at BL-10A. Attenuators made of glass were automatically inserted not to exceed the

counts over 50,000 cps. Under the condition mentioned above, 64 reflections were obtained with a wave length of 1.4 Å and 1.5 Å (λ_k(Cu)=1.380 Å, λ_k(Ni)=1.488 Å). The procedure of data reduction for the present case is as follows. First, the profiles of all reflections were illustrated and examined in their shapes. Second, the integrated intensities, I, was obtained by summing up the count at each step followed by subtracting that of back ground. Third, the squared absolute value of observed structure factor was derived from the following equation;

$$|F_o|^2 = k_s \cdot \sin 2\theta \cdot k_n \cdot k_a \cdot I$$

where k_s is the scale factor, sin2θ the reciprocal of Lorentz factor, k_n the normalization factor derived from the intensities of standard reflections and k_a the attenuator factor.

The data gathered with 1.4 Å were found to be reliable, since a cycle of least-square refinement (LINUS) with a parameter of scale factor gave R-factor 0.09 without introducing an anomalous dispersion effect.

References

- [1] K. Shimizu: J. Cryst. Soc. Japan 23 (1981) 90
- [2] K. Otsuka and C.M. Wayman: A QUARTERLY REVIEW OF PROGRESS IN THE DEFORMATION BEHAVIOR OF MATERIALS, Edit: P. Feltham, Freund Publishing House LTD. Israel.
- [3] K. Otsuka, C.M. Wayman, K. Nakai, H. Sakamoto and K. Shimizu: Acta metall. 24 (1976) 207
- [4] K. Otsuka, M. Tokonami and K. Shimizu: Acta metall. 24 (1978) 965
- [5] K. Otsuka and M. Tokonami: J. Cryst. Soc. Japan 25 (1983) 104
- [6] M. Tokonami and K. Otsuka: in preparation

ideal formula	Cu ₃ Al
space group	Fm3m
a	5.839 ₁
z	4
ρ _c	7.31

Table 1
 Crystal data

site	composition
1	Al
2	Cu. ₈₈₁ Al. ₁₁₉
3	Cu. ₉₂₇ Ni. ₀₇₃

Table 2
 Composition of each site in case of related phase

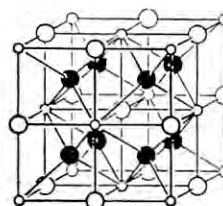


Fig. 1 DO₃ type structure
 ○ site 1
 ○ site 2
 ● site 3

RDF STUDY EMPLOYING ANOMALOUS DISPERSION EFFECT

A.Nukui*, N.Nakazawa*, Y.Hasegawa*, M.Isobe*, T.Tagai**

* National Institut for Research in Inorganic Materials
 ** The University of Tokyo

Utilization of the Diffractometer Constructed for SR

Almost all Radial Distribution Function (RDF) analyses of amorphous states have, hitherto, been carried out by a single scattering experiment. A few experiments have taken consideration of anomalous dispersion effects, from the combination of data obtained using three different radiations (X-ray, neutron and electron) or that from isotope.

While the Synchrotron Radiation (SR) give us the great strong sorce of the range from ultraviolet to hard X-rays (1000-0.1A) with excellent parallel and clean beam natures. Furthermore, a system of a four-circle diffractometer has been constructed in such a way that a whole housing of the machine moves to obtain a aimed incident X-rays, coworking with a monochrometer. Thus to apply this diffractometer for the study on RDF employing the anomalous dispersion effect is powerful and available.

Ge-Se Glass System

The Ge-Se glasses are, at first, chosen for this study, because of (1) an important semiconductor nature, of (2) an interesting vitreous state and of (3) having appropreate wavelengths of absorption edges. RDF studies of amorphous Ge-Se materials have recently been done by Fawcett et al. (1972), Molnar et al. (1973) and Uemura et al. (1975). They observed one or a few film samples in the system. Those are $x=0.29, 0.33, 0.56$ and 0.73 in Ge_xSe_{1-x} . They could obtain average coordinations and atomic distances, because of the single scattering experiment.

While it is possible to seperate a partial structure factor, X, when the anomalous dispersion effect is employed. In the Ge-Se system, for instance, there are three pairs of Ge-Ge, Ge-Se and Se-Se. The observed diffraction intensity of this system is expressed by an expansion of the general formula (Krogh-moe, 1966) as follow;

$$I_{GeSe} = [f_{Ge}^0 + \Delta f'_{Ge}] X_{GeGe} + 2[f_{Ge}^0 + \Delta f'_{Ge}][f_{Se}^0 + \Delta f'_{Se}] X_{GeSe} + [f_{Se}^0 + \Delta f'_{Se}] X_{SeSe}$$

From the formula, the seperation of the partial structure factors, X_{GeGe} , X_{GeSe} and X_{SeSe} are done by using the intensity data at three different wavelengths: one is far from and the other two are at each absorption edge.

Experimental and Results

Chemical compositions of glasses used are $x=0.05, 0.10, 0.15, 0.20$ and 0.25 in Ge_xSe_{1-x} . The glasses are prepared by quenching the melt. Sample was measured in the 2θ range from

3.0 to 100° at every 0.5° . The measurements of all samples were planed to use X-rays of three different wavelengths; $\lambda_1=1.30$, $\lambda_2=1.1165$ (Ge absorption edge) and $\lambda_3=0.9897A$ (Se absorption edge). Unfortunately³ the data were collected at two wavelengths for $Ge_{20}Se_{80}$ glass, because of a limited time.

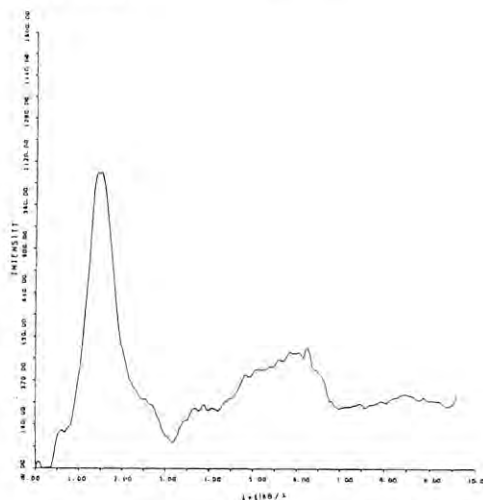


Fig. 1 X-ray diffraction intensity of SiO_2 glass by using $\lambda_1=1.30A$.

Figure 1 shows the typical X-ray diffraction intensity of SiO_2 glass which was taken to check the reliability of the entire optical system. In the figure the intensity does not decrease at higher angle. This indicates that the intensity may be contaminated by some unreasonable scattering. Thus some improvements of the optical system are required.

Further Study

Only from the present preriminal study, it is not enough to discuss about the structures of the Ge-Se glasses and about a possibility of applying this method to the multi-component amorphous materials. This experiment is, however, the beginning of the RDF study with the anomalous dispersion effect using the diffractometer designed to SR. This type of study will be continued.

MEASUREMENTS OF DIFFUSE STREAKS SCATTERED BY FINE SEGREGATES OF β -MnO₂M. Ohmasa*, N. Yamada*, H. Nakazawa**, Y. Sato***, T. Tagai[†] and S. Sueno^{††}

- * Institute of Materials Science, University of Tsukuba, Ibaraki 305, (Japan)
 ** National Institute for Research in Inorganic Materials, Ibaraki 305, (Japan)
 *** KEK, National Laboratory for High Energy Physics, Ibaraki 305, (Japan)
 † Mineralogical Institute, University of Tokyo, Tokyo 113, (Japan)
 †† Institute of Geoscience, University of Tsukuba, Ibaraki 305, (Japan)

Introduction

Six polymorphs (α -, β -, γ -, ϵ -forms and ramsdellite) have so far been described as Mn di-oxides. However, structural relations among them are still not clear, because many of them crystallize not well and only bad single crystals or powder specimens are available for structural studies. β -form of these polymorphs is the most stable phase and fairly good single crystals are obtainable for single crystal works.

Recently we have studied β -MnO₂ by electron diffraction and X-ray diffraction techniques and found that most natural single crystals (pyrolusite) give faint diffuse streaks scattered by sub-microscopic segregations in their diffraction patterns¹⁾. Intensity of these streaks is variable according to samples, but the strongest one is nevertheless too weak to measure using a conventional X-ray generator. Consequently we applied the strong SOR beam of Photon Factory in KEK for measurements of the diffuse streaks of β -MnO₂.

Experiments

Measurements were made by a photographic method at the station of the vertical four-circle diffractometer on BL10A. An oscillation camera with flat film holders was used. The distance between the sample and the film was adjusted to 55mm. Industrial X-ray films (Fuji, Ix150) were used for intensity measurements. A Si flat crystal, parallel to (111), was used to monochromatize incident beam. Two wave lengths, 1.14 and 0.65Å, were selected for the experiment. Since the K-absorption edge of Mn is 1.896Å, longer wavelength than this is suitable for intensity measurements. But the longest wavelength was instrumentally limited to about 1.7Å. Then 1.14Å was selected for the incident beam which is not

strongly affected by absorption effects and is still strong. Diffraction by harmonics of 1.14Å observed in the photographs as discussed in the following chapter. We took photographs also with 0.65Å and could avoid the effects of harmonics. The exposures were 2.5 and 6 hours for the both wavelengths.

The ring was operated at 2.5GeV and the beam current changed from 150mA (after injections) to 50mA (before injections) during the experiment. The intensity of the incident beam was monitored by a scintillation counter. The change of the intensity monitored was less than 30%.

Results and Discussions

An oscillation photographs taken with 0.65Å beam is illustrated in Fig.1. The optical density of the films is roughly comparable to that of the films exposed for more than ten days by a conventional X-ray generator (Zr filtered Mo radiation operated at 40kV, 20mA). In the latter case, the background level was very high and streaks of white radiation was remarkable, hence it was impossible to get accurate intensity by photometry.

Effects of harmonics were not observed on the films taken with the 0.65Å, while many spots by harmonics ($1/3$ and $1/4\lambda$) were observed on the films taken with the 1.14Å.

In Fig.1, Two sets of diffraction patterns are recorded. One of them is the pattern from β -form and another is that from segregations. β -MnO₂, being tetragonal, has rutile type structure with dimensions $a_{\beta}=4.400$ and $c_{\beta}=2.871$ Å. The segregation has orthorhombic symmetry, $a=4.5$, $c=2.87$ Å and b the direction of the diffuse streaks. The mutual orientation is as follows: $a_s // a_{\beta}$, $b_s // b_{\beta} (=a_{\beta})$ and $c_s // c_{\beta}$.

Fig.2 shows a result of photometry of the streak indicated by an arrow in Fig.1. These streaks have maxima with an approximate interval of 9.3Å. These characteristics suggest that the segregation of β -MnO₂ should corresponds to the γ -MnO₂ studied by DeWolff (1959)²⁾ using powder diffraction method. Quantitative analysis of the streak is now in progress.

1) N. Yamada, M. Ohmasa and S. Horiuchi: Abstract Cryst. Soc. Japan (1982) 5p-7.

2) P.M. DeWolff: Acta Cryst. 12, (1959), 341.

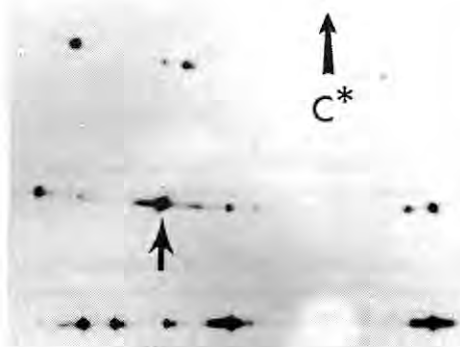


Fig.1. Oscillation photograph.

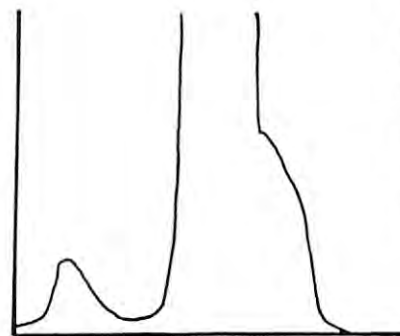


Fig.2. Result of photometry

RADIATION BIOLOGY STUDIES WITH MONOCHROMATIC X-RAYS

Takashi Ito

Radiation Biology Working Group
 Institute of Physics, College of Arts and Sciences
 University of Tokyo, Meguroku, Komaba, Tokyo 153

The working group of radiation biology in the Photon Factory (PF) was established in 1978 to mission for planning necessary facilities for radiation biology studies, and assists in undertaking their constructions, thereby supports the PF. Our basic concept of using synchrotron radiation (SR) in the PF is to have the beam line, BL28, suitable for VUV- and X- regions in the adjacent experimental hall (see related report for details) where radioisotope-labeled biological materials including mammalian cells could be handled. The working group wished first to obtain information on the radiobiological use of X-ray region before designing the complete beam line for radiation effect studies. Although soon realized that X-ray monochromators at the existing stations are not suitable because of the totally different design concept -- they only could provide a beam with extremely narrow size for irradiation purpose for which as much as 4 cm² of target size is desirable, the working group has conducted trial irradiation with various biological materials using part of the diffractometer installed at BL10A during the machine time allotted from June 1982 to June 1983.

Below follow the experiences important for the irradiation experiments with SR, some results worth mentioning at this stage, and a concept of beam line for radiation biology to be installed in BL28, recently worked out, basing on the accumulated experiences, by the collaboration with the in-house staffs.

1. Dosimetry (K. Hieda, K. Kobayashi, and H. Maezawa)

Dosimetry is the essential prerequisite of radiation effects. Biological effect must ultimately be related to the absolute dose expressed

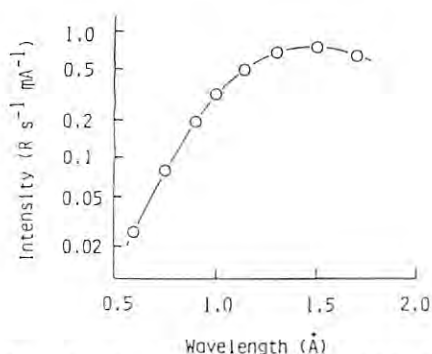


Fig. 1. X-ray spectrum with Si-monochromator at BL10A.

in the units either R or rad. The relative dose can only be used under a limited situation. The calibration of soft X-ray intensity to the rate of absolute dose is a serious problem. A free-air ionization chamber designed with the technical help by Dr. N. Oda was used along with TLD for the monitoring purpose (see Instrumentation). One example of intensity measurements of SR (Si monochromator) in R per unit time per unit stored current is shown in Fig. 1. Two additional points were noted during the course of measurements: (1) The intensity is not necessarily proportional directly to the stored current; and (2) Spacial distribution of intensity is not homogeneous. These results indicate that the irradiation system now planned should be equipped with a simultaneous intensity monitor between the monochromator and the irradiation chamber.

2. Irradiation of Bacteria and Yeast

(a) Experiments with Bromine-Incorporated *E. coli* Cells (H. Maezawa, Y. Furusawa, M. Morimyo and K. Suzuki)

A thymine-requiring mutant of *E. coli* strain B (B₄-1) cells were filtered onto a sample area of a Millipore membrane filter (pore size, 0.45 μm, diameter, 25 mm). The thickness of the layer of loaded cells was estimated as 5 μm. The irradiation was performed with a sample-scanning stage (see Instrumentation). A single crystal

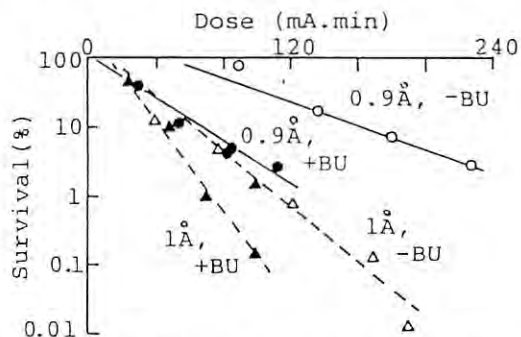


Fig. 2. The effect of irradiation on the survival curves of *E. coli* grown in the presence or absence of BU.

monochromator (graphite 002) designed as part of 4-circle diffractometer was used. The beam size was 6 x 15 mm. The dose rate (intensity) was estimated as 112 rad/mA.min at 0.9 Å (13.8 KeV) and 286 rad/mA.min at 1.0 Å (12.4 KeV). These two wavelengths were chosen just

above and below the K edge for Br (13.473 KeV). As shown in Fig. 2, cells grown with bromouracil (BU) were generally sensitized by the presence of BU. However, to be noted is that the ratio -BU/+BU of D_{10} (the dose required to decrease cell survival to 10%) values was 1.5 at 1 Å and 2.4 at 0.9 Å. Thus, the increased effect in Br-incorporated cells at 0.9 Å could possibly reflect the consequences of the induced Auger processes in the cell.

(b) Experiments with Yeast Cells (K. Kobayashi and A. Ito)

A diploid strain of yeast *Sacchomyces cerevisiae* D7M was used. Stationary phase cells were placed on a Millipore filter in a square of 5 x 5 mm for irradiation. Since the beam size was smaller than the sample area (Jan. 27, 1983, Feb. 10, 1983), the sample holder was scanned. After irradiation, sample cells were assayed for survivors and for convertants at tryptophan 5

Table 1. Induction rate of gene conversion by monochromatic X-ray irradiation.

Wavelength (Å)	Frequency (mA ⁻¹ min ⁻¹)	Calibration factor (R mA ⁻¹ min ⁻¹)	Frequency (R ⁻¹)
1.14	2.59×10^{-6}	33	0.78×10^{-7}
0.90	1.54×10^{-6}	13	1.18×10^{-7}

locus (gene conversion) by plating on the complete and the minimal synthetic (deprived tryptophan) media, respectively. In all experiments gene conversion frequency increased linearly with the dose as in the case of γ -irradiation. Typical results for the induction rate of gene conversion are shown in Table 1. The calibration factor R (roentgen) per mA.min dose was obtained by using free-air ionization chamber. Dividing the frequency by this value gives the frequency per R. The results (last column) would imply that

the induction rate of gene conversion depends on the wavelength of radiation.

3. Irradiation of Mammalian Cells (K. Shinohara, H. Ohara, H. Majima and T. Yamada)

Two cell lines, CHO (derived from Chinese hamster ovary) and HeLa (derived from human cervical carcinoma) were used in the test irradiation. The irradiation experiments are highly motivated, however, since for the first time we could examine with highly monochromatic X-rays of the possibility on the inner-shell ionization of certain elements in mammalian cells. In these cases Br (in the form of BUdR) was incorporated. Although confirmation awaits further experiments, an enhancement of biological effects possibly ascribable to the Auger processes seems measurable (see detail accounts under a separate heading).

4. Basic Concept of Beam Line, BL28

A basic concept of beam line to be installed at BL28 for the radiation effect studies has been worked out recently in collaborating with in-house staffs. Plane view of the proposed beam line is shown in Fig. 3. Available horizontal aperture in this beam line is limited to 10 mrad by a quadrapole magnet just downstream of the bending magnet. In the proposed design, 10 mrad is divided into two branch lines, one is for soft X-ray experiments (2 mrad) and the other for VUV or X-ray experiments (5 mrad). The former is deflected 6° by a mirror (M₁) located 11 m downstream of the source. A mirror (M₂) located at 12.6 m deflects the beam upwards for VUV. The mirror is positioned out of the optical path when X-ray experiments are intended. Appropriate monochromators for respective branch lines to cover 0.8 up to 1900 Å except 4 to 12 Å have been designed. Details will be published elsewhere in the near future.

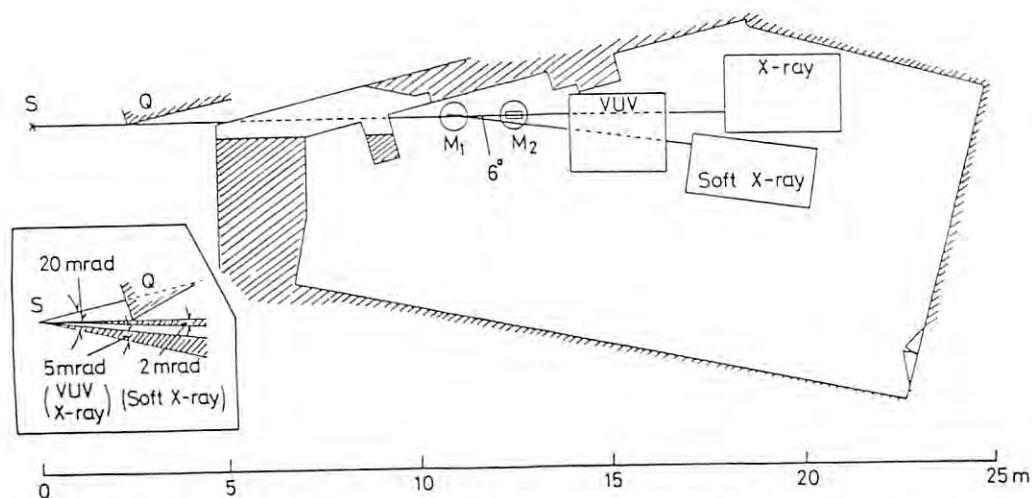


Fig.3. Layout of proposed beam line and monochromators at BL28. S, SR source point; Q, quadrapole magnet; M₁, mirror for soft X-rays; M₂, mirror for VUV.

CHROMOSOME ABERRATIONS INDUCED IN CHINESE HAMSTER
OVARY (CHO) CELLS BY SYNCHROTRON RADIATION

H. Ohara¹, T. Yamada¹, H. Majima², K. Shinohara³, K. Kobayashi⁴,
K. Hieda⁵, H. Maesawa⁶ and Synchrotron Radiation Biology Group⁷

Introduction

Absorption of soft X-rays in biological materials leads to a deposition of energy along electron tracks that may be short compared with cellular or subcellular dimensions. The soft X-rays within the synchrotron radiation can be used, therefore, as a fine probe of the biologically sensitive structure within cells, and to study the size of events in a cell involved in radiobiological processes. In addition, each absorption of mono-energetic X-rays of energy near the characteristic absorption edges of component element of a biomolecule leads to the inner-shell ionization, followed by the Auger effect. This inevitably initiates highly destructive events which are capable of enhancing damage.

In the present study aimed at characterizing biological effects of synchrotron radiation on mammalian cells, we selected the chromosome aberrations as the observation endpoint, since they might directly reflect the damage in DNA molecules. Furthermore, an attempt was made to examine a sensitizing effect of Br incorporated into DNA, possibly resulting from the inner-shell ionization of Br.

Materials and Methods

An established line of Chinese hamster ovary (CHO) cells was used throughout the experiment. The cell culture techniques required for the preparation of irradiation materials of cells and incorporation of BrdU into the cell were followed by the method of Shinohara (1982). About 5×10^4 cells in a log phase of growth were irradiated with 0.9 or 1.0 Å wave length synchrotron radiation in the irradiation chamber attached to Beam line 10A. The irradiated cells were incubated with a mitotic inhibitor, Colcemid, for 5 hr. During the incubation, mitotic cells were arrested by the action of Colcemid at metaphase stage of mitosis. Then, the cells were harvested to prepare the chromosomal specimen for analysis.

Results and Discussion

The chromosome aberrations were classified into two main types, the chromatid and the chromosome types. The former involved the chromatid gaps, breaks and the three different types of inter-chromosome exchanges, while the latter involved the dicentrics, rings, the isochromatid gaps and breaks. A whole set of the chromosomes in an unirradiated control CHO cells was shown in Fig. 1 and several examples of the chromatid type of aberrations induced by synchrotron radiation were in Fig. 2. In Table 1, the summary of the data about the frequencies of chromosome aberrations observed in the BudR-incorporated cells was listed. There is no significant difference in the total aberration frequencies between the two different radiations, although a possible differ-

ence was noted in those of chromosome type aberrations.

From these results, the chromosome aberrations could be recognized as one of the useful observation end-points for characterizing biological effects of synchrotron radiation on mammalian cells. However, the present data are not sufficient to draw any definite conclusion on the differential effect of two radiations. The accurate determination of the absorbed dose of the radiations and the irradiation system specially devised for providing us a sufficient amount of the irradiated cell materials are required for more detailed studies.

Table 1. Frequencies of chromosome aberrations in BudR-incorporated CHO cells by Synchrotron Radiation.

Radiat.	No. cells observed	Chromosome type aberr.	Chromatid type abber.	Total
0.9 Å	107	37	221	258
1.0 Å	100	12	235	247

Fig. 1. Metaphasic chromosomes in unirradiated CHO cells.



Fig. 2. Examples of chromatid type-chromosome aberrations induced by synchrotron radiation



1) Natl. Inst. Radiol. Sci. (Chiba); 2) Univ. of Tokyo (Tokyo); 3) Kobe Univ. (Kobe); 4) Tsukuba Univ. (Tsukuba); 5) Rikkyou Univ. (Tokyo); 6) Tokai Univ. (Hatano); 7) Chairman: T. Ito, Univ. of Tokyo (Tokyo)

IRRADIATION OF CULTURED MAMMALIAN CELLS CONTAINING BROMINE IN THE DNA
BY MONOCHROMATIC SYNCHROTRON RADIATION AT 0.09 AND 0.1 NM

Kunio Shinohara, Hiroshi Ohara*, Hideyuki Majima**, Shigefumi Okada**, Hiroshi Maezawa***, Katsumi Kobayashi****, Kotaro Hieda*****, Atsushi Ito*****, Takeshi Yamada*****, and Takashi Ito*****

Dept. of Radiat. Res., The Tokyo Metropol. Inst. of Med. Sci., Tokyo 113; *Div. of Physiol. and Pathol., Nat'l. Inst. of Radiol. Sci., Chiba 260; **Dept. of Radiat. Biophys., Faculty of Med., Univ. of Tokyo, Tokyo 113; ***Dept. of Radiol., School of Med., Tokai Univ., Kanagawa 259-11; ****Inst. of Biol. Sci., Univ. of Tsukuba, Ibaraki 305; *****Biophys. Lab., Dept. of Phys., Rikkyo Univ., Tokyo 171; *****Inst. of Phys., College of Arts and Sci., Univ. of Tokyo, Tokyo 153; *****Div. of Biol., Nat'l. Inst. of Radiol. Sci., Chiba 260.

The possibility of a new method of radiation therapy of cancer, photon activation therapy, has been proposed recently (1,2). The method is based on the idea that Auger effect enhances the killing effect of the radiation on mammalian cells. To induce this enhancement, the cancer cells should be labeled with significant amount of the compound (e.g., 5-iododeoxyuridine) carrying the special element (iodine in the case of 5-iododeoxyuridine) and irradiated with monochromatic x-rays at the wavelength slightly shorter than the K absorption edge of the element. As the first step to examine this idea, cultured mammalian cells were labeled with 5-bromodeoxyuridine (BUdR) and irradiated with synchrotron radiation at the wavelength of 0.09 and 0.1 nm. The K absorption edge of bromine is 13.474 keV (0.0920 nm).

We have tried two cell lines, CHO (derived from Chinese hamster ovary) and HeLa (derived from human cervical carcinoma). Cells were allowed to attach themselves to a membrane filter disc (3), grown in the presence or absence of BUdR, and irradiated with synchrotron radiation at 0.09 or 0.1 nm. Irradiation was performed on the sample-scanning stage (see Instrumentation) using a diffractometer installed at the BL-10A. The wavelength resolution ($\Delta\lambda/\lambda$) was less than 0.005. Irradiated cells were collected from the membrane filter by trypsinization, plated into 60 mm plastic Petri dishes and incubated for 10-12 days to develop colonies. We wish to report preliminary results with HeLa cells.

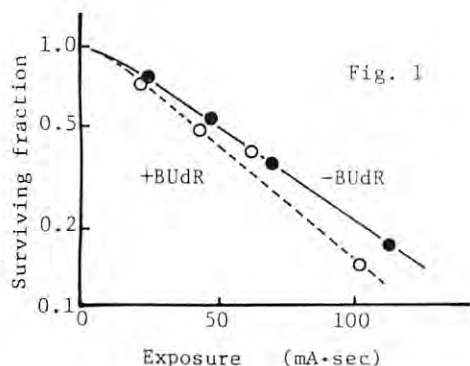


Figure 1 shows the dose survival curve of HeLa cells irradiated with synchrotron radiation at 0.1 nm. In the ordinate, survival was plotted in log scale. In the abscissa, exposure is expressed in the stored current (mA) x irradiation time (sec). Cell survival was smaller in

the presence of BUdR than in the absence of BUdR. Similar curves were obtained with HeLa cells irradiated with 0.09 nm radiation which is shorter than K absorption edge of bromine at which the induction of Auger electrons are expected. Two sets of survival curves obtained at each wavelength were compared (Table 1) by taking a ratio of D_0 with respect to the

Table 1

wavelength (nm)	D_0 (mA·sec) [@]		D_0 (-BUdR)
	+BUdR	-BUdR	D_0 (+BUdR)
0.1	48	57	1.19
0.09	63	88	1.40

@ The conversion factor to R is dependent on the wavelength.

presence and absence of BUdR (D_0 : the dose required to reduce the survival of the linear portion of the response by 63%).

BUdR is a well known radiosensitizer. This effect as sensitizer was observed in both cells irradiated at each wavelength. However, in addition to this effect, there remained additional decrease in survival of the cells irradiated at 0.09 nm. Since the wavelength of 0.09 nm is shorter than the K absorption edge of bromine and 0.1 nm is longer than that, this additional decrease in the survival may be due to the induction of Auger electrons by the radiation at 0.09 nm. The present results suggest a hope for the development of photon activation therapy. Further experiments intended to confirm these results are in progress.

References

- 1) R.G.Fairchild and V.P.Bond: Proc. Tokyo Med. Soc.: Meeting of Neutron Capture Therapy. Tokyo, Japan (1981).
- 2) A.Halpern: Uses of Synchrotron Radiation in Biology (Academic Press, New York and London, 1982) Chap. 10.
- 3) K. Shinohara et al.: Radiat. Res., in press.

EXAFS STUDY OF BEHAVIOR OF $\text{Rh}_6(\text{CO})_{16}$ on Al_2O_3

H. Kuroda, N. Kosugi, K. Asakura and H. Ishii

Department of Chemistry and Research Center for Spectrochemistry, Faculty of Science, The University of Tokyo, Hongo, Bunkyo-ku, Tokyo 113 (JAPAN)

Y. Iwasawa

Department of Applied Chemistry, Faculty of Engineering, Yokohama National University, Tokiwadai, Hodogaya-ku, Yokohama 240 (JAPAN)

For $\text{Rh}_6(\text{CO})_{16}/\text{Al}_2\text{O}_3$ catalyst, Smith et al.¹ proposed a reversible change of the state of the Rh cluster as shown in Table 1, according to their IR study of this system. There are some disagreements in regard to the actual state of the chemical species^{1,2}. The purpose of the present study is to clarify the behavior of this catalyst system by use of XAS technique.

Table 1. Treatments of the sample

Step 1.	$\text{Rh}_6(\text{CO})_{16}$ impregnated on Al_2O_3 in absence of air
	↓ $\text{O}_2/\text{H}_2\text{O}$
Step 2.	Chemical species 1
	↓ $\text{CO}/\text{H}_2\text{O}$
Step 3.	Chemical species 2 (IR spectra similar to $\text{Rh}_6(\text{CO})_{16}$)

The Rh K spectra were measured for the three steps given in Table 1. XAS measurements were done by use of the EXAFS apparatus at BL 10-B as a test experiment of the apparatus.

The Fourier transform for $\text{Rh}_6(\text{CO})_{16}$ dispersed on $\gamma\text{-Al}_2\text{O}_3$ shows two prominent peaks, the peak at shorter distance being attributable to Rh-C and/or Rh-O while the other peak at longer distance to Rh-Rh. The Fourier transform for the chemical species 1 has only a small peak at the position corresponding to Rh-Rh, indicating the destruction of Rh_6 skeleton. The analysis suggests the structure illustrated in Fig.2. The Fourier transform for the species 2 resembles that of the starting catalyst (step 1), showing the peak corresponding to Rh-Rh. The curve-fitting analysis gave $2.78 \pm 0.03 \text{ \AA}$ for Rh-Rh distance, which is the same to the Rh-Rh in $\text{Rh}_6(\text{CO})_{16}$. These facts prove that the Rh cluster once destroyed in the step 2 is regenerated in the step 3.

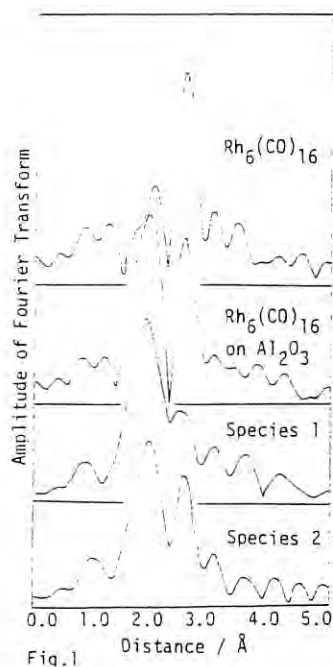


Fig.1

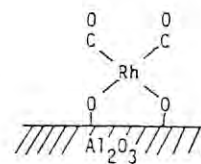


Fig.2

- 1) A. K. Smith, F. Hugues, A. Theolier, J. M. Basset, R. Ugo, G. M. Zanderighi, J. L. Bilhou, V. Bilhou-Bougnol and W. F. Graydon: *Inorg. Chem.* **18** (1979) 3104.
- 2) G. C. Smith, T. P. Chojnacki, S. R. Dasgupta, K. Iwatate, K. L. Watters: *Inorg. Chem.* **14** (1975) 1421.
K. L. Watters, R. F. Howe, T. P. Chojnacki, C. M. Fu, R. L. Schneider and N. B. Wong: *J. Catal.* **66** (1980) 424.

EXAFS AND XANES OF FeCl_3 AQUEOUS SOLUTIONS

H. Kuroda, N. Kosugi, K. Asakura, H. Ishii and M. Nomura*

Department of Chemistry and Research Center for Spectrochemistry, Faculty of Science, The University of Tokyo, Hongo, Bunkyo-ku, Tokyo 113 (JAPAN)

*Photon Factory, National Laboratory for High-Energy Physics, Oho-machi, Tsukuba-gun, Ibaraki 305 (JAPAN)

The structure of the aquo-complexes in the aqueous solution of FeCl_3 has been investigated hitherto by use of X-ray diffraction. There are some disagreements concerning the conclusions given by Wertz et al.¹ and those by Magini et al.² in regard to the dominant chemical species existing in the solutions. In order to give some insight into the actual structure of the aquo-complexes, we have studied the Fe K spectra of aqueous solutions of FeCl_3 .

The XAS spectra were measured by use of the EXAFS apparatus at BL 10-B as a part of the test experiments of the apparatus. The compositions of the studied solutions are given in Table 1 together with the abbreviations of the sample names.

The XANES spectra of the FeCl_3 aqueous solutions are shown in Fig.1, and those of the powders of the reference compounds are shown in Fig.2. The XANES spectra of the solutions, 0.1N and 0.7N, resemble the spectrum of $\text{Fe}(\text{NO}_3)_3 \cdot 9\text{H}_2\text{O}$ indicating that the local chemical structure is $\text{Fe}(\text{H}_2\text{O})_6^{3+}$. On the other hand, the spectrum of DP corresponds to FeCl_4^- , and the spectra of the solutions of high FeCl_3 concentration show an indication for the existence of FeCl_4^- .

The Fourier transforms of the EXAFS oscillations $k^3 \cdot \chi(k)$ are shown in Fig.3. The main peak in these curves in the region of 1.6–1.8 Å is due to the overlap of Fe-Cl and Fe-O peaks. In Fig.4 we plotted the amplitude of this peak against its position. The points fall into two groups. In the GROUP I (0.1N, 0.7N, 0.5A1 and 1A2), the peak is located at about 1.6 Å which is a little longer than the peak position for $\text{Fe}(\text{H}_2\text{O})_6^{3+}$, indicating that main chemical species be $\text{FeCl}(\text{H}_2\text{O})_5^{2+}$ and/or $\text{Fe}(\text{H}_2\text{O})_6^{3+}$. In the GROUP II, the peak is in the region between 1.75–1.85 Å, indicating presence of the species like $\text{FeCl}_2(\text{H}_2\text{O})_4^+$ and FeCl_4^- .

In the Fourier transform for DP shown in Fig.5, we can not find any peak corresponding to Fe-Fe. This means that the dimeric species Fe_2Cl_6 can not be the dominant species in DP. The XAS data can be interpreted by considering the coexistence of $\text{FeCl}_2(\text{H}_2\text{O})_4^+$ and FeCl_4^- .

- 1) D. L. Wertz et al: Inorg. Chem.19(1980) 1652, 20(1981) 3118; J. Phys. Chem.85(1981) 3542.
- 2) M. Magini et al: J. Chem. Phys.71(1979) 4255, 76(1982)1111; Inorg. Chem.22(1983)1001.

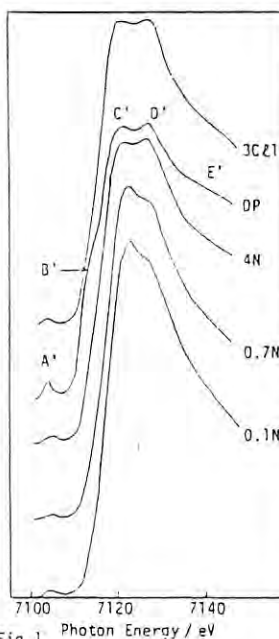


Fig.1 Photon Energy / eV

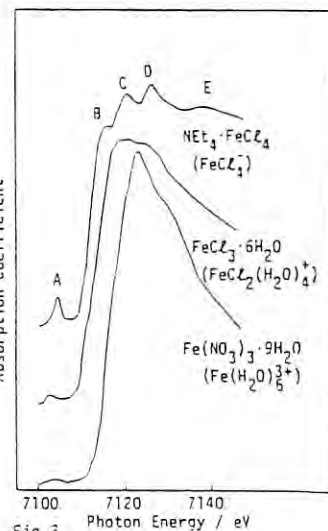


Fig.2 Photon Energy / eV

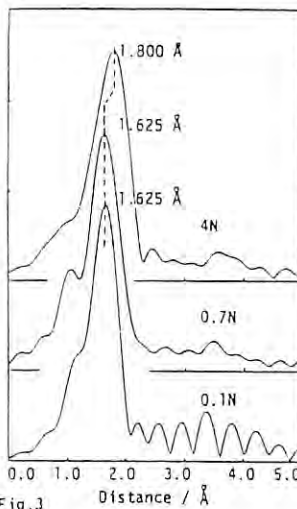


Fig.3 Distance / Å

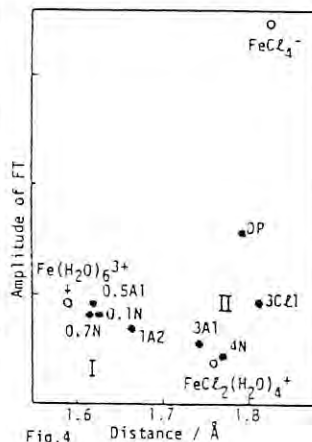


Fig.4 Distance / Å

Table 1

	[Fe ³⁺]	[HNO ₃]	[HCl]
	mol/l	[Fe ³⁺]	[Fe ³⁺]
4N	4.3		
0.7N	0.74		
0.1N	0.14		
3A1	3.0	1.0	
0.5A1	0.50	1.0	
1A2	1.2	2.3	
3C21	3.0		1.0
DP	deliquescent product		

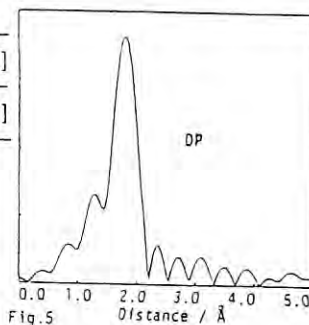


Fig.5 Distance / Å

EXAFS AND XANES OF FeCl_3 DISSOLVED IN ORGANIC SOLVENTS

H. Kuroda, N. Kosugi, K. Asakura, H. Ishii and M. Nomura*

Department of Chemistry and Research Center for Spectrochemistry, Faculty of Science, The University of Tokyo, Hongo, Bunkyo-ku, Tokyo 113 (JAPAN)

*Photon Factory, National Laboratory for High-Energy Physics, Oho-machi, Tsukuba-gun, Ibaraki 305 (JAPAN)

Wertz et al.¹ investigated the structure of the solute in the methanol solution of FeCl_3 by means of X-ray diffraction, and proposed that the solute exists in the state of the dimer Fe_2Cl_6 although they could not find any direct evidence in the radial distribution curve obtained from the analysis of X-ray diffraction data.

We have measured the Fe K spectra of FeCl_3 in the state dissolved in several organic solvents. The solutions studied in the present experiment are 2.7 and 0.45 M in CH_3OH , 1.1 and 0.43 M in CH_3CN , and 0.63 and 0.16 M in CH_3NO_2 .

The XAS data were obtained by use of the EXAFS apparatus at BL 10-B at a test experiment of the apparatus.

Figure 1 shows the Fe K XANES spectra of the powder and the nitromethane solution of $\text{N}(\text{C}_2\text{H}_5)_4 \cdot \text{FeCl}_4$. The spectrum of the nitromethane solution very well resembles that of the powder exhibiting a sharp peak A below the absorption edge and the three peaks B, C and D above the absorption edge. This fact indicates that anions existing in the nitromethane solution are FeCl_4^- .

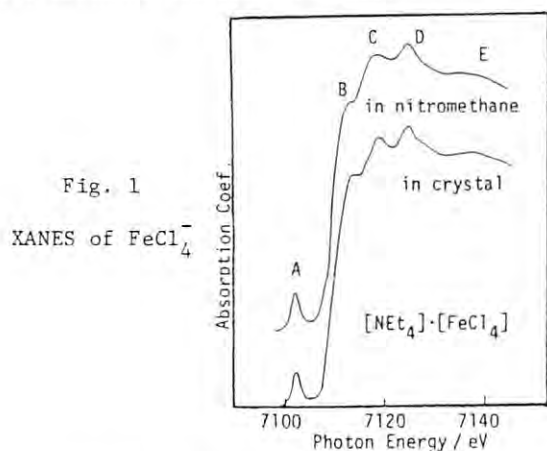


Fig. 1
XANES of FeCl_4^-

The Fe K XANES spectra of the solutions of FeCl_3 are given in Fig. 2. The concentration dependence of XANES spectra could not be observed. Note that the structures A, B, C and D, characteristic of FeCl_4^- , can be found also in these spectra, although the relative intensities more or less vary depending on the solvent. This fact seems to indicate that a considerable amount of the solute is in the state of FeCl_4^- also in these solutions.

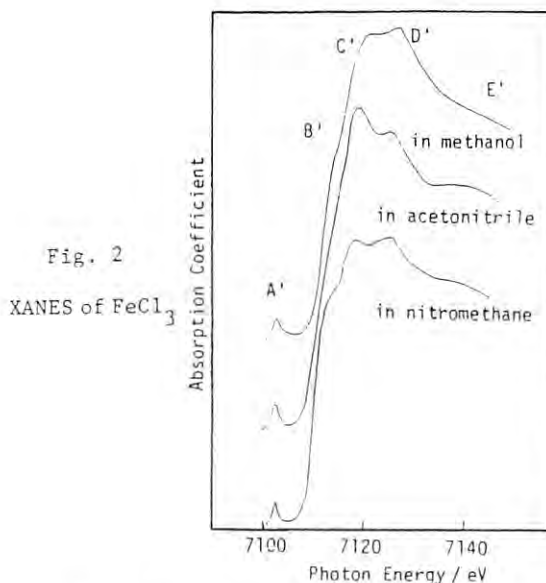


Fig. 2
XANES of FeCl_3

The Fourier transforms of the Fe K EXAFS oscillations observed for the solutions of FeCl_3 are shown in Fig. 3. No peak corresponding to Fe-Fe can be found in Fig. 3. Thus it is quite unlikely that a large part of the solute is in the dimer Fe_2Cl_6 state.

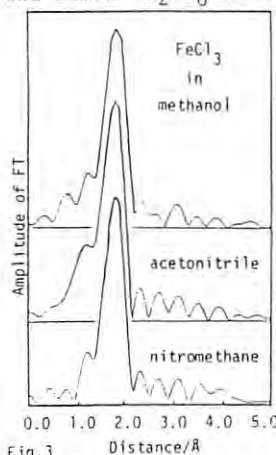


Fig. 3

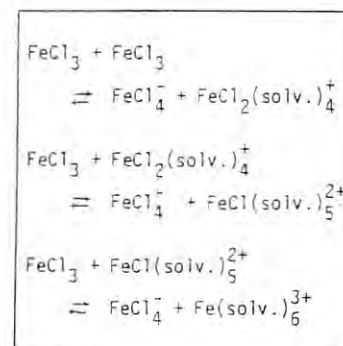


Fig. 4 Solvation mechanism

The Curve-fitting analyses of all the EXAFS data gave $2.22 \pm 0.02 \text{ \AA}$, which agrees with the Fe-Cl distance of FeCl_4^- , and about 3 for the coordination numbers, which is appreciably smaller than expected for FeCl_4^- . This can be understood if we assume that some solvated species $\text{FeCl}_x \cdot (\text{solv.})_{6-x}$ ($x=0,1,2$) are formed besides the main species FeCl_4^- , presumably as shown in Fig. 4.

1) D.L.Wertz and R.F.Kruh: J.Chem.Phys. 50(1969)4013.

POLARIZED XANES STUDIES OF TRANSITION METAL COMPLEXES
I. SQUARE PLANAR CuCl_4^{2-} COMPLEX

H. Kuroda, N. Kosugi, T. Yokoyama, K. Asakura and H. Ishii

Department of Chemistry and Research Center for Spectrochemistry, Faculty of Science, The University of Tokyo, Hongo, Bunkyo-ku, Tokyo 113 (JAPAN)

The shoulder structure on the absorption edge is known to be typical in Cu(II) complexes. Recently Bair and Goddard¹ have ascribed, from the model calculation, this shoulder to a group of dipole-allowed transitions involving $1s \rightarrow 4p$ simultaneous with ligand-to-metal charge transfer (LMCT). This newly proposed phenomenon 'shakedown' is widely received to be a new candidate for the shoulders, which were previously assigned as $1s \rightarrow 4s$ or unexplained. In order to confirm the shakedown phenomenon, we intended to measure polarized XANES spectra of a square planar CuCl_4^{2-} complex, creatininium tetrachlorocuprate, in molecular orientations (out-of-plane and in-plane) different from the previously measured orientation (only in-plane) by Hahn et al.²

The crystal was prepared according to the literature method. The x-ray absorption measurements were carried out at BL 10-B mainly as a test experiment of the EXAFS apparatus. Polarized spectra were obtained with the CuCl_4^{2-} plane perpendicular ($\parallel z$, out-of-plane, π) and parallel ($\parallel y$, in-plane, σ) to the polarization direction. For comparison, spectra of its powder sample and other two powder samples, $\text{CuCl}_4 \cdot 2\text{H}_2\text{O}$ and $[\text{NET}_4]_2[\text{CuCl}_4]$, were also measured.

Figure 1 gives the XANES spectra of the three powder samples. The shoulder in problem is the structure B. Figure 2 gives the polarized XANES for the single crystal together with the powder spectrum. Polarization dependence of B clearly reveals that B should be attributed not to $1s \rightarrow 4s$ but to $1s \rightarrow p\pi$.

We have carried out *ab initio* SCF-CI calculations on D_{4h} CuCl_4^{2-} . The results shown in Table indicate that the shoulder B should be ascribed to $1s \rightarrow 4p\pi$ simultaneous with LMCT. This transition is regarded as the shakedown double excitation. The shakedown phenomenon is expected for $1s \rightarrow p\sigma$ excitation processes as well as $1s \rightarrow p\pi$, and makes the powder spectrum complicated.

The LMCT accompanying $1s$ -to-valence one-electron excitation is presumed to take place generally for d^9 complexes ($n \neq 10$); thus, the shoulder structure typical in Cu(II) complexes can be assigned to the shakedown transition.

- 1) R. A. Bair and W. A. Goddard III: Phys. Rev. B 22 (1980) 2767.
- 2) J. E. Hahn, R. A. Scott, K. O. Hodgson, S. Doniach, S. R. Desjardins and E. I. Solomon: Chem. Phys. Letters 88 (1982) 595.

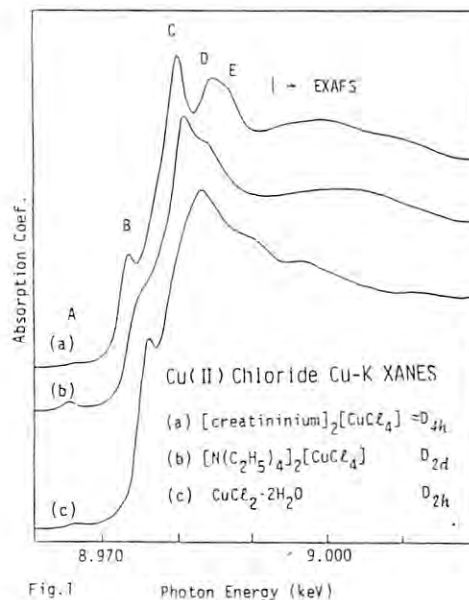


Fig.1 Photon Energy (keV)

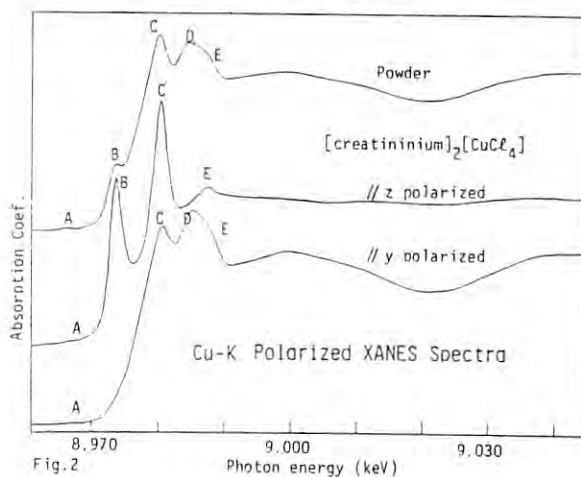


Fig.2 Photon energy (keV)

	obs.	calc.		assignment
		eV *	eV * f**	
A		0.0	0.0	$1s \rightarrow 3d_{x^2-y^2}$
B	$\parallel z$	7.1	8.0	$1s \rightarrow 4p\pi + \text{LMCT}$
-			10.9	$1s \rightarrow 4p\sigma + \text{LMCT}$
C	$\parallel z$	13.6	16.3	$1s \rightarrow 4p\pi$
C	$\parallel y$	13.8	17.8	$1s \rightarrow 5p\sigma + \text{LMCT}$
D	$\parallel y$	18.3	20.7	$1s \rightarrow 4p\sigma$
E	$\parallel z$	20.5	20.0	$1s \rightarrow 5p\pi$
E	$\parallel y$	21.5	24.6	$1s \rightarrow 5p\sigma$

*relative energy **oscillator strength

SHORT RANGE ORDER IN AMORPHOUS GeTe STUDIED
BY MEANS OF EXAFS

H. Oyanagi, K. Tanaka, T. Matsushita,[†] and M. Ito^{††}

Electrotechnical Laboratory, Sakura-mura, Niihari-gun, Ibaraki 305, Japan

[†]National Laboratory for High Energy Physics, Oho-machi, Tsukuba-gun, Ibaraki 305, Japan

^{††}The Institute of Physical and Chemical Research, Hirosawa, Wako-shi, Saitama 351, Japan

INTRODUCTION

X-ray RDF studies of amorphous Ge chalcogenides GeX (X=S, Se, Te) have reported the average coordination of three and shorter nearest neighbor distance than that of crystalline counterparts by 0.2-0.3 Å¹ whereas the coordination of a crystalline phase with a distorted NaCl structure is nearly six-fold. Recent spectroscopic studies² and x-ray absorption fine structure (EXAFS) experiments³ suggested the chemical order and 3-3 coordination in a-GeS and a-GeSe. However, early EXAFS⁴ and differential distribution function (DDF) studies⁵ favored a 4-2 coordination in a-GeSe.

This project is intended to establish the short range order in amorphous Ge chalcogenides. We present the EXAFS results of a-GeTe on the Ge K edge and demonstrate the existence of the chemical order around Ge atoms from the profile analysis of the EXAFS oscillation.

EXPERIMENTAL AND RESULTS

A-GeTe film samples were prepared by a sublimation of a crystalline phase in a vacuum of 10⁻⁸ Torr onto the aluminum-coated Mylar substrates at room temperature. A slow deposition rate (100Å/sec) was used to achieve the stoichiometry in a-GeTe samples. X-ray absorption experiments were performed with the EXAFS apparatus at BL 10B as part of the instrumentation project during the June-July run of 1982. Details of this apparatus are described elsewhere⁶. The energy resolution of the instrument was 1.6 eV at 11.1 keV with the photon flux of 10⁸-10⁹ photons/sec. Several layers of a-GeTe sample with a thickness of 2-3 μm were mounted on a sample holder of a cryostat and measured at low temperature.

Ge K edge EXAFS oscillations of a-GeTe (a) and c-GeTe (b) are presented in Fig. 1 after removing the pre-edge region and background absorption. Fig. 2 shows the Fourier transform results of $k\chi(k)$ multiplied by a window function over a k range between 5 and 16 Å⁻¹. In Fig. 2, (a) and (b) indicate the results for a-GeTe and c-GeTe, respectively. The positions of the peaks in radial distance are displaced from the real positions due to the phase shift. The two peaks observed in (b) are near neighbor Te atoms located at 2.86 Å and 3.17 Å. The most striking result is that the prominent peak observed in a-GeTe (a) is shifted toward smaller r by 0.26 Å and a shoulder peak is absent.

Secondly, the species of the nearest neighbor atoms were examined by comparing the k-dependence of the EXAFS oscillation with the back-scattering amplitude of Ge and Te atom. A brief inspection of Fig. 1 suggests that the scatterer atom is a heavy element in two phases from the profile of the envelope. The back-scattering amplitude of heavy elements show a large magnitude of oscillation at 3-4 Å⁻¹ and the minimum at 6 Å⁻¹ in k. Thus the k-dependence of the EXAFS oscillation in a-GeTe is interpreted as a result of the scattering due to Te atom.

More quantitative analysis has been performed by the least-squares fit of the experimental $\chi(k)$ of a-GeTe by a hypothetical sum of the Ge-Ge and Ge-Te correlations with various fractions. The introduction of a fractional Ge-Ge correlation degraded the R factor of a fit. These results strongly indicate that the chemical order exists in a-GeTe and the random bonding model is therefore not an appropriate description of the near neighbor environments around Ge atoms in a-GeTe.

Fig. 1

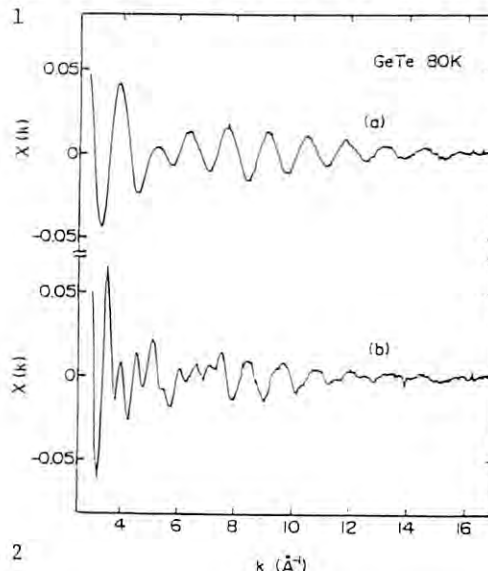
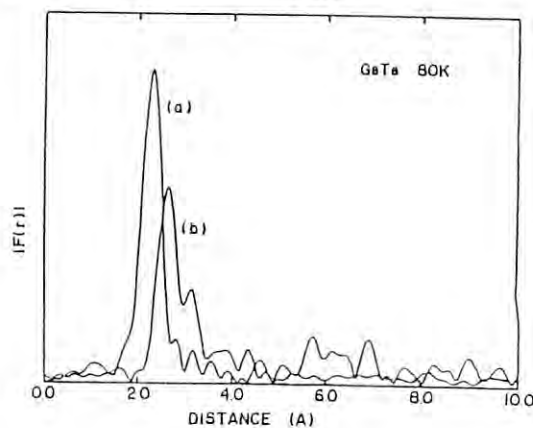


Fig. 2



REFERENCES

- 1) A. Bienenstock, F. Betts, and S. R. Ovshinsky, *J. of Non-Cryst. Solids*, **2** (1970) 347
- 2) P. Tronc, M. Bensoussan, A. Brenac, G. Errandonea, and C. Sebenne, *J. de Physique*, **38** (1977) 2493
- 3) H. Oyanagi, K. Tanaka, S. Hosoya and S. Minomura, *J. de Physique C4* **42** (1981) 221
- 4) D. E. Sayers, "Amorphous and Liquid Semiconductors" ed. by W. E. Spear, University of Edinburgh, Edinburgh (1977)
- 5) P. H. Fuoss, W. K. Warburton, and A. Bienenstock, *J. of Non-Cryst. Solids* **35-36** (1980) 1233
- 6) H. Oyanagi, T. Matsushita, M. Ito, H. Kuroda, and K. Kohra, in preparation.

EXAFS STUDY OF BROMINE-DOPED POLYACETYLENE

M. Tokumoto, H. Oyanagi, T. Ishiguro, H. Shirakawa,[†] H. Nemoto,[†] T. Matsushita,^{††} M. Ito,^{†††}
H. Kuroda^{††††} and K. Kohra^{††}

Electrotechnical Laboratory, Sakura-mura, Niihari-gun, Ibaraki 305, Japan

[†]Institute of Material Science, University of Tsukuba, Sakura-mura, Niihari-gun,
Ibaraki 305, Japan

^{††}National Laboratory for High Energy Physics, Oho-machi, Tsukuba-gun, Ibaraki 305, Japan

^{†††}The Institute of Physical and Chemical Research, Hirosawa, Wako-shi, Saitama 351, Japan

^{††††}Department of Chemistry and Research Center for Spectrochemistry, Faculty of Science,
The University of Tokyo, Hongo, Bunkyo-ku, Tokyo 113, Japan

INTRODUCTION

The room-temperature conductivity of polyacetylene is known to increase by many orders of magnitude on doping with electron acceptor such as iodine and bromine. In the case of iodine doping, the conductivity keeps increasing as the dopant concentration increases up to the saturation composition. In the case of the doping with more reactive bromine, the conductivity initially increases with the increase of dopant content, then its increase saturates at around 10-20% of bromine concentration, and a further doping up to 50-60% of bromine concentration leads to a gradual decrease in electrical conductivity. A more heavy doping results in an abrupt decrease in conductivity, leading to an insulator. This decrease in conductivity on heavy doping has been regarded as an evidence for substitution and/or addition reaction of bromine with polyacetylene. It has been a general understanding that these reactions are not effective at low doping level, say, less than 10% of bromine concentration.¹ Here we report the EXAFS study of the state of bromine in polyacetylene, with an unexpected result that the substitution and/or addition reactions are taking place even at low bromine concentration.²

RESULTS

Figure 1(a) shows the Br K spectrum of a sample taken at room temperature. The inset, Fig. 1(b), shows the EXAFS oscillations $\chi(k)$ as a function of photoelectron momentum k . Figure 2(b) shows the magnitude of the Fourier transform of the $\chi(k)$ curve from 1.8 to 14.0 \AA^{-1} in Fig. 1(b). Similar results for CBr_4 and other samples are also included in the figure. The two prominent peaks A and B in Fig. 2(a) are associated with Br-C and Br-Br distances in CBr_4 , respectively. The Fourier transforms of

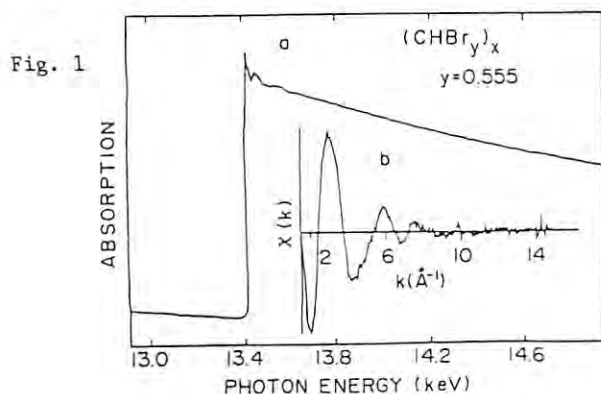


Fig. 1

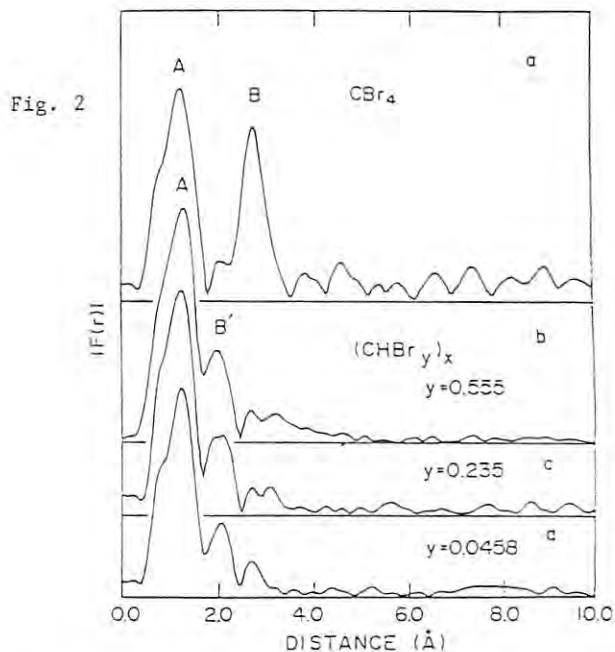


Fig. 2

the EXAFS data of all three $(\text{CHBr}_y)_x$ samples shown in Fig. 2(b) - (d), are characterized by the prominent peak A along with the shoulder peak B'. The peak A corresponds to the bond distance of about 1.95 \AA after the phase shift correction and can be assigned to Br-C bond. This assignment is consistent with the rapid decrease of the EXAFS oscillation with k as shown in Fig. 1(b). The fact that the observed Br-C bond distance lies close to the Br-C distance in CBr_4 indicates that some of the bromine atoms are forming direct chemical bond with polyacetylene chain either by substitution or addition reaction. We assign peak B' to the Br-Br bond since its position is close to the Br-Br distance of Br_3^- anion in brominated $(\text{SN})_x$. Important results are that (i) Br-C bond is clearly observed at Br concentration as low as 5%, (ii) the ratio between Br-C and Br-Br bonds seems to be nearly constant over the wide Br concentration ranging from 60% down to 5%.

REFERENCES

- 1) I. Ikemoto, Y. Cao, M. Yamada, H. Kuroda, I. Harada, H. Shirakawa and S. Ikeda: Bull. Chem. Soc. Jpn. 55, 721 (1982)
- 2) M. Tokumoto, H. Oyanagi, T. Ishiguro, H. Shirakawa, H. Nemoto, T. Matsushita, M. Ito, H. Kuroda and K. Kohra, to be published in Solid State Commun. (1983)

POLARIZED EXAFS STUDIES OF BROMINATED POLYACETYLENE: EVIDENCE FOR STRUCTURAL ORDERING OF BROMINE POLYIONS

H. Oyanagi, M. Tokumoto, T. Ishiguro, H. Shirakawa[†], H. Nemoto^{††}, T. Matsushita,^{†††}
M. Ito^{††††} and H. Kuroda^{†††††}

Electrotechnical Laboratory, Sakura-mura, Niihari-gun, Ibaraki 305, Japan

[†]Institute of Material Science, University of Tsukuba, Sakura-mura, Niihari-gun, Ibaraki 305, Japan

^{††}National Laboratory for High Energy Physics, Oho-machi, Tsukuba-gun, Ibaraki 305, Japan

^{†††}The Institute of Physical and Chemical Research, Hirosawa, Wako-shi, Saitama 351, Japan

^{††††}Department of Chemistry and Research Center for Spectrochemistry, Faculty of Science, The University of Tokyo, Hongo, Bunkyo-ku, Tokyo 113, Japan

INTRODUCTION

The extended x-ray absorption fine structure (EXAFS) studies of brominated polyacetylene¹ have shown that Br-C bonds exist in a wide range of dopant concentration (5-55%) indicating that the substitution and/or addition reactions take place even at the low doping level. These studies also observed Br-Br bonds which are attributed to bromine polyions. However, detailed information on the structure of bromine polyion or its geometrical arrangement were not available. This project aims at the determination of the form of bromine polyions and its geometrical arrangement utilizing the polarized EXAFS technique for oriented samples.

We present an evidence for the existence of highly oriented bromine polyions along the axis of polyacetylene chain.

EXPERIMENTAL AND RESULTS

The *cis*-rich polyacetylene films were prepared as previously described¹ and oriented by uniaxial drawing. Oriented samples were then doped with bromine at room temperature. Samples with different bromine concentration were obtained by controlling the vapor pressure of bromine and the length of time during which samples are exposed to bromine vapor. Special care was taken not to expose the doped samples to air in the course of experiments. Polarized EXAFS measurements were performed with the EXAFS apparatus at BL 10B. Details of the spectrometer are described elsewhere.² With a silicon (311) channel-cut monochromator, an energy resolution of 2.8 eV at Br K edge (13.47 keV) with the photon flux of 10^8 - 10^9 photons/sec was achieved.

The polarization dependence of x-ray absorption spectra were measured using two oriented

samples with the x-ray polarization axis parallel and perpendicular to the axis of orientation.

Fig. 2

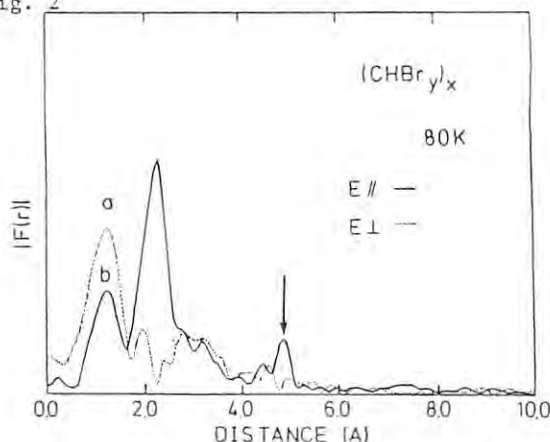


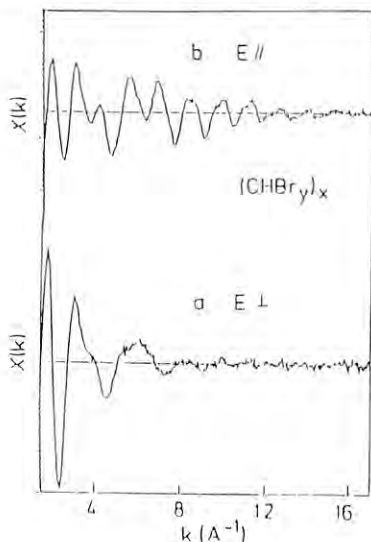
Fig. 1 presents the polarized EXAFS oscillations of brominated polyacetylene on the Br K edge measured at 80 K. In this figure, (a) and (b) indicate the $\chi(k)$ of perpendicularly and parallelly oriented sample, respectively. The bromine content y in $(\text{CHBr}_y)_x$ determined from the weight uptake is 0.145. A large anisotropy observed between (a) and (b) is interpreted as the evidence for the structural ordering of bromine polyions. This anisotropy indicates that the main scatterer atoms are carbon and bromine atoms in (a) and (b), respectively. The scattering amplitude of bromine peaks at a wavenumber k of 6 to 7 \AA^{-1} and extends to higher k of 16 \AA^{-1} while the amplitude of low z element like carbon drops sharply with increasing k .

Fig. 2 shows the results of Fourier transform of $k\chi(k)$ for perpendicularly oriented (a) and parallelly oriented (b) samples. The prominent peak located at 2.2 \AA which is due to the Br-Br bond is observed in a parallelly oriented sample, whereas this peak is not seen in the perpendicularly oriented sample. Further, the existence of the second nearest peak indicated by an arrow at 4.8 \AA suggests that the predominant species is Br_3 or a larger Br_{2n+1} chain. A weaker polarization dependence for Br-C bonds at 1.8 \AA and the structure at 3-3.5 \AA are analyzed and details of the geometrical arrangements of bromine polyions as well as bromine atoms bonded to carbon were obtained.

REFERENCES

- 1) M. Tokumoto, H. Oyanagi, T. Ishiguro, H. Shirakawa, H. Nemoto, T. Matsushita, M. Ito, H. Kuroda, and K. Kohra, to be published in Solid State Comm.
- 2) H. Oyanagi, T. Matsushita, M. Ito, H. Kuroda, and K. Kohra, in preparation.

Fig. 1



POLARIZATION DEPENDENT NEAR EDGE STRUCTURE OF POLYACETYLENE
DOPED WITH BROMINE AND IODINE

H. Oyanagi, M. Tokumoto, T. Ishiguro, H. Shirakawa[†], H. Nemoto^{††}, T. Matsushita,^{††}
M. Ito,^{†††} and H. Kuroda^{††††}

Electrotechnical Laboratory, Sakura-mura, Niihari-gun, Ibaraki 305, Japan

[†]Institute of Material Science, University of Tsukuba, Sakura-mura, Niihari-gun, Ibaraki 305, Japan

^{††}National Laboratory for High Energy Physics, Oho-machi, Tsukuba-gun, Ibaraki 305, Japan

^{†††}The Institute of Physical and Chemical Research, Hirosawa, Wako-shi, Saitama 351, Japan

^{††††} Department of Chemistry and Research Center for Spectrochemistry, Faculty of Science,
The University of Tokyo, Hongo, Bunkyo-ku, Tokyo 113, Japan

INTRODUCTION

Earlier EXAFS studies of brominated polyacetylene¹ have shown that the substitution and/or addition reaction takes place during the doping over a wide range of bromine concentration. The existence of Br-Br bonds indicated that bromines form polyions as well as Br-C bonds.

Recently, the polarized EXAFS studies on oriented polyacetylene films which are doped with bromine have established the structure of polyion and its geometrical arrangements.² This project is part of x-ray absorption studies to obtain the information on the structure and electron states of doped polyacetylene in order to understand the mechanism of doping. In this report, we present the results of polarization dependent near edge experiments for oriented polyacetylene films doped with bromine and iodine intended to study the *anisotropy in the bonding state of incorporated bromine and iodine*.

EXPERIMENTAL AND RESULTS

Sample preparation and doping with bromine was described previously.¹ Doping the oriented samples with iodine was performed in the same manner. Absorption experiments were performed with the EXAFS facility at BL 10B utilizing a silicon (111) double crystal monochromator for iodine L edge measurements whereas a silicon (311) channel-cut crystal was used for Br K edge experiments. Details of the EXAFS apparatus have been described elsewhere. Special care was taken to minimize the high harmonics in iodine L edge experiments. Spectral purity was ensured by a detuning of the parallel setting of two crystals. Samples with the direction of orientation parallel and perpendicular to the electrical field vector \vec{E} were successively measured at 80 K.

Fig. 1

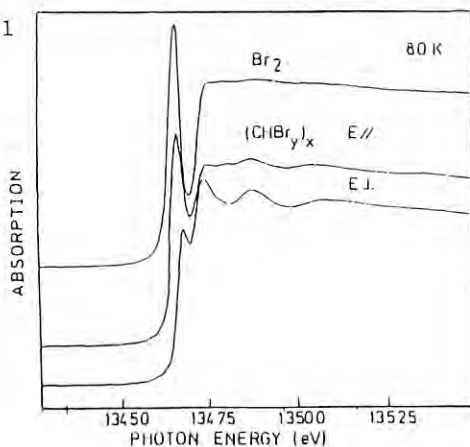
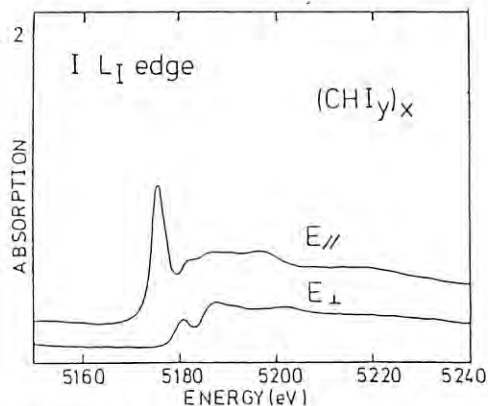


Fig. 1 presents the near edge structure of brominated polyacetylene on Br K edge with the x-ray polarization vector parallel and perpendicular to the axis of orientation. For comparison, the near edge structure of bromine gas is included. The most prominent peak observed at 13.462 keV in the near edge structure of bromine gas is due to the 1s-4p bound state transition. The most striking feature in the near edge structure of parallelly oriented sample is a sharp spike which originates from the same transition with that of bromine gas. These results clearly indicate the presence of Br-Br bonds in the direction of orientation, which is consistent with the polarized EXAFS results.²

Fig. 2



The near edge structure of perpendicularly oriented sample resembles that of brominated carbon compounds and therefore indicates the presence of Br-C bond perpendicular to the direction of orientation. Fig. 2 presents the near edge structures of iodinated polyacetylene on I L₁ edge measured at 80 K. Spectra taken with the photon polarization axis parallel and perpendicular to the axis of orientation are indicated. In the near edge structure of a parallelly oriented sample, a sharp resonance due to 2s-5p transition has been observed. Again, the near edge structure of a perpendicularly oriented sample shows the similar feature with that of brominated polyacetylene.

These results demonstrate the *anisotropy of bonding state which is interpreted as an evidence for structural ordering of bromine and iodine polyions*.

REFERENCES

- 1) M. Tokumoto, H. Oyanagi, T. Ishiguro, H. Shirakawa, H. Nemoto, T. Matsushita, M. Ito, H. Kuroda, and K. Kohra, to be published in Solid State Comm.
- 2) H. Oyanagi, M. Tokumoto, T. Ishiguro, H. Shirakawa, H. Nemoto, T. Matsushita, M. Ito, and H. Kuroda, in this report.

FLUORESCENCE EXAFS STUDIES OF HEMOPROTEIN: THERMAL SPIN EQUILIBRIUM

H. Oyanagi, T. Izuka,[†] R. Makino,[†] T. Matsushita,^{††} and M. Ito^{†††}[†]Electrotechnical Laboratory, Sakura-mura, Niihari-gun, Ibaraki 305, Japan^{††}Department of Biochemistry, Faculty of Medicine, Keio University, Shinano-machi, Shinjuku-ku, Tokyo 160, Japan^{†††}National Laboratory for High Energy Physics, Ohno-machi, Tsukuba-gun, Ibaraki 305, Japan^{††††}The Institute of Physical and Chemical Research, Hirosawa, Wako-shi, Saitama 351, Japan

INTRODUCTION

Fluorescence EXAFS technique has been successfully applied to functional studies of hemoproteins. More recently, the x-ray absorption near edge structure (XANES) attracts attention as a new structural tool which provides more elaborate information of near neighbor environments.²

This project aims at the structural studies of thermal spin equilibrium between high spin and low spin states in some hemoproteins utilizing both EXAFS and XANES by fluorescence detection. We present here the preliminary results of the first attempt to observe the thermal spin equilibrium in alkali-met myoglobin.

EXPERIMENTAL AND RESULTS

The beam time was allocated during the Oct.-Dec. run of 1982 followed by the Feb.-Mar. run of 1983. Experiments were performed at BL 10B using the EXAFS facility with some modifications. The spectrometer is described elsewhere³ in detail. A pure Ge solid state detector was used as a fluorescence detector. Sample solution filled in an aluminum cell with Kapton windows is mounted on a copper holder of a cryostat and placed 45 degrees from the incident beam. The detector is located perpendicular to the beam axis. A single channel analyzer was used to discriminate the fluorescence signal from the background radiation caused by elastic and inelastic scattering of the incident beam.

The photon flux of the incident beam is 10^8 - 10^9 photons/sec with a typical resolution of 1 eV at Fe K edge (7.1 keV). Temperature dependence of Fe K edge absorption spectrum of 20 mM alkali-met myoglobin was measured between 80 K and room temperature. Fig. 1 presents Fe K edge spectra of alkali-met myoglobin at (a) 80 K, (b) 200 K, and (c) 300 K, respectively. These data were obtained by averaging 2-3 runs with 1 second integration per data point. The signal-to-background ratio was roughly 10 above the edge. Summarizing the results, the features extending 50-100 eV above the edge have most changed with temperature. The feature 17 eV above threshold increases its intensity and grows into a shoulder with decreasing temperature.

More detailed discussions are difficult due to a poor signal-to-noise ratio of the spectrum which amounts to a few % in worst cases. Above the Fe K edge, the total fluorescent x-rays were 10^3 counts/sec. With a one second integration, this photon flux gives the photon statistics of several % which is the same order of the EXAFS oscillation in the high k region. Since the scattering amplitude of light atom such as carbon and nitrogen decreases rapidly with the increase of k and hence the modulation in the absorption cross section is on the order of a few %, the photon statistics better than 0.1 % is essential. However, using the unfocused beam and the current

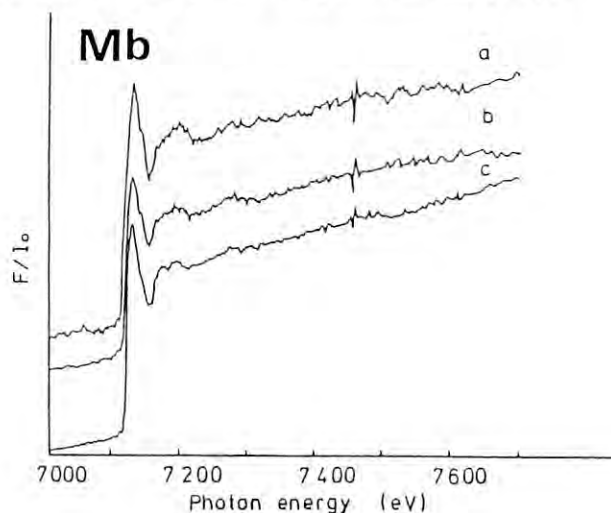


Fig. 1

detector system, this condition is attained by a typical run taking more than 100 hours. This is a serious problem from the viewpoints of radiation damage. The area of a solid state detector is 100 mm^2 and subtends only 1.3 % of 4π steradian in solid angle. Thus it is necessary to build a large area detector system which covers more solid angle to improve the counting efficiency. The total count rate improves with a large area detector system and a focused beam by 10^2 - 10^3 . Based on the results of this project a new multi-detector system was designed and built. Details and performance of this apparatus will be described elsewhere.

REFERENCES

- 1) B. Chance, R. Fischetti, and L. Powers, *Biochemistry*, **22** (1983) 3820.
- 2) P. Durham, S. S. Hasnain, A. Bianconi, L. Incoccia, S. Morante, and J. B. Pendry, *Daresbury Laboratory, SERC DL/SCI/p363T* (1982).
- 3) H. Oyanagi, T. Matsushita, M. Ito, H. Kuroda, and K. Kohra, in preparation.
- 4) Radiation damage was checked by spectroscopy after the experiment which took typically 2-3 hours. No indication of reduction has been observed.

STRUCTURAL STUDIES OF THE SUPERIONIC CONDUCTOR $\text{Rb}_4\text{Cu}_{16}\text{Cl}_{13}\text{I}_7$
BY X-RAY ABSORPTION SPECTROSCOPY

H. Oyanagi, M. Tokumoto, T. Ishiguro, T. Matsushita[†] and M. Ito^{††}

Electrotechnical Laboratory, Sakura-mura, Niihari-gun, Ibaraki 305, Japan

[†]National Laboratory for High Energy Physics, Ohno-machi, Tsukuba-gun, Ibaraki 305, Japan

^{††}The Institute of Physical and Chemical Research, Hirotsawa, Wako-shi, Saitama 351, Japan

INTRODUCTION

The solid electrolyte with the highest room-temperature conductivity ($0.4\Omega^{-1}\text{cm}^{-1}$) has been reported for the quaternary system CuCl-RbCl-CuI^1 . In this system with the chemical formula of $\text{Rb}_4\text{Cu}_{16}\text{Cl}_{13}\text{I}_7$ which has a similar structure with that of RbAg_4I_5 , the charge carriers are Cu ions.

Superionic conductors have been extensively studied by the extended x-ray absorption fine structure (EXAFS)² as well as x-ray and neutron diffraction techniques. Recently, a model structure has been proposed to explain the pair correlation functions obtained from EXAFS experiments².

We present the results of EXAFS and near edge experiments of $\text{Rb}_4\text{Cu}_{16}\text{Cl}_{13}\text{I}_7$ on Cu and Rb K edges to elucidate the average structure and study the conduction mechanism in this novel superionic conductor.

EXPERIMENTAL AND RESULTS

$\text{Rb}_4\text{Cu}_{16}\text{Cl}_{13}\text{I}_7$ samples were prepared as previously described¹ in an inert atmosphere starting from purified CuCl , CuI , and RbI . Samples and reference compounds such as CuI , CuCl , and RbI were ground into a fine powder in a glove box and sandwiched between Scotch tapes. Care was taken not to expose these materials to air during the sample preparation and mounting them on a sample holder of a cryostat. The experiments were performed with the EXAFS apparatus at BL 10B using a silicon (311) channel-cut monochromator. The details of the spectrometer are described elsewhere³. The energy resolution of 1 eV and the photon flux of 10^8 photons/sec were achieved at Cu K edge (9 keV). The beam time was allocated as part of the instrumentation project during the June-July run of 1982.

Temperature dependence of the absorption spectra for $\text{Rb}_4\text{Cu}_{16}\text{Cl}_{13}\text{I}_7$ as well as reference compounds on the Cu and Rb K edges were measured between 8.5 K and room temperature. The temperature dependence of the absorption near edge structure for $\text{Rb}_4\text{Cu}_{16}\text{Cl}_{13}\text{I}_7$ on the Cu K edge is presented in Fig. 1.

The lowest energy feature near threshold

Fig. 1

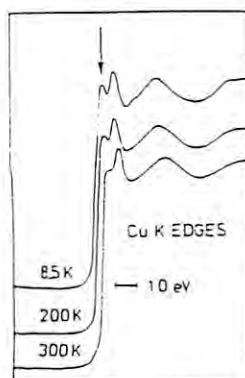
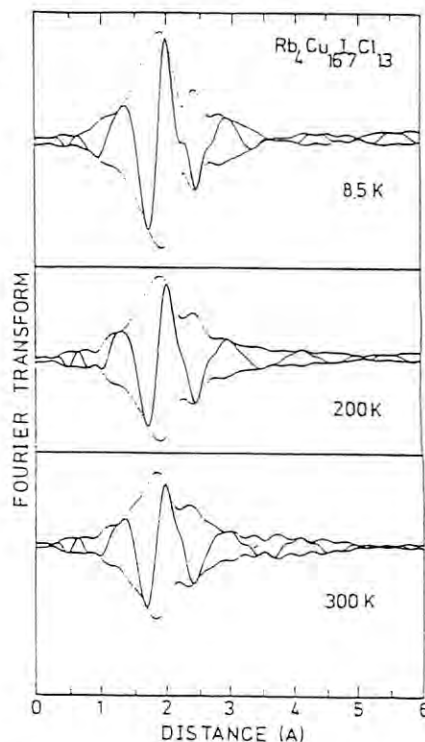


Fig. 2



indicated by an arrow decreases its intensity with increasing temperature due to a wider distribution of mobile Cu ions at higher temperature.

Fig. 2 summarizes the Fourier transform results of $k\chi(k)$ for $\text{Rb}_4\text{Cu}_{16}\text{Cl}_{13}\text{I}_7$ in the k range from 3.5Å^{-1} to 12.0Å^{-1} . The structures observed at 1.5-2.8 Å in radial distance are due to the three pair correlations, Cu-Cl, Cu-I, and Cu-Cu. The most prominent peak at 1.8 Å and the second peak at 2.4 Å are Cu-Cl and Cu-I correlations, respectively. The most striking result is that these peaks are shifted to the smaller r with a broader distribution as temperature increases. This apparent peak shift between 8.5 K and room temperature is roughly 0.1 Å.

The third broad feature at 2.9 Å is interpreted as the Cu-Cu correlation, which is much larger than the average distance between the nearest Cu sites determined by x-ray works. A small anharmonicity in the effective potential felt by mobile Cu ions is predicted from the magnitude of the temperature dependence of the amplitude of the EXAFS oscillation, which is consistent with the weak diffuse background in the x-ray diffraction pattern even at room temperature⁴.

REFERENCES

- 1) T. Takahashi, O. Yamamoto, S. Yamada, and S. Hayashi, *J. Electrochem. Soc.* **126** (1979) 1654
- 2) J. B. Boyce and T. M. Hayes "Physics of Superionic Conductors", Springer-Verlag, Berlin, 1979
- 3) H. Oyanagi, T. Matsushita, M. Ito, H. Kuroda, and K. Kohra, in preparation.
- 4) M. Tokumoto, N. Ohnishi, Y. Okada, and T. Ishiguro, *Solid State Ionics*, **3/4** (1981) 289

NEAR EDGE STRUCTURE STUDIES OF TETRAHEDRALLY BONDED
COMPOUNDS: Ge, GeO₂, GaAs, and ZnSe

H. Oyanagi, T. Fujikawa,[†] T. Matsushita,^{††} M. Okuno,^{†††} and M. Ito^{††††}

Electrotechnical Laboratory, Sakura-mura, Niihari-gun, Ibaraki 305, Japan

[†] Faculty of Engineering, Yokohama National University, Yokohama 240, Japan

^{††} National Laboratory for High Energy Physics, Ohno-machi, Tsukuba-gun, Ibaraki 305, Japan

^{†††} Research Laboratory of Engineering Materials, Tokyo Institute of Technology,
Midori-ku, Yokohama 227, Japan

^{††††} The Institute of Physical and Chemical Research, Hirosawa, Wako-shi, Saitama 351, Japan

INTRODUCTION

Recent interests in the x-ray absorption near edge structure (XANES) which probes into the unoccupied electron states and geometry of the near-neighbor atoms around an excited atom have initiated extensive studies on a number of materials.¹

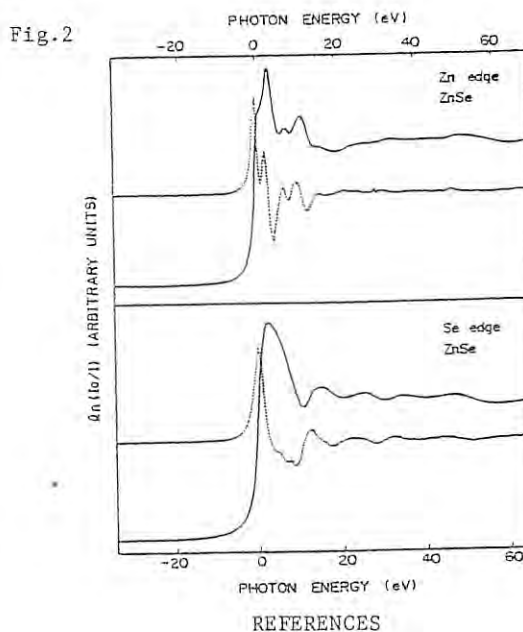
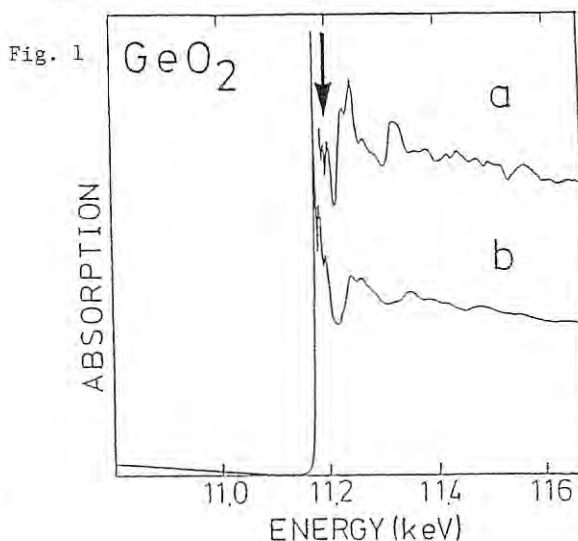
This project is two-fold. Firstly, we intend to analyze XANES of some tetrahedrally bonded covalent materials, Ge, GeO₂, GaAs, and ZnSe based on the multiple scattering theory² and band calculation approach. This study has its goal in understanding the origins of near edge structure based on two different theoretical approaches. Secondly, we attempt to obtain the information on details of unfilled band structure and geometrical arrangements of near neighbor atoms. The latter information is used to analyze the medium range order in glasses and biological systems.

EXPERIMENTAL AND RESULTS

X-ray absorption experiments were performed at BL 10B, Photon Factory, using the EXAFS facility as part of the instrumentation project during June-July run of 1982. Details of the spectrometer are described elsewhere.³ A silicon (311) channel-cut monochromator was used and a resolution with the photon flux of 10^6 photons/sec was achieved at 9 keV. The samples were polycrystalline powders sandwiched between Scotch tapes. For GeO₂, two polymorphs with hexagonal and tetragonal structure were measured. Ge atoms in a hexagonal structure are coordinated with four oxygen atoms whereas Ge atoms in a tetragonal structure are coordinated with six oxygen atoms.

Ge K edge XANES of Ge and GeO₂ were measured at room temperature and 80 K. Both cation and anion K edge data of GaAs and ZnSe were measured at room temperature. Fig. 1 presents the near edge structures of tetragonal (a) and hexagonal (b) GeO₂. Overall features were similar with the previous work.⁴ However, this work has first resolved the fine structures near threshold as indicated by an arrow. This structure is now analyzed by a multiple scattering theory.²

Fig. 2 presents the near edge structures of ZnSe on Zn K and Se K edges. The derivatives of raw spectra are indicated in dotted line. The most striking difference between the two spectra is that a small bump 10 eV above the Zn (cation) edge is absent in the Se (anion) edge. This near edge feature is interpreted in terms of the partial density of states in the lowest conduction band since the near neighbor environments are the same for anion and cation species in a zincblende structure. A band calculation based on a pseudopotential method is in progress.



REFERENCES

- 1) "EXAFS and Near Edge Structure" ed. by A. Bianconi, L. Incoccia, and S. Stipcich, Springer-Verlag, Berlin 1983.
- 2) T. Fujikawa, T. Matsuura, and H. Kuroda, J. Phys. Soc. Jpn. 52 (1983) 905.
- 3) H. Oyanagi, T. Matsushita, M. Ito, H. Kuroda, K. Kohra, in preparation.
- 4) W. F. Nelson, I. Siegel, and R. W. Wagner, Phys. Rev. [2] 127 (1962) 2025.

EXAFS STUDY ON PREMELTING PHENOMENON OF GALLIUM

M. Hida, H. Maeda^{a)}, Y. Ysu^{b)}, S. Iida^{c)}, H. Terauchi^{c)}, N. Kamijo^{d)}, T. Murata^{e)}, I. Watanabe^{f)}

Sch. of Eng., Okayama Univ., Okayama 700, a)Dept. of Chem., Okayama Univ., Okayama 700, b)Res. Inst. of Min'l Dress'g Metall'y, Tohoku Univ., Sendai 980, c)Dept. of Phis., Kwansai-Gakuin Univ., Nishinomiya 662, d)Gov. Ind. Res. Inst., Osaka, Ikeda 563, e)Kyoto Univ. Education, Kyoto 612, f)Dept. of Chem., Osaka 560

Introduction

The absence of premelting in crystalline gallium has been reported in spite of anomalous metal, gallium which increases its density about 3% on melting^{1),2)}. On the other hand, EXAFS spectroscopy and density measurement by using the laboratory facilities confirmed the existence of premelting, not partial melting, phenomenon which has been considered as formation of interstitial or Frenkel-type defects besides vacancies³⁾. Here we report the results of the EXAFS and XANES studies on the local structure of crystalline, premelted and melted gallium with use of a sample through our whole experiment.

Experiments

X-ray absorption measurements near Ga-K edge was made at 25.87°, 29.70° and 32.00°C-- corresponding to crystal(CR-), premelted(PM-) and melted gallium(ML-Ga), respectively-- with synchrotron radiation by use of the EXAFS facilities installed at the beam line 10-B in Photon Factory. The surveying region of X-ray absorption spectra was 10.025 to 11.473 keV. In XANES region(10.325 to 10.474 keV), small step scanning of Si monochromators was carried out in the practice of 0.0011 keV.

High purity(6N) gallium was filed, suitably stacked in thickness on Scotch tape and held together with aluminium foils in the sample holder made of copper. The holder has a small rectangular hole through which X-rays are passed and a water circulating system for controlling the sample temperature. The temperature control for the sample was fixed at a maximum fluctuation of 0.03°C by a precise temperature regulator.

In obtaining the EXAFS function $\chi(k)$, the background level for higher shell and the absorption coefficient for isolated atoms are subtracted from the observed absorption coefficient by using a Victoreen fit and by cubic spline technique⁴⁾.

Results and Discussion

The Fourier transforms of $\chi(k)$ obtained are shown in Fig.1. The first and second peaks marked by arrows in Fig.1 seem to be identified as the first shell(one atom contained) and the second shell(six atoms contained) of RSF. The peak positions of gallium atoms in the above three states are summarized in Table 1.

The premelting state is characterized with a remarkable proximity of the nearest neighbor atomic shell.

Fig.2 shows the results of XANES obtained from the above absorption coefficient of gallium in the three states. The first peak positions

of crystalline and premelted gallium are almost same. The XANES of the crystalline gallium has a substructure being different from that of gallium in other two states. The peak height which means the density state of electrons is maximum for the premelted gallium.

References

- 1) H. Wenzl and G. Mair : Z. Physik B21 (1975) 95.
- 2) G. Mair, K. Hamacher and H. Wenzl : Z. Physik B24 (1976) 301.
- 3) M. Hida, H. Maeda, N. Kamijo, K. Tanabe, H. Terauchi, Y. Tsu and S. Watanabe : Proc. 5th. Int'l Conf. on Liquid and Amorphous Metals, (Los Angeles, August, 1983) to be published.
- 4) H. Maeda, H. Terauchi, K. Tanabe, N. Kamijo, M. Hida and H. Kawamura : Jpn. J. Appl. Phys. 21 (1982) 1342.

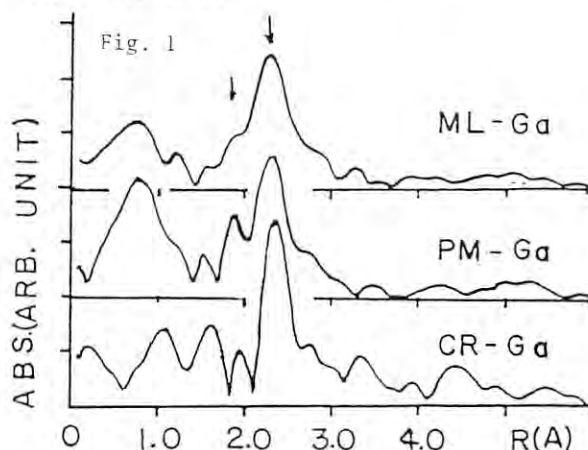
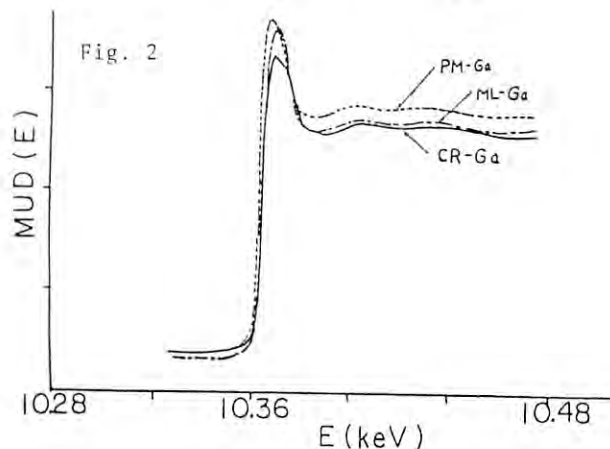


Table 1

	1 st. peak R_1 (Å)	2 nd. peak R_2 (Å)
CR-Ga	1.98	2.37
PM-Ga	1.90	2.30
ML-Ga	1.91	2.27



XAFS STUDY ON LATTICE RELAXATION OF ULTRA FINE NICKEL PARTICLES

M. Hida, H. Maeda^{a)}, N. Wada^{b)}, K. Kimura^{c)}, T. Morimoto^{a)}, Y. Kuroda^{a)}, S. Iida^{d)}, H. Terauchi^{d)}, N. Kamijo^{e)}, Y. Tsu^{f)}, T. Murata^{g)}

Sch. of Eng., Okayama Univ., Okayama 700, a)Dept. of Chem., Okayama Univ., Okayama 700, b)Dept. of Phys., Nagoya Univ., Nagoya 464, c)Instrm. Centr., Inst. for Molec. Sci., Aichi, Okazaki, d)Dept. of Phys., Kwansei-Gakuin Univ., Nishinomiya 662, e)Gov. Ind. Res. Inst., Osaka, Ikeda 563, f)Res. Inst. of Min'l Dress'g and Metall'gy, Tohoku Univ., Sendai 980, g)Kyoto Univ. of Education, Kyoto 612

Introduction

It has been known that ultra fine particles of metal are chemically active less 50 Å in particle size and has no mechanical strain observed by using X-ray diffraction method¹⁾. From this facts it is expected that some kinds of remarkable lattice relaxation on the surface of ultra fine particles unlike usual bulk metal. However it is very difficult to prepare clean surface ultra fine particles as a sample of EXAFS and also difficult to reveal the relaxation effects on the RSF(radial structure function)obtained from EXAFS data. As the first step of lattice relaxation study, here we report the effects of contamination, cold working and heat treatment on the RSF of some kinds of nickel and oxide(NiO) materials.

Experiments and Results

Seven samples used in this study are listed in Table 1. X-ray absorption measurements near Ni-K

Table 1

sample name	description
UFP-Ni	ultra fine nickel particles, estimated to be about 100 Å in size, are made by vaporization in 80 Torr He atmosphere and the paraffin is evaporated in vacuum to prevent the contamination of nickel particles as vaporized.
CMP-Ni	ready made nickel particles on commercial base, about 300Å.
VAP-Ni	prepared from CMP-Ni evacuated at 450° C and kept in vacuum during EXAFS measurement.
FIP-Ni	filed nickel particles, not annealed, less 38 μm.
ANF-Ni	nickel foil annealed in vacuum, 10 μm in thickness. used as a reference sample of Ni.
PYP-NiO	reference sample of NiO particles made by pyrolyzing Ni(OH) ₂ , about 28 μm in size.
VAC-NiO	prepared from PYP-NiO evacuated at 450° C and the same procedure as for VAC-Ni was employed on measuring EXAFS.

edge were made at room temperature with synchrotron radiation by use of the EXAFS port 10-B.

Same data processing and analysis in obtaining the RSF's are applied to X-ray absorption coefficient of nickel(fcc, a=3.52 Å) and nickel oxide(rhombohedral, a=2.95 Å, α=60°.4', close to rock salt lattice a=4.17 Å). Fig. 1 shows the RSF's of the seven samples. Some remarkable characteristics derived from Fig. 1 are summarized as follow :

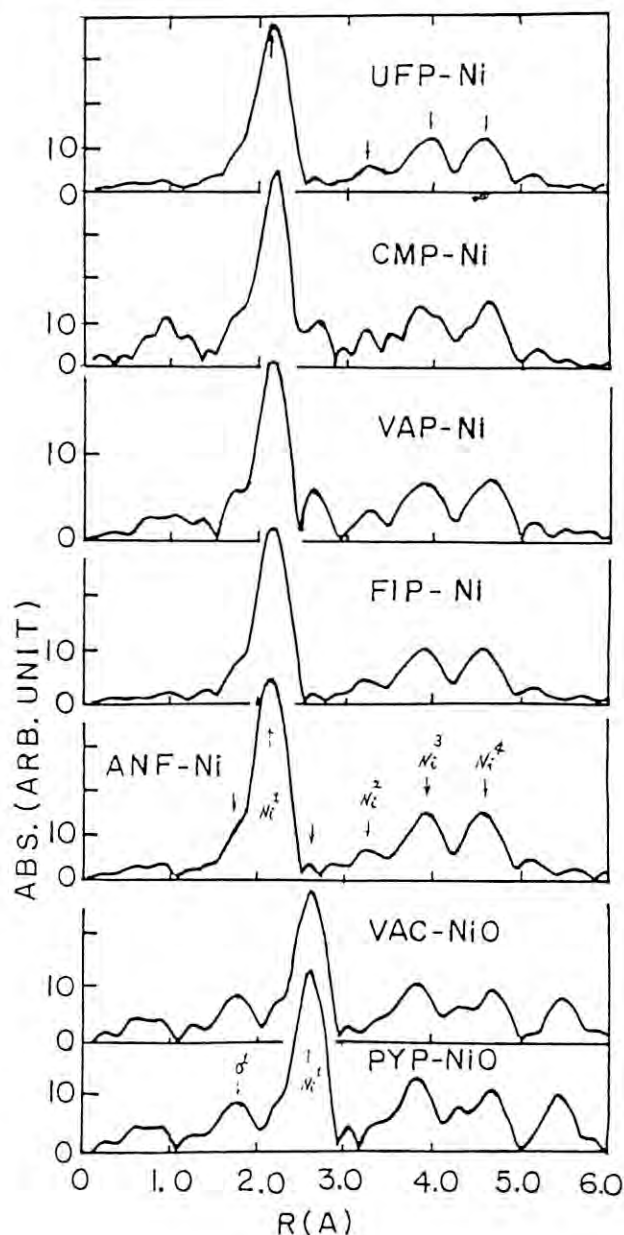


Fig.1

- 1) Our sample of ultra fine particles, UFP-Ni is as clean as the annealed nickel foil sample, ANF-Ni is.
 - 2) The RSF of UFP-Ni(with no lattice strain expected¹⁾) resembles to that of the filed nickel sample, FIP-Ni(with lattice strain) in their profiles. However the former profile seems to be derived chiefly from its atomistic surface roughness.
 - 3) All peak position of RSF for UFP-Ni is in good agreement with that of annealed nickel foil sample ANF-Ni. But both the peak height and width of UFP-Ni are appreciately lower and wider than those of ANF-Ni, respectively.
 - 4) The commercial based fine nickel particles sample, CMP-Ni is very dirty, and its all peak position of RSF with exception of the first peak is considerably differe from those of annealed nickel sample, ANF-Ni. The dirty particles sample has some sharp peaks, and some of them are fairly consistent with the peaks of nickel oxide sample, PYP-NiO.
 - 5) There are atoms with short bond length about 1 A in the commercial based sample of CMP-Ni, and nearly half atoms(estimated from the change of the hight of peak in the RSF) are reduced by evacuation at 450° C . It is assumed that those short bond atoms are related to water molecules adsorpted. The evacuated sample, VAP-Ni has still same magnitude peaks corresponding to the peaks of oxygen and nickel in oxcide on the particle, CMP-Ni
- We are planning to verify the surface structure of clean ultra fine particle(30-100 A) by the electronic and the detail atomistic information obtained from analysing the XANES and applying the curve fitting method to the EXAFS data, respectively.

Reference

- 1) N. Wada : Jpn. J. Appl. Phys., 8(1969) 551.

LOCAL LATTICE STRUCTURE IN SOLID SOLUTIONS OF ALKALI HALIDES

T. Murata, H. Maeda*, M. Hida**, H. Terauchi[†], N. Kamijo^{††}

Dept. of Phys., Kyoto Univ. of Education, Kyoto 612, Dept. of Chem., Okayama Univ., Okayama 700*,[†]
Sch. of Eng., Okayama Univ., Okayama 700**, Dept. of Phys., Kwansai-Gakuin Univ., Nishinomiya 662,^{††}
Gov. Ind. Res. Inst., Ikeda 536.

Introduction

It is well known that heavy halogen ions substitute easily in alkali halide crystals and even form dimers and trimers with increasing concentration, and finally gather into clusters. This effect has mainly been investigated by the observation of the change in the shape of the absorption bands¹⁾ which appears in the tail of the host crystal in the ultraviolet range. This has been interpreted as a localized exciton. The formation of clusters has been confirmed by the analysis of emission spectra excited with the²⁾ photons at the localized exciton energy region.

The optical measurements imply a displacement of the first neighbour ions around the solute ion. EXAFS is the only adequate technique to probe the local environment around a dilute foreign ion and to measure the magnitude of the relaxation.

KCl_{1-x}Br_x solid solution system was chosen to observe the^x above effect by measuring the EXAFS spectrum above the K-edge of Br⁻-ion. The results of the same system were previously reported³⁾ in the case of lower concentration range ($x < 0.10$). The purpose of the present experiment is to extend the concentration range up to $x = 0.50$, and to confirm the effect of the local lattice relaxation which was observed in the previous work.

Experimental

X-ray absorption measurements above the K-edge of Br⁻ (13.475keV) were made at the EXAFS experiment station installed in the BL-10B. Samples were prepared as follows: The powder ground finely from the ingot of the mixture was put into acetone, and was stirred well. The suspended sample in the acetone was filtered with a membrane filter. After the evaporation of the acetone, a homogeneous layer with an appropriate thickness could be obtained. Measurements were made at room and low temperatures (about 60K). Data were analysed with a standard method⁴⁾. Fast Fourier transform (FT) with 2048 points was performed. In Fig. 1 is shown the result of the magnitude of $k\chi(k)$ of KBr at 60K.

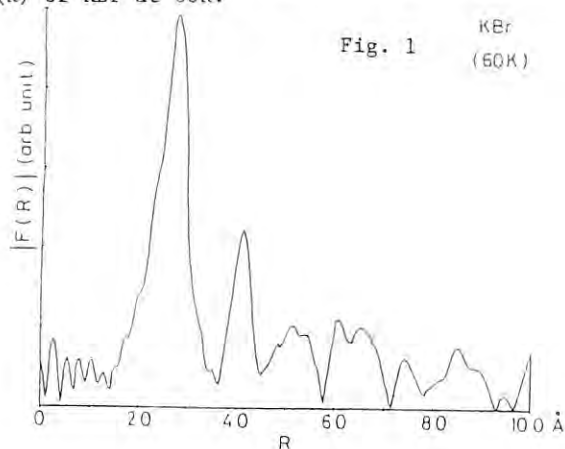


Fig. 1 KBr
(60K)

Discussion

The previous work revealed a large value of the first shell radius around a foreign Br⁻ ion in the host KCl compared to the average interionic distances in the ionic solutions. In Table I are shown the peak positions of the magnitude of FT in various samples at 60K. The results clearly show the similarity of the interionic distance with the value in pure KBr.

Table I. Peak Positions of the Magnitude of FT.

x (concentration of Br ⁻ in KCl)	Peak Positions in Å
1.00 (Pure KBr)	2.695
0.08	2.67
0.10	2.65
0.12	2.65

Recently Mikkelsen and Boyce reported similar effect in a semiconductor alloy system of Ga_{1-x}In_xAs. The system is well known to obey the Vegard's law in the whole concentration range as in the present system, that is, the interatomic distances change linearly with the concentration. This fact has been interpreted with the assumption of the virtual crystal approximation. The analysis of the EXAFS data revealed a very small change of the nearest neighbour distances around Ga and In ions as x varies from 0.01 to 0.99. They concluded that the virtual crystal model does not hold at the atomic level, but holds at least beyond the second neighbour sublattice.

The present results seem to be similar and coherent with the above discussion. The positions of the peak of FT magnitude in the mixtures are not very different from the value of KBr, contrary to a linear change in the lattice constants between the value of pure KCl and KBr³⁾.

Detailed analysis of the curve fitting of the back Fourier transform is in progress.

References

- 1) T. Murata; J. Phys. Soc. Jpn. 25(1968)1632.
- 2) H. Nakagawa; J. Phys. Soc. Jpn. 34(1973)410.
- 3) T. Murata, P. Lagarde, A. Fontaine, D. Raoux; "EXAFS and Near Edge Structure" (Springer Verlag, Berlin and Heidelberg, 1983) p. 271.
- 4) D. Raoux et al.; Rev. Phys. Appl. 15(1980)1079.
- 5) J.C. Mikkelsen, Jr., and J.B. Boyce; Phys. Rev. Letters 49(1982)1412.

EXAFS STUDY ON THE LOCAL STRUCTURE NEAR THE MARTENSITIC PHASE TRANSITION OF AuCuZn_2

H. Terauchi, S. Iida, K. Tanabe, K. Kikukawa, Y. Nishihata, H. Maeda*, M. Hida**, N. Kamijo***, T. Murata****

Dept. of Phys., Kwansai-Gakuin Univ., Nishinomiya 662, Dept. of Chem. Okayama Univ., Okayama 700*, Sch. of Eng., Okayama Univ., Okayama 700**, Gov. Ind. Res. Inst., Ikeda 536***, Dept. of Phys., Kyoto Univ. Education, Kyoto 612****

The Fourier transform method of the EXAFS spectra is one of the powerful techniques for investigating the atom-specific local structure of materials. Here we report the result of the EXAFS study on the local structure near the martensitic phase transition of AuCuZn_2 .

AuCuZn_2 alloy undergoes a martensitic phase transition at about 280K from bcc-based Heusler structure to fcc-based structure with the long period $3R$ stacking order characterized by $3R$.¹⁾ Towards the transition temperature the crystal becomes soft against the shear stress.²⁾ A new premartensitic metastable phase of AuCuZn_2 was found at room temperature.³⁾ Here we discuss the local atomic arrangement of the premartensitic phase.

X-ray absorption measurements near the Au- L_3 , Cu-K and Zn-K edges were made at room temperature with synchrotron radiation by use of the EXAFS facilities installed at the beam line 10-B. In obtaining the EXAFS function $X(k)$, the background level is subtracted from the observed absorption coefficient by using a Victoreen fit and the absorption coefficient for an isolated atom is obtained by the cubic spline technique.⁴⁾

The Fourier transform of $X(k)$ obtained near the Au- L_3 edge is given in Fig. 1, where the magnitude and imaginary part are shown. There are

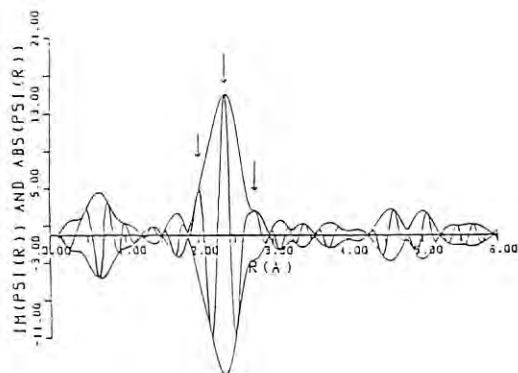


Fig. 1

three peaks in the range from 1.8 Å to 3.0 Å. The atomic distances from Au atom are summarized in Table I. The actual distances are given by assuming the phase shift for a Zn atom (0.20 Å). The calculated Au-Zn distances are also given in the table where the displacement of the Au atom along the $[110]$ direction is estimated to be 0.50 Å. Almost same results are obtained from

Table I. Atomic distances from Au

atoms	$R_{\text{obs.}} (\text{Å})$	$R_{\text{act.}} (\text{Å})$	$R_{\text{calc.}} (\text{Å})$
2Zn	1.99	2.19	2.16
4Zn	2.35	2.56	2.60
2Zn	2.75	2.95	2.97

the Fourier transforms of $X(k)$ near the Cu and Zn edges. There is a fairly good agreement between the actual and calculated distances. This implies that the local atomic displacements of the premartensitic phase are related to the $3R$ structure and also the temperature dependent soft phonon mode observed by inelastic neutron scattering.³⁾ The detailed analysis of the temperature dependent EXAFS spectra and the least squared parameter fitting are in progress.

The authors wish to express their thanks to N. Nakanishi and Y. Yamada for supplying good specimens and fruitful discussions.

References

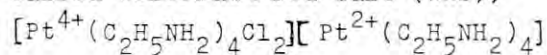
- 1) Y. Murakami, N. Nakanishi and S. Kachi: Jpn. J. Appl. Phys. **11** (1972) 1591
- 2) N. Nakanishi, Y. Murakami and S. Kachi: Scripta Metal. **5** (1971) 433
- 3) M. Mori, Y. Yamada and G. Shirane: Solid State Commun. **17** (1975) 127
- 4) H. Maeda, H. Terauchi, K. Tanabe, N. Kamijo, M. Hida and H. Kawamura: Jpn. J. Appl. Phys. **21** (1982) 1342

XANES STUDY ON THE LOCAL STRUCTURE OF A QUASI-1D MIXED VALENCE CRYSTAL
WOLFFRAM'S RED SALT

H. Terauchi, S. Iida, K. Tanabe, K. Kikukawa, Y. Nishihata, H. Maeda*, K. Hida**,
N. Kamijo***, T. Murata****

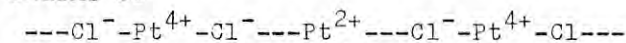
Dept. of Phys., Kwansai-Gakuin Univ., Nishinomiya 662, Dept. of Chem., Okayama Univ.
Okayama 700*, Sch. of Eng., Okayama Univ., Okayama 700**, Gov. Ind. Res. Inst.,
Ikeda 536***, Dept. of Phys., Kyoto Univ. Education, Kyoto 612****

A number of insulating chain crystals have been investigated extensively because of interest in the fascinating phenomena due to a strong electron-phonon coupling. Here we report the result of the x-ray absorption near edge structure (XANES) study on a quasi-one-dimension (1D) crystal called Wolfram's red salt (WRS),



$\cdot\text{Cl}_4\text{H}_2\text{O}$, in order to clarify the nature of the local electronic state.

WRS is considered to be a mixed valence crystal consisting of linear chains of



where each Pt^{4+} or Pt^{2+} ion is coordinated by four ethylamines. The crystal structure is body-centered-tetragonal containing chains parallel to the c -axis.¹⁾ There is no long-range order in the chain structure because of occasional slips in the packing of the chains.²⁾

X-ray absorption measurements were made with synchrotron radiation by use of the EXAFS facilities installed at the beam line 10-B. The XANES spectra near the Pt- L_3 edge of WRS, K_2PtCl_6 (Pt^{4+}) and K_2PtCl_4 (Pt^{2+}) were carefully observed. The results are given in Fig. 1. The near edge structure of Pt^{4+} is fairly different from that of Pt^{2+} . There is fairly good agreement between the spectrum of WRS and the convolution of the spectra of Pt^{4+} and Pt^{2+} . We have directly found that there are Pt^{4+} ions and Pt^{2+} ions in the ground state of WRS.

The charge transfer excitation from the chain $\text{---Pt}^{4+}\text{---Cl}^-\text{Pt}^{2+}\text{---Cl}^-\text{---}$ to the chain of $\text{---Pt}^{3+}\text{---Cl}^-\text{Pt}^{3+}\text{---Cl}^-\text{---}$ is expected in WRS. The optically excited state was studied by measuring optical

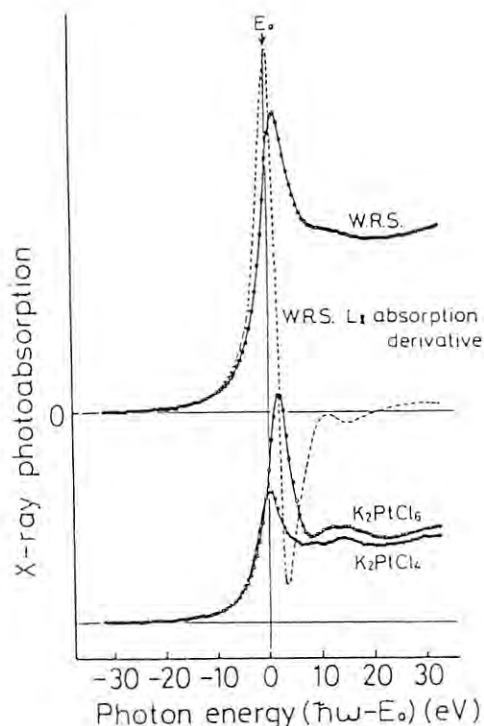


Fig. 1

absorption, resonance Raman and luminescence.³⁾ The XANES study on the lattice relaxation due to the charge transfer excitation in WRS is in progress.

The authors wish to express their thanks to H. Tanino and K. Kobayashi for their fruitful discussions.

References

- 1) B. M. Craven and D. Hall: Acta Cryst. 14 (1961) 476
- 2) S. Iida, T. Iwasumi and H. Terauchi: J. Phys. Soc. Jpn. 52 (1983) No. 8
- 3) H. Tanino and K. Kobayashi: J. Phys. Soc. Jpn. 52 (1983) 1446

EXAFS STUDY ON LOCAL STRUCTURE OF AMORPHOUS AND LIQUID Ge - Se SYSTEM

H. Maeda (a), A. Terauchi (b), S. Iida (b), M. Hida (c), T. Murata (d), N. Kamiyo (e)

Dept. of Chem., Okayama Univ., Okayama 700(a), Dept. of Phys., Kwansei-Gakuin Univ., Nishinomiya 662 (b), Sch. of Eng., Okayama Univ., Okayama 700(c), Dept. of Phys., Kyoto Univ. of Education, Kyoto 612 (d), Gov. Ind. Res. Inst., Ikeda 536(e)

In recent years, a lot of experimental and theoretical work has been done on the amorphous state in order to understand their electronic and structural properties(1). From these works, it has become apparent that the nearest neighbour distance in the amorphous materials are 0.2 to 0.3 Å less, and the coordination numbers are significantly lower than those in the corresponding crystals.

The average energy gap of the amorphous Se-Ge alloy *vs.* atomic content of germanium was obtained from measuring the optical dielectric constant(2). From this experiment, it can be seen that the average gap has a maximum at 33% of germanium content and a minimum at 50% of germanium content. This result suggests that the structure of the amorphous GeSe was contained the considerable distortion than crystalline GeSe.

As discussed previously(3), the near neighbour arrangement in amorphous GeSe shows a striking change from crystalline GeSe. In order to elucidate whether or no this specific structure in amorphous state is maintained in the liquid state, we present structural data for amorphous and liquid $\text{Ge}_{1-x}\text{Se}_x$, containing $x=0.33$ and 0.50 germanium, obtained with the EXAFS technique.

The measurement of the EXAFS spectra were done in transmission at KEK Synchrotron Radiation Laboratory using EXAFS beam line 10-B with a Si (311) channel-cut monochromator. A detailed description of the X-Ray absorption apparatus is given elsewhere(4). Absorption data were taken at 298 K for amorphous and crystalline GeSe and at discrete temperature in the range 298 K to 823 K of GeSe_2 . The EXAFS interference function $\chi(k)$ was determined by numerical procedures in detail in ref. (3).

The Fourier transforms of $k^3\chi(k)$ are given

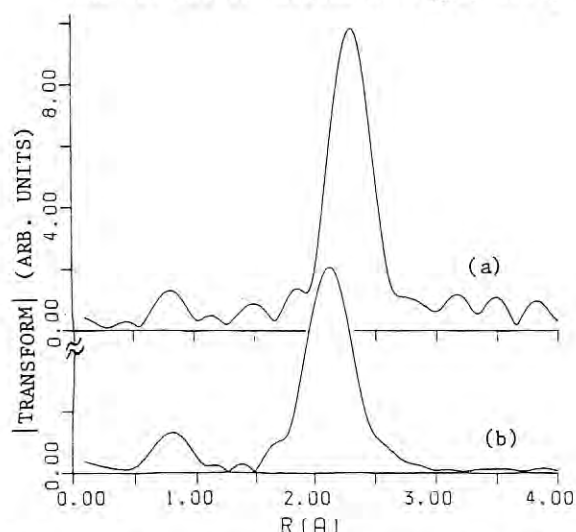


Fig. 1. Magnitude of Fourier transform of $k^3\chi(k)$ data (a) for crystalline GeSe and (b) for amorphous GeSe.

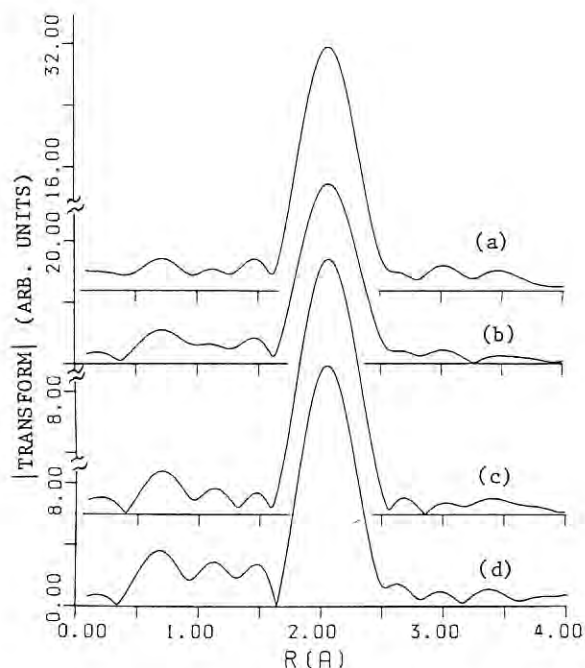


Fig. 2. Magnitude of Fourier transform of $k^3\chi(k)$ data (a) for crystalline GeSe_2 at 298 K and (b) for amorphous GeSe_2 at 298 K, (c) at 748 K, (d) at 848 K.

in Fig. 1 and Fig. 2 for the K edge of Ge in GeSe at 298 K, and in GeSe_2 at 298 K (amorphous), 723 K (58 K above the glass transition temperature) and 823 K (17 K above the crystallization temperature), respectively, where only the magnitude function are shown.

A comparison of Fig. 1(a) and (b) indicates that the first peak at 2.12 Å is considerably shorter than crystalline distance, 2.29 Å. This has been explained by allowing changes in the bond characters of relevant atoms. In the case of GeSe_2 on the other hand, structural rearrangements do not occur in the nearest neighbour shell between crystalline form and amorphous form. Further, the peak shift does not arise from glass transition. The height of the peak above the glass transition point is less than amorphous state.

The detail analysis of the temperature dependent EXAFS spectra and EXAFS measurement on liquid GeSe are in progress.

The authors thank prof. H. Kawamura for supplying good specimens.

Reference

- (1) G. S. Cargill III: Solid State Phys. 30(1977)227.
- (2) H. Kawamura, M. Matsumura and S. Ushioda: J. Non-Cryst. Solids, 35-36(1980)1215.
- (3) H. Maeda, H. Terauchi, K. Tanabe, N. Kamiyo, M. Hida and H. Kawamura: Jpn. J. Appl. Phys. 21(1982)1342.
- (4) H. Oyanagi and T. Matsushita: to be published.

STUDIES ON THE LOCAL STRUCTURE OF THE PHASE TRANSITION IN INVAR ALLOYS

O. Yamada, H. Maeda*, I. Nakai, K. Kamon, Lui Wan Li, H. Tokuhara, M. Mimura

Dept. of Physics, Faculty of Science, Okayama University, Tsushima-Naka, Okayama 700

* Dept. of Chemistry, Faculty of Science, Okayama University, Tsushima-Naka, Okayama 700

One of the unsolved subjects in the Invar problem is to elucidate unusual properties of Fe-Pt Invar alloys at low temperatures. The FCC Fe-Pt Invar alloys show no deviation of the magnetic moment from the Slater-Pauling curve, if the magnetic moment is determined from magnetization values at low temperatures¹⁾, while Fe-Ni Invar alloys show an evident deviation of the spontaneous magnetization at 0 K from the Slater-Pauling curve²⁾. The Fe-Pt Invar alloys have a small forced volume magnetostriction at low temperature³⁾ and their bulk modulus increases with decreasing temperature: the alloys behave as normal metal alloys rather than Invar alloys at low temperatures in contrast with Fe-Pt Invar alloys. In order to explain these peculiarities of Fe-Pt Invar alloys at low temperatures, a model of strong itinerant electron ferromagnets has been proposed⁴⁾. Although this model gives a reasonable explanation for the characteristics that the magnetization decreases almost linearly with increasing Pt concentration without showing any

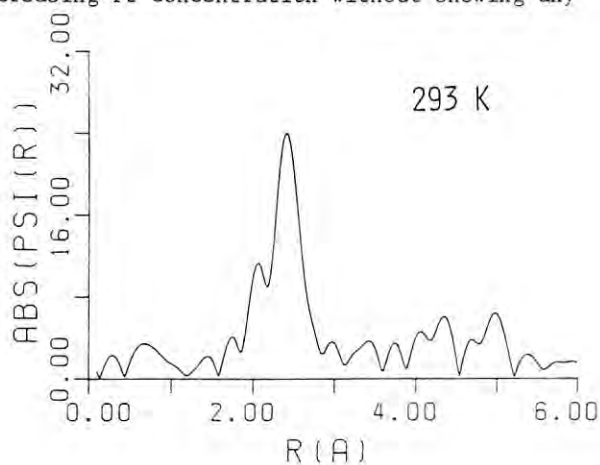


Fig.1

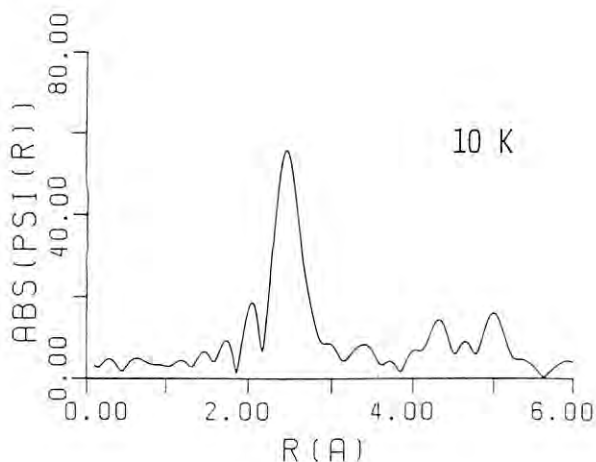


Fig.2

deviation from the Slater-Pauling curve, the correlation between the strong ferromagnet character observed at low temperatures and the weak ferromagnet character observed at room temperature is still far from clear understanding.

According to our neutron experiments⁵⁾ for a disordered single crystal of 28.3 at%Pt-Fe Invar alloy, an integrated neutron intensity of the (400) reflection, contained both magnetic and nuclear contributions, shows a hysteresis against temperature, which suggests the existence of a sort of transformation, being maybe called a pre-martensitic transformation.

In order to investigate how Fe or Pt atoms begin to move in the step of the premartensitic transformation in Fe-Pt Invar alloys, we have carried out EXAFS experiments at the KEK Synchrotron Radiation Laboratory. Powder samples of ordered and disordered Fe-Pt alloys were prepared and annealed at 600°C during one hour.

The EXAFS spectra of the Fe and Pt edges for these samples were obtained at 293 and 10 K. In obtaining the EXAFS function $\chi(k)$, the background level is subtracted from the observed absorption coefficient by using a Victoreen fit and the absorption coefficient for an isolated atom is obtained by the cubic spline technique⁶⁾. The Fourier transformations of the EXAFS spectra of Fe edge in a 26.0 at%Pt-Fe ordered alloy are shown in Fig.1 for 293 K and in Fig.2 for 10 K. Although this alloy shows clearly premartensitic characters in magnetic properties at low temperatures, the results of Fig.1 and Fig.2 indicate that the differences of EXAFS spectra between at 293 K (Fig.1) and at 10 K (Fig.2) are not so much: Fe-Fe distance changes from 2.41 to 2.42 Å, whereas Fe-Pt distance from 2.06 to 2.04 Å, when the temperature of the sample decreases from 293 to 10 K. Also we can hardly find any essential difference for the XANES spectra between at 293 and 10 K. These obtained results are rather unexpected. Probably the EXAFS spectra at 10 K might not yet be those in the pre-martensitic state. This would be caused by the powder form of the samples, which could suppress the martensitic transformation. Farther detailed analyses are now proceeding.

References

- 1) Y. Nakamura, K. Sumiyama and M. Shiga: *Inst. Phys. Conf. Ser.* **39**(1978) 522.
- 2) E. I. Kondorsky and V. L. Sedov: *J. App. Phys.* **31**(1960) 331S.
- 3) K. Sumiyama, M. Shiga, M. Morioka and Y. Nakamura: *J. Phys.* **F9**(1979) 1665.
- 4) Y. Nakamura, K. Sumiyama and M. Shiga: *J. Magn. & Magn. Mater.* **12**(1979) 127.
- 5) O. Yamada, F. Ono, I. Nakai, H. Maruyama, F. Arae and K. Ohta: *Solid State Commun.* **42**(1982) 473.
- 6) H. Maeda, H. Terauchi, K. Tanabe, N. Kamijo, M. Hida and H. Kawamura: *Jpn. J. App. Phys.* **21**(1982) 1342.

EXAFS STUDY ON THE PREMELTING PHENOMENON OF RUBIDIUM

Y. Tsu^{a)}, M. Hida^{b)}, H. Maeda^{c)}, S. Watanabe^{a)}, N. Kamiyo^{d)}, S. Iida^{e)}, H. Terauchi^{e)}, T. Murata^{f)}, I. Watanabe^{g)}

a)Res. Inst. of Min'l Dress'g Metll'y, Tohoku Univ., Sendai 980, b)Sch. of Eng., Okayama Univ., Okayama 700, c)Dept. of Chem., Okayama Univ., Okayama 700, d)Gov. Ind. Res. Inst., Osaka, Ikeda 563, e)Dept. of Phys., Kwansei-Gakuin Univ., Nishinomiya 662, f)Kyoto Univ. Education, Kyoto 612, g)Dept. of Chem., Osaka 560

Introduction

Melting of metals is usually classified as a first order phase transition, solid-liquid, without critical phenomena. Nevertheless experimental investigations on specific heats and electrical conductivity of Na and K indicated the possibility of the existence of a critical point, which would be correlated with premonitory effects, at temperatures close to the melting points.¹⁾ In search for experimental evidence of premelting effects several investigations have been performed on gallium. Recent experiments have shown the absence of premelting in crystal gallium from results of the Debys-Waller factor and lattice parameter measurements using anomalous diffraction of X-rays and thermal expansion coefficient measurement.^{2,3)}

However, a certain premelting phenomenon in gallium was recently found by using EXAFS spectroscopy and density measurements.⁴⁾ The structure of crystal gallium consists of elementary cells with the pairs of Ga-atoms arranged in a face centered orthorhombic structure. Even though a premelting phenomenon is found in such a complex metal, it could not be decided hastily to exist in other structure metals.

Therefore, the purpose of the present investigation is to study whether a premelting phenomenon can be found or not in crystal rubidium having simple bcc structure.

Analysis are still continuing; we report the results obtained so far.

Experiments and Results

To make the suitable shape of sample was very difficult as rubidium is a very high active metal. In order to obtain samples, at first, rubidium film was evaporated on a polymer plate and protected with an overcoat of evaporated paraffin. But the sample was immediately burn out when it was exposed to the air. Therefore, the following technique was used: a high purity rubidium (99.95%) contained in an ampule was melted in kerosene heated about 50°C and the molten metal was sucked up into a thin cell (0.12mm×5mm×15mm) made of polymer film by using an injector (the thickness of 0.12mm was calculated from $\mu d = 2.5$). According to this method, however, oxidation on the surface of the sample metal could not be completely prevented. The rubidium foil enclosed in a polymer cell was used as the experimental sample. The temperature of specimen held in the sample holder was controlled at given temperature with a maximum fluctuation of $\pm 0.03^\circ\text{C}$ by a precise temperature regulator.

The EXAFS spectra were obtained on the crystalline (25.73°C), premelted (38.05°C) and melted (43.98°C) state of rubidium (hereafter abbreviated as CR-Rb, PM-Rb and ML-Rb, respectively). Data processing and analysis applied to these EXAFS spectra were the same as described in the previous papers.^{4,5)}

Figure 1 shows parts of the Fourier transformation for the EXAFS spectra. The first and second peaks of the radial structure function of CR-Rb were identified as that the nearest neighbour shell contains eight atoms at 4.94Å and the second neighbour at 5.70Å, respectively. The peaks corresponding to the shell radii at each state of rubidium were listed in Table 1.

The result suggests that the premelted state of rubidium may exist at temperature about 1°C below the melting point. However, there remains some uncertainty as to the conclusion because of the existence of noise in the Fourier transformation spectra. Further investigation is necessary.

Table 1. The structure parameters obtained from the fourier transformation

Sample	Shell	$R_j + \sigma$ (Å)	N_j
CR-Rb	1	(4.94)	(8.0)
	2	(5.70)	(6.0)
PM-Rb	1	4.97	1.0
	2	5.61	0.5
ML-Rb	1	5.03	1.0
	2	5.66	0.9

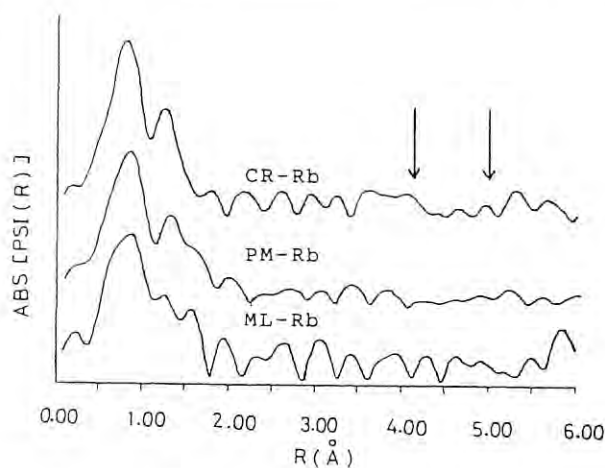


Fig. 1 The radial structure function of CR-Rb, PM-Rb and ML-Rb.

References

- 1) A.R. Ubbelohde: Melting and Crystal Structure, Clarendon Press, Oxford, (1965).
- 2) H. Wenzl et al.: Z. Physik S21(1975), 95.
- 3) G. Mair et al.: ibid B24(1976), 301.
- 4) M. Hida et al.: The 5th Int'l Conf. of Liquid and Amorphous Metals, Los Angeles, Aug., 1983.
- 5) H. Maeda et al.: J. J. Appl. Phys., 21 (1982), 1342.

EXAFS AND XANES STUDIES OF CHEMICALLY FIXED Mo AND Cr CATALYSTS
I. Mo₂/SiO₂ CATALYST

H. Kuroda, N. Kosugi, H. Ishii, K. Asakura and T. Yokoyama

Department of Chemistry and Research Center for Spectrochemistry, Faculty of Science, The University of Tokyo, Hongo, Bunkyo-ku, Tokyo 113 (JAPAN)

Y. Iwasawa

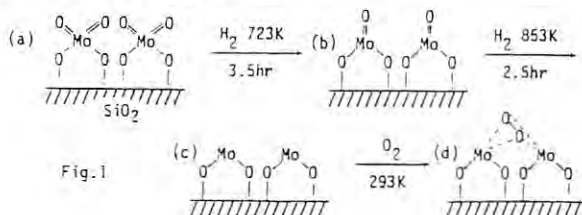
Department of Applied Chemistry, Faculty of Engineering, Yokohama National University, Tokiwadai, Hodogaya-ku, Yokohama 240 (JAPAN)

One of the present authors has developed the method to prepare Mo₂/SiO₂ catalyst by the chemical reaction of Mo₂(π-C₃H₅)₄ with OH groups on the surface of silica, and has shown that the catalyst thus obtained has very unique catalytic activities.¹ This catalyst system seems to provide a way to understand the relation between the surface structure and the catalytic activity. Thus we studied the surface structure and its changes with the treatment of this catalyst by means of X-ray absorption spectroscopy.

The catalyst was prepared by the method described elsewhere.¹ XAS measurements were carried out by use of the EXAFS apparatus installed at BL 10-B.

Since the reduced form of the catalyst is unstable in air, all the oxidation and reduction treatments of the catalyst were carried out *in situ* by use of a specially constructed sample chamber.

The models of the surface structure for several different oxidation stages of the catalyst, which have been proposed, are illustrated in Fig.1, together with the conditions of treatments.



The Mo K XANES spectra obtained for the four stages are shown in Fig.2. The spectrum for the stage (a) resembles to the Mo K XANES of K₂MoO₄, indicating that the valency state and the chemical environment of Mo is in the state very much like MoO₄²⁻ ion. On going from this stage to the stages (b), (c) and (d) the sharp peak before the absorption edge decreases its intensity, indicating the disappearance of Mo=O bonds and the loss of Td symmetry.

The Fourier transforms of the EXAFS oscillations are shown in Fig.3. The prominent peak in the Fourier transform for the stage (a) corresponds to Mo-O bonds, and no peak corresponding to Mo-Mo bond can be found. The result is similar for the stage (b), except a slight decrease of the peak height of Mo-O bonds. On going to the stages (c) and (d), a new peak corresponding to Mo-Mo bond appears at about 2.5 Å and the peak due to Mo-O bond shifts to longer distance. The interatomic distances obtained from curve-fitting analysis are given in Table 1.

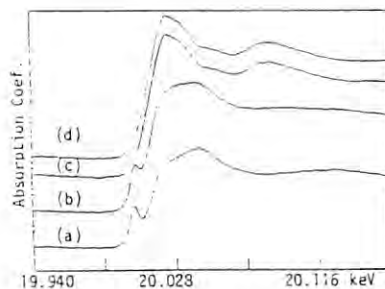


Fig.2 Mo K-Edge XANES Spectra

Table 1
Curve-Fitting Results

	Mo-O	Mo-Mo
(a)	1.71 Å	—
(b)	1.74	—
(c)	2.04	2.53
(d)	2.05	2.53

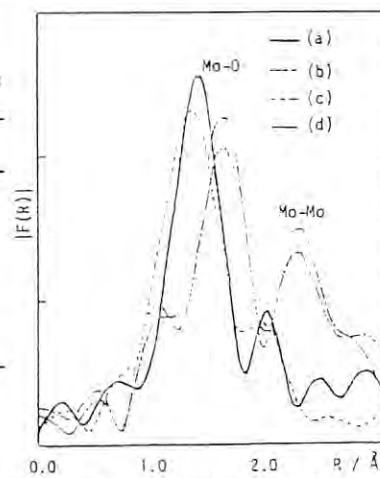


Fig.3 Fourier Transforms of (a) - (d)

The present results provide a direct evidence for the presence of Mo₂ group on the surface of the catalyst. It is interesting to see that Mo-Mo peak does appear only in the highly reduced stages where the formation of chemical bond between Mo atoms is expected. The present results also indicate that, in the stage (d), oxygen molecule is only loosely bound to the Mo₂ site without causing a significant change in the geometrical and electronic structure surrounding Mo atoms.

The results described above provide very important information for understanding the catalytic activity of this unique catalyst.

- 1) Y. Iwasawa, H. Kubo, M. Yamagishi and S. Ogasawara: Chem. Lett.(1980) 1165;
Y. Iwasawa, M. Yamagishi and S. Ogasawara: J. Chem.Soc.Chem.Commun.(1980) 871;
Y. Iwasawa and M. Yamagishi: J. Catal. 82 (1983) 373.

XANES OF METAL CARBONYL MOLECULES
I. GAS- AND LIQUID-PHASE $\text{Fe}(\text{CO})_5$

H. Kuroda, N. Kosugi, T. Yokoyama, K. Asakura and H. Ishii

Department of Chemistry and Research Center for Spectrochemistry, Faculty of Science, The University of Tokyo, Hongo, Bunkyo-ku, Tokyo 113 (JAPAN)

Understanding of XANES spectra of transition metal compounds is still qualitative. If the compound is in a solid state, precise investigation for its XANES spectrum is difficult due to solid-state and many other effects. In order to investigate XANES phenomena in detail both experimentally and theoretically, it is better to analyze XANES spectra for gas-phase compounds.

In the present experiment, we measured XANES spectra of gas- and liquid-phase $\text{Fe}(\text{CO})_5$ at room temperature by use of the EXAFS apparatus at BL 10-B.

The measured spectra are shown in Fig.1. The spectra reveal some fine structures with low intensity in the pre-edge region. The electronic structure of the ground state of D_{3h} $\text{Fe}(\text{CO})_5$ is a closed-shell system with eight d electrons, where the d_{z^2} orbital is unoccupied. Based on the simple one-electron model, we have proposed a tentative assignment to the fine structures A, B and C indicated in Fig.1 as follows:

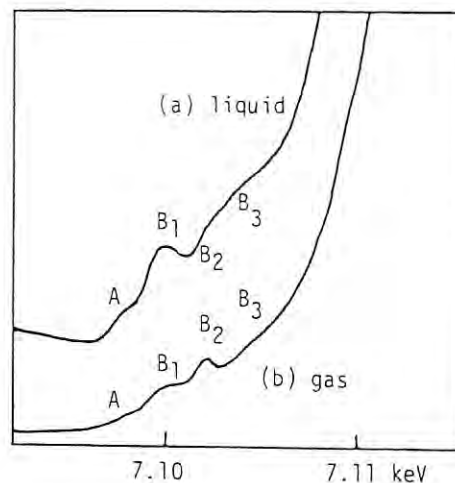
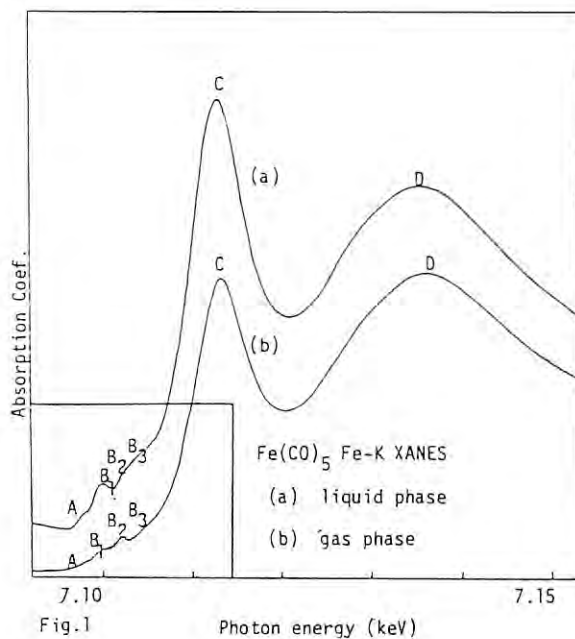
- A $\text{Fe } 1s \rightarrow \text{Fe } 3d_{z^2}$
- B $\text{Fe } 1s \rightarrow \text{CO } 2\pi^* (+\text{Fe } 4p\pi)$
- C $\text{Fe } 1s \rightarrow \text{Fe } 4p$

Both A and B are in rather low intensity, because A corresponds to a dipole-forbidden and quadrupole-allowed transition and B has charge-transfer character from metal to ligand.

On the higher energy side of the structure C, there are transitions from Fe 1s to the continuum states. Below the ionization threshold, transitions to the Rydberg-type orbitals could not be observed in the present gas-phase spectrum.

The edge-energy difference between the two spectra is not observed. This suggests that the molecular interaction in the liquid phase be not so large to shift the edge energy. However, there is a distinct difference in the structure B. This is probably because the CO $2\pi^*$ orbitals are in the exterior region of the molecule and are liable to suffer interaction with the surrounding molecules in the liquid.

We are planning to analyze the XANES spectrum of gas-phase $\text{Fe}(\text{CO})_5$ theoretically by means of the *ab initio* SCF-CI method.



EXAFS AND XANES STUDIES OF METAL-HALIDE-DOPED POLYACETYLENES
I. FeCl₃-DOPED POLYACETYLENE

H. Kuroda, I. Ikemoto, N. Kosugi, K. Asakura, H. Ishii, H. Shirakawa*, T. Kobayashi*, H. Oyanagi** and T. Matushita***

Department of Chemistry and Research Center for Spectrochemistry, Faculty of Science, The University of Tokyo, Hongo, Bunkyo-ku, Tokyo 113 (JAPAN)

*Institute of Material Science, University of Tsukuba, Sakura-mura, Niihari-gun, Ibaraki 305 (JAPAN)

**Electrotechnical Laboratory, Umezono, Sakura-mura, Niihari-gun, Ibaraki 305 (JAPAN)

***Photon Factory, National Laboratory for High Energy Physics, Oho-machi, Tsukuba-gun, Ibaraki 305 (JAPAN)

Recently, Pron et al.¹ reported that FeCl₃ can be doped into a polyacetylene film to give metallic conductivity. They studied ⁵⁷Fe Mössbauer spectra of FeCl₃-doped polyacetylenes [CH(FeCl₃)_y]_x and concluded that the dopant exists in the state of some Fe(II) compound. We investigated Fe-K absorption spectra of FeCl₃-doped polyacetylenes for the purpose to obtain information concerning the structure and chemical state of the dopant.

Polyacetylene films were prepared by the polymerization over a Ziegler-Natta catalyst.² The doping with FeCl₃ was carried out by immersing polyacetylene films into a nitromethane solution of FeCl₃.

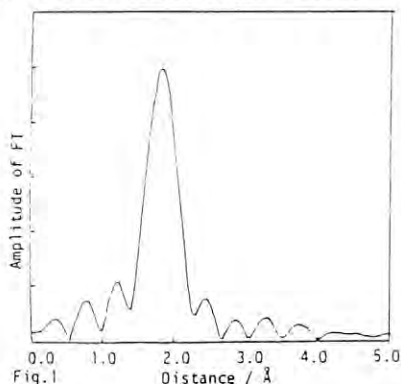
X-ray absorption spectra were measured by use of the EXAFS apparatus installed at the beam line BL 10-B, partly as a test experiment of the apparatus.

Fe K spectra were measured on three doped films of different dopant contents. The values of the apparent dopant contents and the electrical conductivities of the samples are given in Table 1.

Table 1. Samples of [CH(FeCl₃)_y]_x

Sample	Dopant conc. y	Conductivity (S/cm)
Sample 1	0.024	10-80
Sample 2	0.087	700-850
Sample 3	0.13	~200

The Fourier transform of the EXAFS oscillation $k^3 \cdot \chi(k)$ for Sample 3 is shown in Fig.1. Only one prominent peak was found at the same distance for all the three samples. The peak in the Fourier transform can be attributed to the Cl atoms surrounding Fe atom.



The distance and coordination number obtained by the curve-fitting analysis are given in Table 2. The observed Fe-Cl distance corresponds to that of FeCl₄⁻.

Table 2. Results of analysis of EXAFS data by use of empirical parameters*)

Sample	Bond length (Å)	Coordination No.	R(%)
Sample 1	2.193	3.2	13.4
Sample 2	2.182	3.6	7.4
Sample 3	2.180	3.8	3.7

*The model compound used was [N(C₂H₅)₄][FeCl₄] with Fe-Cl distance 2.18, coordination number 4.

The XANES region of the Fe K spectrum of FeCl₃-doped polyacetylene is compared with the corresponding spectra of the chloride ions of Fe in Fig.2. It shows clearly that the former corresponds to the XANES of FeCl₄⁻ ion.

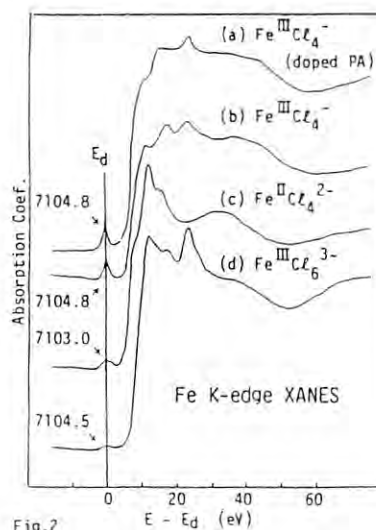


Fig.2

All the results described above prove that the dopant is in the state of FeCl₄⁻ ion, not in a state of Fe(II) compound.

- 1) A. Pron, I. Kulszenwicz, D. Billaud and J. Prylowski: J. Chem. Soc. Chem. Commun. (1981) 783.
- 2) H. Shirakawa and S. Ikeda: Poly. J. 4 (1971) 460.

EXAFS AND XANES STUDIES OF METAL-HALIDE-DOPED POLYACETYLENES
 II. MoCl₅- AND WCl₆-DOPED POLYACETYLENES

H. Kuroda, I. Ikemoto, N. Kosugi, K. Asakura, H. Ishii, T. Yokoyama, H. Shirakawa*, T. Kobayashi*,
 H. Oyanagi**, M. Nomura*** and T. Matushita***

Department of Chemistry and Research Center for Spectrochemistry, Faculty of Science, The University of Tokyo, Hongo, Bunkyo-ku, Tokyo 113 (JAPAN)

*Institute of Material Science, University of Tsukuba, Sakura-mura, Niihari-gun, Ibaraki 305 (JAPAN)

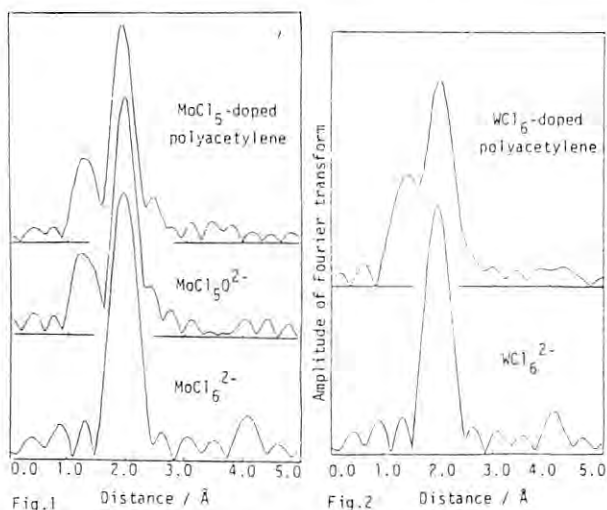
**Electrotechnical Laboratory, Umezono, Sakura-mura, Niihari-gun, Ibaraki 305 (JAPAN)

***Photon Factory, National Laboratory for High Energy Physics, Oho-machi, Tsukuba-gun, Ibaraki 305 (JAPAN)

Various metal halides can be doped into polyacetylene to give metallic high conductivity. We have previously elucidated the chemical state and geometrical structure of the dopant in the FeCl₃-doped polyacetylene from the analyses of the XANES and EXAFS. In the present study we have investigated MoCl₅- and WCl₆-doped polyacetylenes.

The doping of metal halide was carried out by immersing a polyacetylene film into anisole solution of the dopant. The XAS measurements were performed by use of the EXAFS apparatus at BL 10-B. The samples were kept at 100 K during the measurements.

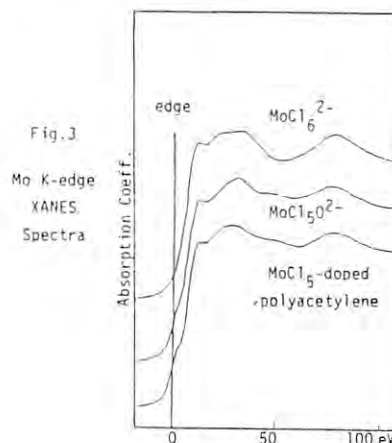
The Fourier transform of the Mo K EXAFS oscillation of MoCl₅-doped polyacetylene and that of the W L_{III} EXAFS oscillation of WCl₆-doped polyacetylene are shown in Figs.1 and 2, respectively, together with those of the reference compounds.



As compared with the Fourier transform obtained for K₂MoCl₆, the height of the main peak at about 2 Å is lower and there appears a new peak at the shorter distance in the Fourier transform of MoCl₅-doped polyacetylene, which resembles very much the Fourier transform obtained for (NEt₄)₂MoCl₅O where the main peak can be attributed to Mo-Cl and the short-distance peak can be attributed to Mo-O.

In the case of WCl₆-doped polyacetylene, the Fourier transform shows again two peaks, the stronger one being attributed to W-Cl and the weaker one probably being attributable to W-O.

The Mo K XANES spectra are shown in Fig.3. Note that the spectrum of MoCl₅-doped polyacetylene resembles the spectrum of (NEt₄)₂MoCl₅O and is appreciably different from the spectrum of K₂MoCl₆.



The curve-fitting analyses were successfully carried out on the EXAFS oscillations observed for MoCl₅- and WCl₆-doped polyacetylenes by assuming the presence of O atom besides Cl atoms. The results are given in Table.1

Table 1. Curve-fitting results

doping	Weight ratio of dopant to (CH) _x		distance/Å	Coord. No.
MoCl ₅ /anisole	1.41	Mo-Cl	2.37 ± 0.03	4.9 ± 0.5
		Mo-O	1.66 ± 0.04	1.2 ± 0.2
(NEt ₄) ₂ MoCl ₅ O *	—	Mo-Cl	2.38 ± 0.03	5*
		Mo-O	1.67 ± 0.03	1*
WCl ₆ /anisole	1.47	W-Cl	2.35 ± 0.03	**
		W-O	1.74 ± 0.03	

*standard **under investigation

All the present results indicate that the chemical species in the MoCl₅-doped polyacetylene is not MoCl₆²⁻ but MoCl₅O²⁻. At present we do not know the origin of the oxygen atom. Presumably the oxygen atoms of the dopants came from the oxygen and/or water contained in the solutions used in the doping processes.

XANES OF HIGHLY-CONDUCTIVE MIXED-VALENCE ORGANIC CHARGE TRANSFER SALTS
I. (TMTSF)₂X AND RELATED MATERIALS

H. Kuroda, I. Ikemoto, K. Kikuchi, N. Kosugi, K. Asakura, H. Ishii and T. Yokoyama
Department of Chemistry and Research Center for Spectrochemistry, Faculty of Science, The University of Tokyo, Hongo, Bunkyo-ku, Tokyo 113 (JAPAN)

The charge transfer salts of tetramethyl-tetraselenafulvalene (TMTSF)₂X are known to exhibit the behaviors characteristic to the quasi-one-dimensional metal. Some of them have been found to show superconduction at low temperature. It is known that their behaviors concerned with the electrical conduction as well as those concerned with the metal-insulator (M-I) transition vary rather widely depending on the anion. For example, (TMTSF)₂PF₆ shows the M-I transition at 12 K, below which the lattice shows SDW distortion, while (TMTSF)₂ReO₄ shows the M-I transition at much higher temperature 180 K which seems to be associated with the anion ordering. We have previously investigated the XPS spectra of (TMTSF)₂X salts.¹ In connection with this study, we have examined the Se K XANES spectra.

(TMTSF)₂PF₆ and (TMTSF)₂ReO₄ were prepared by the electrochemical method.² The Se K XANES spectra were measured by use of the EXAFS apparatus at BL 10-B.

In the present experiment, all measurements were done on the powder samples at 10.8 and 295 K. The Se K XANES spectra of (TMTSF)₂PF₆ and (TMTSF)₂ReO₄ are shown in Figs. 1 and 2, respectively. There seems to be little change in the spectrum of (TMTSF)₂PF₆ between 10.8 and 295 K. However, in the case of (TMTSF)₂ReO₄, a shoulder appeared in the lower-energy side of the first peak A, and the position of the first peak was shifted to higher energy on going from 295 K to 10.8 K. This must be associated either with the splitting of Se K level or with a change in the band structure.

The present experiments are just preliminary ones. We are planning to measure the XANES spectra on single crystals of (TMTSF)₂X salts varying the polarization direction of X-rays in respect to the crystal axis, as the experiments in the next machine time.

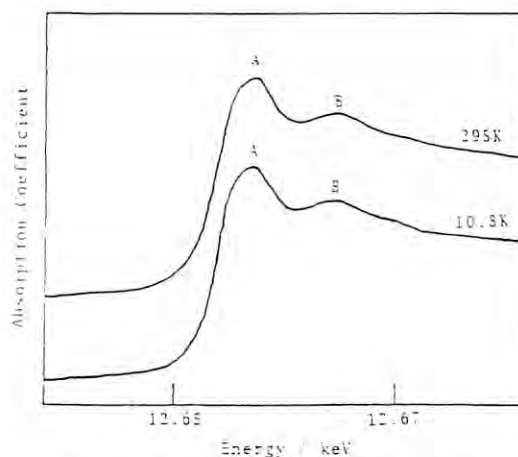


Fig. 1 The spectra of Se-K XANES of (TMTSF)₂PF₆

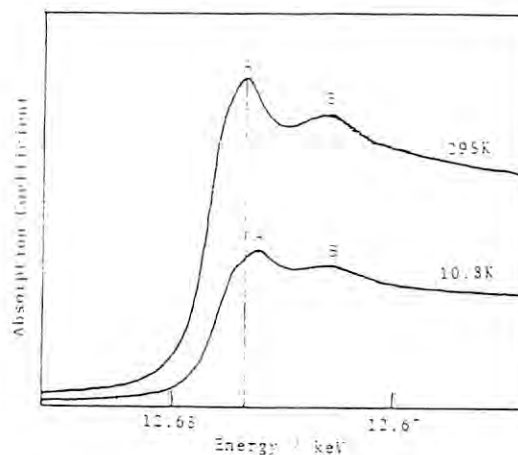


Fig. 2 The spectra of Se-K XANES of (TMTSF)₂ReO₄

- 1) I. Ikemoto, K. Kikuchi, K. Yakushi, H. Kuroda, and K. Kobayashi: Solid State Commun. 42(1982) 257.
- 2) K. Bechgaard, K. Carneiro, F. B. Ramussin, M. Olsen, G. Rindorf, C. S. Jacobsen, H. J. Pedersen and J. C. Scott: J. Amer. Chem. Soc. 103(1981) 2440.

SURFACE STRUCTURE OF SMSI CATALYST
I. Rh/TiO₂ CATALYST

H. Kuroda, N. Kosugi, K. Asakura, H. Ishii and T. Yokoyama

Department of Chemistry and Research Center for Spectrochemistry, Faculty of Science, The University of Tokyo, Hongo, Bunkyo-ku, Tokyo 113 (JAPAN)

Y. Iwasawa

Department of Applied Chemistry, Faculty of Engineering, Yokohama National University, Tokiwadai, Hodogaya-ku, Yokohama 240 (JAPAN)

Tauster et al.¹ first found a very peculiar behavior for the catalysts, noble metals supported on metal oxides, that such catalyst systems when reduced at high temperature in H₂ lost the H₂ (or CO) adsorbing ability although the supported metal still remained in a highly-dispersed state. This peculiar phenomenon is called SMSI (strong metal support interaction), and has been presumed to be associated with a bond formation between the supported metal atom and the metal atom of the support. However no direct experimental evidence is known for the formation of such metal-metal bond. We have tried to see if SMSI phenomenon is actually associated with the above-mentioned mechanism by studying the surface structures of SMSI systems using X-ray absorption spectroscopy.

A highly-dispersed Rh/TiO₂ catalyst was prepared by the reaction of Rh(C₃H₅)₄ with fine powder of TiO₂. After the necessary treatments, the catalyst was transferred to the sample cell for XAS measurements without exposing to air. All XAS measurements were done at room temperature by use of EXAFS apparatus at BL 10-B.

Figures 1-3 show the EXAFS oscillations $k \cdot X(k)$ obtained for the SMSI and normal states of Rh/TiO₂ catalyst and that for Rh metal. The Fourier transform curves corresponding to these EXAFS oscillations are shown in Figs.4-6, respectively. In all cases, the Fourier transform exhibits one prominent peak at about 2.5 Å. The fact that the observed EXAFS oscillation shows the largest amplitude at about $k=8 \text{ \AA}^{-1}$, indicates that the peak of the Fourier transform is not due to O or Ti atoms, but due to heavy atoms possibly Rh atoms. This interpretation is supported from the curve fitting analysis, the results of which are summarized in Table 1. According to the results of the present EXAFS study of Rh/TiO₂ catalyst, Rh atoms are forming clusters with a structure similar to the Rh metal.

In the present experiment, we were not able to find any definite indication for the formation of a direct chemical bond between Rh and Ti. However, we found that the Rh K absorption edge is shifted to lower energy as large as 0.9 eV on going from the normal state to the SMSI state. This fact seems to indicate that a significant electron transfer from the substrate to the supported Rh atoms are taking place in the SMSI state. Thus the SMSI phenomenon is likely to be associated not with the direct Rh-Ti bond, but by the charge density increase in the supported Rh metal particle. But we are investigating further other SMSI systems in order to get more information concerning the surface structure of the SMSI state.

1) S. J. Tauster, S. C. Fung, R. T. K. Baker and J. A. Horsley: Science 211(1981) 1121.

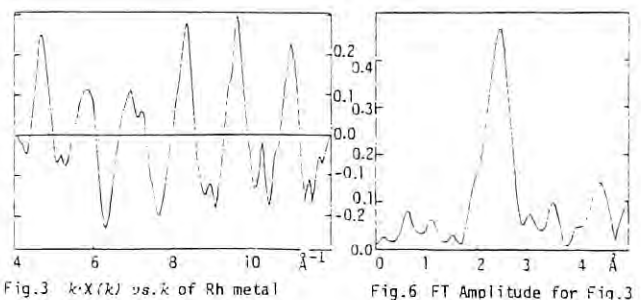
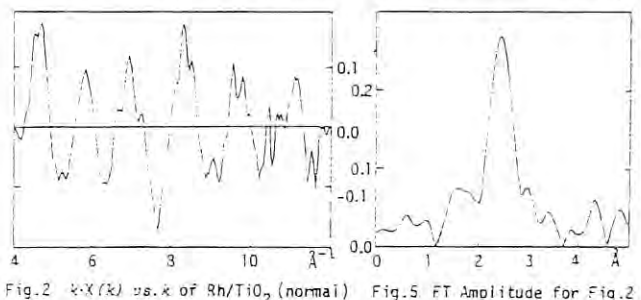
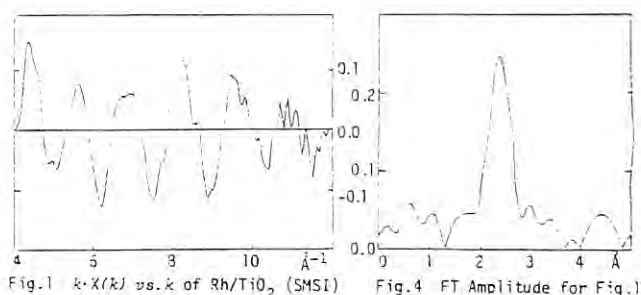


Table 1. Theoretical Curve-Fitting Results

sample name	Rh-Rh distance/Å	Coord.No.
Rh/TiO ₂ (SMSI)	2.64 ± 0.03	8.5 ± 1.0
Rh/TiO ₂ (normal)	2.65 ± 0.03	9.3 ± 1.0
Rh metal (standard)	2.67 ± 0.03	(12)
(crystallography)	(2.69)	(12)

Table 2. Energy Shifts of Rh K-Edge

Sample	Relative Energy (eV)
Rh metal	0.0
Rh/TiO ₂ (SMSI)	3.1 ± 0.5
Rh/TiO ₂ (normal)	4.0 ± 0.5

STUDY ON THE STRUCTURE OF THE ACTIVE SITES FOR THE FORMATION
OF OXYGENATED COMPOUNDS FROM CO-H₂ UNDER MILD CONDITIONS

S.Naito, N.Kosugi, K.Asakura, H.Ishii, T.Yokoyama, K.Tamaru and H.Kuroda
Department of Chemistry, Faculty of Science, The University of Tokyo,
Hongo, Bunkyo-ku, Tokyo 113, (JAPAN)

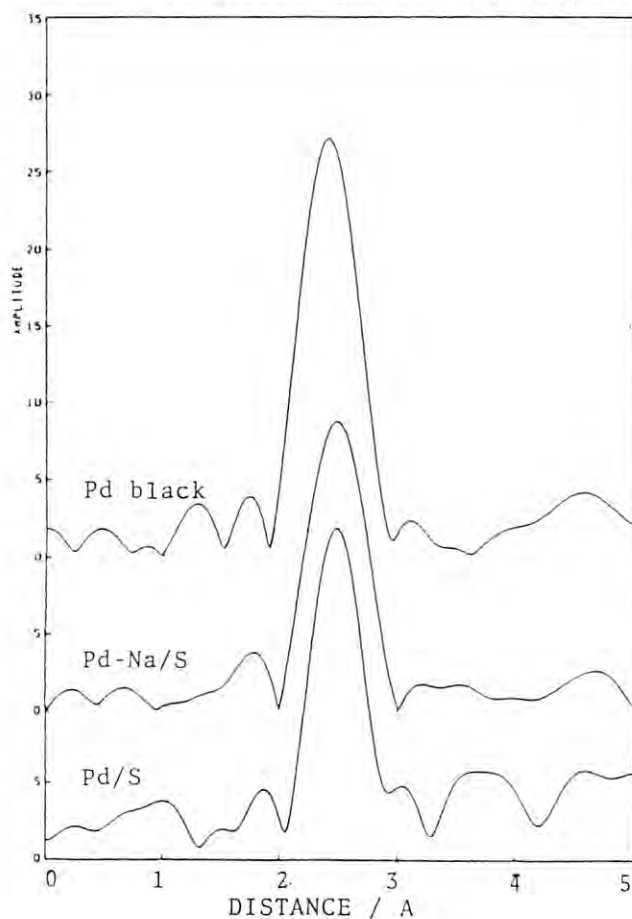
Palladium metal is a good catalyst for the formation of methanol from CO-H₂ reaction under high pressures, although it produces only methane under atmospheric pressure. Recently we have found that by adding alkali metal cations like lithium or sodium to the supported palladium catalysts, methanol formation was enhanced drastically even under atmospheric CO-H₂ pressures. From the investigations of infrared spectroscopy during the reaction and isotope labelled experiments, it was considered that there exists some surface oxygen at the vicinity of the palladium metal particle and the support, which can stabilize the reaction intermediate for methanol formation as a surface formate ion. And alkali metal cations may act as a stabilizer for surface oxygen. To prove above mentioned structure of active sites, EXAFS study was carried out for these catalysts.

To form uniformly dispersed active sites, following method was employed for the preparation of sample catalysts. First of all, a certain amount of Na⁺ was impregnated on a silica support, which was evacuated at 823 K to control the amount of surface OH group. Then pentane solution of Pd(C₃H₅)₂ was added on this support at 230 K to produce Si-O-Pd(C₃H₅) group on the surface. After removing pentane, the catalyst was reduced by hydrogen at 473 K over night (Pd-Na/S). For the reference, the sample without Na⁺ on the surface was also prepared by the same procedure (Pd/S). Pd black from Nippon Engerhard Co. Ltd. was also used without further treatment.

The results of EXAFS measurements are shown in the figure. It is interesting

to note that the bond distance of the Pd-Pd metal of the supported palladium catalysts is apparently larger than that of palladium black. It is also concluded that supported palladium metal is more negatively charged than unsupported palladium black. But unfortunately, no difference of EXAFS between sodium doped and non-doped supported palladium catalysts was observed so far. Further investigation should be needed to interpret these phenomena.

Fig. EXAFS of various palladium catalysts



EXAFS STUDY OF CATALYSTS FOR PHOTODECOMPOSITION OF H₂O

K. Domen, A. Kudo, T. Onishi
 Research Laboratory of Resources Utilization,
 Tokyo Institute of Technology,
 4259 Nagatsuta, Midori-ku, Yokohama (Japan)

N. Kosugi, K. Asakura, H. Ishii, T. Yokoyama and K. Kuroda,
 Department of Chemistry, Faculty of Science, University of Tokyo,
 7-3-1 Hongo bunkyo-ku, Tokyo (Japan)

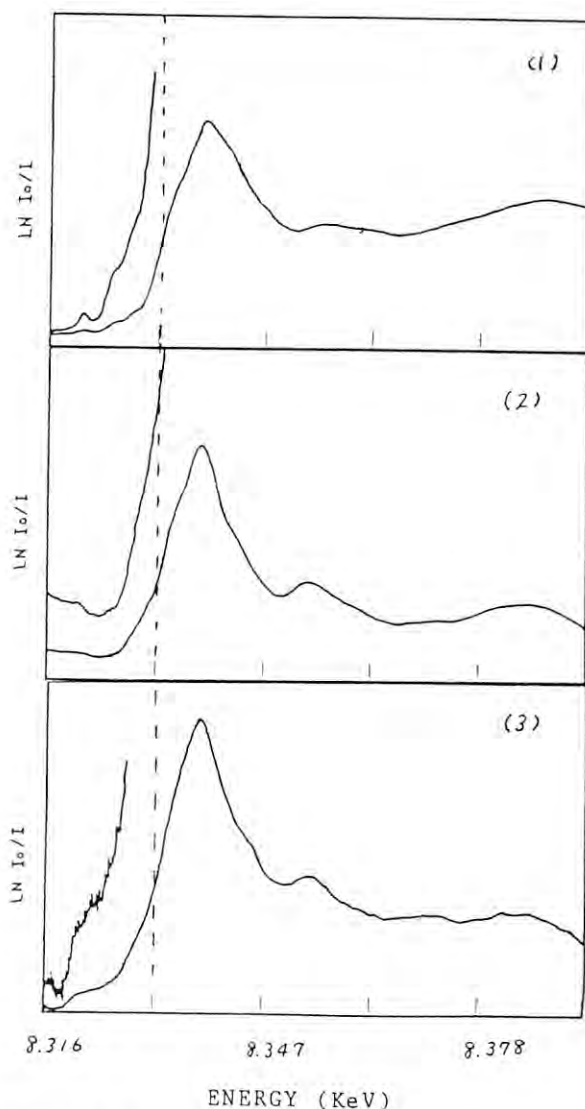
Introduction

Photocatalytic decomposition of water into H₂ and O₂ is interesting subject in view of utilization of solar energy. To use a semiconductors as a mediator for energy transfer from photon to water seems to be one of the intense approaches to accomplish the reaction. Strontium titanate (SrTiO₃) is a semiconductor with a band gap of 3.2 eV. Some of authors have found that SrTiO₃ powder supported with NiO can decompose water efficiently to H₂ and O₂ under band gap irradiation. The catalyst, NiO(2wt%)-SrTiO₃, is prepared by impregnation method. SrTiO₃ powder is impregnated with Ni(NO₃)₂ aq. and calcined at 400°C in air. After the calcination, Ni(NO₃)₂ on the SrTiO₃ decomposes into NiO. However, the activity of the catalyst is very small as it is. When the catalyst is reduced by H₂ and reoxidized by O₂, the activity of the catalyst for photodecomposition of water increases by Ca. 1000 times. It is not known clearly what is happen on the catalyst by this pretreatment. To study the difference of the catalysts before and after the pretreatment is necessary for the improvement of the activity. The XPS has been applied to investigate the catalysts. The oxidation state of Ni was determined as +2 before and after the pretreatment. It seems that the form of NiO on SrTiO₃ changes by the activation process. EXAFS study may be one of the effective methods to study this catalyst.

Experimental and Results

Three different samples were prepared; (1) NiTiO₃ as reference, (2) NiO(2wt%)-SrTiO₃ before pretreatment, (3) NiO(2wt%)-SrTiO₃ after pretreatment. The measurements of the EXAFS and XANES were done using the EXAFS apparatus installed at the BL10-B. The adjustment of the thickness of the sample to obtain the EXAFS of Ni was difficult because of the intense absorption of Ti near the Ni absorption. So, the experimental time was not enough to measure the EXAFS of sample (2) and (3). The results of preliminary experiment, measurements of XANES, are shown in the figure. The coincidence of main peak positions of all samples suggests that the valences of Ni in these catalysts are +2. Although

the line shapes of (2) and (3) are almost same, there may be some difference between the shapes at the edges of X-ray absorption. Further extended study of EXAFS will be expected to give some information on these catalysts.



XANES of Ni
 (1) NiTiO₃
 (2) NiO(2wt%)-SrTiO₃ before pretreatment
 (3) NiO(2wt%)-SrTiO₃ after pretreatment

XANES STUDIES ON MIXED-VALENCY AND ABNORMAL VALENCY
IN THE COMPLEXES OF FERROCENE DERIVATIVES

Kumiko SATO, Makoto IWAI, Yasuo WATANABE, Satoru NAKASHIMA, Hirotoishi SANOn, and Isao IKEMOTO
Department of Chemistry, Faculty of Science, Tokyo Metropolitan
University, Fukasawa, Setagaya-ku, Tokyo 158
Nobuhiro KOSUGI, Kiyotaka ASAKURA, Hiromu ISHII, Toshihiko YOKOYAMA, and Haruo KURODA
Department of Chemistry, Faculty of Science, The University of
Tokyo, Hongo, Bunkyo-ku, Tokyo 113

Introduction

The authors have reported the preparation and characterization of triiodide salts of mixed-valence biferrrocene-type compounds.¹⁾ The compounds are classified roughly into two types: one is the trapped-valence type which contains ferrocene-like bivalent and ferrocenium-like trivalent iron atoms; the other is the averaged-valence type which contains equivalent iron atoms. Recently, it was reported that 1',1'''-diethyl and 1',1'''-dipropyl-biferrrocenium⁺I₃⁻ salts give rise to a transition from the averaged-valence state of iron atoms to the trapped-valence state as temperature is lowered.²⁾

Although Mössbauer spectroscopy can distinguish whether or not the rate of the thermal electron transfer between two iron atoms in these salts is higher than $\alpha. 10^7 s^{-1}$, the X-ray-absorption near edge structure (XANES) spectroscopy involves a different time scale of $\alpha. 10^{15} s^{-1}$. We show the XANES spectra of ferrocene, ferrocenium⁺I₃⁻, 1',1'''-diiodobiferrrocene, biferrrocenium⁺I₃⁻ and 1',1'''-dibromobiferrrocenium⁺I₃⁻.

Results and Discussion

For simplicity we first compare ferrocene and ferrocenium⁺I₃⁻ where the iron atoms are in the site of D_{5h} symmetry. Figure 1 shows that iron atoms have a very weak absorption peak at the threshold, followed by a shoulder on a rising absorption curve which culminates in a strong peak. We identify this strong peak as the allowed transition 1s + 4p, the lower energy shoulder as the forbidden transition 1s + 4s, and the small peak at the threshold as the forbidden transition 1s + 3d. Although these assignments are based on the previous results,³⁾ this conclusion will be confirmed by comparing the measured transition intensities and energies with the quantitative theoretical calculations based on atomic states. No change in the intense 1s + 4p transitions was observed in these compounds. The transitions confirm that upon oxidation of ferrocene the iron atom's electronic structure barely changes. The previous analysis of Mössbauer isomer shifts also suggested that the iron atom did not change its charge upon oxidation.

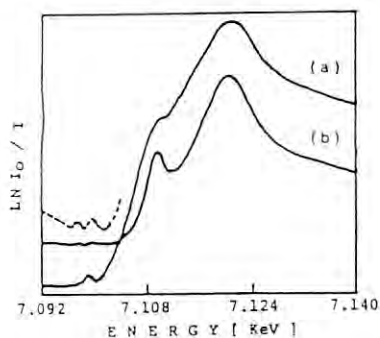


Fig. 1. The XANES spectra of (a) ferrocene and (b) biferrrocenium⁺I₃⁻. The incomplete dashed and solid curve is the absorption under magnification.

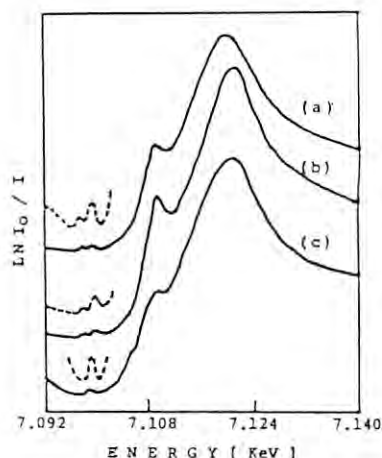


Fig. 2. The XANES spectra of (a) 1,1'''-dibromobiferrrocenium⁺I₃⁻, (b) biferrrocenium⁺I₃⁻ and (c) 1,1'''-diiodobiferrrocene.

The weak 1s + 3d transition in ferrocene consists of a single peak. The splitting of 2eV in the 1s + 3d transition of ferrocenium⁺ was observed and is explained by crystal field splitting of the ground state. The electronic ground states of the ferrocene and ferrocenium ion are the orbitally degenerate ¹A_{1g} and ²E_{2g} states made from the a_{1g}² e_{2g}⁴ and a_{1g}² e_{2g}³ configurations, respectively. The 1s + 3d transition of ferrocene is assigned to the transition from the 1s to the e_{1g} state. Two possibilities of the 1s + 3d transition of ferrocenium⁺ are the transitions from the 1s state to the e_{1g} or e_{2g} states. This agrees with the crystal field splitting of ferrocenium⁺ observed in the electronic absorption data assigned to the d-d transition which corresponds to about 2eV.

Figure 2 shows the XANES spectra of binuclear ferrocenes. The neutral species, diiodobiferrrocene, gives ferrocene-like parameters. In the mono-oxidized biferrrocene and dibromobiferrrocene, the 1s + 3d transition consists of the asymmetric doublet characterized by overlapping of ferrocene- and ferrocenium-like spectra. Although Mössbauer spectra of dibromobiferrrocenium⁺ show the averaged-valence state, the XANES spectrum exhibits the trapped-valence state. This fact indicates that the rate of the thermal electron transfer between two iron atoms in dibromobiferrrocenium⁺ is higher than $\alpha. 10^7 s^{-1}$, but lower than $\alpha. 10^{15} s^{-1}$.

References

- 1) I. Motoyama, K. Suto, M. Katada and H. Sano, Chem. Lett., 1215 (1983).
- 2) S. Iijima, R. Saida, I. Motoyama and H. Sano, Bull. Chem. Soc. Jpn., 54, 1375 (1981).
- 3) R. G. Shulman, Y. Yafet, P. Eisenberger and W. E. Blumberg, Proc. Natl. Acad. Sci. USA, 73, 1384 (1976).

XAS STUDIES ON BIMETALLIC Rh-Co CARBONYL-DERIVED CATALYSTS
I. PRELIMINARY EXPERIMENTS ON Rh/SiO₂ CATALYST

H. Kuroda, N. Kosugi, T. Yokoyama, H. Ishii and K. Asakura

Department of Chemistry and Research Center for Spectrochemistry, Faculty of Science, The University of Tokyo, Hongo, Bunkyo-ku, Tokyo 113 (JAPAN)

M. Ichikawa and T. Fukushima

Sagami Chemical Research Center, Nishi-Ohmura 4-4-1, Sagamihara, Kanagawa 229 (JAPAN)

The catalyst, Rh₄(CO)₁₂ supported on silica, is known to give methanol and other oxygen-containing compounds when used for the CO-H₂ reaction, whereas Co₄(CO)₁₂/SiO₂ catalyst gives C₁ ~ C₄ hydrocarbons. When Rh and Co are used together as carbonyl metals, the catalysts Rh_xCo_{4-x}(CO)₁₂/SiO₂ (x=1,2) give the oxygen-containing C₁ ~ C₄ compounds; these catalysts have catalytic properties intermediate between Rh₄(CO)₁₂/SiO₂ and Co₄(CO)₁₂/SiO₂ catalysts. The catalysts derived from Rh_xCo_{4-x}(CO)₁₂ are considered to be in a state of highly dispersed cluster with the Rh_xCo_{4-x} skelton kept. However no direct evidence has been known so far for the existence of such clusters. It is the purpose of this study to examine the existence of the Rh_xCo_{4-x} cluster on the surface of the Rh-Co bimetallic carbonyl-derived catalysts by means of x-ray absorption spectroscopy (XAS).

There are several experimental difficulties in the XAS study of this kind of catalysts: first, the supported metal carbonyl should be kept in low concentration in order to obtain a good catalyst, and secondly the intensity of the radiation available from the PF storage ring significantly decreases in the photon-energy region around 23 keV. Thus, in the present experiment, we aimed to examine the possibility of obtaining reliable XAS spectra and the necessary experimental conditions by using a Rh/SiO₂ catalyst of 2 wt % Rh as a test sample for Rh_xCo_{4-x}(CO)₁₂/SiO₂.

The observed XAS spectrum is shown in Fig.1. The S/N ratio is rather low as was expected. Figure 2 shows the Fourier transform of the observed EXAFS oscillation. The prominent peak at about 2.5 Å can be attributed to Rh-Rh distance. The result of curve-fitting analysis by use of theoretical parameters is given in Table 1 together with that obtained for Rh metal.

We were able to confirm that EXAFS data sufficient at least for the information about the first shell are obtainable for Rh/SiO₂ catalysts of considerably low Rh concentration.

In the next machine time, we are planning to measure the XAS spectra of Rh_xCo_{4-x}(CO)₁₂/SiO₂ catalysts (x=0,1,2,4) treated under different conditions.

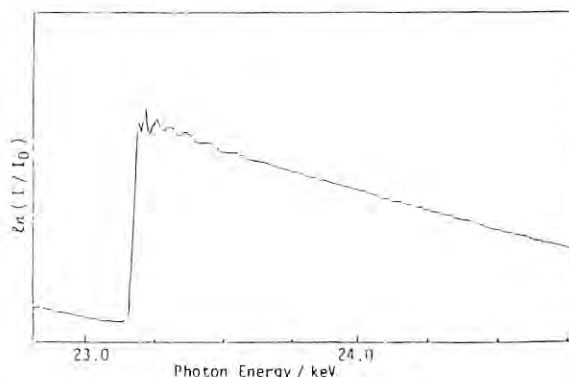


Fig.1 X-Ray Absorption Spectrum of Rh/SiO₂

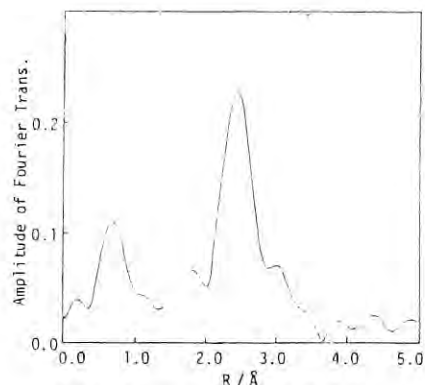


Fig.2 Fourier Transform of Rh/SiO₂

Table 1. Results of the curve-fitting analysis with theoretical parameters

	Rh-Rh distance / Å	Coord. No.
Rh / SiO ₂	2.66 ± 0.03	9.5 ± 1.0
Rh metal	2.67 ± 0.03	(12)*
	(2.69)**	(12)**

*standard **crystallographic data

EXAFS STUDY ON THE STRUCTURE OF HETEROPOLYMOLYBDATES IN SOLUTION

Yukiyoshi SASAKI, Akiko KOBAYASHI, Tomoji OZEKI,

Haruo KURODA, Nobuhiro KOSUGI, Kiyotaka ASAKURA, Hiromu ISHII, Toshihiko YOKOYAMA

Department of Chemistry, Faculty of Science, The University of Tokyo, Hongo, Tokyo 113 (JAPAN)

Introduction

When a mixture solution of MoO_4^{2-} and AsO_4^{3-} is acidified, a series of heteropolyanions containing As and Mo is formed. Potentiometric titrations have revealed the existence of heteropolyanions of the composition, $(\text{MoO}_4^{2-})_p(\text{H}^+)_q(\text{HASO}_4^{2-})_r$, where $(p,q,r) = (8,5,2)$, $(10,6,2)$, $(11,6,2)$ and $(12,6,2)^{1)}$ in solution.

The present study concerns with the structure of this (12,6,2) species. From a solution of pH 2, containing As and Mo in a ratio of 1:3, colorless crystals have been separated. The crystals of $[(\text{CH}_3)_4\text{N}]_2\text{Na}_2[\text{H}_2\text{As}_2\text{Mo}_6\text{O}_{26}] \cdot 8\text{H}_2\text{O}$ have been studied by the single crystal X-ray diffraction technique and it has been found that they contain polyanion of the structure shown in Fig. 1.²⁾

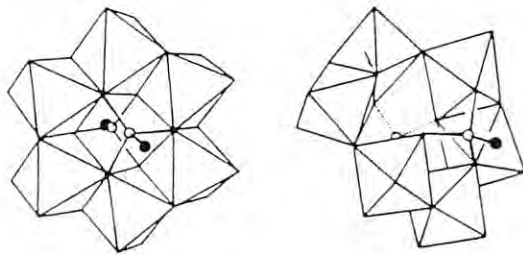


Fig. 1

Fig. 2

Fig. 1. Structure of $[(\text{CH}_3\text{As})_2\text{Mo}_6\text{O}_{24}]^{4-}$
 • denotes OH group.

Fig. 2. Proposed structure of the ion (12,6,2)
 • denotes OH. $[(\text{C}_6\text{H}_5\text{As})_2\text{Mo}_6\text{O}_{24}(\text{H}_2\text{O})]^{4-}$
 has same structure, but in this case,
 • represents a carbon atom of the phenyl groups. + points OH_2 .

At the beginning, it was believed that this structure is stable also in solution.¹⁾ But this model failed to explain the data obtained by the large-angle X-ray scattering of a solution having the upper mentioned composition.³⁾ This disagreement suggests that the structure of the polyanion in solution state is considerably different from that found in crystals (Fig. 1).

Figure 2 shows the model of the (12,6,2) species in solution proposed alternatively by the present authors which gave a better agreement between the solution X-ray diffraction data and theoretical calculations using models.⁴⁾ The composition of the ion having this structure is different from that of Fig. 1 only by one extra water molecule contained. This difference can not be detected by the potentiometry because the two forms have the same charge of 4-. We expected that use of EXAFS may throw some more light on the structure difference of this anion in solution and in solid phase.

Crystals of hexamolybdiarsenate (12,6,2) salt having the structure proposed (Fig. 2) have never been prepared. But an organoarsenate

derivative of the same structure $(\text{C}_6\text{H}_5\text{As})_2\text{Mo}_6\text{O}_{24}(\text{H}_2\text{O})^{4-}$ has been prepared as guanidinium salt.⁵⁾

Our research plan is to compare EXAFS of the solution with those of these crystals, to see coordination around the Mo atoms are similar in both cases, that is the skeleton of the (12,6,2) complex in solution is similar to the structure in Fig. 2.

Experimental

Solution sample containing 0.6 M MoO_4^{2-} , 0.2 M HASO_4^{2-} and HCl which adjusts the pH to 2.2, was used for measurements. In this solution, more than 90% of the total Mo is present in the state of (12,6,2) species. The liquid cell was constructed by an acryl frame and polyester (Mylar) film (<4 micron). The thickness of the liquid was 3 mm. The other sample was powdered crystals of $(\text{CN}_3\text{H}_6)_4[(\text{C}_6\text{H}_5\text{As})_2\text{Mo}_6\text{O}_{24}(\text{H}_2\text{O}) \cdot 4\text{H}_2\text{O}]$. The spectra were registered at EXAFS apparatus BL-10B.

Results

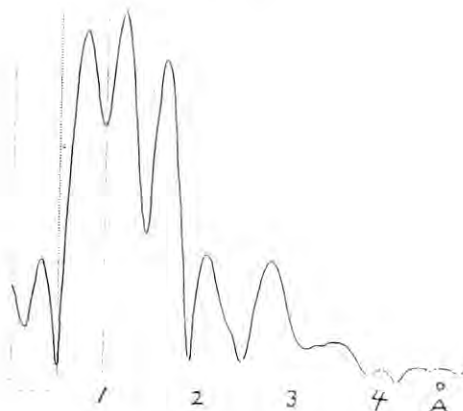


Fig. 3. Fourier transform of solution sample EXAFS.

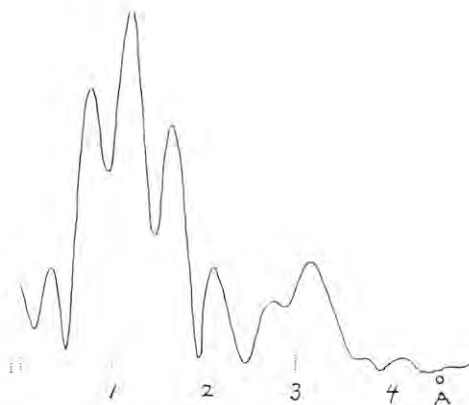


Fig. 4. Fourier transform of EXAFS of $(\text{CN}_3\text{H}_6)_4[(\text{C}_6\text{H}_5\text{As})_2\text{Mo}_6\text{O}_{24}(\text{H}_2\text{O})] \cdot 4\text{H}_2\text{O}$.

Figures 3 and 4 show the Fourier transforms of the EXAFS registered (without the correction for phase shifts) of the liquid and crystal samples. They appear similar, but we need more detailed analyses to draw a clear conclusion on the similarities of the structures of two samples.

Reference

- 1) L. Pettersson: Acta Chem. Scand. A29(1975)677.
- 2) Y. Takeuchi: to be published.
- 3) G. Johansson, L. Pettersson and N. Ingri:
Acta Chem. Scand. A32(1978)681.
- 4) G. Johansson: private communication.
- 5) K. Y. Matsumoto: Bull. Chem. Soc. Jpn.
51(1978)492.

INFLUENCES OF VARIOUS LIGANDS ON JAHN-TELLER EFFECT OF COMPLEXES IN SOLUTION

N.Matsubayashi, I.Watanabe, K.Murata and S.Ikeda
 Department of Chemistry, Faculty of Science, Osaka University
 Toyonaka, Osaka 560 (JAPAN)

Introduction

It is well known that six coordinate Cu^{2+} complexes have the distorted octahedral structures in solid. This effect, known as a Jahn-Teller effect, has also been reported in the solution by X-ray diffraction technique¹⁾. Although a number of Jahn-Teller Cu^{2+} complexes have been studied with EXAFS²⁾, the axial bonds have not been clearly observed on the radial distribution function (RDF) obtained by Foulrier transform (FT). We have measured EXAFS spectra of various Cu^{2+} complexes in solution by Synchrotron Radiation (SR) at Photon Factory in order to clarify the applicability of the EXAFS method for the structure study of the Jahn-Teller effect.

Experimental

Samples below were prepared for measurements: 0.2M $\text{Cu}(\text{NO}_3)_2/5.4\text{M}$ en (ethylene diamine), 0.2M $\text{Cu}(\text{NO}_3)_2/13.5\text{M}$ NH_3aq , 1M $\text{Cu}(\text{NO}_3)_2/x\text{M}$ $\text{LiCl}+(5-x)\text{M}$ LiNO_3 , 1M $\text{Cu}(\text{NO}_3)_2/7\text{M}$ $\text{LiCl}+0.01\text{M}$ HNO_3 , 1M $\text{CuCl}_2/12\text{M}$ HClaq .

The solution samples were put into the polyethylene pouch sandwiched between the two stainless steel holders. All of the EXAFS spectra of Cu K-edge were obtained with the monochromator having a channel cut Si(3,1,1) crystal and the collection time was fixed at 1 sec and total measurement time was about thirty minutes for a single scan. The SR ring was operated at 2.5 GeV and the beam current was between 50 - 150 mA.

Results and discussion

The EXAFS spectra obtained are now under investigation and so far, the analysis of EXAFS data for 1M copper nitrate solution gave a peak at 2 Å from central copper atom corresponding to nearest neighbor Cu-O bond distance. But the peak corresponding to Cu-O bond which should lie around 2.4 Å due to the Jahn-Teller effect could not be clearly observed. If the shoulder peak around 2.35 Å is the one, this is too weak to be distinguished from the ripple peaks which appear by the termination error on FT. The further analysis is now carried out by maximum entropy method in order

Table 1. Result of FT analysis for Cu^{2+} in Cl^- solution

[Cl ⁻]	O			Cl		
	R/Å	h	hR ²	R/Å	h	hR ²
0	2.00	1.15	4.6			
0.25	1.98	1.14	4.6	2.28	0.20	1.0
0.5	2.00	1.15	4.6	2.32	0.21	1.1
1	2.02	1.03	4.2	2.36	0.21	1.1
2	2.00	0.85	3.4	2.32	0.27	1.4
3	2.00	0.75	3.0	2.30	0.30	1.6
5	2.00	0.60	2.4	2.30	0.36	1.9
7	2.04	0.48	2.0	2.30	0.47	2.5
14	1.94	0.25	0.9	2.28	0.66	3.4
				N		
0.2M $\text{Cu}(\text{NO}_3)_2/5.4\text{M}$ en				2.06	0.91	3.9
0.2M $\text{Cu}(\text{NO}_3)_2/13.5\text{M}$ NH_3				2.08	0.98	4.2

to get higher resolution than by FT.

Some of the RDFs by FT with k ranges of 3.6 - 16.85 Å⁻¹ obtained from the EXAFS spectra for copper chloride complexes were shown in Fig. 1. The RDFs were corrected for phase shift and back-scattering amplitude by using the parameters for Cu-O bond given by Teo and Lee³⁾. The result in Fig. 1 indicates that the higher the concentration of Cl^- , the smaller the peak of oxygen of H_2O at 2 Å and the higher the peak of Cl^- at 2.3 Å. The peak position R and the peak height h and hR^2 as the value proportional to the coordination number were determined and are given in Table 1. These values were obtained by correcting for back-scattering amplitude and phase shift of the atoms not only of O, but also Cl^- and N. Although the low peaks are possibly influenced by ripple peaks and it is necessary to deconvolute to separate two peaks, the result indicates that Cl^- substitutes for equatorial H_2O at the first stage and that even in the case of CuCl_2 in concentrated HCl solution four equatorial H_2O are not substituted completely and axial Cl^- is not found.

Moreover, detailed analysis using curve fitting method should be applied to the EXAFS spectra to obtain the coordination number of Cu^{2+} which should give the important information about the formation of copper chloride complex in aqueous solution.

It should be noticed that whereas the peak around 2.3 Å corresponding to Cu-Cl could be observed on RDF, the peak corresponding to Cu-O bond which should lie around 2.4 Å owing to the Jahn-Teller effect could be clearly observed.

We wish to thank Drs. T.Matsushita, H.Oyanagi and M.Nomura for the help for measurement.

References

- 1) H.Ohtaki and M.Maeda: Bull. Chem. Soc. Jpn., 47(1974) 2197
- 2) T.K.Sham, J.B.Hastings and M.L.Perlman: Chem. Phys. Lett., 83(1981) 391
- 3) B.K.Teo and P.A.Lee: J. Am. Chem. Soc., 101(1979) 2815

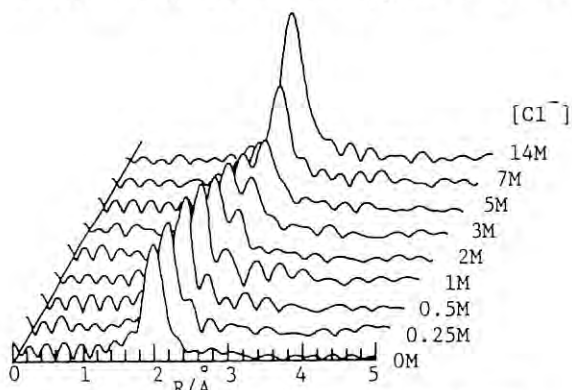


Fig. 1. The RDFs of Cu^{2+} in the solutions of various concentration of Cl^-

EXAFS STUDY OF FLUORITES

N. Kamijo, K. Koto*, Y. Ito*, K. Tanabe**, K. Kikukawa**, H. Maeda***, M. Hida****, T. Murata*****, H. Terauchi**

Government Industrial Research Institute, Osaka., Ikeda Osaka 563, Inst. of Sci. and Ind. Res. Osaka Univ., Suita Osaka 565*, Dept. of Phys., Kwansai-Gakuin Univ., Nishinomiya 662**, Dept. of Chem. Okayama Univ., Okayama 700***, Sch. of Eng., Okayama Univ., Okayama 700****, Dept. of Phys., Kyoto Univ. Education, Kyoto 612*****

Many compounds with calcium fluoride type structure show an anomaly in the specific heat at an elevated temperature, a few hundred degree below their melting temperature. This anomaly is associated with an order-disorder phase transition which is accompanied by arise in ionic conductivity. β -PbF₂ has the lowest transition temperature (705 K) and high ionic conductivity among these compounds.

Single crystal X-ray and powder neutron diffraction studies of this compound at various temperatures have been published^{1)~4)} which were carried out to investigate the diffusion mechanism of mobile ions at elevated temperature. In these investigations it was found that the occupation probability of fluorine ion at normal site decreases and the anharmonic thermal vibration is pronounced with increasing temperature: fluorine ion does not occupy the center of Pb tetrahedron but is displaced into four split positions with an occupation probability of 1/4 for each position.⁴⁾ Here we present the way of disorder of fluorine ion about this compound at 80 K and 293 K using the EXAFS spectroscopy which is one of the powerful techniques for determining the local atomic arrangement.

The X-ray absorption measurements were carried out at the KEK Synchrotron Radiation Laboratory on beam line 10-B (EXAFS). The EXAFS spectra of the Pb-L₃ edge of the crystalline β -PbF₂ (80 K and 293 K) were obtained. In obtaining the EXAFS function $\chi(k)$, the background level is subtracted from the observed absorption coefficient by using a Victoreen fit and the absorption coefficient for an isolated atom is obtained by the cubic spline technique.⁵⁾

Fig. 1 shows the Fourier transformations of the EXAFS spectra ($k=3.0\sim 16.9 \text{ \AA}^{-1}$) multiplied by k^3 , (a) at 80 K and (b) at 293 K.

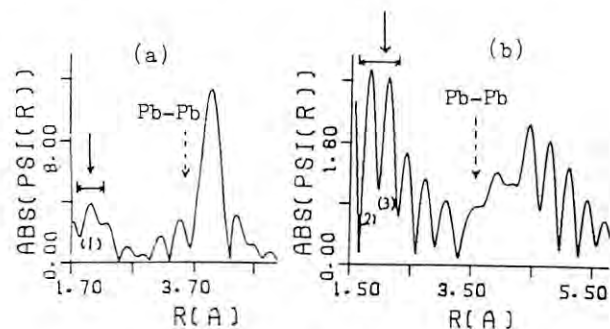


Fig. 1

The magnitude (ABS in Fig. 1) of each transformation provides the radial structural function (RSF), where no phase shift correction being

made. Arrows indicated by solid and dotted lines in each RSF show the position of normal fluorine and lead ion sites respectively in ideal fluorite structure at room temperature. In Fig. 1 it is found that the broad first peak in (a) indicated by (1) splits into sharp double peaks as shown (2) and (3) in (b).

There are many peaks within the Pb-Pb distance, 4.20 Å in each RSF. From these RSF features it is found that fluorine ion does not occupy the center of the normal sites but is displaced into several separate sites along the body diagonals in the direction of the Pb tetrahedral faces even in 80 K and this tendency remarkably increase as temperature increased. These interstitial anions will play a key role in ion conduction process indicating the hopping model being a probable one.

For the first and second peaks in (a) and (b) in Fig. 1 indicated by arrows, curve-fitting method is applied using Fourier filtering method (reference sample: α -PbF₂). The atomic distances between Pb and F ions and coordination numbers around Pb ion thus obtained are shown in Table 1.

The data analysis of the high temperature EXAFS measurement of β -PbF₂ and that of SrF₂ are now in progress.

Table 1. Atomic distances (R) and coordination numbers (N)

shell	80 K		293 K	
	R(A)	N	R(A)	N
Pb-F (1)	2.53	3.2	2.53	2.4
Pb-F (2)	2.63	3.2	2.66	2.4

References

- 1) S.M. Shapiro and F. Reidinger, in: Physics of superionic conductors, ed. M.B. Salamon (Springer Berlin, 1979) P. 45
- 2) M.H. Dickens, W. Hayes, C. Smith and M.T. Hutchings, in: Fast ion transport in solids, eds. P. Vashishta, J.N. Mundy and G.K. Shenoy (North-Holland, Amsterdam, 1979) P. 225
- 3) K. Koto, H. Schulz and R.A. Huggins, Solid State Ionics 1 (1980) 355
- 4) K. Koto, H. Schulz and R.A. Huggins, Solid State Ionics 3/4 (1981) 381
- 5) H. Maeda, H. Terauchi, K. Tanabe, N. Kamijo, M. Hida and H. Kawamura: Jpn. J. App. Phys. 21 (1982) 1342

ANOMALOUS SCATTERING PHENOMENA APPLIED TO THE STUDY OF
SHORT-RANGE ORDER IN TERNARY ALLOYS

S. Hashimoto, H. Iwasaki, Y. Watanabe, K. Ohshima*, J. Harada*, M. Sakata*,
H. Terauchi**, T. Matsushita***, T. Nakajima*** and T. Ishikawa***

The Research Institute for Iron, Steel and Other Metals, Tohoku University, Sendai

* Faculty of Engineering, Nagoya University, Nagoya

** Faculty of Science, Kwansai Gakuin University, Nishinomiya

*** KEK, National Laboratory for High Energy Physics, Oho, Ibaraki

Introduction

Measurement of X-ray diffuse scattering is the most direct method available for deriving an information on the short-range ordered structure of metallic solid solutions and a number of data have been accumulated on a variety of binary alloy systems. In recent years much attention has been focused on ternary alloys which often exhibit physical properties different from those of binary alloys and are becoming important materials for industrial use. These properties are known to be sensitive to the state of order present in the alloys, but no investigation has hitherto been made to reveal their short-range ordered structure. The reason is found in that there are three kinds of parameters, in contrast to one for binary alloys, to describe the state of order but it is not possible to determine these parameters with recourse to an ordinary method of intensity measurement. Denoting these parameters by α_{λ}^{AB} , α_{λ}^{BC} and α_{λ}^{CA} , the diffuse scattering intensity from short-range ordered ternary alloys is written as

$$I_{SRO}(\mathbf{q}) = N \{ m_A m_B |f_A - f_B|^2 \alpha_{\lambda}^{AB}(\mathbf{q}) + m_B m_C |f_B - f_C|^2 \alpha_{\lambda}^{BC}(\mathbf{q}) + m_C m_A |f_C - f_A|^2 \alpha_{\lambda}^{CA}(\mathbf{q}) \}, \quad (1)$$

where $\alpha_{\lambda}^{AB}(\mathbf{q}) = \sum_j \alpha_{\lambda}^{AB} \exp(2\pi i \mathbf{q} \cdot \mathbf{R}_j)$, etc., N is the total number of atoms, \mathbf{q} a vector in reciprocal space, \mathbf{R}_j an interatomic vector, m_j the fraction of the j th kind of atom and f_j its scattering factor. Eq.(1) indicates that what one can measure is a superposition of the partial intensities carrying an information on the spatial correlation of the respective pairs of atoms.

It is possible, however, to obtain α_{λ}^{AB} , α_{λ}^{BC} and α_{λ}^{CA} separately if one makes intensity measurements with changing scattering power of atoms, solves three sets of intensity equations of the form (1) containing three unknowns and

performs Fourier transformation. The most effective way of doing this type of measurements is to utilize the anomalous scattering phenomena of X-rays by atoms, i.e., to perform the measurements using X-rays of the three kinds of wavelength lying near the absorption edges of the constituent atoms.

We present here a preliminary report of the investigation done at the photon factory of KEK.

Experimental Procedures

Cu-20at%Ni-24at%Zn alloy single crystal was chosen as the sample which had been quenched from a temperature of 600°C. It has an fcc structure with the lattice parameter $a=3.633 \text{ \AA}$. A slab (6 mm in diameter and 4mm in thickness) was cut from the ingot so that the surface was parallel to a (210) plane.

The sample crystal was mounted on a single crystal orienter capable of doing ϕ - and χ -motion, which was fixed on the θ - 2θ goniometer developed originally for the crystallographic study at low temperatures, the details of which are given in this issue. This composite diffractometer was installed at the beam line 10-C, where X-rays monochromated by a pair of silicon single crystals and focused at sample position by a curved mirror were available. The wavelength spread $\Delta\lambda/\lambda$ is 4

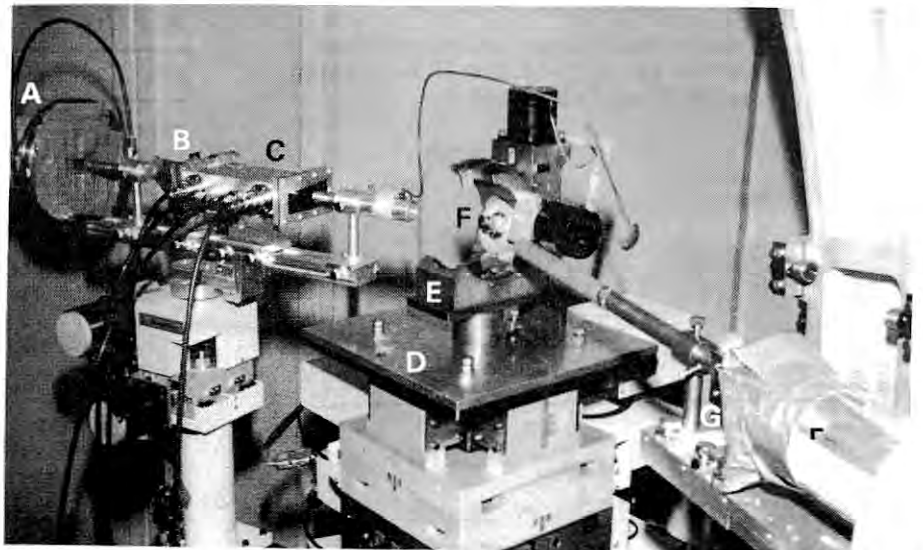


Fig. 1. X-ray diffuse scattering measurement system installed at the beam line 10-C.

$\times 10^{-4}$ at $\lambda=1.5 \text{ \AA}$. Scattered radiation from the sample was detected by a versatile solid state-detector (pure Ge). Any variation of the incident beam intensity was monitored using an ion chamber placed behind the divergence slit system. The beam divergences of the present X-ray optical system gave a parallelepiped of the sizes of $(0.02)^3$ in reciprocal lattice unit. Figure 1 shows a photograph of the whole experimental set up. All procedures of adjustments and measurements were controlled by a micro-computer (not shown in Fig. 1).

X-rays of the following three kinds of wavelength selected from the band of continuous spectrum were used; 1.32, 1.41 and 1.59 \AA , which are respectively slightly longer than the wavelength of the absorption edges of zinc, copper and nickel. The gate width of the pulse-height analyser was set so that it accepted scattered radiation of the same wavelength as that of the incident radiation but rejected fluorescent $K\alpha$ and $K\beta$ radiation emitted from the sample. The measurements were performed throughout the reciprocal space volume commonly adopted in the study of short-range order in the fcc alloys. Intensity data were collected at points separated by 0.02 reciprocal lattice unit along the cubic axis, except for the region containing no diffuse intensity peaks in which measurements were made at larger intervals. Measured intensities were put into an absolute scale by making comparison with the intensity scattered from amorphous polystyrene kept under the identical experimental condition. Correction was made for the Compton scattering effect by calculating its intensity using the International Tables III.

Experimental Results

Figure 2 shows the intensity contour maps, expressed in electron unit, of Cu-20at%Ni-24at%Zn alloy obtained using X-rays of the three kinds of wavelengths. A peak located at the 110 position is undoubtedly due to the short-range order

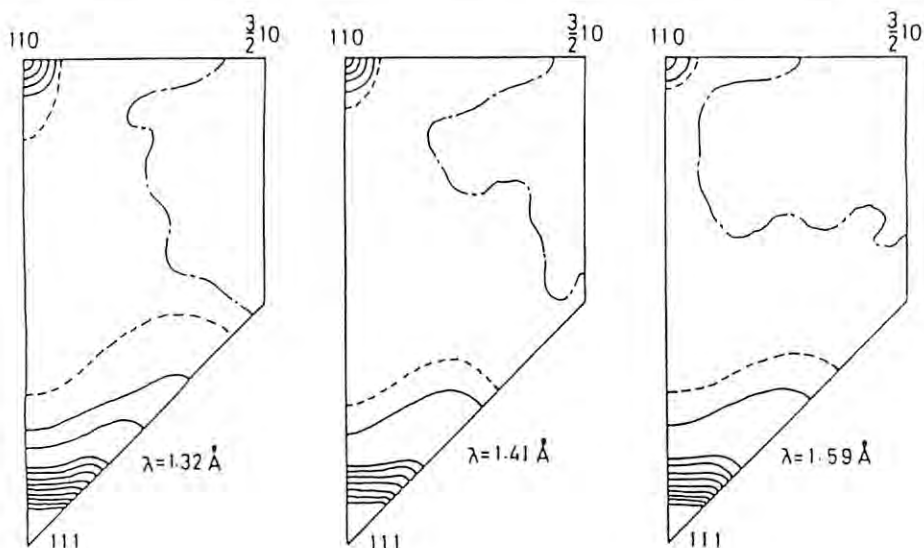


Fig. 2. Intensity contour maps in $(h \ 1 \ l)$ section of the reciprocal lattice of Cu-20at%Ni-24at%Zn alloy measured using X-rays of the three kinds of wavelengths.

present in the alloy, which, because of the small difference in atomic number between the three elements here concerned, would be very weak in intensity if measured using the characteristic radiation usually available. The enhancement of intensity particularly notable for the radiation of the wavelengths 1.32 and 1.41 \AA is due to the anomalous scattering effect. The intensity observed around the 111 position consists of two parts; one with a distribution like that of temperature diffuse scattering and the other with a long tail along the $\langle 111 \rangle$ direction.

The three sets of the observed intensity $I_{\text{SRO}}(q)$ now allow us to obtain the partial intensities $\alpha^{\text{CuNi}}(q)$, $\alpha^{\text{NiZn}}(q)$ and $\alpha^{\text{ZnCu}}(q)$. In this procedure the anomalous scattering factors given by Cromer and Lieberman¹⁾ were used. Owing to insufficient counting statistics, there remains some fluctuation in the resulting partial intensity contour maps, but it is certain that the 110 diffuse peak is due to an ordering type correlation of Cu-Ni and Zn-Cu atomic pairs, while there is a clustering type correlation, though not much remarkable, for the Ni-Zn pair. The ordering tendency found for the Cu-Ni pair is of particular interest, since the existence of clustering of atoms was revealed for the binary Cu-Ni alloy system²⁾. The results of the present investigation suggest that the nature of interaction between atoms in ternary alloys is not necessarily the same as that observed in binary alloys.

We thank Dr. Kashiwara of Nagoya University and Mr. Nishihata of Kwansai Gakuin University for their help in this experiment.

References

- 1) D. T. Cromer and D. J. Liberman: J. Chem. Phys. 53(1970) 189; Los Alamos Scientific Lab. Rep., LA-4403(1970).
- 2) B. Mozer, D. T. Keating and S. C. Moss: Phys. Rev. 175(1968) 868.

DYNAMIC BEHAVIOUR OF BIOPOLYMERS STUDIED BY SMALL-ANGLE SCATTERING (I)

T. Ueki¹, Y. Hiragi², Y. Izumi³, H. Tagawa⁴, M. Kataoka⁵, Y. Muroga⁶, T. Matsushita⁷
and Y. Amemiya⁷

1. Faculty of Engineering Science, Osaka University, Toyonaka, Osaka 560 (JAPAN)
2. Institute for Chemical Research, Kyoto University, Uji, Kyoto 611 (JAPAN)
3. Faculty of Science, Hokkaido University, Sapporo, Hokkaido 011 (JAPAN)
4. Faculty of Science and Technology, Nihon University, Chiyoda-ku, Tokyo 100 (JAPAN)
5. Faculty of Science, Tohoku University, Sendai, Miyagi 980 (JAPAN)
6. Faculty of Engineering, Nagoya University, Nagoya, Aichi 464 (JAPAN)
7. Photon Factory Instrumentation Group, KEK, National Laboratory of High Energy Physics, Oho-machi, Tsukuba-gun, Ibaraki 305 (JAPAN)

Introduction

A "tunable" small-angle X-ray scattering apparatus for "enzyme" (SAXES - Small-Angle X-ray Equipment for Solutions) was designed and constructed in Photon Factory, KEK, mainly for use of the experiments on non-crystalline materials such as aqueous solutions of biological polymers, synthetic polymers, metals and alloys that give continuous scattering in small-angle region.

This is an activity report of SAXES working group in evaluating the performance of apparatus. A number of preliminary experiments were carried out on various specimens of biological materials and synthetic polymers, during the machine time of 14-th to 24-th of June, 1983. Since the specimen chambers for the time-resolved problems are not finished yet, experiments were limited to the static at present. Out of experiments, we report typical results of scattering from collagen and polystyrene latexes that have large dimensions.

Experimental

Experiments were performed with the storage ring operated at the energy of 2.5 GeV with the beam current of 50 ~ 130 mA. The X-ray used was the wavelength of 1.4881 Å which corresponds to the absorption edge of nickel foil. The specimen to detector distances were either 2,010 mm for film recording or 2,180 mm with the one-dimensional PSPC. The PSPC was operated with a mixture of argon 90 % + CH₄ 10 % at the gauge pressure of 1 atm. The high voltage applied to PSPC was 2,000 volts. Since the scattering from specimen, in addition to the parasitic, was too intense to handle with the present PSPC, attenuators of aluminum plates with various thickness were used, depending on the counting rate. With film recording, no attenuators were used.

Results

The meridional X-ray diffraction pattern from collagen, soaked in Locke's solution, is shown in Fig. 1. The diffraction photograph was recorded in 5 min with Fuji film at the beam current of 105 mA. Collagen has a long repeat distance of 670 Å, along its fibre axis and is a specimen frequently used to test the small-angle resolution. As seen in the figure, the first order reflection can be clearly resolved apart from the beam stop and reflections up to

the twelveth can easily be recognized in the photograph. The slightly assymmetric feature of reflections is attributed to the shape of the direct beam since the back focal plane was somewhat displaced from its ideal position. The same collagen specimen was used in the experiments with PSPC. The intensity profile

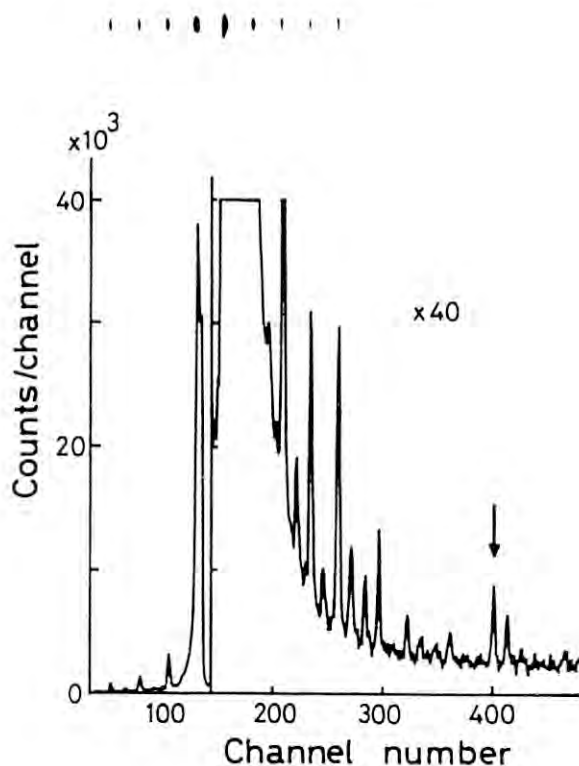


Figure 1. The diffraction photograph and the intensity profile measured with PSPC from collagen soaked in Locke's solution. The profile with channel numbers higher than 156 (right three quarters of the profile) is 40-fold. The first order reflection of period, 670 Å, is seen at about 120 channel in the left quarter. The arrow shows the 20-th order reflection.

of the diffraction pattern is also shown in Fig. 1. The counting time was 100 sec at the beam current of 100 mA. An attenuator of aluminum plate with a thickness of 0.22 mm was inserted in front of the specimen. The attenuation factor of this aluminum plate is about 1/12, and hence the effective counting time is about 8 sec without attenuator. In the left quarter of the figure, the first order reflection can be clearly visible at the channel number of 120, whereas, in the right hand side, reflections up to the 25-th order of 670 Å repeating structure can be seen (the arrow in the figure shows the 20-th order reflection).

Polystyrene latexes, dried on mica, gave a scattering intensity with the counting rate of 55,000 cps at the beam current of 91 mA. Without attenuator, the counting rate is estimated to be more than 6×10^5 cps/chamber. Figure 2 shows the intensity profile, $\log(I)$, of scattering. It consists of five broad scattering rings with its innermost ring at the Bragg spacing of 550 Å. From this raw data, the size of the latex was estimated although it stays as the approximate since the data were not corrected for background scattering and so on. The dashed line in the figure is the scattering intensity calculated for sphere with a radius of 475 Å. The peak positions of the scattering from the sphere coincide very well with scattering rings observed. This radius of sphere is consistent with the result of electron microscopy, 500 Å.

Discussions

The SAXES constructed in PF was proved to have the performance as designed, for instance the small-angle resolution of 1,500 Å with the wavelength at 1.5 Å. The intensity at the specimen was found to be more than 10^{11} photons/sec although the full width of the incident beam was not utilized with the specimen yet because of the thickness of the specimens. The spatial resolution is less than 1 mrad since the direct beam size in vertical direction is about 1.5 mm, and is slightly better than the value designed. However, the angular resolution was found not to be satisfactory to record the fine details of the scattering from polystyrene latexes, as seen in Fig. 2.

The time-resolved experiments, as stopped-flow and temperature jump technique, are planned to be performed in the machine time in fall, and the results will follow in the next report. The manuscript of SAXES is in preparation and will appear elsewhere.

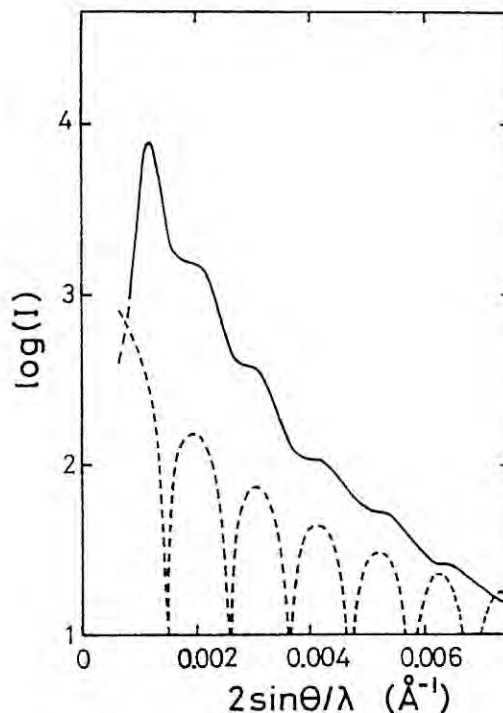


Figure 2. The intensity profile, $\log(I)$, of the scattering from polystyrene latexes, dried on mica. Five broad maxima are visible in the figure with the innermost at 550 Å. The dashed line is the calculated intensity profile from sphere with radius of 475 Å.

PERFORMANCE OF MULTI-DETECTOR SYSTEM FOR FLUORESCENCE EXAFS EXPERIMENTS

H. Oyanagi, T. Ishiguro, T. Matsushita⁺, and K. Kohra⁺

Electrotechnical Laboratory, Sakura-mura, Niihari-gun, Ibaraki 305

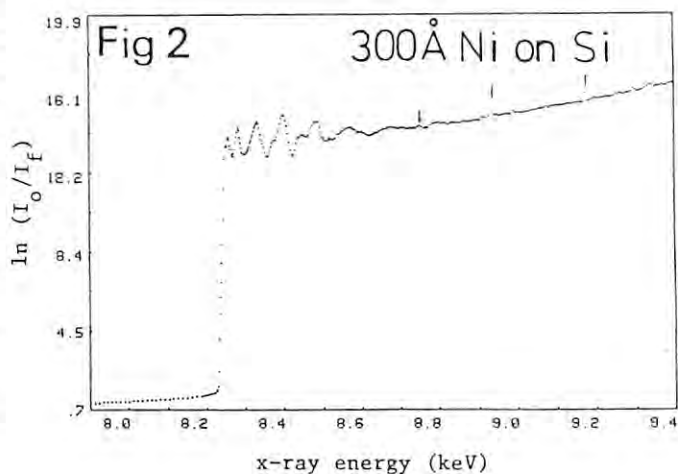
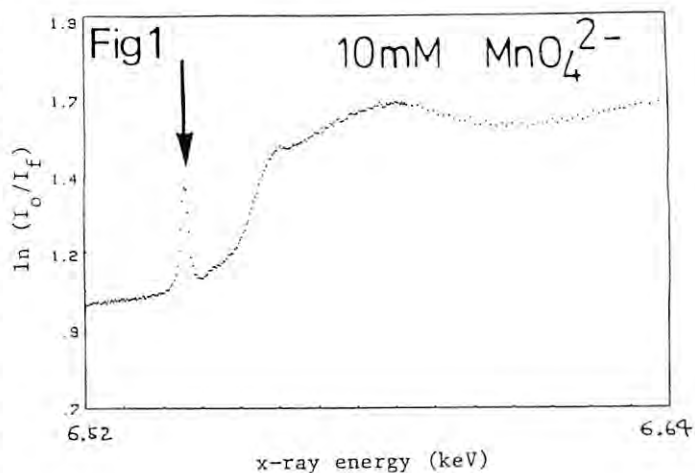
⁺ National Laboratory for High Energy Physics, Oho-machi, Tsukuba-gun, Ibaraki 305

A multi-detector system for fluorescence EXAFS experiment has been designed and constructed under a cooperative program between the Electrotechnical Laboratory and the Photon Factory. It has nine NaI detectors arranged almost perpendicularly to the incident beam direction subtending 18% of 4π steradian in solid angle. Each detector is equipped with a 2-dimensional soller slit in order to reduce fluorescent X-ray intensity from a metal foil which filters out the elastically scattered X-rays. More details of this system is reported in § V.3.1 in this report.

During the June-July run of 1983, this detector system was first tested on the focused beam line, 10C. The optics of this line consisted of a double crystal monochromator (up stream) and a bent cylindrical mirror. An intensity of the order of 10^{10} photons/sec is obtained at the focus (approximately 6 mm(H) \times 1.5 mm(V)) with an energy resolution of better than 2 eV at 9 keV. As the beam height of the focused beam does not change by scanning the X-ray energy with the monochromator on this beam line, the height of the detector system is kept constant during the measurement of fluorescence EXAFS spectra.

Figure 1 shows a spectrum near the Mn K-absorption edge for 10 mM K_2MnO_4 solution. A sharp spike indicated by an arrow in this figure is observed with a high resolution. This indicate that a high resolution study in the near edge region is possible in a fluorescence detection mode with a combination of the optics of BL-10C and this multi-detector system.

Figure 2 shows a Ni-K edge EXAFS spectrum for a 300 Å thick nickel film deposited on a single crystal of silicon. A typical accumulated photon number is more than 2 million counts per data point of this spectrum for an integration time of 6 seconds. It took about an hour to take the spectrum shown in Fig. 2.



FINE STRUCTURE OF Ti $L_{2,3}$ EDGES IN Ti, TiS AND TiS₂

Shun-ichi Nakai, Masanao Ohashi, Kazutsugu Ogata,
Mihiro Yanagihara* and Hideki Maezawa*
Department of Applied Physics, Faculty of Engineering,
Utsunomiya University, Utsunomiya 321, JAPAN
*Photon Factory, National Laboratory for High Energy Physics,
Oho-machi, Ibaraki-ken 305, JAPAN

The 3d transition-metals and their compounds have various interesting characters in their magnetic and electrical properties which are related to the unoccupied 3d states. Therefore, it is worthwhile to investigate the $L_{2,3}$ absorption spectra of the transition from the 2p core levels to the unoccupied 3d states. Fine structure of the $L_{2,3}$ edges of 3d transition-metals and their compounds have been previously measured by several authors.^{1),2),3)} A crystal monochromator has been usually used in the wavelength region 10-30 Å, where the $L_{2,3}$ edges of the 3d transition metals lie. However, the x-ray radiation caused sometimes damage the analyzing crystal, then it has been difficult to obtain a high resolution spectrum. The use of synchrotron radiation combine with a grating monochromator allows us to collect well-resolved data at soft x-ray region. As is now, the PF light source has become to available to use, then in this study, we tried to measure the $TiL_{2,3}$ absorption spectra of Ti, TiS and TiS₂.

The absorption measurements were performed at the BL11-A line at 2.5 GeV electron storage ring (KEK-PF) by use of a grazing incidence monochromator "Grasshopper". The monochromatized x-ray I_0 was monitored by a ceratron and the transmitted x-ray intensity I was detected by a HTV R595 CuI photoelectron multiplier. A TN-4000 microcomputer stored and displayed the spectrum. The absorption film of Ti metal was prepared by electron-beam evaporation onto a thin collodion film, while the absorption specimens of TiS and TiS₂ were prepared in form of powders and spreaded them mixing with ethanol onto a thin collodion film. The vacuum in the sample chamber was about 10^{-8} Torr.

Figure 1 shows the $TiL_{2,3}$ absorption spectra of Ti, TiS and TiS₂ recorded with a resolution of < 1 eV. The spectrum of Ti metal is composed of two peaks "white lines" arise through transitions from the 2p core levels to the narrow unoccupied 3d states. The lower energy peak is the transition from the $2p_{3/2}$ level (L_3) and the higher one is the $2p_{1/2}$ level (L_2). The L_3 - L_2 spin-orbit splitting is estimated as 5.5 eV in Ti metal which agrees closely with the XPS binding energy data (6.1 eV). The intensity ratio of L_2 to L_3 is estimated roughly as 1 : 2.5 in contrast to the ratio of 2 : 1 as expected theoretically. Our data is differ from a previous Fisher's one in spectral profile which was performed using self-absorption technique, while consistent with the electron energy loss spectrum (EELS) by Leapman et al.⁴⁾ In the case of TiS and TiS₂ spectra, each of the L_3 and L_2 peaks is split into two components separated by 1.5 eV. Similar structure was also observed in the EELS data of TiO₂ and interpreted in terms of the crystal field which splitted the degenerate unoccupied 3d states into a lower energy $2t_{2g}$ molecular orbital

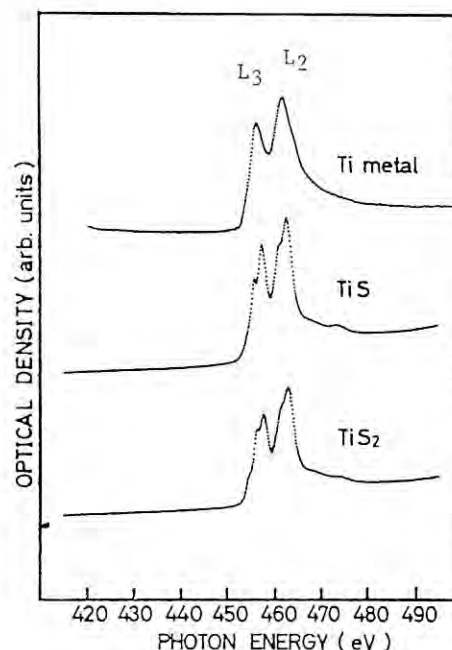


Fig. 1

(MO) level and a higher energy $3e_g$ level. In our observed spectra of TiS and TiS₂, the Ti atom is also octahedrally coordinated, therefore lower peak of L_3 is attributed to $2t_{2g}$ and higher one to $3e_g$ MO levels, respectively. The SK absorption spectrum of TiS₂ obtained by Ohno et al.⁶⁾ also showed that the $t_{2g}^-e_g$ peak splitting was 2.0 eV. In addition, in the case of the spectrum of TiS₂, an additional shoulder structure is located at the 1.7 eV lower energy side of the $2t_{2g}$ peak. This structure has no MO interpretation, then may be attributed to a core exciton absorption. Recently, Grunes⁵⁾ has measured a corresponding structure in the TiK absorption edge of TiO₂ and also interpreted as a core exciton.

Now, we intend to take further refined spectra of these materials at coming beam time.

References

- 1) C. Bonnelle, Ann. Phys. (Paris) 1, 439 (1966).
- 2) D.W. Fischer, J. Appl. Phys. 41, 3561 (1970).
- 3) S. Kiyono, Y. Hayasi, S. Kato and S. Mochimaru, Jpn. J. Appl. Phys. 17, 212 (1978).
- 4) R.D. Leapman, L.A. Grunes and P.L. Fejes, Phys. Rev. B26, 614 (1982).
- 5) L.A. Grunes, Phys. Rev. B27, 2111 (1983).
- 6) Y. Ohno, K. Hirama, S. Nakai, C. Sugiura and S. Okada, Phys. Rev. B27, 3811 (1983).

SENSITIVE Z DEPENDENCE OF $M_{4,5}$ GIANT RESONANCE
 ABSORPTION SPECTRA OF $Z=49-57$ ELEMENTS

Y.Iguchi, H.Maezawa*, M.Yanagihara*, Y.Suzuki* and T.Sasaki*

Institute of Applied Physics, University of Tsukuba
 Sakura, Ibaraki 305 (Japan)

* Photon Factory, National Laboratory for High Energy Physics
 Oho, Ibaraki 305 (Japan)

The nd-f (n=3,4) transitions of the elements around $Z=54$ play a special role in the study of atomic spectra¹⁾. A notable coexistence of discrete and continuum features appears in the absorption spectra near the $M_{4,5}$ and $N_{4,5}$ thresholds in the range $Z>55$ ²⁾. Centrifugal potential barriers have major influence on these spectra to form the so-called 'giant resonances'.

We have measured a series of the $M_{4,5}$ giant resonance absorption spectra of elements $Z=49-57$ in solid thin films, except Xe gas, by means of a 'Grasshopper' monochromator connected to the BL 11A beam line in the photon energy range 440 to 890eV to explore Z dependence of the giant resonance of atomic nature and to find solid state effects.

Fig.1 shows optical density curves of In, Sn, Sb, Te, CsI, KI, NaI, Xe, CsCl, BaF₂, LaF₃ and a photoelectric yield curve of La₂O₃. The abscissae of the graphs are photon energies measured from the onset of the M_5 absorption cross-section. Two main peaks observed for $Z>52$ correspond to M_4 and M_5 giant resonances. photon energy difference between the onset and the peak of the M_5 giant resonance becomes smaller as Z increases. Shape of the resonance becomes sharper as Z increases, and this tendency is abrupt for $Z>55$. Decrease of the absorption continuum is also observed as Z increases. The gross structures of the spectra do not depend on the other component of the compound in I $M_{4,5}$ spectra of CsI, KI and NaI, Cs $M_{4,5}$ spectra of CsI and CsCl, and La $M_{4,5}$ spectra of LaF₃ and La₂O₃ showing themselves to have an atomic origin. The M_4 and M_5 spectra are well separated and appear relatively simpler than $N_{4,5}$ spectra because the 3d spin-orbit interaction is dominant and the exchange interaction between the 3d shell and the 4f shell is small. This circumstance makes us easy to see the abrupt changeover of f-wave functions from collapsed state to uncollapsed state through the Z dependence of the shape of $M_{4,5}$ giant resonances around $Z=54$. The FWHM of the M_5 resonance decreases from 4.3eV for Ba(BaF₂) to 2.2eV for La(La₂O₃), in which 4f state almost completely collapses. This fact coincides with the one observed in atomic vapour³⁾. The abrupt change of the spectra corresponds closely with the abrupt change of potential barrier calculated by the use of HS potential⁴⁾. This fact is also supported by HF calculation⁵⁾

Weak but clear structures present below the M_5 giant resonances showing edges at the thresholds for $Z=49$ to 54. These resonances would lead to the 3d- ϵ_p continua because the f continua are expected to be very small at the thresholds. We consider the fine structures observed for solid samples near the thresholds to be the solid state effects due to the density of p-like states.

References

- 1) S.T.Manson: in Photoemission in Solids I, M.Cardona and L.Ley eds. (Springer-Verlag, 1978) p.135.
- 2) M.Elango, A.Maiste and R.Ruus: Phys. Letters 72A (1979) 16.
- 3) B.Sonntag and A.Yagishita: this activity report.
- 4) F.Herman and S.Skillman: Atomic Structure Calculations, (Prentice-Hall, 1963).
- 5) J.P.Connerade and M.W.D.Mansfield: Proc. R. Soc. Lond. A346 (1975) 565.

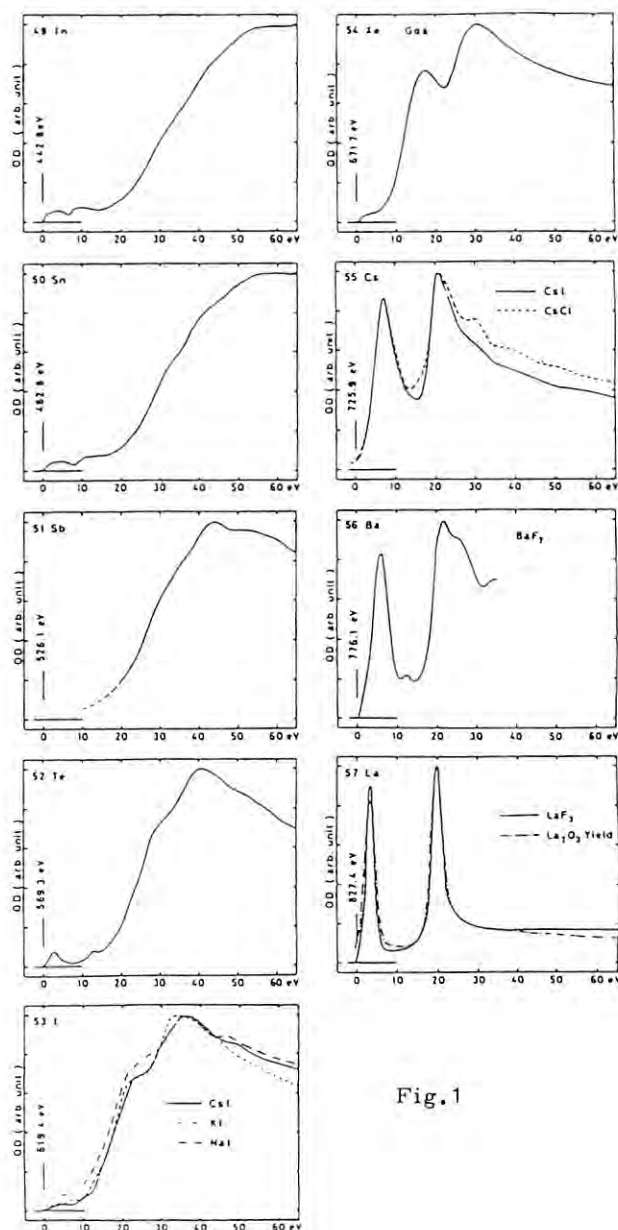


Fig.1

COLLAPSE OF THE f-SYMMETRIC FINAL STATE WAVE-FUNCTION
IN THE 3d-EXCITATION SPECTRA OF ATOMIC Xe, Cs and Ba

B. Sonntag^{1*}, T. Nagata², U. Sato³, Y. Satow¹,
A. Yagishita¹ and M. Yanagihara¹

- 1) Photon Factory, National Laboratory for High Energy Physics,
Oho-machi, Tsukuba-gun, Ibaraki-ken 305, Japan
- 2) Research Institute for Scientific Measurements, Tohoku University,
2-1-1 Katahira, Sendai 980, Japan
- 3) Department of Science and Technology, Meisei University,
337 Hodokubo, Hino 191, Japan

Introduction

In the ground state of Xe, Cs and Ba the f-symmetric wave functions are localized in the outer valley of the double valley effective potential. Going from Ba to La the 4f wave-function collapses into the inner potential well. This sudden transfer of the wave-function from the outer to the inner well critically depends on the width and the depth of the inner well and the height of the potential barrier and thus can be influenced by excitation or ionization.

Experiment

The synchrotron radiation emitted by the 2.5 GeV electron storage ring of the Photon Factory was monochromatized by a Grasshopper monochromator. The spectral bandwidth was 2 eV for Xe and Cs and 1 eV for Ba. The atoms were contained in a heat pipe (length of the vapour column < 60 cm) mounted behind the exit slit of the monochromator. Thin film Al windows and a differential pumping stage separated the heat pipe from the ultrahigh-vacuum of the monochromator. The temperatures ranged from 900°C to 1000°C for Ba and from 200°C to 250°C for Cs. This corresponds to vapour pressures between 0.1 and 1 mbar. A Ne buffer gas retarded the escape of the metal atoms from the hot zone of the furnace. The energy scale was calibrated by means of the Ne K absorption (uncertainty of the energy scale ± 1 eV). The efficiency of the open photomultiplier was greatly enhanced by using a CuI cathode.

Results

The experimental 3d-absorption spectra of atomic Xe, Cs and Ba are presented in Fig. 1. Since the number of the metal and Ne atoms in the vapour column has not been determined only the relative spectral dependence of the cross sections is given. The figure nicely displays the dramatic change of the broad and overlapping Xe absorption bands into the sharp and well separated Ba absorption lines. Our results for Xe are in agreement with those reported by Deslattes (1968). The weak structure centered at 673 eV is ascribed to $4d \rightarrow 6p$ transitions. The broad bands above the corresponding ionization limits are due to transitions of 4d electrons to f-symmetric continuum states.

For Ba the low energy absorption line lies well below the M_V ionization threshold and the high energy well below the M_{IV} threshold. In LS coupling the line centered at 783.8 ± 1 eV is ascribed to $3d^{10} 1S_0 + 3d^9 4f 3D_1$ transitions the line centered at 798.4 ± 1 eV to $3d^{10} 1S_0 +$

$3d^9 4f 1P_1$ transitions. $3d^{10} 1S_0 + 3d^9 4f 3P_1$ excitations are responsible for the weak shoulder at 780.2 ± 1 eV. The intensity ratio $1P_1 / 3D_1 = 1.3 \pm 0.2$ agrees neither with the value for pure LS coupling nor the statistical ratio 2/3 for pure jj coupling. The importance of both, the spin orbit splitting of the 3d level and the interaction of the excited electron with the open 3d shell corroborates the localization of the final state wave-function. The asymmetry of the $1P_1$ line is mostly due to the $3d^9 3/2 4f + 3d^9 5/2 \epsilon f$ autoionization channel.

The 3d spectrum of atomic Cs represents an interesting intermediate case. The centers of the two absorption lines (733.7 ± 1 eV; 747.6 ± 1 eV) lie above the corresponding $3d 5/2$, $3d 3/2$ ionization limits. On the other hand, the spectral dependence of the cross section is close to that of Ba than that of Xe. The intensity ratio of the low energy peak to the high energy peak, determined in various sensible ways, always comes out smaller than the statistical ratio.

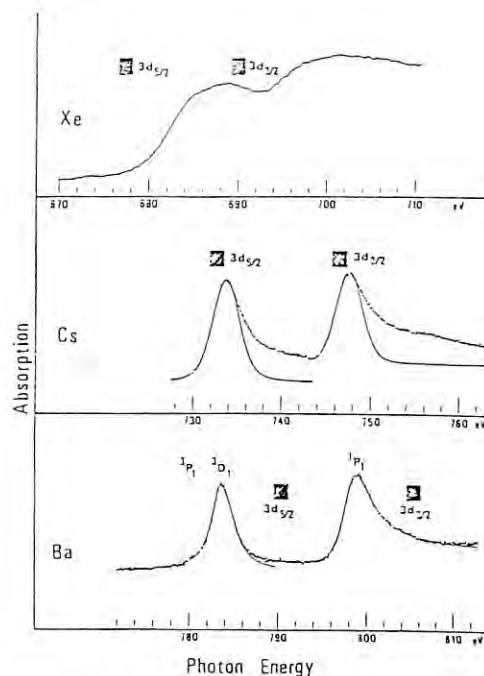


Fig.1 3d-absorption spectra of atomic Xe, Cs and Ba.

* On Leave from the University of Hamburg, Hamburg, Germany

References Deslattes, R.D., 1968, Phys. Rev. Lett. 10 483.

X-RAY LITHOGRAPHY : SOFT X-RAY SPECTRAL
CHARACTERIZATION OF RESIST POLYMER

Kozo Mochiji, Takeshi Kimura, Hidehito Obayashi

Mihiro Yanagihara⁺ and Taizo Sasaki⁺

Central Research Laboratory, Hitachi, Ltd.,
Kokubunji, Tokyo 185

⁺ National Laboratory for High Energy Physics
Ohomachi, Tsukuba, Ibaraki 305

The soft X-ray absorption spectra of an X-ray resist film and its spectral sensitivity are studied using synchrotron radiation.

The X-ray resist studied here was poly-2-methylpentene-1-sulfone (PMPS).¹⁾ The beam line used in the experiment was BL 11A and the electron acceleration energy was 2.5 GeV. For monochromatizing the synchrotron radiation, a two degree grazing incident monochromator (Grasshopper) was employed. The optical resolution was about 0.03 Å at $\lambda = 50$ Å.

The absorption spectra of PMPS film is shown in Fig.1. Some fine structures can be observed near the absorption edges of carbon and sulfur. The doublet peaks at about 285 eV can be assigned to Rydberg transition, that is, from C_{1s} orbital to unoccupied orbitals lower than continuum states. Splitting is brought about by the effect of chemical shift in the molecular structure. This is the first observation of chemical shift of carbon atoms in a polymer film. The sharp band at 170 eV among the three peaks around the ionization threshold of S_{2p} orbital at about 175 eV is due to a Rydberg transition. The other two broad bands at the higher energy side are considered to be part of XANES (X-ray Absorption Near Edge Structure).²⁾

The sensitivity of this resist to monochromatized radiation was measured. The change in sensitivity brought about by incident photon energy can be seen to be in correspondence with the absorption coefficient. If the degradation efficiency of the resist per unit absorbed energy changes marginally at different photon energies, the resist sensitivity should vary proportional to the absorption coefficient. However, as shown in Fig.2, this is not the case and drastic sensitivity enhancement is observed at higher absorption coefficients.

Following these results, it is considered that the degradation efficiency of PMPS depends upon incident photon wavelength. A specific excitation such as the Rydberg transition from C_{1s} or S_{2p} is effective for the scission of the main chains in PMPS.

References

- 1) M. J. Bowden: J. Polymer Sci., 12 (1974) 499.
- 2) J. B. Pendy: Comments Solid State Phys., 10 (1983) 219.

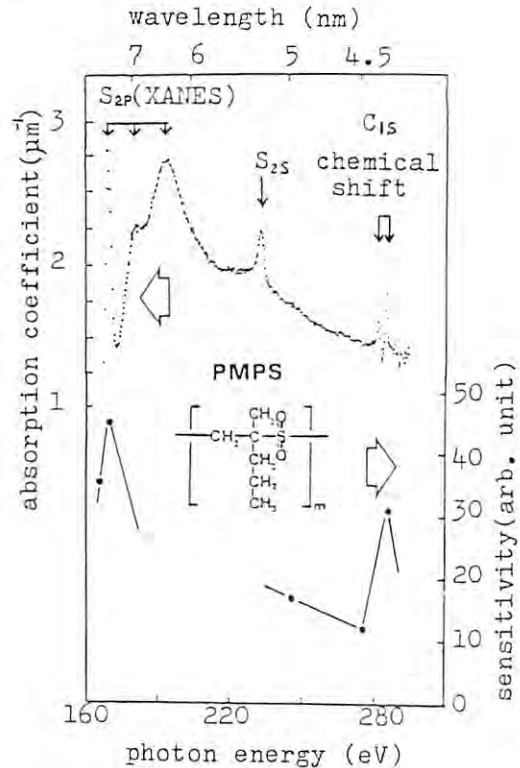


Fig.1 Absorption Spectra and Sensitivity of PMPS

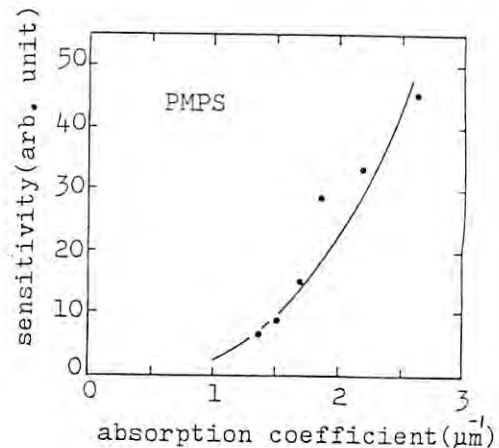


Fig.2 Dependence of Sensitivity upon Absorption Coefficient

PHOTOEFFICIENCY EVALUATION OF PHOTOCATHODES
FOR SOFT X-RAY EXPERIMENTS

A. Sawaki, T. Yamashita
Hamamatsu Photonics K.K., Ichino-Cho, Hamamatsu 435

Y. Iguchi
Tsukuba Univ., Sakura-Mura Niiharu-Gun Ibaraki 305
and

H. Maezawa, Y. Yanagihara, Y. Suzuki, and T. Sasaki
KEK, Oho-Machi, Tsukuba-Gun, Ibaraki 305

Introduction

There has been increased interest in high-sensitivity soft x-ray detectors in various studies such as experiments using synchrotron radiation, plasma diagnostics and satellite astronomy. Although a photomultiplier is a useful detector not only for visible light but also for soft x-rays, the photoefficiency profile in the soft x-ray region is not well known. In this study the photoefficiency curves were evaluated for many kinds of materials as candidates for the photocathode in the energy range of 0.1 - 1 keV by using synchrotron radiation.

Experimental procedures

The experiment was carried out at the beam line BL-11A, where monochromatic soft x-rays from a Baker grasshopper monochromator in the energy range of 0.1 - 1 keV are available. A gold mesh was used as a monitor for an input soft x-ray intensity. The photoelectrons emitted from it are led to a channel electron multiplier (CEM) and detected by a pulse counting system. The samples were attached as photocathodes to a diode-type holder. This holder was designed to hold ten photocathode samples so that ten kinds of samples could be measured without venting the vacuum chamber. The monochromator was scanned by a microcomputer control, and the synchronized data from the CEM and the sample were analyzed and stored by a Tracor Northern TN4000 system. The following photocathode samples were prepared mainly by evaporation on the stainless steel substrates: CsI, RbBr, CuI, RbI, RbCl, RbI, TlI, BiTe, CdTe, PbTe, Au, and BeO. The photoefficiency calibration of the samples was carried out by using an NBS Al_2O_3 standard photodiode in the wavelength region longer than 50 Å and an Au photocathode in the region shorter than 50 Å on the basis of the photoefficiency value of Au as given by Henke."

Results

The photoefficiency curves measured for CsI, RbBr, CuI, BeO, and Au are shown in Fig.1. Alkali-halides such as CsI and RbBr make high-sensitivity photocathodes. RbBr has no steep structures in its photoefficiency curve in the energy range of 0.1 - 1 keV. Although it is rather hygroscopic, it is a useful material as photocathode if handled carefully.

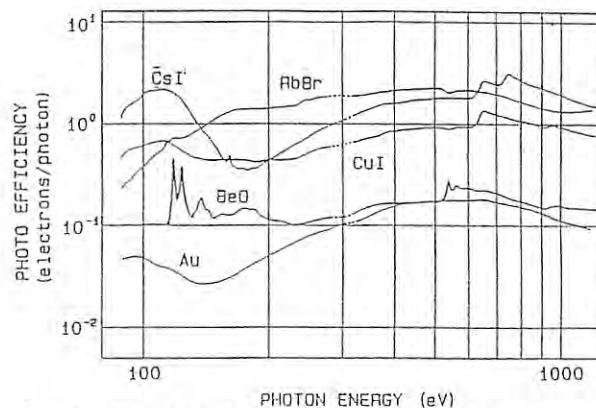


Fig.1 : Photoefficiency curves of CsI, RbBr, BeO, CuI, Au photocathodes

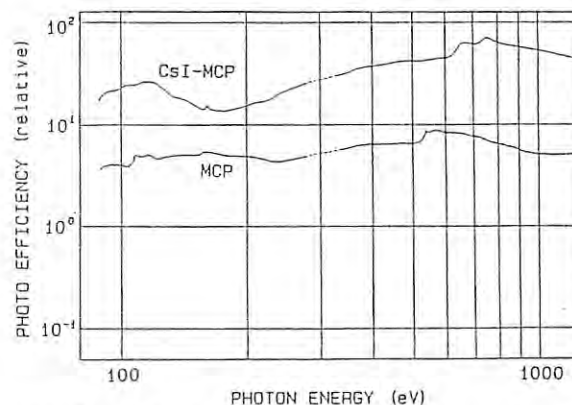


Fig.2 : Relative sensitivity curves for MCP with and without CsI photocathodes

Figure 2 shows the relative sensitivity curves for MCP's with and without a CsI photocathode. The MCP overcoated with CsI shows 5 to 10 times higher output than the bare MCP, which is due to increases in both photoefficiency and electron multiplication by the CsI. It should be noted that the sensitivity curve of the CsI coated MCP differs from that of CsI itself in Fig.1. This is due to the grazing incidence of the soft x-rays onto the channel walls and then their multiple reflections in the channels.

- 1) B.L. Henke ; Nucl. Instr. & Meth. 177
(1980) 161

REFLECTION OF VUV LIGHT FROM MIRROR SURFACES

M.Yanagihara, T.Koide, M.Niwano, T.Miyahara,
S.Sato, Y.Iguchi*, and T.Sasaki

KEK, National Laboratory for High Energy Physics
Oho-machi, Tsukuba-gun, Ibaraki 305

*Institute of Applied Physics, University of Tsukuba
Sakura-mura, Niihari-gun, Ibaraki 305

For the purpose of obtaining the optical constants of mirror materials in VUV region, we measured the reflectivity spectra of quartz, silicon carbide, and gold at glancing angles at BL-11A (grasshopper monochromator)¹⁾ using the reflectometer designed by the authors.²⁾

The data is now under analysis.

The measurement was carried out in the following manner. The VUV beam is focused on the 0.2-mm wide slit of a detector by a refocusing mirror.³⁾ In order to collimate the incident beam, an entrance diaphragm of 0.1-mm wide is employed at 120 mm before the sample.

The gold was evaporated on a glass substrate with relatively low speed. The mirrors are about 45 mm in length.

The sample holder is tilted a few degrees from the rotational axis by a linear feedthrough to pass the incident beam. The reflectivities were obtained by normalizing the reflection intensity with the incident light intensity and the stored electron current in the ring.

References

- 1) F.C.Brown, R.Z.Bachrach, and N.Lien: Nucl. Instrum. & Methods 152 (1978) 73. see also "BL-11A: Grasshopper Monochromator" in this report.
- 2) See "VUV and Soft X-Ray Reflectometer" in this report.
- 3) See "The Refocusing Mirror for the Grasshopper Monochromator" in this report.

$K^+L_{2,3}$ ABSORPTION SPECTRA OF POTASSIUM HALIDES

M. Yanagihara, Y. Iguchi,* H. Maezawa, and T. Sasaki
 KEK, National Laboratory for High Energy Physics
 Oho-machi, Tsukuba-gun, Ibaraki 305

* Institute of Applied Physics, University of Tsukuba
 Sakura-mura, Niihari-gun, Ibaraki 305

We obtained contamination-free $K^+L_{2,3}$ absorption spectra of KCl, KBr, and KI films at room temperature using synchrotron radiation from the 2.5-GeV PF storage ring as a light source and the grasshopper monochromator¹⁾ at BL-11A.

The samples were prepared by vacuum evaporation on collodion substrates supported by nickel mesh. Their thickness was about 3000 Å. They were mounted on a turret, and then put into a sample chamber. The pressure of the chamber was 2×10^{-8} Torr realized by a turbomolecular pump. The time dependence of the incident light intensity was monitored with a gold mesh before the sample. The VUV transmissions through a reference collodion film and the samples were detected with an electron multiplier R595 (Hamamatsu) and picoammeter (Takeda). The optical densities were obtained from these with the correction of incident light intensity. The optical band pass was about 0.15 eV with the slits of 15–15 μ m.

Figure 1 shows the absorption spectra of the $K^+L_{2,3}$ levels between 290 and 330 eV. The photon energy was calibrated by the argon $L_{2,3}$ absorption. The spectra in Fig. 1 are displaced vertically. The three spectra can be divided into two energy regions, I and II as indicated in Fig. 1. In the region I two peaks A and B are predominantly seen at 296.2 and 299.0 eV (± 0.1 eV) accompanying smaller peaks A' and B' in each lower energy sides. The position of these peaks are almost independent on the halide ions. The energy difference between A and B is 2.8 eV, which is in good agreement with the spin-orbit splitting of the $K^+L_{2,3}$ levels.²⁾ These facts suggest strongly that the two peaks A and B are due to the localized transition from the 2p to 3d-like levels at the potassium ion K^+ .

On the other hand, the splitting of the peaks A' and B' from A and B (~ 0.8 eV) can not be explained only by atomic transitions, indicating the existence of the solid state effect as the ligand field in the crystal.

The peak intensity ratio of A and B is likely to be discrepant from the statistical value of 2:1. The deconvolution analyses are now continued.

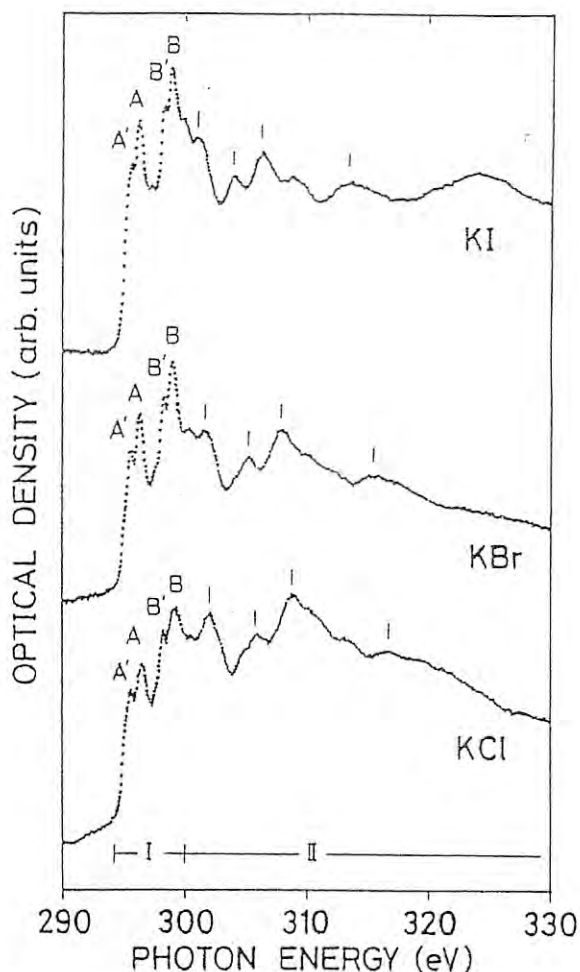


Fig. 1 The $K^+L_{2,3}$ absorption spectra of KI (upper), KBr (middle), and KCl (lower) evaporated films at room temperature.

References

- 1) F.C. Brown, R.Z. Bachrach, and N. Lien: Nucl. Instrum. & Methods 152 (1978) 73. see also "BL-11A: Grasshopper Monochromator" in this report.
- 2) J.A. Bearden and A.F. Burr: Rev. Mod. Phys. 39 (1967) 125.

CONTACT MICROSCOPY WITH SYNCHROTRON RADIATION
X-RAYS USING TRANSMISSION GRATING

Sadao AOKI, Toshiaki OHTA[†], Masaharu NOMURA[†] and Seishi KIKUTA^{††}

Institute of Applied Physics, University of Tsukuba,
Sakura, Ibaraki 305

[†] Photon Factory, National Laboratory for High
Energy Physics, Oho, Ibaraki 305

^{††} Department of Applied Physics, Faculty of Engineering,
University of Tokyo, Hongo, Bunkyo-ku, Tokyo 113

X-ray contact microscopy has been made considerable improvements by the technique of x-ray lithography and the development of the synchrotron radiation source¹⁾. It can be applicable in many fields of biology, medicine, and chemistry. Soft x-rays are especially useful for imaging biological specimens which consist of low-Z elements. It is possible to make use of the wavelength variation of the absorptivity to produce several images revealing different structures of the specimen. The basic bandwidth requirement for x-ray microscopy is quite modest: $\lambda/\lambda\Delta \approx 10$ is typically adequate. Although the transmission grating is a low dispersive element, it is very convenient to obtain a broad wavelength band in a simple geometrical condition.

Coupling the transmission grating with the condensing mirror an effective optics for x-ray microscopy can be build. The present note shows that x-ray micrographs obtained with different wavelengths reveal different structures in the object.

Experiments were made at BL11B Station in PH Tsukuba. The synchrotron radiation from the electron storage ring has a broad continuum of radiation and the intensity peak lies at a wavelength of about 3.1 Å in the present case. Schematic diagram of the experimental arrangement is shown in Fig. 1. Synchrotron radiation was focussed by a platinum coated bent cylindrical mirror and dispersed vertically by the transmission grating. The mechanically bent mirror had a long radius of curvature of 1000 m. As the grazing angle was 17 mrad x-rays shorter than 2.2 Å were cut off. The commercially available gold transmission grating (Option Co.) has a grating period of 1.0 μm and the bar-slit ratio is 1. In this case, even orders of spectra are calculated to be omitted²⁾. The diffraction efficiency is 6% in both first orders in the range of 10 Å up to 600 Å. The first order dispersion in the resist plane is 0.2 mm/Å; the spectral resolution, however, is limited by the beam width of 0.5 mm (FWHM) and amounts to 2.5 Å in the first order. No filters were used to eliminate higher order spectra because these intensities were lower than 10% of the first order. A 0.8 μm thick PMMA (poly-methyl methacrylate) film spun on a silicon wafer was used as the x-ray resist. The sensitivity of the resist is 1.2 J/cm² at $\lambda = 5.4$ Å (MoKα).

The specimen was brought in contact with x-ray resist, and the resulting x-ray copy of the absorption profile in resist was subsequently viewed with a scanning electron microscope. As a specimen we used a lycopodium clavatum, a kind of a spore, whose diameter was about 30 μm. Figure 2(a) shows an x-ray micrograph of a

lycopodium obtained with the zeroth order spectrum which consists of a spectral range from 2.2 Å to visible. However, a large contribution to the exposure came from soft x-rays shorter than 10 Å. An exposure time was 40 min under the operating condition of average electron current of 50 mA at 2.5 GeV. Figure 2(b) is a scanning electron micrograph of the specimen. X-ray micrograph taken with different wavelength is also shown in Fig. 2(c). X-rays longer than 20 Å were absorbed in the central part of the objects. Different fine structures of the outer part of the image can be seen. A resolution better than 1000 Å is easily obtained. All our micrographs were obtained with the specimen in a vacuum. Some modifications of our exposure station are necessary to allow exposure in air, so that wet specimen may be observed.

We would like to thank Dr. T. Kitayama and Dr. K. Harada of Musashino Electrical Communication Laboratory, NTT, for the preparation of the x-ray resist.

References

- 1) E.Spiller, R.Feder, J.Topalian, D.Eastman, W.Gudat and D.Sayre: Science 191(1976)1172.
- 2) H.W.Schnopper, L.P.Van Speybroeck, J.P. Delvaile, A.Epstein, E.KHllne, R.Z.Bachrach, J.H.Dijkstra and L.Lantward: Appl. Opt. 16 (1977)1088.

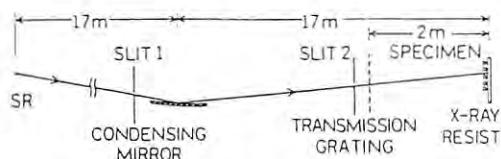


Fig. 1

The experimental arrangement. The condensing mirror is 60 cm long and 10 cm wide. The width of the entrance slit 1 and slit 2 are 1 mm and 2mm, respectively.

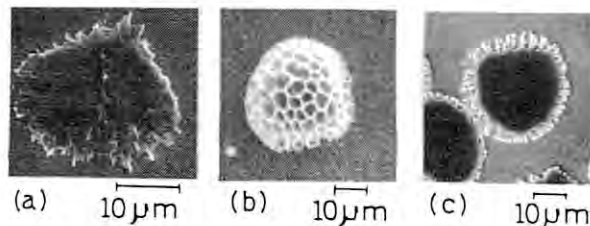


Fig. 2

X-ray micrographs of lycopodium clavatum (a and c) in the x-ray resist. (a) Zero order beam ($\lambda \approx 2.2 \text{ \AA} \sim 100 \text{ \AA}$). (b) Scanning electron micrograph of the object. (c) $\lambda \approx 20 \text{ \AA}$.

S-L_{2,3} EMISSION SPECTRA OF SULFURE COMPOUNDS
EXCITED BY SYNCHROTRON RADIATION

K.Taniguchi, T.Ohta* and M.Nomura*

Department of Solid State Electronics, Faculty of Engineering,
Osaka Electro-Communication University,
18-8, Hatsucho, Neyagawa, Osaka 572 (JAPAN)

*KEK, National Laboratory for High Energy Physics,
Oho-machi, Tsukuba-gun, Ibaraki 305 (JAPAN)

Introduction

The X-ray emission spectrum originated from the electronic transition between the valence band and the inner shell level has been studied very extensively, because it gives much information about the valence state¹. It is the purpose of the present work to report of the results of construction of the simple soft X-ray grazing incidence spectrometer for secondary excitation using S.R., and the X-ray spectra obtained by the use of this spectrometer.

Experiment

The incident soft X-rays are obtained from the storage ring operated at 2.5 GeV at Photon Factory of National Laboratory for High Energy Physics in Japan. The incident X-rays by S.R. are limited from visible and violet rays with a thin carbon film supported on polyvinyl-formal film and from higher energy components with a mirror. The incident X-rays are focused by a pyrex mirror 2 coated with Pt whose curvature radius is 12m. The mirror can be controlled from outside in order to select the optimum region of the specimen.

The mirror chamber, sample chamber and spectrometer were evacuated by Turbo Molecular pumps. The concave grating spectrometer with 1/1200 mm of 3m radius was used at the incident angle of 85.70°. In order to reduce the impurity lines of high order and the electric noise signal, a gas flow proportional counter was used as a detector. The counting gas is Propane gas at 60 mmHg pressure and sealed in the counter with the polyvinyl-formal film. The ceratron is used as a monitor counter and monitors 0th order of the reflection spectrum. The spectra were recorded automatically by means of step-scanning method at the fixed count of intensity for monitor.

Results and Discussion

S=L_{2,3} emission spectrum of Na₂SO₄

An example of such a high-resolution spectrum obtained in the present spectrometer the S-L_{2,3} spectrum of Na₂SO₄ is shown in Fig.1. The vertical slit width and the horizontal slit width were chosen to be 200-200μm and 8mm,

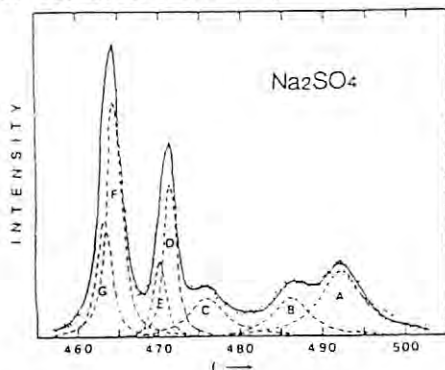


Fig. 1.

respectively, and the energy resolution of 1.0eV was achieved. Using a small laboratory computer-plotter system with a simple iterative procedure, we have decomposed the S-L_{2,3} spectra of Na₂SO₄ into the seven allowed components. The relative by higher intensity peaks D, E, F and G show the contribution of spin orbital splitting of the inner core level, and are originated from the electron transition from valence molecular orbital 4a₁ and 3t₂, respectively. The peak C can not be assigned with the electron transition. It should be noted that the peak A is considerably small compared with the case of the spectra measured with the crystal analyzer¹. It seems reasonable that the peak A, due to overlapping with 2nd order reflection of C-Kα, and C-Kα components is negligible small in the case of the present grating spectrometer.

S-L_{2,3} emission spectra of metallic sulfide compounds.

Figure 2 shows the comparison between the S-L_{2,3} emission spectra of TiS, FeS, CoS and CuS. There are two main components (A and B) and small structures between A and B. L_{2,3} emission spectra result from the transitions from valence orbital levels to the 2p level in the second row elements. This fact means that by measuring these spectra, we can investigate the 3s and 3d character in the valence band. The main peak A should be ascribed to the electron transition from 3s character and the peak B that from 3d character in valence band. The structures between A and B are originated from the electron transition from the 3p level with small contributions of 3s or 3d character to the inner 2p level. The typical change is appeared at the peak B by the chemical condition of the surrounding atom. The extent of 3d orbital participation in the chemical bonding is very important in the discussion of electronic structure of valence band. This is a subject for future study in our work.

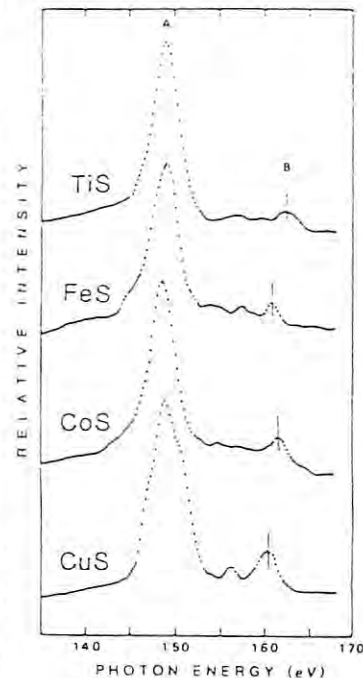


Fig. 2.

References

- 1) K.Taniguchi and B.L. Henke, J. Chem. Phys. 64, (1976), 3021.
- 2) B.L. Henke and K.Taniguchi, J. Appl. Phys. 47, (1976), 1017.

EXTREME ULTRAVIOLET ABSORPTION SPECTRA OF K-Na ALLOYS

I. FUKUI,^a S. SUZUKI,^b T. HANYU,^c H. FUKUTANI,^a H. KATO,^d H. SUGAWARA,^e
I. NAGAKURA,^e S. NAKAI,^f T. HIROSAWA,^g T. ISHII,^g and T. MIYAHARA^d

a: The University of Tsukuba b: Tohoku University
c: Tokyo Metropolitan University d: KEK
e: Gunma University f: Utsunomiya University
g: Institute for Solid State Physics, University of Tokyo

The optical absorption spectra of K-Na alloys were measured in the photon energy region from 10 to 40 eV. One purpose of this measurement is to study the edge shape problem which is still controversial because recently D. Gibbs et. al performed the optical measurements using Cs-Na alloys and observed Cs 5p linear absorption edges in alloys with dilute Cs.¹⁾ They claimed the edge singularity comes from a local effect associated with the bonding between the same alkali atoms.

The other purpose is to examine the character of the broad absorption structure which in the previous report seemed to persist in solid solutions.²⁾ In the present case, however, K-Na alloys do not form solid solutions. Therefore some change is expected in the spectral shape of the broad absorption band.

The absorption spectra of pure K and pure Na were measured by S. Sato et. al³⁾ in photon energy region from 10 to 38 eV. The result was confirmed in this work and is shown in Fig. 1. As the present result the absorption spectra of an alloy with dilute Na is shown in Fig. 2 where a new broad structure are around 30eV. Apparently this structure is due to Na, but it does not have any sharp edge expected from the many-body theory (MND theory).

Fig. 3 shows the result for 36 at. % K-Na alloy. It is seen that the small structure A and B appearing in Fig. 1 are much weakened in the result.

D. Gibbs et. al considered the condition under which a linear absorption profile occurs in alkali metal alloys.¹⁾ According to their theory Na edges in K-Na alloys should not show

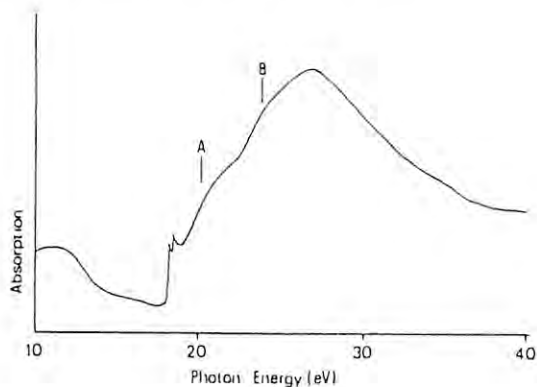


Fig. 1

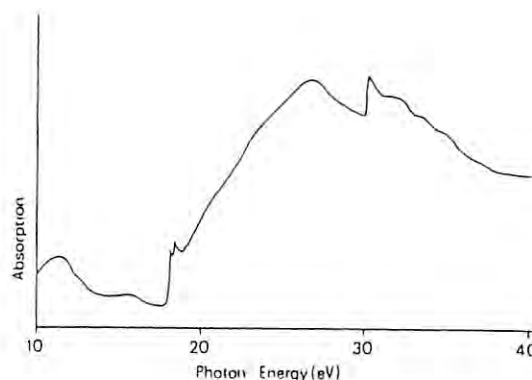


Fig. 3

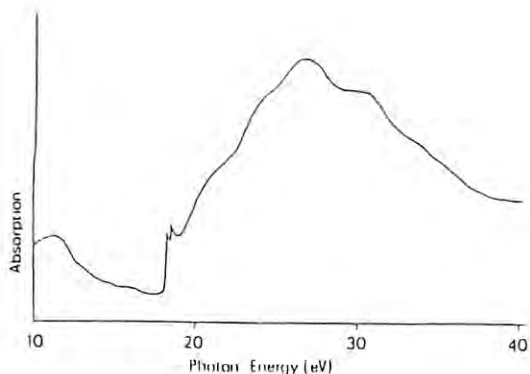


Fig. 2

a linear profile. Contrary to their theory, a broad profile is found for the Na absorption threshold. A tentative explanation of this broad structure is that the broad edge comes from a superposition of absorption edges with different threshold energies. In moderately dilute alloys there are some probability that a Na atom is isolated from other Na atoms, and probability that a Na atom meets another Na atom, and probability that a Na atom meets two other Na atoms, and so on. In each case the absorption threshold energy is different from others due to chemical shifts. The amount of the chemical shifts is supposed to be large because the Fermi level as well as the lattice constant of K largely differ from those of Na.

In the previous experiment,²⁾ however, the concentrations were such that the probability that each alkali atom meets another same kind of alkali atom should be close to unity. The similar situation might happen in a extremely dilute case, where almost all of the minority atoms are supposed to be isolated. In both cases the threshold should show a sharp edge because the chemical environment is nearly uniform.

Unfortunately the experiment for extremely dilute cases has not been done yet as far as the authors know. If this kind of experiments is carried out, the result would be a good check for the present interpretation.

Next the reduction of the structure A and B in the 36% Na-K alloy is considered. In the alloy the hexagonal Na₂K structure is predominant according to the phase diagram, where K-K spacing is roughly 3 times larger than Na-Na spacing. In addition K atoms are distributed two-dimensionally in this hexagonal structure. Thus the local density of states around K atoms should be different from those of K atoms in solid solutions such as K-Rb alloys. This may cause the change in the structure A and B.

references

- 1) Doon Gibbs, T.H.Chiu, J.E.Cunningham, and C.P.Flynn: Phys. Rev. Lett. 49, 815(1982)
- 2) T.Miyahara, S.Sato, T.Hanyu, A.Kakizaki, S.Yamaguchi, and T.Ishii: J.Phys. Soc. Jpn. 49, 194(1980)
- 3) S.Sato, T.Miyahara, T.Hanyu, S.Yamaguchi, and T.Ishii: J.Phys. Soc. Jpn. 47, 836(1979)

INNER CORE EXCITATION SPECTRA OF ALKALINE EARTH AND RARE EARTH METALS

Takaaki Hanyu, Tsuneaki Miyahara⁺, Toru Kamada, Ken-ichiro Asada, Haruo Ohkuma, Hiroyoshi Ishii, Kenzo Naito⁺⁺, Hiroo Katō and Shigeo Yamaguchi
 Department of Physics, Tokyo Metropolitan University, Tokyo, 158
⁺ Photon Factory, National Laboratory for High Energy Physics, Oho-machi, Ibaraki-ken 305
⁺⁺ Institute of Materials Science, University of Tsukuba, Sakura-mura, Ibaraki-ken 305-

The absorption spectra of the light rare earths in the extreme ultraviolet region have been measured by our group¹⁾. In those measurements the contribution of the 4f electrons to the optical absorption spectra has not been confirmed in the photon energy region from 6 eV to 40 eV. Moreover the 5p threshold of the light rare earth metals did not show sharp edges due to the Fermi level. This study has been performed in order to confirm systematically these optical properties on the series of the lanthanides.

As a light source the storage ring at Photon Factory, National Laboratory for High Energy Physics. Light is monochromatized by 1 m Seya-Namioka type monochromator. The energy range is 7 eV to 40 eV. The resolution is about $\lambda/\Delta\lambda \approx 2000$. The pressure of the chamber was kept at 4×10^{-10} Torr. During the evaporation the pressure of the chamber was raised up to about 2×10^{-8} Torr. Evaporation of the sample was performed from E-gun. The pressure of the monochromator was 2×10^{-9} Torr. The thickness of the evaporated films, which were produced on the polycarbonate film supported by Ni meshes, were controlled by quartz oscillator. The samples were cooled at liquid nitrogen temperature. The absorption spectra were measured by using a filter to eliminate the higher order radiation from the grating. The filters are In and LiF films with the thickness of about 1000 Å. Such filters were used in different photon energy range; In film from 10.2 eV to 17.8 eV, and LiF from 7 eV to 12.4 eV.

Figure 1 shows the absorption spectra of the rare earth and barium metals. Overall profiles

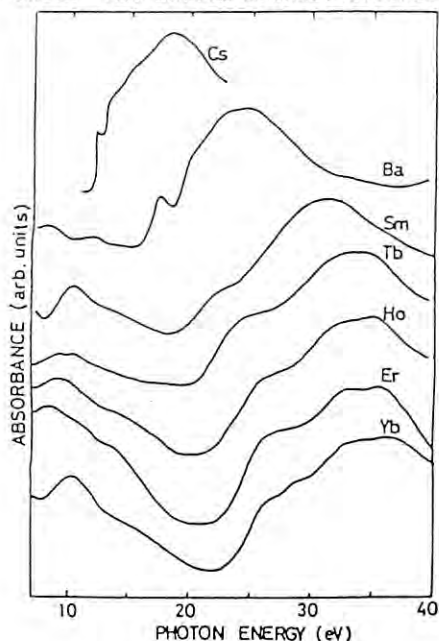


Fig.1

are similar to each other. The 5p threshold of cesium²⁾ was shown in order to compare the shape of those thresholds as a function of the atomic number. Barium metal situates just at the right-hand of cesium in the periodic table. Comparison of Cs and Ba leads to the interesting results. The rising of the threshold of Ba was far slow respective to that of Cs. For all elements, which have been measured until lately, the widths of the edge were measured. The widths were estimated by the energy position from 10 to 90 % of the height of the rising portion at the threshold. The widths were plotted as a function of the atomic number as shown in Fig.2. For all the elements of the lanthanides the measurements have not been performed, and the broken lines indicate the values expected to measure. The widths of the 5p edges have minimum

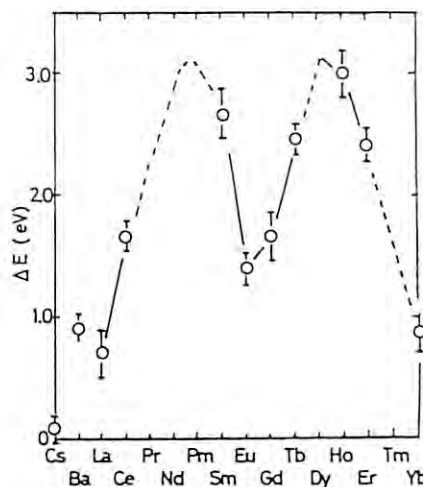


Fig.2

values for the lightest and heaviest elements; La has no 4f electrons and Yb is completely filled. For Eu and Gd the widths are comparable to those of La and Yb. Eu and Gd are half-filled. Dependency of the widths on the elements shows the double-peaked shape with the minimum at La, Eu and Gd, and Yb. The unpaired 4f electrons produce the multiplet structure near the 5p threshold. The energy position and the shape of the structure can not be known, but the existence of the unpaired 4f electrons can be considered as one of the origins of the edge broadening. For light rare earth the trace of the 4f electron could not be confirmed and the 4f transition would be delayed far above the binding energy. For the heavy elements the similar results were obtained.

1) T. Miyahara et al.: J. Phys. Soc. Jpn 51(1982)1834.
 2) T. Ishii et al.: J. Phys. Soc. Jpn 42(1977)876.

ELECTRON CORRELATIONS IN PHOTOIONIZATION OF ATOMS

Y. Itikawa,¹ Y. Sato,² J. Murakami,² T. Nagata,³ B. Sonntag,^{4*} A. Yagishita,⁴ M. Yoshino⁵
¹Institute of Space and Astronautical Science, Komaba, Meguroku, Tokyo 153, ²Research Institute for Scientific Measurements, Tohoku University, 2-1-1 Katahira, Sendai 980, ³Department of Science and Technology, Meisei University, 337 Hodokubo, Hino, 191, ⁴Photon Factory, National Laboratory of High Energy Physics, Oho-machi, Ibaraki 305, and ⁵Faculty of General Education, Shibaura Institute of Technology, 307 Fukasaku, Omiya 330

Electron correlations play an important role in photoionization or photoexcitation of atoms and molecules. One of the explicit ways to reveal the effects of the electron correlation is to investigate multiple ionization induced by photoabsorption. The single-electron model cannot account for the simultaneous ejection of two or more electrons at the incidence of one photon. The multiple ionization has been studied rather extensively for rare-gas atoms. Only fragmentary data, however, are available for other atoms. The effects of electron correlation should be dependent on the number of electrons and the shell structure of atoms. For further understanding of the electron correlation we have started to measure multiple-ionization cross sections of alkali and alkaline-earth elements. This is the first report of the work and concerned with the double ionization of Ca atoms.

The present study has been performed by means of time-of-flight (TOF) mass spectrometer coupled with a source of monochromatized synchrotron radiation and an atomic Ca beam. The synchrotron radiation from the KEK 2.5 GeV storage ring was dispersed vertically by a 1 m Seya-Namioka monochromator equipped with a 1200 lines/mm grating blazed at 500 Å. A spectral bandwidth of 2 Å was used in the wave length region of 350 to 450 Å. The monochromatized radiation was focused onto a differentially pumped interaction region where the photon beam crossed at right angles with a collimated beam of Ca atoms effused from an oven operated at a temperature of about 700 °C. The oven orifice was located at 4 cm apart from the interaction region. An electrostatic deflector and a collimating aperture were placed between the oven orifice and the interaction region. The deflector was used to prevent thermal ions produced by the oven from entering the interaction region. The drift tube of the TOF mass spectrometer was placed at right angles to both the photon and atomic beams.

The photoelectrons and photoions were accelerated in the opposite directions each other by a static electric field applied in the interaction region. The TOF spectra of photoions were obtained by a method of delayed coincidence between the photoions and photoelectrons. The photoelectrons were detected by a channel electron multiplier on one end of the TOF spectrometer, while the photoions were detected by a microchannel plate on the other end after traversing the drift tube of a length of 45 cm. The signals of the photoelectrons and the photoions were fed into the start and stop inputs, respectively, of a time-to-amplitude converter coupled

with a multichannel pulse height analyzer. Thus the differently charged ions are dispersed at different delay times corresponding to the individual flight times.

In the present wave length region (350-450 Å or the photon energies of 35.4-27.6 eV), only the singly and doubly charged ions (Ca^+ and Ca^{++}) were observed in the TOF spectra. The relative dependence of the ion yield, $n(\text{Ca}^{q+})$, on the photon wave length was obtained both for the Ca^+ and Ca^{++} by using two sets of delayed coincidence units, each being gated for the Ca^+ and Ca^{++} ions. Though the detection efficiencies of the differently charged ions are yet to be calibrated relatively, the apparent ratio of the yields, $n(\text{Ca}^{++})/n(\text{Ca}^+)$, increased remarkably at about 31 eV and 35 eV of the photon energies. At those two photon energies, both the yields, $n(\text{Ca}^+)$ and $n(\text{Ca}^{++})$, increased, but $n(\text{Ca}^{++})$ was enhanced much more than $n(\text{Ca}^+)$. This enhancement may be partly due to the higher efficiency of the detection of Ca^{++} . The Auger process following the innershell excitation or ionization may also account for those enhancement of $n(\text{Ca}^{++})/n(\text{Ca}^+)$. More detailed experiment and analysis of this process are in progress.

* On leave from University of Hamburg.

DYNAMIC MEASUREMENT OF PHOTOIONIZATION PROCESSES OF GASES

M.Nakamura , M.Watanabe , Y.Morioka , Y.Kageyama , T.Hayaishi[†]

Institute of Physics, University of Tsukuba, Sakura-mura, Niihari-gun, Ibaraki 305
[†]Institute of Applied Physics, University of Tsukuba, Sakura-mura, Niihari-gun, Ibaraki 305

Introduction

Most molecules ionize and dissociate with irradiation of the light in the V.U.V. region. The study of these processes provides information on the interaction between V.U.V radiation from the sun and molecules in the upper-atmosphere.

In February and June 1983, we measured the photoionization and photo-dissociation of O₂, N₂, H₂, D₂, H₂O and D₂O at the BL-12A beam line in Photon Factory. By using the time of flight method, in February the relative partial photoionization cross sections were measured, and in June the threshold photoelectron-photoion coincidence spectra were taken.

Experimental

A schematic of the experimental apparatus are shown in Fig.1. The light from the BL-12A beam port were monochromatized by Im-Seya-Namioka-monochromator with the grating of 2400 lines/mm and collimated at the collision region by three mirrors (one is toroidal). The target molecules are effused through a single capillary tube to the collision region. The time of flight analyser consists of a photoelectron detector, a photoion detector and a signal analysing system. The ejected electrons and ions are pulled by the electric field to the opposite directions and detected by the multi-channel-plates(MCP's). In analysing system, the interval time between the electron and the ion arrival times is translated to the pulse height and analysed by a pulse height analyser.

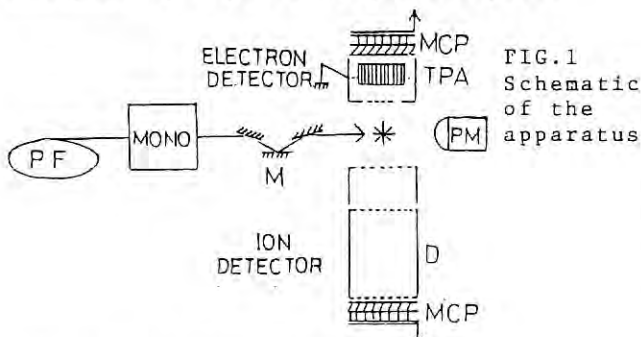


FIG.1 Schematic of the apparatus

PF: Synchrotron ring. M: Mirrors
 TPA: Threshold photoelectron analyser (only in June). PM: Photomultiplier.
 D: Drift tube. MCP: Multi-channel-plate.

In June, to analyse the threshold photoelectron, we used the honey-comb structured electron analyser which had many holes of 1 mm in diameter and 16 mm in length. The threshold photoelectron spectrum of Ar observed to test this analyser is shown in Fig.2. The Ar 2P_{3/2} peak has 34.5 meV FWHM.

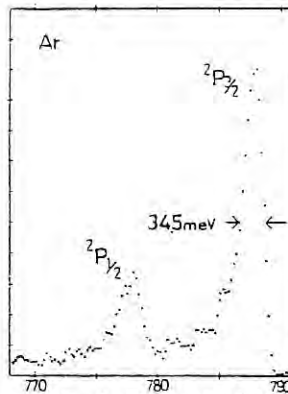


FIG.2 Threshold photoelectron spectrum of Ar

Results and Discussion

Results and Discussion

Many data were taken in the present experiment. Here we show some of these data. The relative partial photoionization cross sections of O₂ are shown in Fig.3. In both the O⁺ and O₂⁺ spectra in Fig.3, we can see the autoionizing peaks due to the transitions to Rydberg states converging to the C_u⁴ state of O₂⁺. Fig.4 shows the threshold photoelectron and photoion coincidence spectrum of O⁺ at 558.5 Å. The kinetic

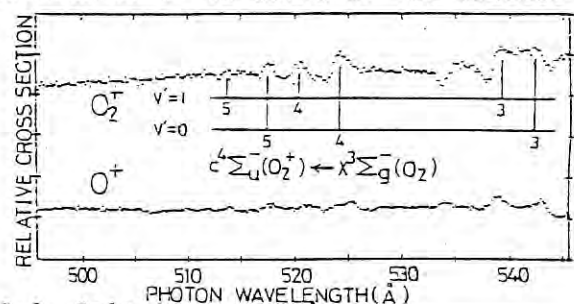


FIG.3 Relative partial cross section of O₂

energies of ions are separated in this spectrum (0.07 eV and 0.72 eV). It suggests the existence of two dissociative potential curves of O₂⁺ which dissociate to the limits (O(3P) + O⁺(2D) and O(1D) + O⁺(4S^o)).

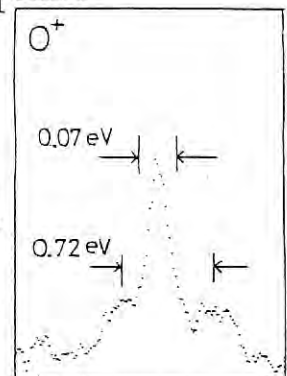


FIG.4

IONIZATION AND DISSOCIATION OF HIGHLY EXCITED MOLECULES

Y. Hatano, K. Shinsaka, H. Koizumi, T. Yoshimi, M. Toriumi, M. Ukai
 S. Arai, E. Suzuki, Y. Tanaka, M. Morita, A. Yagishita*, and K. Ito*
 Department of Chemistry, Tokyo Institute of Technology, Meguro-ku,
 Tokyo 152, Japan, and *Photon Factory, KEK, National Laboratory for
 High Energy Physics, Oho-machi, Tsukuba-gun, Ibaraki 305, Japan

Introduction

There exists in the vacuum ultraviolet region the most important part of optical oscillator strength distribution of atoms and molecules. The measurements of optical oscillator strength or absorption cross section (σ_t), ionization cross section (σ_i), and therefore ionization efficiency, $\eta = \sigma_i/\sigma_t$, in this region are of great importance to understand interaction of photon with atoms and molecules, and their reaction dynamics. For various atoms and molecules, however, these basic quantities are still unknown because of the absence of suitable light source. A synchrotron radiation has been considered as the most suitable light source to measure these quantities. We have constructed an ionization chamber with four ion-collector plates and measured these quantities using the synchrotron radiation of PF which is dispersed through a 1m Gas Seya-Namioka (GSN) monochromator at the BL-12A station.

Experimental

Figure 1 shows the ionization chamber used in this experiment which is made of stainless steel and teflon, and has a light trap on a rear side. This was put in a large vacuum chamber as shown in figure 2. A beam intensity of synchrotron radiation from GSN was monitored by a piece of gold mesh. This was electrically insulated and positive charges produced on it by photoionization were measured. The ion current in the sample gas and the current of the intensity monitor were measured by a picoammeter and counted by a counter and a MCA through a VF-converter. These detection systems and the monochromator were controlled by a computer (NEC PC-8001).

An absorption coefficient, μ , can be obtained from the ion current, i_1 , i_2 , i_3 , and i_4 using the following equation:

$$\mu = \sigma_t N = \ln(i_1/i_2)/L = \ln(i_2/i_3)/L = \ln(i_3/i_4)/L \quad (1)$$

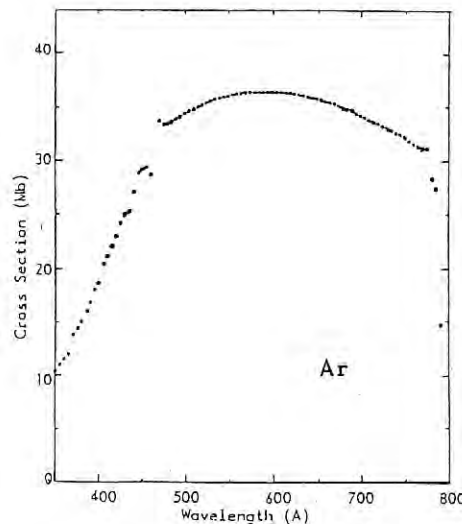
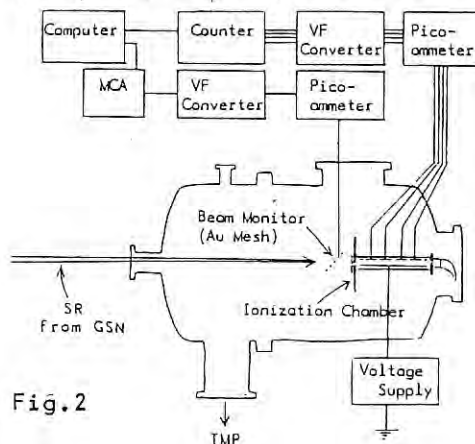
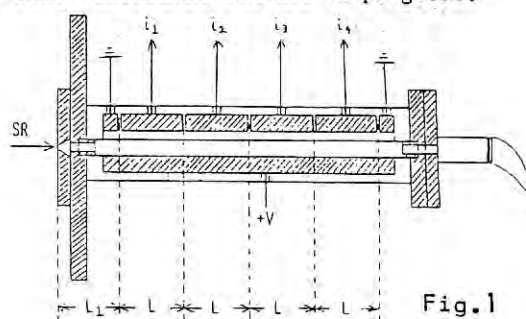
Equation (1) gives the three μ values, which is an advantage of this method. This makes it possible to check some errors caused by a gradient of the sample gas pressure, etc.

The value of $I_0\eta$, where I_0 is the incident light intensity, is also obtained using the following equation.

$$I_0\eta = \frac{i_1/e}{\exp(-\mu L)(1 - \exp(-\mu L))} \quad (2)$$

If I_0 is determined for a particular gas sample whose η is known, the ionization efficiency can be measured. The absorption cross section for Ar, Xe, and CH₄, the ionization efficiency of CH₄ at the wavelength region of 1000Å - 350Å were measured as the above procedure (figure 3), and systematic measurements of these quantities

for other molecules are now in progress.



Acknowledgement

The authors thank Dr. Y. Morioka of the University of Tsukuba for his valuable support during this experiment. They are also indebted to Dr. T. Nagata, Mr. M. Uematsu, and Mr. Y. Fukuda from Prof. Kuchitsu's group of the University of Tokyo for their valuable cooperation in the preliminary stage of this experiment in 1982.

Reference

1) A. L. Di Domenico et al.: Int. J. Mass Spectrom. Ion Phys. 33(1980)349

PERFORMANCES OF THE MUSCLE DIFFRACTOMETER

K. Wakabayashi^a, T. Hamanaka^a, Y. Amemiya^b, H. Tanaka^c, T. Wakabayashi^d and H. Hashizume^e

a Department of Biophysical Engineering, Faculty of Engineering Science, Osaka University, Toyonaka, Osaka.

b Photon Factory, National Institute for High Energy Physics, Oho-machi, Tsukubagun, Ibaragi.

c Department of Physiology, Faculty of Medicine, Teikyo University, Kaga, Itabashi-ku, Tokyo.

d Department of Physics, Faculty of Science, University of Tokyo, Hongo, Bunkyo-ku, Tokyo.

e Research Institute of Engineering Materials, Tokyo Institute of Technology, Nagatsuda, Midori-ku, Yokohama.

Introduction

The design and construction of the small-angle X-ray diffractometer built at Beam Line 15A was reported earlier¹⁻²). Since July 1982, the working group has made a series of experiments to evaluate the performances of the focusing optics together with progressive improvements. The optics is now in a final stage of construction to achieve a high resolution. A linear detector system for time-resolved data collection has been installed and preliminary experiments have been made on contracting muscle.

Optics

The double focusing optics uses a tandem of seven bent silica mirrors, each 20 cm-long, placed horizontally at 13 m from the light point. The mirror assembly accepts the whole vertical divergence of 0.36 mrad of synchrotron radiation at 1.5 Å wavelength. The horizontal focusing is achieved by a bent triangular silicon crystal, 7.8°-cut to the 111 plane, placed 4.5 m downstream of the mirror. This optics has been designed to give a demagnified image of the source with a focus size of 1.0(V) x 2.6 mm (H) (4σ value) at the focal plane 22 m from the light point¹⁻²).

Focusing property of the mirror

In the first operation in July 1982, seven 15 mm-thick silica mirrors were used and pressed against the bottom surface of the bending H-beam by two aluminum clamping pieces per mirror. It was found that the global surface figure of the mirrors were already curved to a short radius by the self weights of the mirrors and the bending mechanism. Coil springs were then implemented to cancel the weight of the force-applying arms. It was also found that individual mirrors were bent to a radius shorter than the bottom surface of the elastically bent H-beam. The number of clamping pieces per mirror was then increased to six and finally to ten. This progressively improved the focusing property of the mirrors.

Fig. 1 shows the beam images observed at the focal plane. Images a - c have been recorded by illuminating only the upstream, central and downstream one-thirds of the total length of the mirror assembly, while image d is produced from the whole mirror. The densitometer tracings of

image d show a beam size of 1.27 (v) x 2.6 mm (H) in 4σ values, which is only slightly larger than the design value. To examine the reflections from individual mirrors, the incidence slit was closed to 0.3 mm aperture and translated in the vertical direction in steps of 0.25 mm. Some mirrors were found to produce reflected beams at slightly different vertical heights at the focal plane. Furthermore, reflections from some mirrors are not uniform in intensity distribution. So there still remain some problems in the clamping of the mirrors. In fact, a greatest care is needed in positioning and clamping seven mirrors on the bottom surface of the H-beam. Securing screw bolts is critical in producing a uniform curvature of individual mirrors. Once well-aligned the mirror produces a good focus, but the beam size undergoes a gradual increase in a week, which can not be corrected by changing the bending couple applied to the H-beam. It seems that some thermal or elastic relaxation occurs in aluminum clamping pieces. We plan to test 7 mm-thick mirrors in the next run.

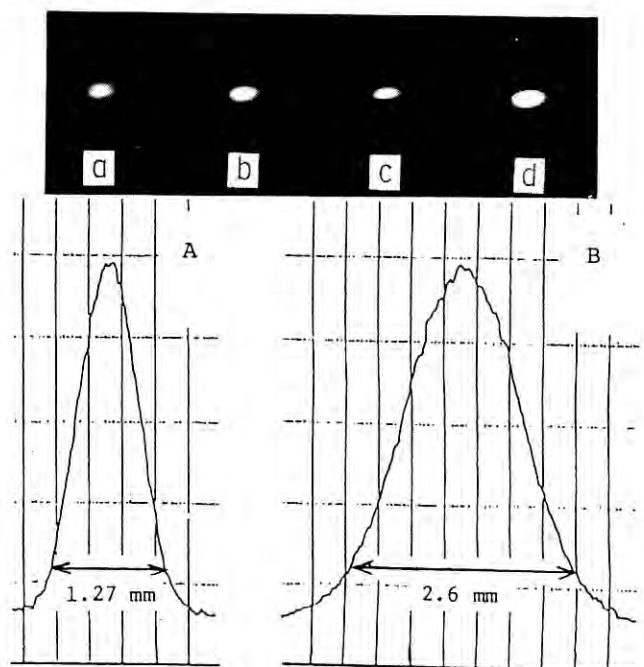


Fig. 1 Images of the focused beam. Images a, b and c are recorded from the upstream, central and downstream one-thirds of the total mirror length, respectively. Lower curves are densitometer tracings of image d. A: traced in the vertical direction, B: traced in the horizontal direction.

Parasitic scattering

In early runs, strong parasitic scatterings were observed around the focused beam even when the incidence slit was closed to a very small aperture. We then inserted three lead plates with 20 x 15 mm aperture in the vacuum pipe after the bent-crystal monochromator. The flat edge blades of the guard slit, placed at the specimen position, were replaced by tapered blades. These, however, did not dramatically change the parasitic scatterings. Finally the origin of the strong scattering was identified with the 0.3 mm-thick beryllium window, positioned just upstream of the specimen. When this window was replaced by a 0.02 mm-thick Kapton window, the scattering was reduced to a level acceptable in muscle works.

Resolutions

The optics is designed to give small-angle resolution of about 1000 Å and 80 Å at 1.5 Å wavelength with angular resolutions of 0.8 and 0.6 mrad in the vertical and horizontal directions respectively, at a specimen-to-detector distance of 2.6 m¹⁻²⁾.

Fig. 2 reproduces meridional diffraction diagrams recorded from a dried chicken collagen. These diagrams were recorded with the fiber axis vertical in 5 min on a Fuji Ix-150 X-ray film and in 10 sec with the linear proportional counter, when the PF storage ring ran at an energy of 2.5 GeV and a current of 90 mA. Collagen has a columnar structure with a long repeat distance

of about 670 Å (in native state) along the fiber axis. In Fig. 2 the first-order reflection of 653 Å (corresponding to the repeat of the dried chicken collagen used) is clearly resolved from the direct beam as well as from the parasitic scattering around the beam stop. Higher-order reflections up to the 11th are recorded with a good order-to-order resolution. This shows that the optics gives a small-angle resolution better than 1000 Å with an angular resolution of 2.3 mrad in the vertical direction at a specimen-to-detector distance of 2.3 m. The angular resolution in the horizontal direction has been examined by recording diffraction diagrams from crab muscle in the relaxed state. The intensity distribution on the 145 Å meridional layer line was not deformed appreciably.

Beam intensity

The intensity of the focused beam was measured with a scintillation counter by attenuating the beam with copper foils. When the PF storage ring ran at an electron energy of 2.5 GeV and a current of 13.4 mA, an intensity of 2.5×10^{10} photons/sec was observed at 1.5 Å wavelength. This can be increased by a factor of 20 when a maximum current of 250 mA is accumulated in the storage ring.

Position sensitive detector and data-taking system

A linear position sensitive proportional detector system has been installed and tested. The detector, 20 cm in sensitive length, uses an internal delay line of a 400 ns delay time for position encoding. Several anode wires are used to minimize the reduction of gas multiplication factor at high counting rates. The detector outputs are processed by ORTEC's NIM modules and fed to a LeCroy 4202 encoding digitizer followed by a LeCroy 3588 histogramming memory. Computer programs for a LSI 11/23 have been completed to setup the CAMAC modules for collecting data in time-resolved modes. The data collected in the histogramming memory is read by the 11/23 to be displayed on the graphic screen.

At low counting rates, the detector has given a spatial resolution of 0.35 mm, and the response is uniform within $\pm 3\%$ over the whole sensitive length. At average counting rates exceeding some 20,000 cps the encoding digitizer inhibits data taking and the router operates in an unexpected way. In spite of our frequent contacts with the dealer and the manufacturer, this problem remain unsolved at present.

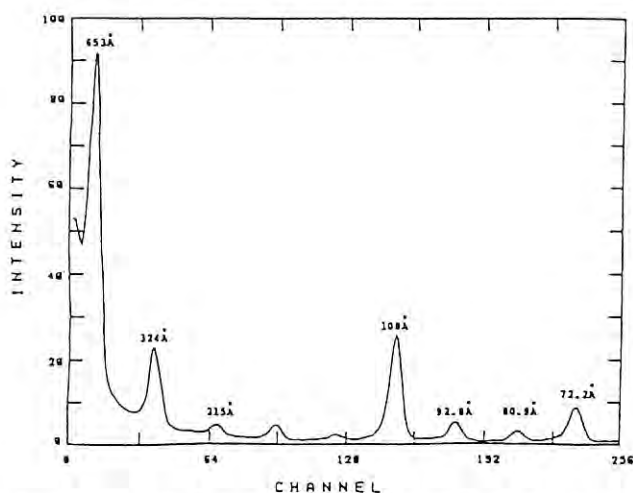
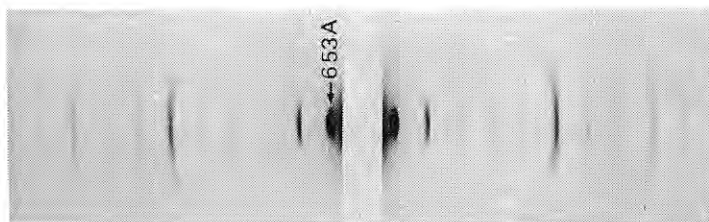


Fig. 2 Diffraction patterns of a dried chicken collagen. Upper: a photographic recording, lower: recorded with the linear proportional detector.

Preliminary time-resolved experiments on contracting muscle

Preliminary observations of time-resolved diffraction diagrams from contracting muscle were done in July 1982. Fig. 3 reproduces a series of equatorial reflection diagrams recorded from frog sartorius muscle slowly stretched during isometric tetanus. The muscle, placed with its fiber axis horizontal, was stimulated with 3 sec trains of 3 msec pulses at 33 Hz and was stretched by about 5 % of its initial length with a velocity of 10 mm/sec by actuating the vibrator 1 sec after the initiation of the stimulation. Equatorial reflection diagrams were detected by a 5 cm-long linear proportional counter bollowed from Prof. H. Sugi and recorded with a time resolution of 500 msec. The data were accumulated from two cycles of stimulation and stretch. The 1,0 and 1,1 reflections are clearly resolved and show intensity changes.

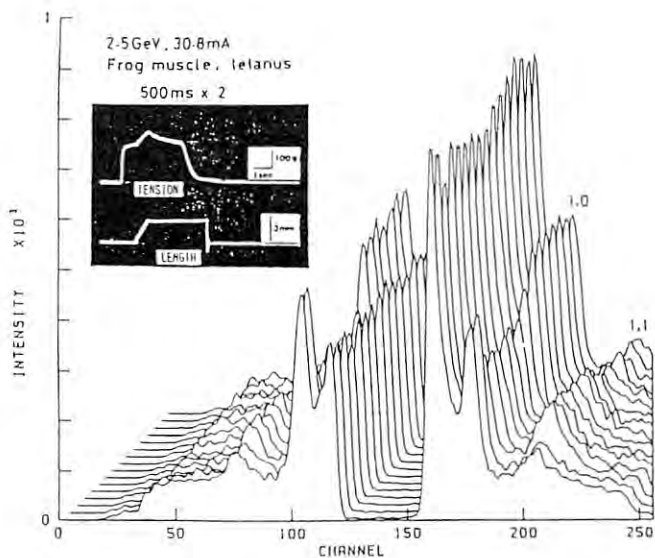


Fig. 3 Time-resolved diffraction diagrams of frog sartorius muscle slowly stretched during isometric tetanus.

References

1. H. Hashizume, K. Wakabayashi, Y. Amemiya, T. Hamanaka, T. Wakabayashi, T. Matsushita, T. Ueki, Y. Hiiragi, Y. Izumi and H. Tagawa: KEK Internal 81-11, March (1982).
2. Y. Amemiya, K. Wakabayashi, T. Hamanaka, T. Wakabayashi, T. Matsushita and H. Hashizume: Nucl. Instrum. Methods 208, 471 (1983).

TIME-RESOLVED X-RAY DIFFRACTION OF CONTRACTING SKELETAL MUSCLE

Hidehiro Tanaka¹, Takakazu Kobayashi¹, Hiroo Hashizume², Yoshiyuki Amemiya³ and Haruo Sugii¹

¹ Department of Physiology, School of Medicine, Teikyo University, Kaga, Itabashi-ku, Tokyo

² Research Laboratory of Engineering Materials, Tokyo Institute of Technology, Nagatsuda, Midori-ku, Yokohama

³ Photon Factory, National Laboratory for High Energy Physics, Ohomachi, Tsukuba-gun, Ibaraki-ken (Japan)

Introduction

Muscle contraction is believed to result from the alternate formation and breaking of cross-links between the projections on the thick filaments, i.e. the cross-bridges, and the sites on the thin filaments. It still remains, however, to be a matter of debate and speculation how the cross-bridges produce force and motion in muscle. Because of the hexagonal lattice formed by the thick and thin filaments, skeletal muscle exhibits clear equatorial and meridional X-ray diffraction patterns. When a muscle is stimulated to develop isometric force, the intensity of equatorial 1,0 reflection decreases while that of 1,1 reflection increases.

The present experiments were undertaken to study the dynamic properties of the cross-bridges (1) when a muscle is stretched during tetanus to result in a production of larger force at the stretched length despite the decrease in the amount of overlap between the filaments, and (2) when a muscle is stimulated with two successive brief pulses so that summation of isometric twitches takes place.

Materials and Methods

The sartorius muscle isolated from the bullfrog (*Rana catesbeiana*) was mounted between the length and force transducers. Time-resolved X-ray diffraction methods with synchrotron radiation have been described elsewhere. The experimental procedures were as follows: (1) the muscle was tetanized with repetitive 2 msec pulses at 30 Hz, and when the isometric force reached a maximum, the muscle was stretched by 5% in 1 sec and kept at the stretched length for 2 sec. The resulting changes in the equatorial reflections were examined with a time resolution of 0.5 sec; (2) the muscle was stimulated with two 2 msec pulses given at an interval of 80 msec, and the resulting changes in the equatorial reflections during summation of isometric twitches were examined with a time resolution of 5 msec. All experiments were made at 5-15°C.

Results and Discussion

The changes in the equatorial reflections when a tetanized muscle is stretched are shown in Fig.1. Despite a distinct force increment in response to applied stretch, no appreciable change in the intensity ratio between the 1,0 and 1,1 reflections was observed, suggesting that the force increase by stretch results from a mechanism other than the increase in the number of the cross-bridges attached to

the thin filaments.

The changes in the equatorial reflections during summation of two isometric twitches are shown in Fig.2. It was found that, during the first twitch, the changes in the equatorial reflections showed maximal changes prior to the peak twitch force, while during the second twitch the corresponding maximal changes of the equatorial reflections took place in parallel with the twitch force. This indicates that the behaviour of the cross-bridges during the first twitch is different from that during the second twitch.

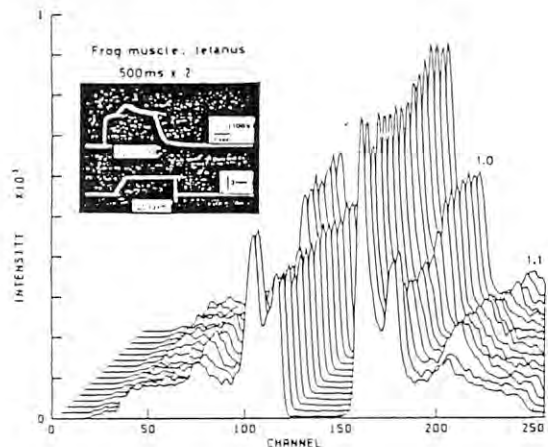


Fig.1

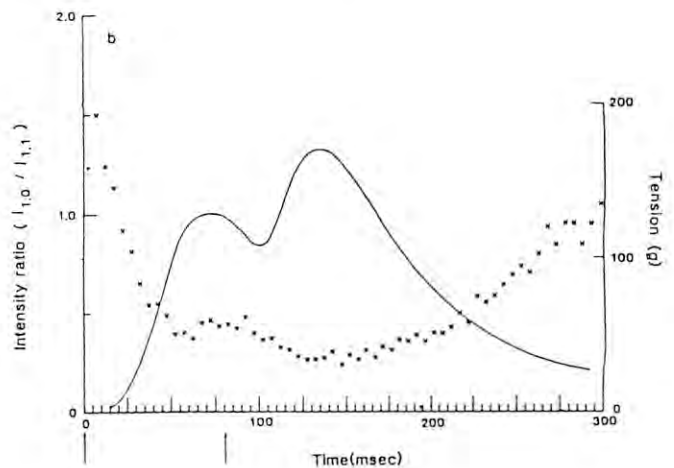


Fig.2

1. Amemiya et al. (1983) Nucl.Instrm.Methods, 208, 471.

X-RAY DIFFRACTION STUDIES OF STRUCTURAL CHANGE OF MUSCLE FILAMENTS IN CONNECTION WITH MUSCLE CONTRACTION

K. Wakabayashi, T. Hayashi, A. Fujishima, T. Hamanaka
 Department of Biophysical Engineering, Faculty of Engineering Science, Osaka University, Toyonaka, Osaka 560 (JAPAN)

M. Konishi, S. Kurihara, Y. Umazume
 Department of Physiology, The Jikei University School of Medicine, Nishi-Shinjuku, Minato-ku 105 (JAPAN)

Y. Amemiya
 Photon Factory Instrumentation Group, KEK, National Laboratory for High Energy Physics, Oho-machi, Tsukuba-gun, Ibaraki 305 (JAPAN)

Synchrotron X-ray diffraction studies of structural change of muscle filaments in connection with the muscle contraction have been done using the muscle diffractometer installed at BL 15A.

A study of structural change of muscle filaments at low ionic strengths

X-ray diffraction using rotating anode sources indicated that the binding of myosin heads to the thin filaments in glycerinated crab (and rabbit psoas) muscle fibres took place with lowering ionic strengths at low temperature (<6°C) in the presence of ATP without Ca ions. This work was extended to obtain the structural data at high temperature (~20°C) during the force generation using synchrotron radiation. Prior to studies, we recorded two-dimensional diffraction patterns from crab muscles in the rigor and relaxed states to compare the speed of recording with films and quality of the patterns with those obtained using rotating anode sources. Fig. 1 shows a diffraction pattern from a rigor crab muscle obtained with synchrotron radiation. The pattern by synchrotron radiation was recorded in 40 min with similar quality to the pattern recorded in 25 hrs by a laboratory source. In an example of Fig. 1, the high diffuse scattering has appeared in the small-angle region. This scattering could be suppressed by using Mylar for the window materials and the diffraction pattern should be recorded with much higher S/N ratio.

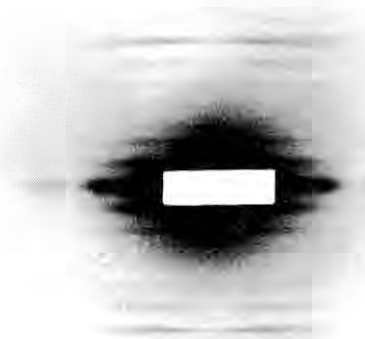


Fig. 1 X-ray diffraction pattern from crab muscle fibres in rigor
 Fibre axis, vertical. Specimen-to-film distance, 92cm. Exposure time, 40 min (2.5Gev, 55mA).

A study of the muscle contraction induced by caffeine

In order to study the structural changes of muscle filaments during contraction in the presence of caffeine by rapid cooling method, X-ray diffraction has been done using frog toe muscles. Fig. 2 shows the preliminary results of changes of equatorial diffraction patterns, in which (a) denotes the pattern from the muscle in the absence of caffeine at room temperature, (b) in the presence of caffeine at room temperature and (c) in rapid cooling from room temperature to 4°C in the presence of caffeine. When the muscle was cooled rapidly to 4°C in the presence of caffeine, it was found that the intensity ratio of I(1010)/I(1120) decreased and small changes in lattice spacing occurred in connection with the force generation.

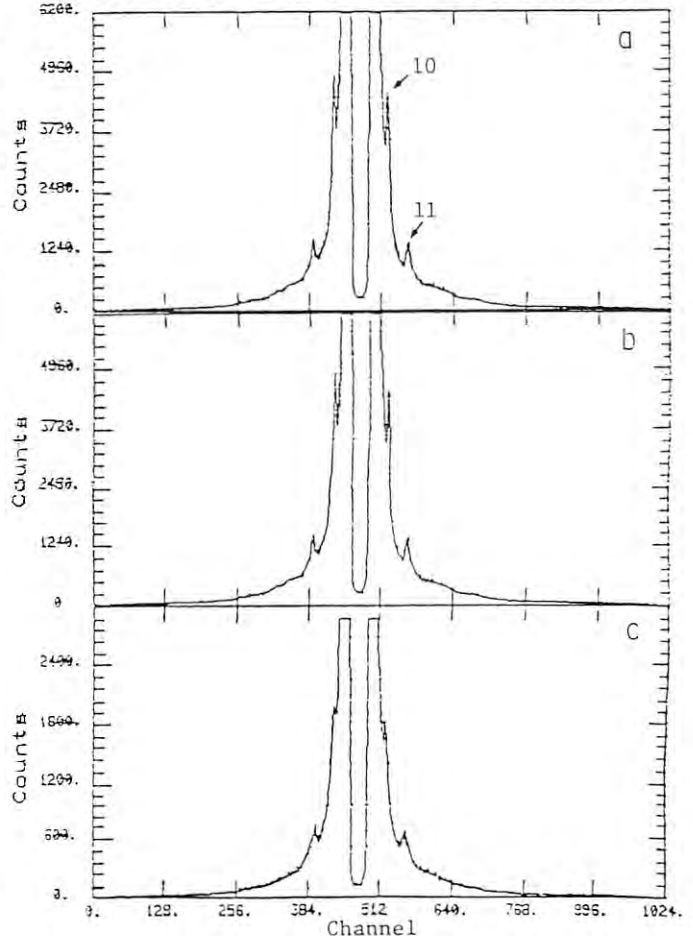


Fig. 2 Changes of equatorial diffraction patterns from frog toe muscle fibres in the presence of caffeine of 1.2mM
 Intensity data were recorded by a 20cm long-PSPC.

TEST OF INTEGRAL TYPE POSITION-SENSITIVE DETECTOR AND ITS APPLICATION TO SMALL ANGLE SCATTERING EXPERIMENTS

Ken-ichi Hasegawa and Koh-ichi Mochiki
 Faculty of Engineering, University of Tokyo
 7-3-1, Hongo, Bunkyo-ku, Tokyo 113 (JAPAN)

Introduction

Synchrotron radiation sources delivering intense X-ray beams have placed new demands on the quality of instrumentation. The main requirement in using intense X-ray beams, especially in time-resolved X-ray diffraction experiments is to reduce the necessary recording times sufficiently to obtain statistically meaningful information in the time scale of interest. The integral type¹ has no counting loss, and the applied voltage and the accumulation time are appropriately adjustable to the intensity of incident X-ray flux, thus the attainable maximum count rate of the integral type is higher than that of any other type, such as the delay line type and the wire/scaler type^{2,3}. The minimum rate of this system depends on the leakage current and the noise of associated electronics and the gas gain. When the gas gain is about 10^4 , this limit is about 40 counts/sec/channel.

Detectors

The integral type position-sensitive proportional chambers are divided into two groups, the single anode - multistrip cathode type and the multianode type. The cathode type can be used in lower intensity than the anode type. In the early stage of this development, we made large detectors; a cathode type (2.54 mm pitch, 128 ch) and an anode type (1 mm pitch, 128 ch) and measured basic characteristics of these detectors because the experimental requirements were not confirmed and such large detectors were convenient to test the performance.

Application

Figs. 1 and 2 show the diffraction patterns recorded from frog muscle at resting state and during contraction, respectively with a cathode type detector with 1 mm pitch. The data shown in Fig. 2 were obtained in only 100 msec with the X-ray intensity about 10^5 counts/sec over the whole detector and about 6×10^3 counts/sec at the peak channel. In the case of Fig.3, data were summed from 10 twitches, each time slot being of 10 msec duration, that is, corresponding to 100 msec total exposure. The X-ray intensity is about 6×10^4 counts/sec over the whole detector and about 5×10^3 counts/sec at the peak channel. These data show the availability of this type of detector to high intensity experiments and synchrotron radiation sources can be used effectively.

Future Development

Now we are constructing a cathode type detector with 0.5 mm pitch and it will be tested in the next machine time.

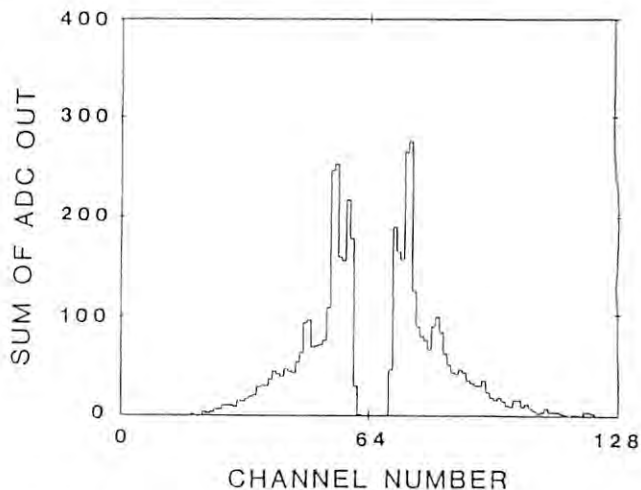


Fig. 1. 100 msec resting pattern from frog muscle.

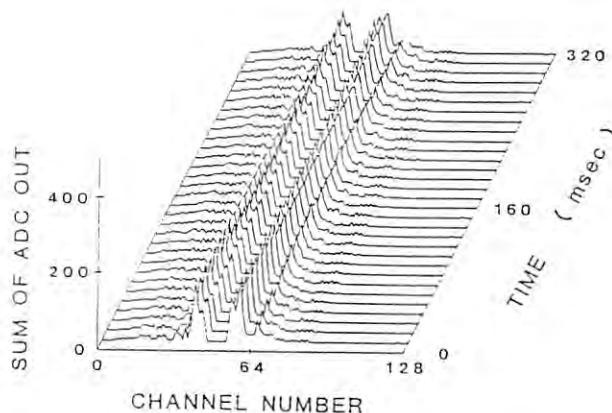


Fig. 2. Time-resolved diffraction diagrams. Data are summed from 10 twitches, each time slot being of 10 msec duration.

Acknowledgments

These experiments have been carried out with Dr. Tanaka and Dr. Kobayashi of Teikyo University, Dr. Amemiya of Photon Factory and Professor Hashizume of Tokyo Institute of Technology. We would like to thank them for experimental arrangements and many helpful suggestions.

References

- 1) K. Hasegawa, K. Mochiki and A. Sekiguchi: IEEE Trans. Nucl. Sci. NS-28(1981)3660.
- 2) H.E. Huxley and A.R. Faruqi: Ann. Rev. Biophys. Bioeng. 12(1983)381.
- 3) A.R. Faruqi: IEEE Trans. Nucl. Sci. NS-30(1983)358.

Supplement

POSITION-SENSITIVE IONIZATION CHAMBER
AS A BEAM MONITOR DEVICE

Koh-ichi Mochiki, Atushi Ogata*
and Ken-ichi Hasegawa; * KEK

We expect that the position-sensitive detector with integral type readout electronics is useful also as a beam monitor device¹. It can be used in the circumstances where any other detectors are saturated or damaged. One will be equipped in the TRISTAN accumulation ring, where radius of critical X-ray beam of the synchrotron radiation will be about 2.5 mm for electrons at the detector position. Bearing the application in mind, we have tested a prototype detector with high space resolution at the PF beam channel.

The prototype detector consists of uniformly-spaced anode wires and a uniform conducting cathode block; 50 gold-plated tungsten wires with 20 μm diameter are stretched at intervals of 100 μm as the anode. Spacing between cathode and anode is 1.6 mm, where 200 V voltage was applied. The detector was operated as a position-sensitive ionization chamber either in flowing argon gas or in open air. Structure of the detector is shown in Fig. 1. Among 50 anode wires, 11 were found to be of no use; they are short-circuited or broken. Therefore the center part with successive sound 19 wires was employed to test the detector performance. Figure 2 shows the response of the anodes to a uniform beam. The lack of the outputs expresses the broken channels and the large output channels are short-circuited. A uniformity of 7.7 percent was obtained in the center part.

Data of successive 19 channels covered 2 mm in horizontal direction of the PF X-ray beam. The whole detector was shifted 1 mm after each measurement. Such a procedure was repeated 5 times. Five data sets were thus obtained which covers 6 mm as a whole. They were used to estimate the intensity distribution of the X-ray. The result is shown in Fig. 3.

We conclude that this position-sensitive detector has no problem as a beam monitor device in principle. Besides the advantages previously mentioned, the fact that it is operatable in open air is also notable, because beam monitoring favors a maintenance-free device. Another prototype with more robust structure is under construction.

We are grateful to Prof. T. Hongo and Mr. K. Sato of KEK Workshop who have constructed the anode of the detector.

Reference

- 1) Y. Hosono, K. Hasegawa and A. Sekiguchi:
Oyo Buturi Vol.52, No.4 (1982)344.

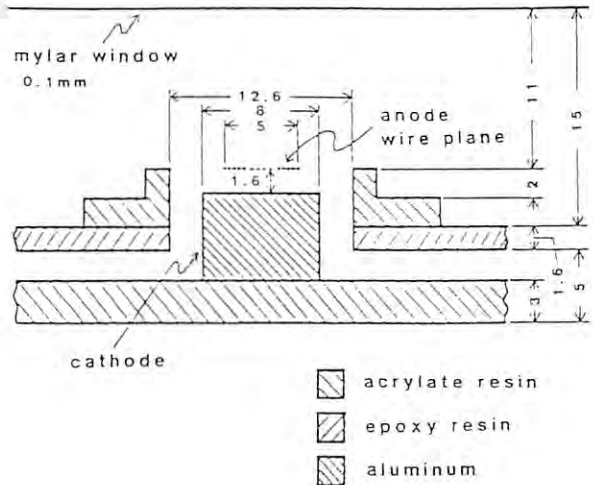


Fig. 1 Structure of the prototype detector.

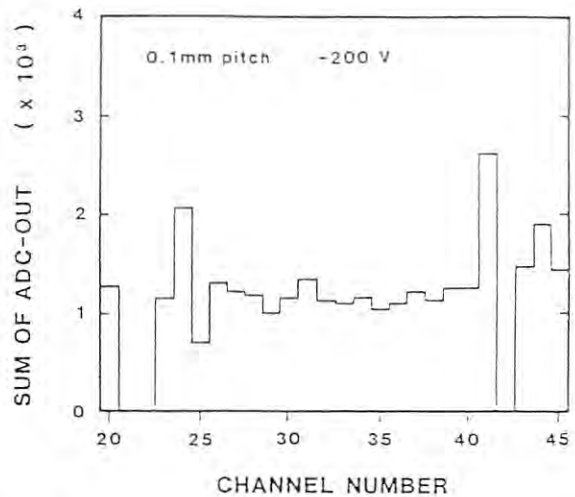


Fig. 2 Response of anodes to a uniform beam.

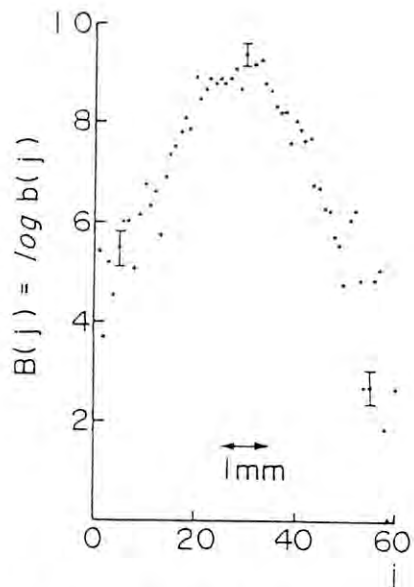


Fig. 3 X-ray intensity distribution of the BL-15A1 beam channel.

TIME-RESOLVED X-RAY DIFFRACTION STUDIES OF TMV AND THEIR PROTEIN ASSEMBLIES.

M.Taniguchi¹, Y.Amemiya², K.Wakabayashi³, T.Taniguchi⁴, Y.Sato², and Y.Kamiya⁵

1. Department of Physics, Faculty of Science, Nagoya University, Nagoya 464 (Japan)
2. Photon Factory, National Laboratory for High Energy Physics, Ohomachi, Tsukuba-gun, Ibaraki-ken 305 (Japan)
3. Department of Biophysical Engineering, Faculty of Engineering Science, Osaka University, Toyonaka, Osaka (Japan)
4. Plant Pathology Laboratory, Faculty of Agriculture, Nagoya 464 (Japan)
5. Department of General Education, Faculty of Engineering, Toyota Technological Institute, Nagoya (Japan)

Introduction

Tobacco mosaic virus (TMV) is a complex of a single ribonucleic acid (RNA) molecule and identical protein subunits. We have found that three strains of TMV (TMV-OM, TMV-T and TMV-B) differ from one another in their physico-chemical and electric properties¹⁻³. In order to understand the molecular development of TMV, it is necessary to know their detailed structures and dynamic properties. Comparative study of TMV strains has been done using small angle X-ray diffraction apparatus⁴.

Experimental results and discussions

Three strains of TMV were used in the experiment; the ordinary strain (TMV-OM) from the virus infected tobacco leaves (*Nicotiana tabacum*, L. var Bright Yellow), the tomato strain (TMV-T) from infected tomato leaves (*Lycopersicon esculentum*, Mill) and the cruciferous strain (TMV-C) from infected cruciferous leaves (*Brassica campestris* L.). The viruses were extracted and purified by several cycles of low speed and high speed centrifugation, and suspended in a 10 mM phosphate buffer of pH 7.0 and 0.4 mM Na₃. Oriented specimens were prepared essentially according to the method of Gregory & Holmes.⁵ Three sets of X-ray diffraction photographs from oriented fibers of TMV-OM., TMV-T and TMV-C have been collected on precession camera (at static position) at station 15 A at the Photon Factory Synchrotron Radiation Source. Each photograph was recorded with an exposure time of 15 mins for a beam of 80-100 mA and 2.5 GeV. and analyzed by microdensitometer. The main features of TMV-T and TMV-C are closely similar to that of TMV-OM; the 3rd(23Å⁻¹) and 6th layer lines show strong near-meridional reflections and the first order layer line(69Å⁻¹) corresponds the axial repeat period of three turns of the helix (See Fig.1) Clear differences in the near-meridional reflections between TMV-OM and TMV-T appear in the second and 4th layer lines. (See arrow in Fig.1). (These reflections are observed in TMV-T, but not in TMV-OM). Significant differences between the X-ray diagrams of TMV-C and TMV-OM have also been detected in the laboratory.

In the near future we plan to use the synchrotron source to study the dynamic structure of TMV molecules obtained from various strains.

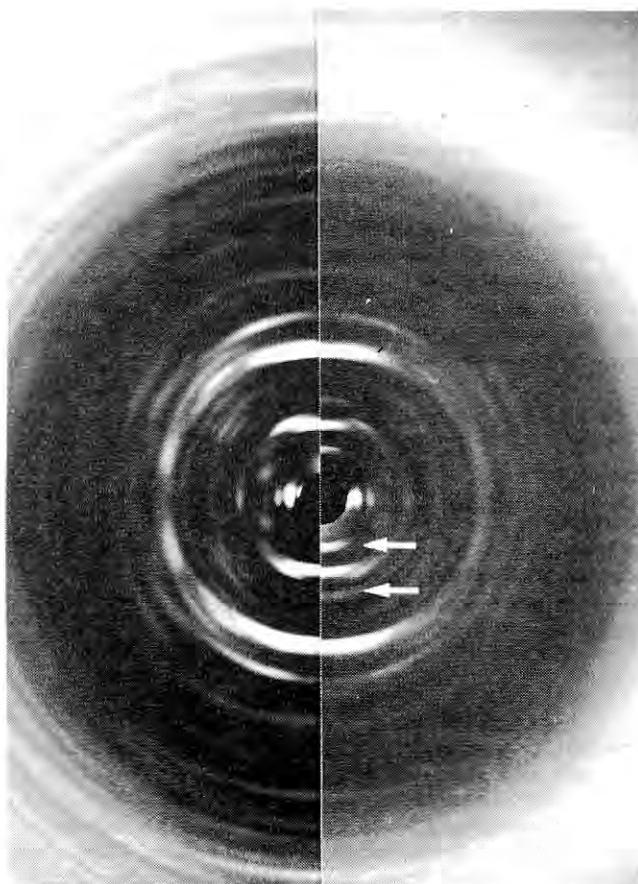


Fig.1 X-ray diffraction pattern of oriented TMV-T gel compared with that of oriented TMV-OM gel. Arrow in photograph indicates the second and 4th layer lines. TMV-OM(left) and TMV-T(right)

References

1. M.Taniguchi, S.Kobayashi and A.Yamaguchi
Biochim. Biophys. Acta., 188(1969)140-146
2. M.Taniguchi, A.Yamaguchi, and T.Taniguchi
Biochim. Biophys. Acta., 251(1971)164-171
3. M.Taniguchi and T.Taniguchi,
Biochim. Biophys. Acta. 386(1975)1-17
4. Y.Amemiya, K.Wakabayashi, T.Hamanaka,
T.Wakabayashi, T.Matsushita and H.Hashizume,
Nucl. Instrum. methods 208(1983)471
5. J.Gregory and K.C.Holmes,
J.Mol.Biol. 13 (1965)796-801

LOCALIZATION OF PHYSIOLOGICALLY ACTIVE TYROSINES IN PURPLE MEMBRANE
AND THEIR LOCALIZATION CHANGE ON ABSORPTION OF LIGHT

F. Tokunaga, M. Kataoka, N. Sato, K. Takeda, O. Hisatomi, M. Hirai
and
Y. Amemiya*

Faculty of Science, Tohoku University, Sendai, Miyagi 980
PF Instrument, KEK, National Laboratory for High Energy Physics, Ibaragi 305*

INTRODUCTION

Purple membrane (PM) of *Halobacterium halobium* is composed of only one species of protein, bacteriorhodopsin (bR). BR molecules in PM form a two-dimensional hexagonal lattice (p3) with $a=63\text{\AA}$.¹ Physiologically, bR acts as a light-driven proton pump.² It is clarified spectroscopically that some of tyrosine residues play an important role in the photoreaction of bR.^{3,4} In order to understand the molecular mechanism of bR's photoreaction, it is essential to identify the physiologically active tyrosines and their sites in bR. Tyrosine can be labelled with iodine. Iodinated PM regards as a heavy atom derivative of PM.

Purpose of present experiment is application of heavy atom replacement to biomembrane, PM, to define the active tyrosines. We report preliminary results of X-ray diffraction experiment on PM and iodinated PM which was performed at Muscle Diffractometer, BL-15A.^{5,6}

EXPERIMENTAL

PM was isolated from *H. halobium* with ordinary method.⁷ PM was iodinated with lactoperoxidase.³ Centrifugal pellet sealed into glass capillary and dried specimen were used for X-ray diffraction experiment ($\lambda=1.5\text{\AA}$). Diffraction patterns were recorded on Fuji Industrial 400 X-ray films or with PSPC. Sample to detector distance was 890 mm.

RESULTS

X-ray diffraction patterns from native PM (pellet), native PM (dried) and iodinated PM (dried) are shown in Fig. 1. Bragg reflections up to (21) reflection were clearly observed. These photographs were recorded in 1 hr exposure. With ordinary X-ray source, it requires more than 20 hrs. Judging from diffraction pattern, iodination causes slight distortion of crystalline structure of PM. Because of high level of background scattering, exact diffraction profiles could not be obtained.

We note here two points of remarkable findings. One is two reflection lines existing in the small angle region whose spacings correspond to 180Å and 130Å (designated A in Fig. 1). The other is new reflection lied outside of (10) reflection, clearly seen in the case of dried native PM (designated B in Fig. 1). The latter reflection was stronger than ordinary (10) reflection in the case of iodinated PM. Native PM (pellet) did not show the latter reflection. Some deterioration may occur in the process of drying or iodination. So far, it is believed that drying procedure does not affect the structure of PM, because such a reflection has not been observed. The former reflection is not observed for iodinated PM. For dried PM, the former is not clear in the film but can be observed with PSPC. One of possible interpretation

of the former reflection is that PM possesses superlattice structure. This is the first description of both reflections. Origins and other characteristics are yet unknown. Both reflections cannot be observed with ordinary laboratory apparatus. We hope to continue the project in order of detailed analysis. We are grateful to members of Muscle Diffractometer WG.

REFERENCES

1. Blaurock, A.E. & Stoeckenius, W. (1971) *Nature New Biol.* **263**, 152
2. Stoeckenius, W. *et al.* (1974) *B.B.A.* **505**, 215
3. Iwasa, T. *et al.* (1983) *Biosci. Rep.* **2**, 949
4. Lemke, H.D. & Oesterhelt, D. (1981) *Eur. J. Biochem.* **115**, 595
5. Hashizume, H. *et al.* (1981) KEK Internal 81-11
6. Amemiya, Y. *et al.* (1983) *Nucl. Instrum. Methods* **208**, 471
7. Oesterhelt, D. & Stoeckenius, W. (1974) *Method. Enzymol.* **31**, 667

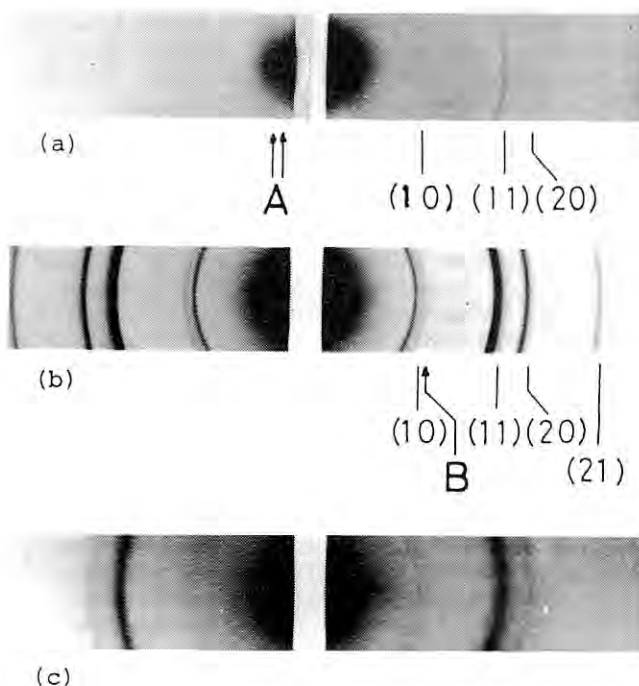


Fig. 1. X-ray diffraction photographs of a) native PM (pellet), b) native PM (dried) and c) iodinated PM (dried). Bragg indices according to p3 with $a=63\text{\AA}$ are indicated. A: newly found small angle reflections (clearly seen in the original film). B: newly found reflection outside of (10) reflection, corresponding spacing is 51Å. Intense scattering near beam stop is due to scattering from Be window.

FOTOGRAFIC INVESTIGATION OF A HUMAN TOOTH (15 B 1, Dec. 1982)

by Peter Spieker

Using one axis of the "3-axes diffractometer" at station 15 B 1 a 50 μm thick slice of a human tooth has been investigated in two ways:

- a) absorption contrast and
- b) phase contrast.

The sample has been provided by Prof. Suga from Nihon Shiga Daigaku / Tokyo. A human tooth was imbedded in a plastic material and than a 50 μm thic slice was cut out of this bloc. The aim of the investigation is the process of mineralisation at the border between the living tissue of the tooth and the mineralized part.

a)
Using a special channel cut monochromator (see section 2.4 of this report), absorption contrast pictures are taken over a wavelengh range from 1 \AA to 3.4 \AA (see figure 1).

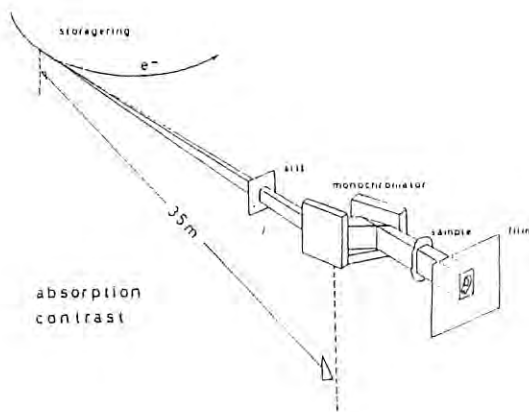


fig: 1
Sketch of the set up for absorption contrast

Special attention is payed to the neighbourhood of the K-absorption edge of Calcium at 3.07 \AA .

b)
Using a LLL x-ray interferometer (see section 2.4 of this report) phase contrast pictures of the same sample are taken. The set up is shown in figure 2. The phase contrast fotos contain a much more detailed structure as the ones with absorption contrast, but they are also more difficult to understand. Inhomogenities caused by the slicing procedure produce unwanted interference patterns.

At 2.5 GeV and about 40 mA the exposure times are around 1 minute.

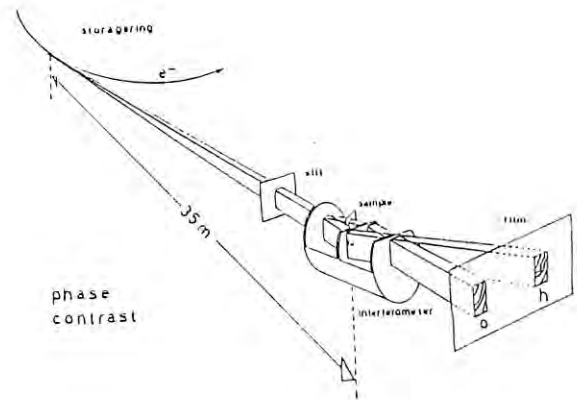


fig: 2
Sketch of the set up for phase contrast

For the longer wavelenghs (above 2 \AA) the whole set up was covered with a helium tent to reduce absorption in the air. The background is also lowered by this measure.

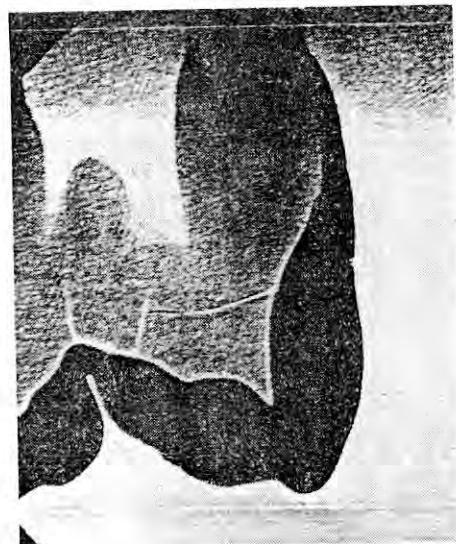


fig: 3
Fotograph with absorption contrast at 1.7 \AA

Figure 3 shows one example of the pictures. Bringing the sample in contact with the film, will enhance the sharpness in the case of absorption- and a better slicing will reduce the disturbing superposition in the case of phase-contrast in further experiments.

TEST OF AN X-RAY INTERFEROMETER (15 B 1, Jun. 1982)

by Peter Spieker

Using only one axis of the "Three Axis Diffractometer" at station 15 B 1 the performance of a LLL x-ray interferometer has been checked. The device itself is described in section 2.4 of this report.

When an interferometer is used in an experiment the interference pattern in the output is recorded on film, with TV or by a counter. This pattern is a superposition of the one produced by the phaseshift caused by the sample (wanted pattern) and a "built in" pattern (unwanted) originating from the imperfections of the crystal material and the manufacturing process of the interferometer.

A check is necessary to prove that there is no or only a simple, reproducible "built in" pattern in the outgoing beams of the empty interferometer. In the test the crystal is placed in the primary beam from the storage ring and the resulting O- and H-beam are photographed. A separate monochromator is not necessary, because the interferometer acts already in this way. In our case the empty interferometer caused no structure.

This can be interpreted as:

- a) the interferometer is nearly perfect and
- b) the "built in" fringe system has a spacing that can not be resolved.

Case b) would mean a useless interferometer, because the insertion of a sample would usually result in an even finer structured interference pattern. To distinguish these two cases, a wedge (acryl) is placed in one of the internal beams.

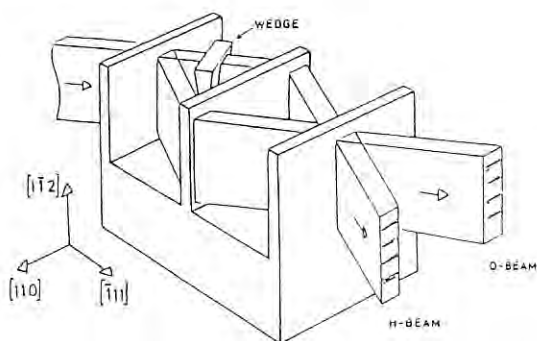


fig: 1

Shown is a schematic drawing of an LLL x-ray interferometer. It is cut in such a way, that 220-reflections are used. The wedge inserted in one of the internal beams produces a phase shift proportional to the material thickness. This is the reason, that parallel, equidistant fringes are formed in the output.

In case a) an equally spaced system of parallel fringes is produced, because no complicated "built in" pattern is superimposed. In case b) nothing visible is changed.

fig. 1 shows the setup and fig.2 the result.

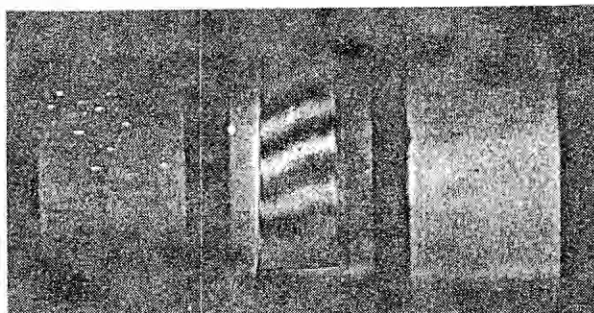


fig: 2

Picture taken with the set up of fig 1. The inclination of the fringes comes from an unsymmetrically fabricated wedge. The unstructured regions on both sides of the fringed part occur, because not the whole internal beam passes through the wedge. The exposed areas left and right have no structure, because the beams which reach here travelled only over one path through the interferometer.

The described experiment tests only a small part of the mirror area. To cover more, interferometer and film are moved like in a Lang-camera. This scanning produces fringes covering nearly the whole width of a mirror. Together with the first result (fig.2) this tells, that the device is suitable for further experiments.

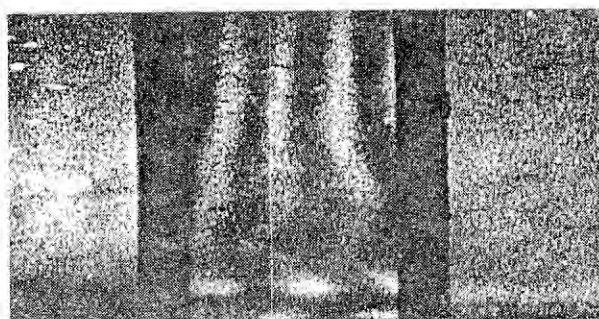


fig:3

This picture shows the interesting result obtained after slightly heating the third lamella of the interferometer. Because of thermal expansion this "dilatation moire" is produced.

TEST OF A "MONOLITHIC FIXED EXIT BEAM MONOCHROMATOR" (15 B 1, Jun./Jul.1983)

by Peter Spieker

Using the "3-axes diffractometer" at station 15 B 1 the alignment procedure and performance of a "Monolithic fixed exit beam monochromator" for x-rays (described in section 2.4 of this report) has been checked. Because of the not-flat reflecting surface the following had to be done.

a)

The geometrical condition for a proper working demands, that the axis of rotation for selection of the wavelength runs through the center of symmetry of the crystal and that all beams pass over this center (see figure 1).

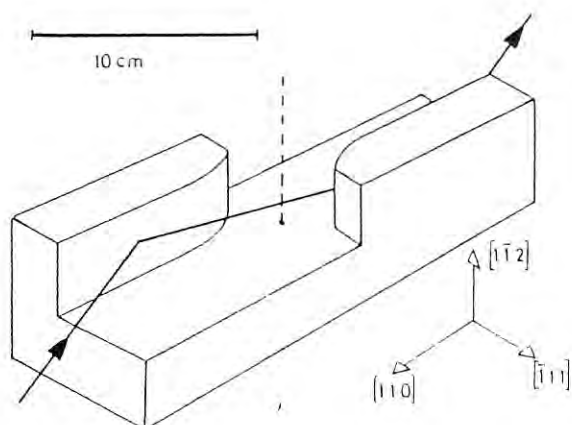


fig: 1

Sketch of the monochromator

All beams must pass over the center of the crystal.

Only when this is fulfilled, the asymmetry effects in both reflection points cancel each other and no intensity is lost due to a mismatch in angular reflection ranges. Because no mark made by the manufacturer (CANON) indicates the center, it has to be determined by taking the geometrical dimensions of the crystal. To position the device with respect to the primary beam, a 0.5 mm thick copper wire is placed above the center. When the crystal is shifted sidwise, the intensity of an 0.5 mm wide x-ray beam passing through the monochromator is cut, when the proper position is reached. Because of uncertainties in the location of the symmetry center this position can only be reached with an accuracy of a few hundred microns.

b)

Because the crystal is large (220 mm) it is not trivial, that the perfectness necessary for two successive reflections is given over the whole length. This is simply checked by scanning the wavelength over the spectrum of a bending magnet and by taking an EXAFS spectrum. One compares the results with those obtained with other methods.

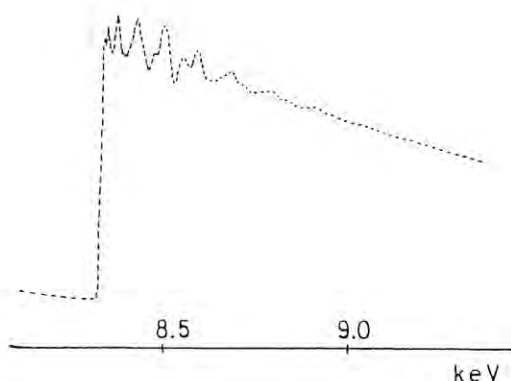
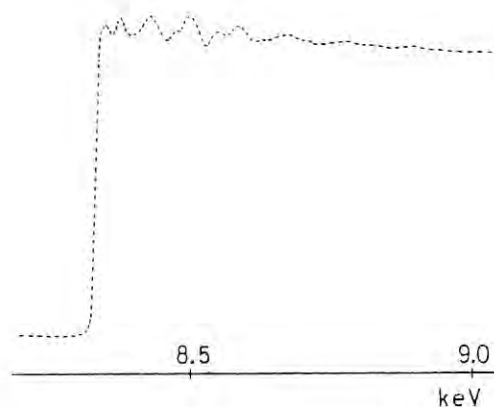


fig: 2

upper part: EXAFS spectrum taken with this monochromator at the Ni-K edge in a scanning mode.

lower part: EXAFS spectrum of the Ni-K edge taken point by point at another experimental station.

Both experiments show a good coincidence.

HIGH SPEED X-RAY TOPOGRAPHY

Working Group of High Speed X-Ray Topography[†]

Introduction

X-ray topography is now widely used for characterization of single crystals and observation of secondary structures in crystals such as magnetic and/or ferroelectric domains. Today, dynamic observation of defects and magnetic domain walls is possible using an x-ray sensing television camera and high power x-ray generator with a rotating target. However, the resolution of this type of observation is limited to low resolution (20 to 30 μm). Synchrotron radiation provides 10~100 times higher diffracted intensities than such a high power x-ray generator and, in principle make it possible to observe rapid structural changes with a higher resolution and better signal-to-noise ratio. If this is materialized, we can expect significant development in modern crystallography as well as industrial applications. For this end, a working group of "High Speed X-Ray Topography" has been organized from 1978 and has worked on design and construction of the entire system for synchrotron radiation topography (SRT).

Observation System

The system was designed along the following guide lines:

- (1) A high resolution TV system should be developed for SRT.
- (2) Merits due to white radiation from synchrotron should be fully utilized.
- (3) Preparation for experiments such as specimen setting can be made quickly to use machine time effectively.

TV camera

Both indirect and direct types of TV cameras were developed. In the former type, x-ray images are first converted into visible light images to be observed by the usual electro-optical system. It has an advantage to adjust viewing area (magnification) by a zoom lens placed behind a fluorescent screen (gadolinium oxysulfide film). Whereas, the direct type converts x-ray input images directly into video signals and provides very high resolution: A camera tube with an

amorphous Se-As alloy photoconductive layer was developed, and a limiting resolution of 6 μm and low lag characteristic (less than 1% after one frame) were achieved by employing a narrow electron beam from a diode-type gun having a barium-impregnated tungsten cathode. Its sensitivity for a wavelength of 0.71 Å was nearly half of that of the conventional camera tube with a PbO target layer. These characteristics were confirmed by imaging individual dislocations in a silicon wafer with synchrotron radiation.

Goniometer

The goniometer was designed primarily for the use of synchrotron radiation with the vertical E polarization from a PF superconducting wiggler which will be operated from November 1983, i.e., θ and 2θ rotation are in horizontal (vertical rotation axis). This geometry is convenient for holding liquid, e.g., in in-situ observation of melting and growth processes. Its special features are as follows:

- (1) Various accessories such as a magnet or cryostat can be loaded up to 30 kg in weight.
- (2) Using the white radiation, simultaneous observation of topographic images for two reflections are possible by employing two TV cameras (Fig. 1), so that in-situ identification of defects may be made.
- (3) Almost all operation can be remote-controlled with the aid of microcomputer. Alignment of specimen orientation can be made quickly by monitoring Laue patterns on the fluorescent screen using a low light level TV camera (TV-3 in Fig. 1).

Experiment

Various kinds of specimens have been investigated as listed in Table 1. Using specimen-heating and cooling accessories, phase transition of quartz (846 K), melting of GaAs (1520 K) and olivine (2170 K), and domain structure in TbVO₄ due to Jahn-Teller transition (34 K) have been observed. Some of these experiments are reported in the following pages.

Table 1. Specimens observed during April 1982 - July 1983.

Metals and alloys	Al, W, Cr, Nb, Sn, Fe-Si [*] , Sn-In, In-Pb [†]
Minerals	Beryl [Be ₃ Al ₂ (Si ₆ O ₁₈)], Diamond Olivine [(Mg,Fe) ₂ SiO ₄] [#] , Fluorite [CaF ₂], Quartz [SiO ₂]
Semiconductors and others	Si, Web Si [#] , GaAs [#] , KDP, Al ₂ O ₃ , SiO ₂ [#] , TbVO ₄ [†] , Rochelle salt, TTF-TCNQ, (TMSF) ₂ ClO ₄ , Fe ₃ O ₄ [†]

* Under magnetic fields,
At high temperatures,
† At low temperatures and under magnetic fields.

[†] M.Ando, J. Chikawa, H. Hashizume, K. Hayakawa, T. Imura, T. Ishikawa, S. Kishino, S. Nagakura, O. Nittono, S. Suzuki

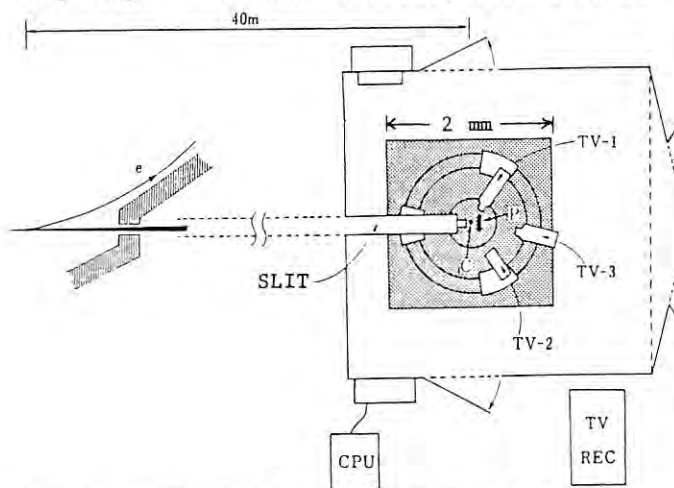


Fig. 1. Apparatus for SR topography. C: Crystal, P: Fluorescent screen, TV-1 and TV-2: X-ray TV cameras, TV-3: Low light level TV camera.

STUDIES ON DYNAMICAL BEHAVIOR OF
LATTICE DEFECTS IN ICE BY RAPID X-RAY TOPOGRAPHY

Ice Topography Group*
Dept. of Applied Physics, Faculty of Engn.
Hokkaido University, Sapporo 060 (JAPAN)

Introduction

We are planning to clarify the dynamical behavior of lattice defects in ice crystals by using the SOR X-ray topography. Although it had been known that the ice crystal did not suffer any radiation damages even after a long period irradiation of X-ray from a strong source like RU-1000 C2 (Rigaku Denki, 60 kW), it was feared that the radiation damage should occur when ice specimen was irradiated by a very strong X-ray from the SOR. Therefore, preliminary experiments were carried out for the first step to observe the degree of radiation damage under various conditions of taking SOR topographs. This paper is a brief report of the experiments which brought satisfactory results for performing real experiments.

Experimental

Single crystals of ice artificially grown in our laboratory by the modified Bridgman method were used for the topographic observations. In blank tests to measure the temperature rise of specimens owing to the irradiation, natural ice single crystals from the Mendenhall Glacier, Alaska were used. Thin planar specimens were cut from these single crystals so that the specimen surface was approximately parallel to (0001).

A specimen was mounted on a specimen holder which was kept at subzero temperature in a polyurethane foam container. This container was installed on the goniometer head of the SOR topograph. Fig. 1 is a schematic diagram of the apparatus. X-ray was incident perpendicular to the sheet through 2 cm thick foam.

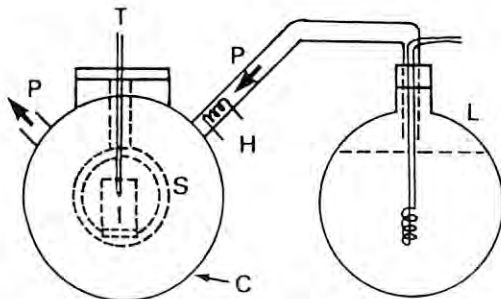


Fig. 1 I: ice specimen, S: specimen holder, C: container, P: passage of N₂ gas, T: thermocouple, H: heater for controlling temperature of N₂ gas, L: liquid N₂ tank

After several blank tests for measuring the temperature rise of specimens, SOR transmission topographs were taken with a specimen of the artificially grown single crystal of ice, of which thickness was 5.2 mm. The specimen was properly protected by the absorber of Al foils to avoid the temperature rise. Distance between the specimen and the X-ray film (Fuji Ix-50) was 100 mm. Several topographs were taken, changing the angle between the beam and the <0001> direction of the specimen, keeping the <11 $\bar{2}$ 0>

direction vertical to the beam. In this way, the wavelength of diffracting X-ray was changed.

Results

The direct radiation effects like the vacancy formation was not observed after several minutes irradiation by the SOR beam of 70~80 mA current. However, an appreciable temperature rise was observed during irradiation. It was found that the absorber of 9 sheets of Al foil of 15 μ m thickness protected the specimen from temperature rise.

Fig. 2 is an example among several SOR topographs taken with 3 sec exposure time. The beam current was 54 mA and the specimen temperature was -3.1°C with a protection as described above. Photograph (b) is an enlargement of dark spot on a topograph (a) which was taken by the diffracting plane of (1 $\bar{1}$ 00). In the photograph, we can clearly observe images of dislocation loops and stacking faults, exhibiting the same patterns as were observed hitherto by the ordinary X-ray topographs. It was found from a topograph taken next to Fig. 2 that stacking fault area became larger than that in Fig. 2, owing to a little temperature drop during 15 min. interval between two topographs.

In the present preliminary experiments, it was shown that the temperature rise of ice crystal specimens due to the SOR beam could be avoided by using proper absorbers. Even when the absorber of 9 sheets of Al foil was used, the incident beam intensity was high enough to make the exposure time as short as a few seconds. Observed topographic images were clear. Therefore, we can expect that the dynamical behavior of lattice defects in ice could be well observed by the SOR topography. We still need to develop a method to estimate real temperature of the specimen from the measurement by a thermocouple mounted on the specimen holder.

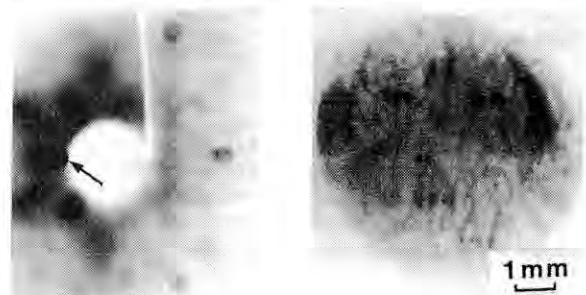


Fig. 2 (a) Original SOR topograph of ice single crystal
(b) Enlargement of a spot indicated by an arrow in (a)

* A. Higashi, T. Hondoh, K. Goto, S. Amakai, K. Katsuta, Y. Mori

AN EXAMINATION OF THE X-RAY MAGNETIC BRAGG REFLECTION AND ITS APPLICATION TO THE FUNDAMENTAL MAGNETISM

Kazumich NAMIKAWA, Masami ANDO*, Tetsuo NAKAJIMA*, Peter SPIEKER* and Sukeaki HOSOYA
 The Institute for Solid State Physics, The University of Tokyo, Roppongi, Minato-ku, Tokyo 106
 * KEK, National Laboratory for High Energy Physics, Oho-machi, Tsukuba-gun, Ibaraki 305

Introduction

X-ray magnetic scattering is a well known relativistic phenomenon in photon scattering. Existence of the magnetic Bragg reflection has been almost confirmed by several experiments related to its characteristics. However, the scattering amplitude of the reflection is no more than 10^{-3} ~ 10^{-4} of the regular Bragg reflection. Moreover, these experiments by no means exclude the possibilities of detecting the X-rays due to any other scattering process. Therefore, each of these experiments includes some ambiguities.

The purpose of the present experiment is to confirm the existence of the X-ray magnetic Bragg reflection. We examine, by means of synchrotron X-ray radiation, the spin dependence and the imaginary phase of the magnetic scattering amplitude. Thomson scattering and the magnetic scattering from magnetic crystals interfere each other, provided that the periodicity of the chemical lattice and that of the spin lattice coincide each other. In this case, we define an asymmetrical ratio of the Bragg reflection by R_a , as follows:

$$R_a = \frac{I_n^\uparrow - I_n^\downarrow}{I_n^\uparrow + I_n^\downarrow}$$

where, I_n^\uparrow and I_n^\downarrow mean the normalized intensity of the Bragg reflection from ferromagnetic crystals when the applied magnetic field perpendicular to the scattering plane is downward and upward, respectively. Thus this asymmetrical ratio R_a is proportional to the cross term of those scattering amplitudes. The cross term become detectable only under the resonance condition due to the imaginary part of the anomalous scattering factor. Anomalous scattering factor is a function of the incident energy, and can be distinguished by its characteristic behaviour near the absorption edge. Therefore, examining the characteristic variation of R_a , we can identify the magnetic Bragg reflection.

Experimental

The present experiment has been carried out at the X-ray topography station BL-15B2. We set up, in this station, an apparatus which consists of a monochromator, an incident beam monitor, a goniometer, a magnet, a solid-state detector and

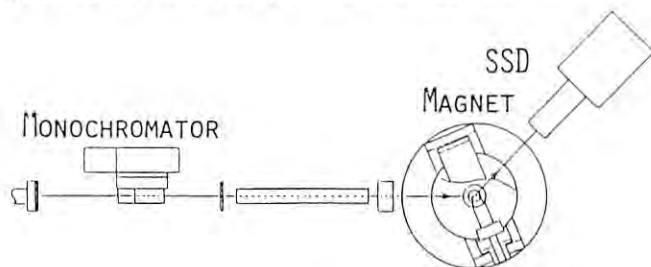


FIG. 1

counting circuits. These equipments are arranged as shown in Fig. 1. Incident X-rays are monochromated by means of 220 reflection from Si (110) channel-cut monochromator mounted on a goniometer with its rotational axis horizontal. The intensity of the incident X-rays are monitored by an ion chamber set behind the monochromator. The sample is a 10 mmφ, 1 mm thick nickel (111) disk single crystal attached to the top of the goniometer-head fitted sideways to the yoke of the magnet. The magnet was mounted on the XRT goniometer so that the vertical axis of the goniometer lies in the sample surface. Scattered X-rays are measured by a pure Ge solid-state detector.

Intensities of the Ni 111 reflection were measured in alternate direction of the field at three different energy near the absorption edge. A magnetic field of about 5 kG was applied parallel to the sample surface in order to align the spin parallel to the [112] direction about 19.5° off an easy axis. It took about 10 to 30 minutes for accumulating 2×10^5 to 2×10^6 counts.

Results and Discussion

In table I, we show the results of the present measurements and the experimental asymmetrical ratio R_a^{ex} obtained. Where, Σ and Δ are the sum and the difference of I_n^\uparrow and I_n^\downarrow , respectively. In the last column we show R_a^{cal} calculated values for R_a^{cal} after Parratt and Hempstead.

Table I

(keV)	I_n^\uparrow	I_n^\downarrow	Σ	Δ	$R_a^{ex} \times 10^3$	$R_a^{cal} \times 10^4$
8.328	3.2180	3.2439	6.4620	-0.0259	-4.01	+1.08
8.342	1.1764	1.1556	2.3321	+0.0208	+8.92	+4.75
8.441	2.9838	3.0032	5.9870	-0.0194	-3.25	+3.49

Large discrepancies are observed between the experiment and the calculation in sign and order of magnitude. There are two reason we can imagine for these discrepancies: a different deviation of the diffraction condition due to the two opposite directions of the magnetic field, and a variation in the polarization of the incident beam during the measurements. The deviation of the diffraction condition could be discriminated by examining a Bragg reflection off resonance. The effects of the variation in the polarization could be suppressed by using a 90° reflection in monochromator or by adopting a forward scattering from the sample. More comprehensive experiment are in progress.

We are indebted T. OHTA for the loan of a nickel single crystal, Y. SATO for the facilities of the I_n^0 monitor and T. SAKAMAKI for the calculation of the anomalous scattering factors. We thank S. SUZUKI, N. KAMIYA, T. OGAWA and O. NITTONO for their help in experiment. Finally, we acknowledge the PF crew for their permission to use the beam over the user's beam time.

REAL TIME X-RAY TOPOGRAPHIC STUDY OF PHASE
TRANSITION OF Fe_3O_4 AND TbVO_4 CRYSTALS

S. Suzuki(TIT), H. Unoki(ELH), S. Chikazumi(Keio U),
S. Todo(ISSP), T. Nakajima(KEK) and M. Ando(KEK)

Introduction

Phase transitions of magnetite and terbium vanadate crystals at low temperatures have been studied with X-ray topographic techniques using nuclear plates, a real time topography camera and 2.5 GeV synchrotron radiation of the Photon Factory. The main purpose of this experiment was to find out how the phase transitions of these crystals would be disclosed by this technique and to get the information for further experimental progress.

Experimental method

Experiments have been performed using a microprocessor controlled high speed camera for synchrotron radiation topography which is one of the users' dedicated machines in the Photon Factory. Details of this apparatus have been reported in 2.4 of this activity report. White radiation from the normal bending magnet at beam line No. 15 was used to form a Laue pattern on a fluorescence screen which was put a few centimeters behind the crystal. The specimen was oriented in the desired orientation by looking at the symmetry of the Laue spots. An ordinary photographic method was used to observe the static pattern, but the dynamical behaviour of the domain pattern was recorded by the live topography camera using a fluorescence screen and an image intensifier.

The specimen was cooled in a continuous flow type cooling-system. This system provides refrigeration in the temperature range from 2 K to 100 K by a controlled transfer of liquid He. The specimen temperature was measured with a chromel vs. gold (0.07 atomic percent iron) thermocouple.

The spatial resolution of the TV image is poor compared with the one of a topograph taken

by a nuclear plate. TV image on the other hand quickly follow dynamical phenomena.

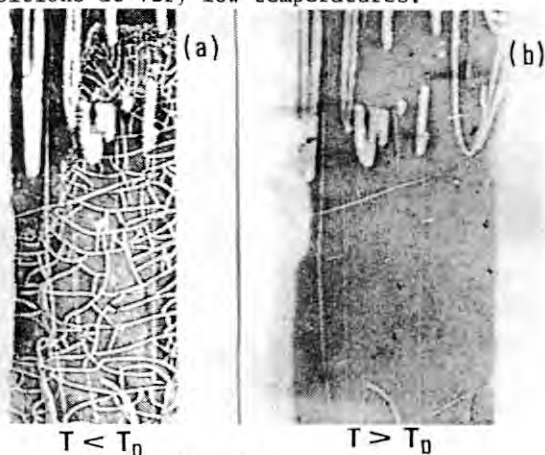
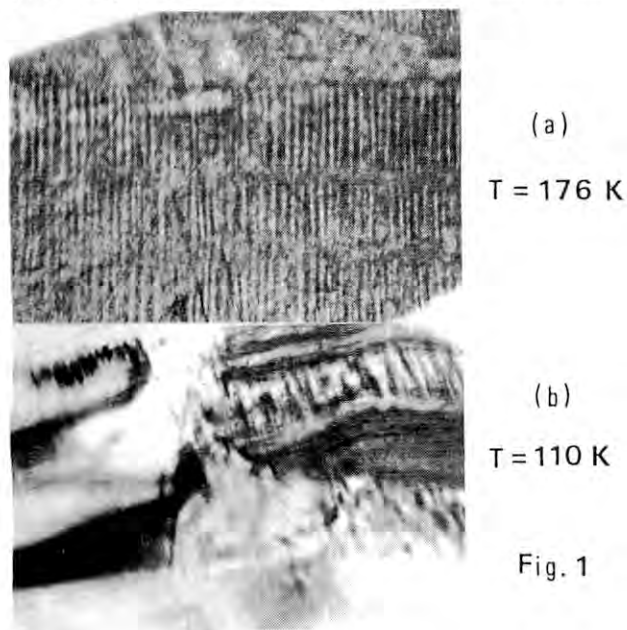
Magnetite

Magnetite is a familiar ferrimagnetic crystal at room temperature and undergoes a phase transition at the Verwey temperature ($T_V = 120$ K). We have tried to see how the crystal^Y line state changes while changing the specimen temperature and applying an external magnetic field. Figure 1a is a 511 transmission topograph taken at 176 K with a nuclear plate. The wavelength of the contributing radiation is 0.62 angstrom. The vertical parallel lines seem to be ferrimagnetic domain structures. These pattern has disappeared after an external magnetic field of $H = 2000$ Oe was applied. Figure 2b was taken at 110 K without field. The parallel lines disappear completely and a very strong contrast due to lattice strain appeared. Such contrast fluctuated with the temperature change and was visible down to 4.2 K.

Terbium vanadate

The rare earth vanadate, TbVO_4 , which crystallizes in the tetragonal zircon-structure, shows a cooperative Jahn-Teller effect (CJTE) at about 35 K (T_D). This phase transition corresponds to the condensation of a zone center lattice distortion of B_{2g} symmetry. The direction of the distortion^{2g} is controllable by an external magnetic field. In this preliminary work, we observed very complicated pattern as shown in Fig. 2a in the low temperature phase. These pattern disappeared above T_D (Fig. 2b). They might be due to the stress which was introduced by gluing the specimen to a holder. The origin of the contrast is not clear at this moment. Further work is in progress now in order to gain better understanding of the crystal lattice state at the phase transition.

In conclusion, synchrotron radiation live topography combined with ordinary photographic methods is a promising way to study phase transitions at very low temperatures.



REAL TIME X-RAY TOPOGRAPHY CAMERA USING
FLUORESCENCE FILM AND IMAGE INTENSIFIER

S. Suzuki(TIT), H. Kawata(KEK) and M. Ando(KEK)

Introduction

An apparatus for video display of X-ray topograph by an indirect method has been developed for the purpose of synchrotron radiation experiments. Care was taken that several functions can be remote-controlled.

Camera system

An apparatus for live topography is schematically shown in Fig. 1 together with a photograph of the camera installed on an arm of the goniometer of BL-15B in the Photon Factory. The camera consists of a fluorescence gadolinium oxysulfide film (P) of 10-20 μm thickness, optical magnifying lens (L) and a detector (image intensifier: II, relay lens: RL and TV camera). The image is recorded by a cassette video recorder and is displayed on a monitor. The fluorescence particles with diameters ranging in 2-4 microns have been selected from the commercial powder using the difference in sedimentation rates of the particles in a fluid (isoamyl acetate + small amount of collidion). The selected powder was spread on a mylar film of 5 μm thickness and was supported by a frame.

Lens and detector can be shifted independently along the optical axis of the camera by a synchronous motor, leaving the fluorescence film P in place. Thus the researcher can change the magnification of the image between 60-300, can focus the image and adjust the aperture size (brightness) controlled by looking at the TV image. The distance between the specimen and the fluorescence film can be changed by sliding the whole set of the camera. This distance and the orientation of the whole camera set around

the specimen can be changed by giving appropriate data to a microcomputer. The fluorescence film was put into a dark box. Therefore this camera can be used with lights on in the hutch.

Resolution

The resolution of the camera was estimated by measuring the modulation transfer function (MTF) which was defined by Dr. Chikawa (Chikawa; 1974). In Fig. 2 is shown a MTF measured by tracing the TV image of a shadow of an X-ray test chart along a scanning line by a synchroscope. The shadow was formed by synchrotron radiation which were diffracted from a Si (111) surface. An extrapolation of the curve to 5 percent gives 20 μm as the limit of the spatial resolution. The limit of the resolution of the indirect method is almost the same as the thickness of the fluorescence film. A resolution better than 10 microns can be expected if we prepare a thin film, about 5 μm thick which will be made without much difficulty.

Applications

Live topography cameras using the indirect method have been applied to real time topography of various specimens under various conditions.

- (a) Room temperature: Fe-Si, Synthetic quartz, Si, web S etc.
- (b) High temperature: Alpha-beta transition of synthetic quartz (573 C), melting phenomenon of olivine (1900 C).
- (c) Low temperature: Phase transition of magnetite (35 K) and terbium vanadate (120 K).

Reference

Chikawa, J.: J. Crystal Growth, 24/25 (1974) 61-68.

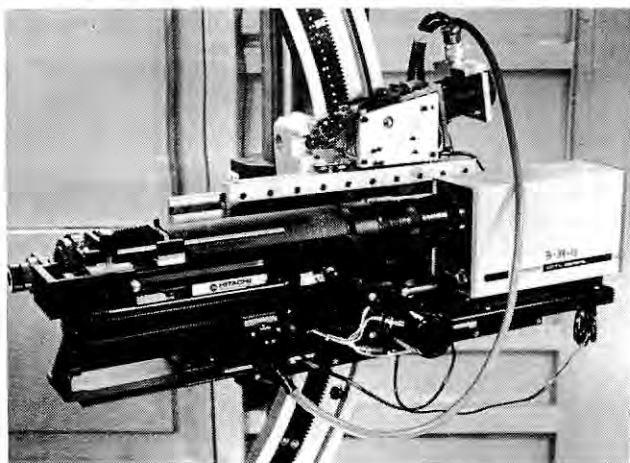
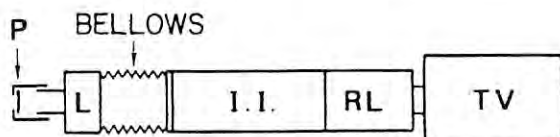


Fig.1

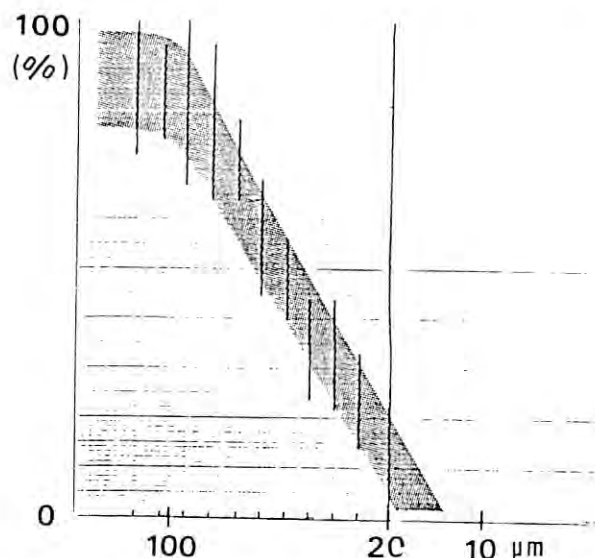


Fig.2

X-RAY TOPOGRAPHY OF GaAs CRYSTAL

H.Takaoka, K.Ikeda, Y.Homma, Y.Ishii,* M.Ando
 Electrical Communication Laboratory NTT
 Midoricho, Musashinoshi, Tokyo 180, Japan
 *KEK,National Laboratory for High Energy Physics
 Oho-machi Tsukuba-gun,Ibaraki 305, Japan

Introduction

GaAs crystal is an important material for high speed GaAs ICs. One of the most-pressing problems in the practical application of this material, however, is the lack of uniformity in its electrical properties. This non-uniformity is considered to be related to the dislocation density distribution. XRT is a suitable method for evaluating such uniformity. A high quality topograph of GaAs, however, was found to be very difficult to record due to high absorption and fluorescence. The thickness for $\mu t=1$ (μ :absorption coefficient, t :thickness) is about $29 \mu\text{m}$ with a wave length of 0.7\AA (MoK α). In practical application thick wafers of a few hundred μm are required. The recording must be carried out under anomalous transmission conditions and an intense X-ray beam from an SR has an advantage for short time exposure. A double crystal topography experiment was performed using a 15-C beam station at Photon Factory in KEK during the 1983 dedicated run.

Experiment and results

A white x-ray topography and a monochromatic topography were carried out. Exposure time was as short as 1 minute at 2.5 GeV 50 mA in the anomalous transmission case for a white X-ray beam using a Ilford L4 plate. There was a very large background due to fluorescence. This background decreased when a 0.5 mm aluminum sheet was used.

Large size topography is necessary to evaluate GaAs wafers in practical use. The beam must be expanded or scan a wafer when large size topography is carried out using SR. There has been difficulty in setting up the scanning instrument, because the wafer must be translated vertically due to the polarization of SR X-ray beam. An asymmetric double crystal method was adopted to expand the beam. The experimental arrangement for large size topography is shown in Fig.1. Two sets of Huber goniometer were attached vertically to an aluminum panel. There was no degradation in the accuracy of this goniometer as a result of the tilt of the rotation axis. A GaAs(012) crystal grown by the Horizontal Bridgeman method was used as a monochromator crystal. The diffractive net plane used was (022) inclined 18.4° to the (012) surface. The incident angle of the primary beam was 13° . The Asymmetric factor in this arrangement was 6.9, and the expanded beam size was $36(w)\times 40(h)\text{mm}$. A topograph of a GaAs wafer cut from an LEC grown GaAs boule parallel to the growth axis was recorded. The thickness of the wafer was $300 \mu\text{m}$. Ilford L4 nuclear plates were used for recording. Figure 2 shows an anomalous transmission topograph of a GaAs wafer under in the parallel (220) condition. The topographs could be recorded with an exposure time of 5-10minutes. The dislocation distribution was clearly defined. These results provide good information on the analysis of dislocation introducing mechanism in GaAs crystal growth. In-situ observation is also planned using image intensifier (I.M).

Acknowledgment

Authors wish to thank to Dr. Nittono, Dr. Suzuki and Dr. Spieker for their useful advice and assistance with the goniometers, and K.Hoshikawa for providing GaAs wafers.

Reference

- 1)J.Bonnafe, et al: Mat. Res. Bull. 16 (1981) 1193
- 2)M. Scott: SSRL Activity Rep. (1982) VIII 3

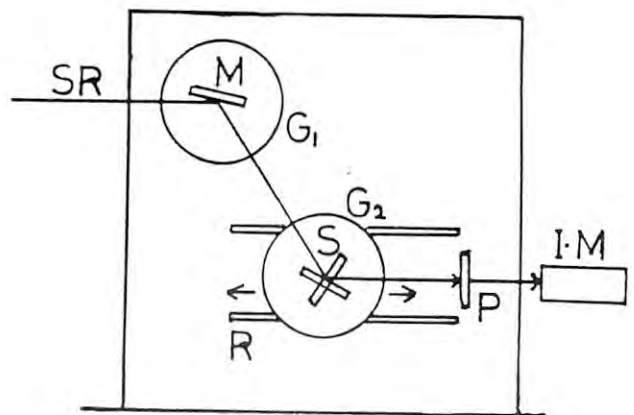


Fig.1 Experimental arrangement for double crystal X-ray topography.

G1,G2:Goniometer ($1/5000^\circ$ pulses), M:Monochromator GaAs(012), S:Specimen GaAs(100)
 P:Nuclear plate, I.M:Image intensifier
 R:Sliding groove

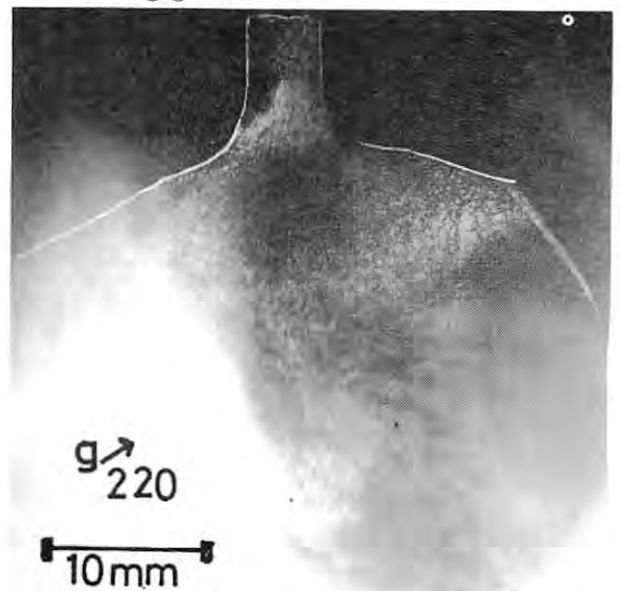


Fig.2 Anomalous transmission topograph of GaAs wafer. Wafer thickness:300 μm

SYNCHROTRON X-RAY SECTION TOPOGRAPHY

Y. Sugita and H. Kawata*

Physics Department, Toyama University
3190 Gofuku, Toyama 930

Introduction

Section topography can be very valuable in providing information on imperfections in a nearly perfect crystal through the observation of Pendellösung fringes and the margin effect as well as through the observation of fine structure of defects and their depth distribution. Since x-ray beams are limited by very narrow slit system, long exposure time is needed for obtaining a section topograph for a normal x-ray source. Section topography with synchrotron radiation may allow us to perform in-situ observation with saticon image converter tube system or step by step observation with nuclear films. One of the application of this technique is the study of dynamic process of precipitations. For example, precipitation process in silicon containing supersaturated oxygen, in which traverse topography fails to detect oxide precipitates because traversing causes to blur out of defect images.

In this report we describe the preliminary results on section topography.

Experimental Procedures and Results

The experimental set up used for section topography is the double-crystal arrangement utilizing non-parallel (+,-) setting with asymmetric reflection in the first crystal and illustrated in Fig.1. Monochromatic beams with the wavelength close to that of $MoK\alpha_1$ radiation are diffracted in the (333) planes of the first crystal and leave the crystal at an angle of

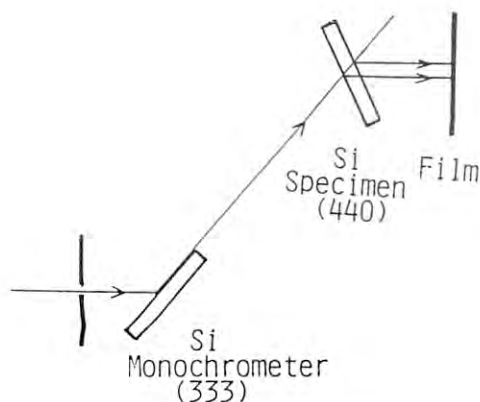


Fig.1

about 0.5 degrees to the surface.

A specimen used was (100) oriented, 0.55 mm thick, Czochralski silicon wafer, with initial oxygen concentration of 1.08×10^{18} atoms. cm^{-3} . This specimen was heat treated at 1000 C° for 48 hours for oxide precipitation.

The parameters of the storage ring were $E=2.5$ Gev, $I=60$ mA.

The section topograph obtained is shown in Fig.2 and the similar topograph obtained for a normal x-ray source is shown in Fig.3 for comparison. The exposure time on a nuclear plate was 5 minutes. Defect images from oxide precipitates were recorded, though they became blurred to a some extent due to the spread in beam size.

The experiment is in progress and the blur in the defect images shall be improved by use of a proper slit system. In near future, using the wiggler line, in-situ section topography may become feasible.



Fig.2

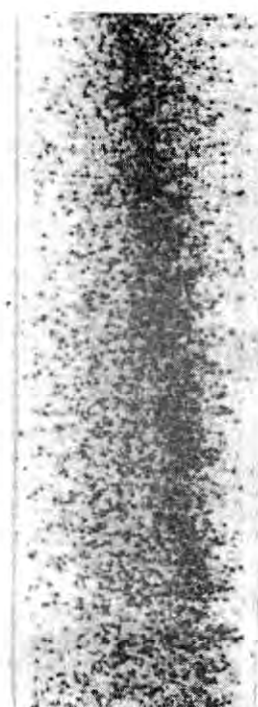


Fig.3

* Present address ; KEK, National Laboratory for High Energy Physics. Oho-machi, Tsukubagun, Ibaraki 305.

A Study on Defects in CaF_2 Single Crystals

Cui Cheng-Jia* and Tomoya Ogawa
 Dept. of Physics, Gakushuin Univ.
 Mejiro, Tokyo, 171.

CaF_2 crystals transmit over a wide spectral range, possess relatively low refractive indices, exhibit small absorption and scattering losses. These properties are of interest for applications as components required to transmit high-power laser beams, such as window applications HF and DF lasers.

In order to realize low absorption and low scattering in the crystals, they were grown in a high-temperature furnace similar to that of Stockbarger-Bridgman out of well selected fluorite (mineral) or synthetic CaF_2 . The crystals grown in Chanchun Institute were 180 mm in diameter with about 15 kg.

A study on defects in the crystals was started from July 1982 at Gakushuin University by optical microscopy, light-scattering tomography and x-ray topography. SOR topographs were taken along the program at the Photon Factory and one of them is shown in the figure comparing light-scattering tomograph. Analytical studies on these figures are still advancing.

Fig.(a) shows a SOR topograph on (331) plane of a CaF_2 single crystal. Some sub-grain boundaries are observed as shown in this figure. The defects on $\{331\}$ plane are similar to that of on $\{551\}$ one. Fig.(b) shows a light scattering tomograph on (001) plane and the scattering vector of this tomograph is $\langle 011 \rangle$ direction. The slip system of this crystal is $\{110\}$ plane and $\langle 110 \rangle$ direction. Since the strain in the crystals is continuity, there are only two slip systems. Clear patterns of the strain were easily observed by a polarized transmitted light.

The authors express their cordial thanks to Prof. Kohra and Andow for giving a beneficial experience in the Photon Factory.

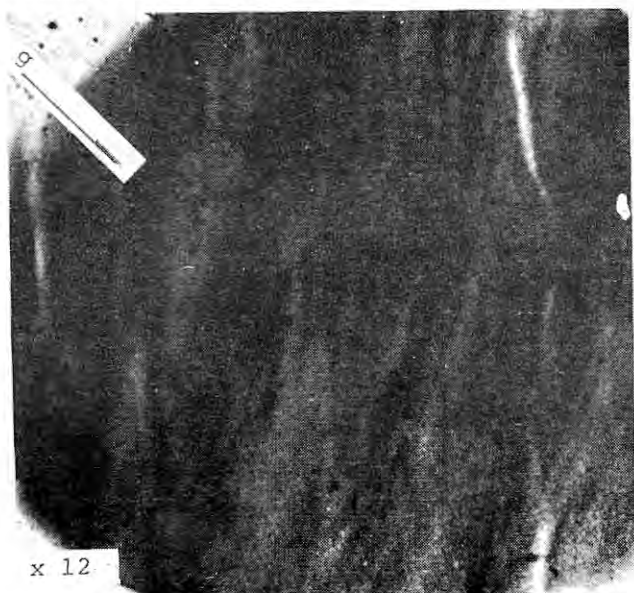


Fig.(a) SOR topograph on (331) plane

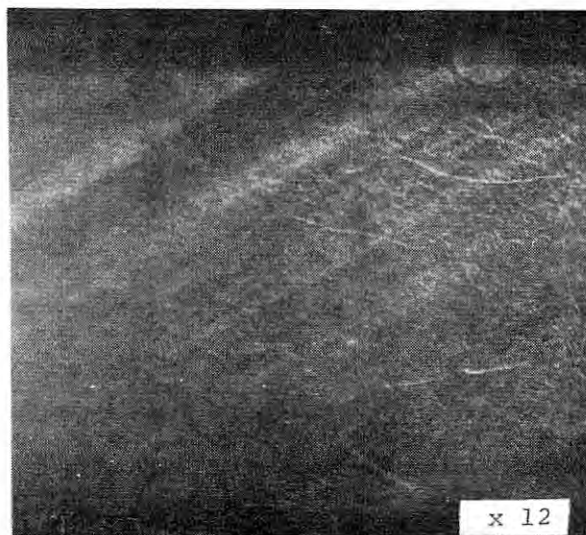


Fig.(b) light scattering tomograph on (001) plane

* On leave from Changchun Institute of Optics and Fine Mechanics, Academia Sinica, Peoples' Republic of China.

Study on the melting mechanism of forsterite Mg_2SiO_4
by means of X-ray topography

Y. Takéuchi, T. Yamanaka and K. Ogata
Mineralogical Institute, Faculty of Science, University of Tokyo
Hongo, Tokyo 113 (Japan)

Introduction

Forsterite Mg_2SiO_4 has cell dimensions¹ $a=4.7503(4)$ Å, $b=10.187(1)$ Å, $c=5.9771(7)$ Å, and space group Pbnm. The tetrahedra formed by the oxygen atoms about the tetrahedral cations in this structure type are inherently distorted, yielding three independent bonds having different lengths. In the specific case of forsterite, the three bonds are : Si-O(1) = 1.614 Å, Si-O(2) = 1.654 Å, and Si-O(3) = 1.635 Å. Our single-crystal X-ray diffraction study of the forsterite structure as a function of temperature up to 1600°C has revealed a salient feature that at temperatures above 1000°C the difference in Si-O bond length is decreased with increasing temperature (the Si-O bond lengths were corrected for thermal motion of a rigid-body mode). The change is such that the bonds would have the same value¹ of about 1.63 Å at the melting point of 1890°C. The melting point of forsterite may then be structurally defined as the temperature at which the three Si-O bond lengths are equalized.

As an extension of such a high-temperature X-ray study of forsterite, we have undertaken the study on the melting phenomenon of this mineral species by means of X-ray topography with the use of synchrotron radiation. It was anticipated that we would be able to observe the formation and propagation of solid-liquid interface. The present report presents the result of our preliminary test experiment carried out for the above-mentioned *in situ* observation.

Experimental and observation

From a synthetic single crystal of forsterite², cuts parallel to (001) or (010) were prepared, each having the shape of a thin square plate; their dimensions were approximately 5 x 10 x 0.1 mm. The X-ray sample thus prepared was mounted on an alumina rod. As heat source, we decided to use the heater system utilizing gas flame which was originally designed for X-ray single-crystal diffraction study³. The feasibility of applying such a high-temperature technique to our planned experiment at the topography station was found to be successful.

As the effective size of the gas flame was smaller than the crystal plate, the direction of the flame was chosen so that it heated a corner of the plate. That portion of the crystal shown in a selected Laue spot was then observed through the video system designed for the station. The temperature was raised with manual operation of the gas-flow rate.

Although it was not possible to observe the formation of solid-liquid interface, evidence was observed of the development of dislocation

bunches from the melting front. Figure 1 shows portion of the Laue spot which was recorded on X-ray film after the crystal was quenched to room temperature. This spot, which has not yet been indexed, was in a Laue pattern from a crystal plate parallel to (001), the X-ray beam being parallel to c . In the corresponding portion of the crystal (Fig. 2, under crossed nicols), we observe the formation of quenched crystals.

References

- 1) Y. Takéuchi, N. Haga, and T. Yamanaka: J. Japan. Assoc. Min. Petr. Econ. Geol., Spec. Paper, No.3 (1982) 51.
- 2) H. Takei and S. Hosoya: Advances in Earth and Planet. Sci. Vol. 12: High-Pressure Res. in Geophysics. Ed. S. Akimoto and M.H. Manghani (1982) pp.537.
- 3) T. Yamanaka, Y. Takéuchi and R. Sadanaga: Z. Krist. 154 (1981) 147.

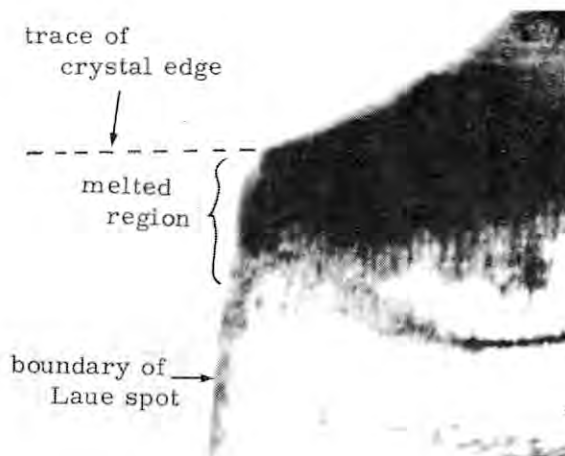


Fig. 1 (x50)



Fig. 2 (x50)

SYNCHROTRON RADIATION TOPOGRAPHS OF AS-GROWN TIN SINGLE CRYSTAL PLATES

Osamu NITTONO, Taro OGAWA and Sigemaro NAGAKURA
 Department of Metallurgy, Tokyo Institute of Technology
 Oh-okayama, Meguro-ku, Tokyo, 152 (JAPAN)

Introduction

Previously, the present authors proposed a new and simple method of preparing nearly perfect crystal plates such as Cd, Zn and Sn for X-ray topography⁽¹⁾. In the present study, several Sn plates were subjected to topographic observations using synchrotron radiations (SR), and image quality as well as resolving power was investigated. The results showed that the crystal plates prepared by the present method are appropriate to observe dynamical phenomena such as crystal growing, dislocation motion and phase transformation.

Experimental

Flat single crystal plates of Sn(99.999% purity) with low dislocation density were prepared by a solidification technique⁽¹⁾ similar to G'Sell, Champier and Iwasaki's method⁽²⁾. Cold-rolled Sn sheets 0.2 to 0.4 mm thick were placed between 2 glass plates separated by alumina spacers 0.5 mm thick. Grown crystals were cooled at a rate of less than 5 K/h. The slow cooling is essential for reducing residual lattice defects. In order to avoid to give any damage to the as-grown crystals, each of them was fixed to a Cu rod of 1 mm in dia. with cement (Aron ceramic, K-45), and further manipulations were done by handling this rod. After crystal surfaces were slightly etched by an etchant ($\text{H}_3\text{PO}_4:\text{CH}_3\text{COOH}:\text{HF}:\text{HNO}_3=12:5:2:1$)⁽³⁾, they were subjected to SR Laue topography. The crystal thickness was 0.1 to 0.2 mm. The experiments were carried out by using a microprocessor-controlled high-speed goniometer (BL-15). For taking SR Laue topographs, a device which can be put on the top part of the swivel table of the goniometer was constructed so as to make the specimen-plate distance as short as possible. The shortest distance was less than 25 mm, and the use of a small stopper was effective for reducing the distance. Laue spots were recorded on nuclear plates (Ilford, L-4 type, emulsion thickness 25 and 50 μm , 115 mm sq. in size) Exposure time varied from 1 to 30 sec according to the specimen thickness and beam currents. Topographic images were enlarged optically as large as 100 times, and image quality as well as resolving power was evaluated. Furthermore, several nearly perfect crystals were also observed by an indirect TV method⁽⁴⁾, in which visible images are magnified optically and subsequently intensified by an image intensifier.

Results and discussion

Melted Sn surfaces tended to be stuck by a soot film coated on the glass plates. Accordingly, smooth soot films were essential for preparing nearly perfect crystals. SR Laue topographs contain a large number of spots having different reflection indices and provide a lot of information on growth mode such as angular and spatial distribution of subgrains. Thus, SR Laue topography is appropriate to study the solidification and growing processes. Fig. 1(a)-(c) show topographs of

of a tin crystal plate with low dislocation density. Fig. 1(a) is taken by using a fine-focus X-ray generator (100x100 μm^2 , 45 kV, 3 mA), (b) is an enlarged Laue spot in an SR Laue topograph, and (c) is a TV image recorded by the indirect live topography camera. Individual dislocations can be recognized in each topograph, but the resolution of dislocation image varies from 5 μm in (a) to 20 μm in (c) according to the ways and means used. The resolution of TV image was sufficient for determining the Burgers vector of dislocation.

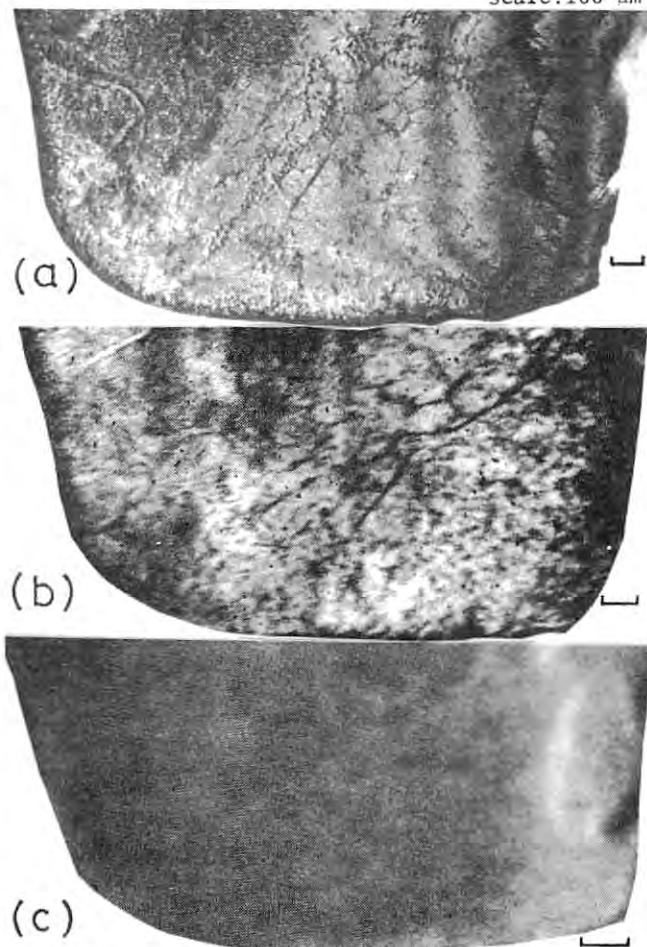
References

- (1) O. Nittono, M. Hyugaji and S. Nagakura : Jpn. J. Appl. Phys., 20 (1981), 1329.
- (2) C. G'Sell, G. Champier and Y. Iwasaki : J. Crystal Growth, 24/25 (1974), 527.
- (3) R. Fiedler and A. R. Lang : J. Mater. Sci., 7(1972), 531.
- (4) S. Suzuki and H. Kawata : J. Cryst. Soc. Jpn. 24 (1982), 299. (in Japanese).

Fig. 1 X-ray topographs of a tin crystal plate

- (a) Conventional Lang projection topograph
- (b) SR Laue topograph (2.5 GeV, 61.7 mA, 7 sec)
- (c) TV image recorded by the indirect method.

scale:100 μm



MAGNETIC DIFFRACTION OF X-RAYS FROM A Fe-3%Si CRYSTAL

Shinichiro NAKATANI, Yoshiyuki USHIGAMI, Tetsuya ISHIKAWA⁺, Seishi KIKUTA
 Hiroyasu SAKA⁺⁺ and Toru IMURA⁺⁺

Department of Applied Physics, Faculty of Engineering,
 University of Tokyo, Hongo, Bunkyo-ku, Tokyo 113
⁺Photon Factory, National Laboratory for High Energy Physics
 Oho-machi, Tsukuba-gun, Ibaraki 305
⁺⁺Department of Metallurgy, Faculty of Engineering,
 Nagoya University, Chigusa-ku, Nagoya 464

Introduction

As is well known, X-ray diffraction is based on Thomson scattering caused by the interaction of X-rays with the charge of electrons and provides information on the electron charge distribution. Recently diffraction of X-rays by magnetic materials has been observed and the formula for magnetic diffraction has been given by de Bergevin and Brunel.^{1,2)} Since magnetic scattering of X-rays comes from the interaction between X-rays and magnetic moments of electrons, it is expected to get information on the spin density in magnetic materials. This will be complementary to neutron diffraction.

The diffracted intensity due to magnetic scattering is estimated to be about 10^{-6} times as large as that due to Thomson scattering. In addition the very weak intensity of magnetic diffraction from ferromagnetic substances overlaps that of Thomson diffraction in the same Bragg peak. In this study it was attempted to enlarge the intensity ratio of magnetic diffraction to Thomson diffraction to some extent by using the polarization dependence of magnetic scattering. In the scattering amplitude of magnetic diffraction the matrix of polarization contains non-diagonal elements.

Experiment and Result

The experiment was carried out by SR X-rays available from the beam line 15C. The precision multi-axis diffractometer installed there was used. The experimental arrangement is shown

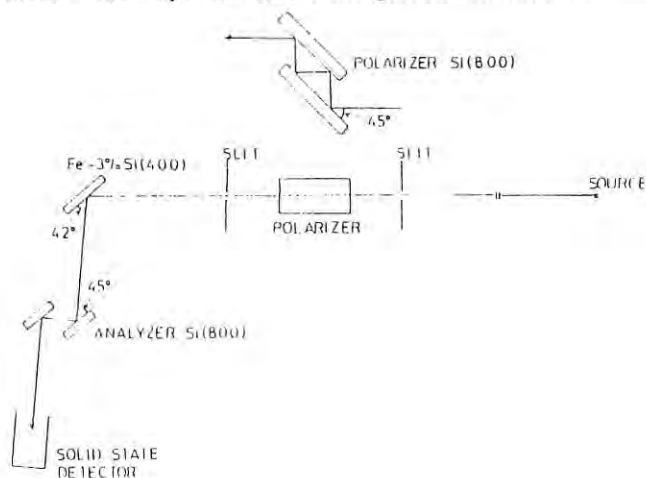


Fig. 1 A plane figure of the experimental arrangement. A side view of the polarizer is shown in the insert.

schematically in Fig. 1. The first crystal is a channel-cut polarizer made of silicon. Since 800 reflection with the Bragg angle of 45° takes place 4 times in the polarizer, the reflected X-ray beam with the wavelength of 0.960\AA is highly polarized, whose electric vector is parallel to the electron orbit. This polarized beam is incident on a Fe-3%Si crystal and the symmetric 400 Bragg-case diffraction occurs. In the diffracted beam from the sample the vertically polarized component was selected by an analyzer which is the same design as the polarizer except for the number of multiple reflections, and the integrated intensity was measured by rotating the analyzer. The magnetic field was applied to the specimen from the four directions lying in a plane parallel to the surface of the specimen as shown in Fig. 2. The integrated intensities increase in the case of horizontal directions 1 and 2 of the magnetic field compared to that in the case of vertical directions 3 and 4 (Fig. 2). The difference between the integrated intensities in the horizontal and vertical directions is attributed to the component of magnetic diffraction. The integrated intensities in the vertical directions, correspond to Thomson diffraction, which come from the vertically polarized component of synchrotron radiation remaining after reflection in the polarizer. The intensity ratio of magnetic diffraction to Thomson diffraction is about 6% for the present experimental geometry.

The authors would like to thank the members of Photon Factory-Precision X-Ray Optics Working Group for their cooperation in the present study.

- 1) F. de Bergevin and M. Brunel: Acta Cryst. A37(1981)314.
- 2) M. Brunel and F. de Bergevin: Acta Cryst. A37(1981)324.

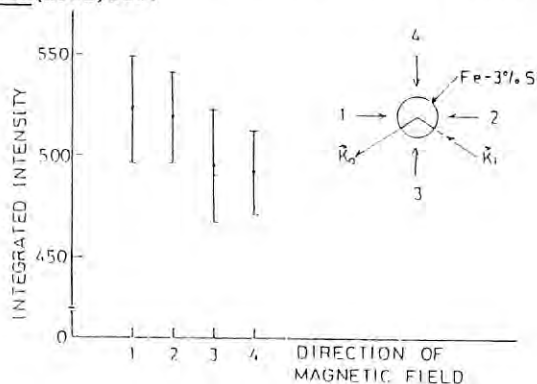


Fig. 2 Change of integrated intensities of magnetic diffraction from a Fe-3%Si crystal with the direction of applied magnetic field.

STRUCTURE ANALYSIS OF THE NiSi₂/(111)Si INTERFACE
BY THE X-RAY STANDING WAVE METHOD

Koichi AKIMOTO, Tetsuya ISHIKAWA⁺, Toshio TAKAHASHI and Seishi KIKUTA

Department of Applied Physics, Faculty of Engineering,
University of Tokyo, Hongo, Bunkyo-ku, Tokyo 113
⁺Photon Factory, National Laboratory for High Energy Physics
Oho-machi, Tsukuba-gun, Ibaraki 305

Introduction

According to the dynamical theory of X-ray diffraction, X-ray standing wave fields are formed by interference between incident and diffracted beams not only inside the crystal but also outside the crystal. Recently this X-ray standing wave method has been used to determine accurately the position of impurity atoms in the crystal¹⁾ or adsorbed atoms on the crystal surface²⁾.

In the present paper the X-ray standing wave method was applied to the determination of atomic structure of a silicide/Si interface. The angular yield of Ni K fluorescent X-rays emitted from Ni atoms in the NiSi₂ film was measured in the diffraction process of X-rays on the (111)Si substrate. Judging from the profile of the yield curve, the position of Ni atoms was determined and hence the atomic structure of the NiSi₂/(111)Si interface was analyzed.

Experimental Results and Discussion

An experimental arrangement is shown in Fig. 1. The (+,-) arrangement of parallel setting was adopted. The wavelength of X-rays incident on the specimen is 0.80 Å which can

excite Ni K fluorescent X-rays of $\lambda=1.66 \text{ \AA}$. The yield of Ni K fluorescent X-rays were measured by a Ge solid state detector set normal to the specimen with a distance of 3-5 cm.

The experimental results are shown in Fig. 2. The angular-yield of Ni K fluorescent X-rays emitted from NiSi₂ films produced by Ni films of 5 nm and 10 nm thickness was measured. Cherns et.al³⁾ proposed two models (Fig. 3) and concluded by TEM studies that the calculation for the model of Fig. 3(a) gives good fit to the observation of NiSi₂/Si interface lattice images. Fig. 4 shows the calculation of the yield curve for the model of Fig. 3(b). It appears that the model of Fig. 3(b) gives better fit to the results of our experiments rather than the model of Fig. 3(a).

The authors acknowledge the members of Photon Factory-Precision X-Ray Optics Working Group for their cooperation in the present study.

- 1) J. A. Golovchenko, B. W. Batterman and W. L. Brown: Phys. Rev. B 10 (1974) 4239
- 2) P. L. Cowan, J. A. Golovchenko and M. F. Robbins: Phys. Rev. Lett. 44 (1980) 1680
- 3) D. Cherns, G. R. Anstis and J. L. Hutchison: Phil. Mag. 46 (1982) 849

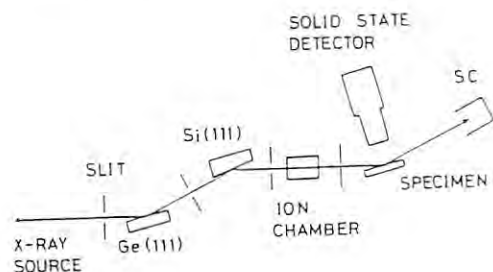


Fig. 1

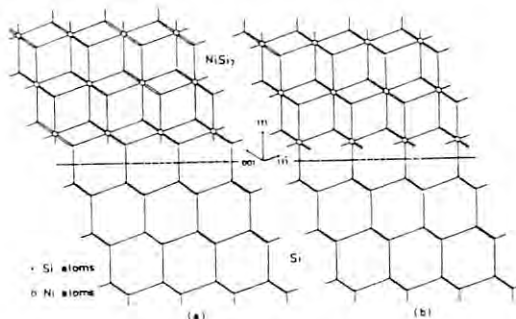


Fig. 3

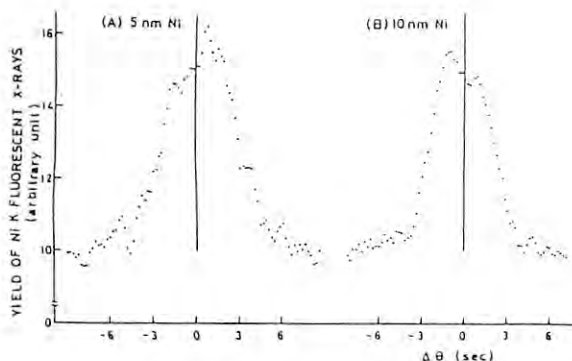


Fig. 2

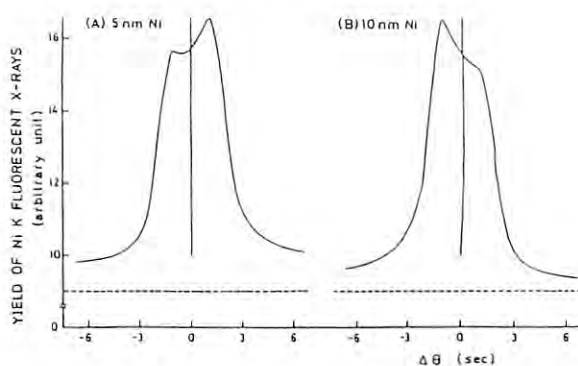


Fig. 4

POLARIZATION RATIO AND ROTATION OF THE ELECTRIC VECTOR OF SYNCHROTRON RADIATION

T. Ishikawa, S. Annaka[†] and K. Kohra
 KEK, National Laboratory for High Energy Physics
 Oho-machi, Tsukuba-gun, Ibaraki 305 (JAPAN)

[†]Tokyo University of Mercantile Marine
 Etchujima 2, Koto-ku, Tokyo 135

Introduction

As the synchrotron radiation (SR) is linearly polarized in the electron orbit plane, it is useful for the study of polarization phenomena in the x-ray wavelength region.^{1,2)} The SR is also elliptically polarized outside the plane and so it is important to analyse the polarization ratio of an incident beam in the diffraction experiments.³⁾ In order to study the above subjects a $\chi\phi$ -circle was made for x-ray polarization measurements. The polarization of the SR was observed with analysing crystals of Ge and Si. An experiment on a rotation of the electric vector (E-vector) of the SR by 45° was also carried out with a grooved monochromator.

 $\chi\phi$ -circle

A diagram of the $\chi\phi$ -circle is shown in Fig. 1. The χ -circle plane (A) about 300 cm in diameter is located 5 cm outside the ϕ -circle axis. The scintillation counter (B) is fixed to the χ -circle plane so as to measure x-ray reflections with the Bragg angle of 45° . The goniometer head (C) is mounted on the adjustable tilting table

, which is fixed to the χ -circle. The χ -circle and the ϕ -circle are rotated by stepping motors with accuracies of 0.002° /pulse and 0.0025° /pulse respectively. The $\chi\phi$ -circle mounted on the precision turntable can be also used for the usual dynamical diffraction experiments.

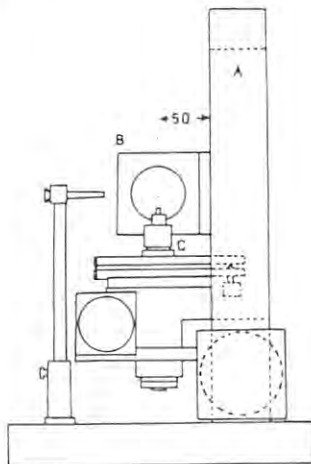


Fig. 1. $\chi\phi$ -circle.

Polarization measurements of the SR

The polarization state of the SR from the 2.5 GeV storage ring was measured by using the $\chi\phi$ -circle. The analyser was Ge with the (111) plane. The x-ray beams deflecting at 90° to the incident beam were measured against an angle χ , which was a rotation angle of the χ -circle. The counter system was adjusted to measure only the 333 reflection (wavelength $\lambda=1.54 \text{ \AA}$). But the 444 reflection ($\lambda=1.155 \text{ \AA}$) might be contained to a little extent. The beam size was as large

as $0.2 \times 0.2 \text{ mm}^2$. The experimental result is shown as solid circles in Fig. 2, where a horizontal position of the counter corresponds to $\chi=0$. Fig. 2 shows that the radiation of 1.54 \AA is linearly polarized with the horizontal E-vector.

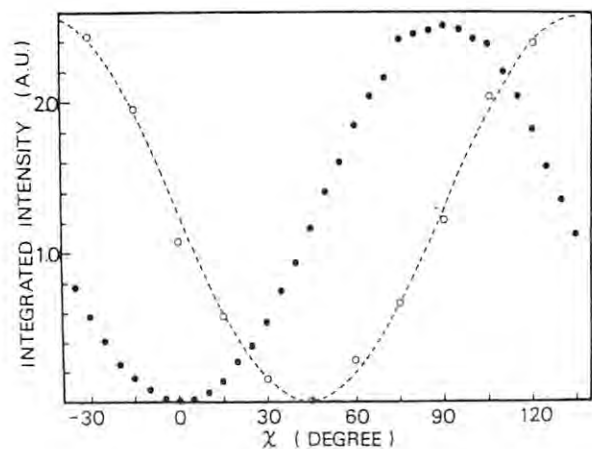


Fig. 2. Integrated intensities of the 333 reflections from the Ge analyser against the rotation angle χ of the χ -circle. Solid circles correspond to the case of the incident SR ($\lambda=1.54 \text{ \AA}$). Open circles correspond to the 333 reflection beam from the skew-grooved monochromator of Ge.

It is known that the SR is left-hand elliptically and right-hand elliptically polarized above and below the orbit plane, respectively. Owing to a finite size of the SR source it is rather difficult to measure the horizontal and vertical components of the E-vector separately. But, by using the Si 333 reflection and the $\chi\phi$ -circle, the polarization state was observed against the angle χ at each deviation angle θ from the orbit plane relatively. Relative integrated intensities of the 333 reflections ($\lambda=1.48 \text{ \AA}$) are shown in Fig. 3, where solid circles, squares, open circles and triangles correspond to $\theta=0, 2 \times 10^{-5}, 4 \times 10^{-5}$ and 6×10^{-5} rad, respectively. The vertical component of the E-vector of the SR is shown clearly to increase with the angle θ .

Rotation of the E-vector

As the SR is linearly polarized in the orbit plane and elliptically polarized outside

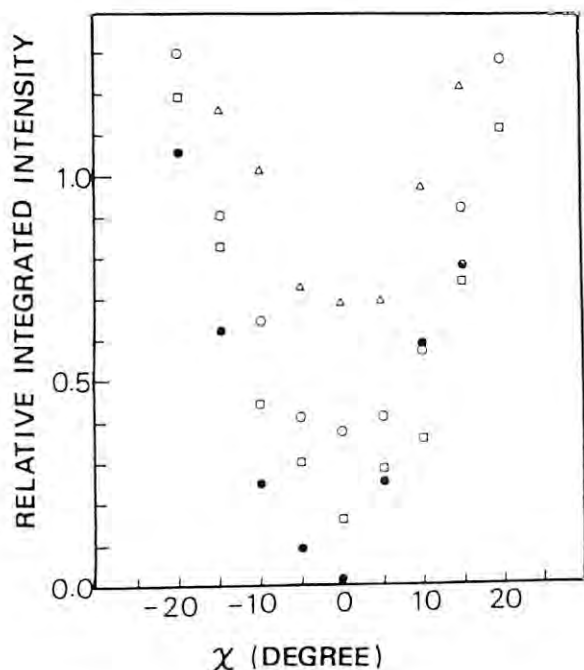


Fig. 3. Relative integrated intensities of the 333 reflections from the Si analyser against χ . Solid circles show the intensity change of the SR in the orbit plane. Squares, open circles and triangles show the changes of the SR inclined at 2×10^{-5} , 4×10^{-5} and 6×10^{-5} rad to the orbit plane, respectively.

the orbit plane, it is useful in some diffraction experiments to obtain the monochromated beam with the known E-vector inclined at 45° to the orbit plane. For this purpose an effective method is to use a grooved monochromator with the Bragg angle of 45° , whose plane of incidence is set to be inclined at 45° to the orbit plane. The E-vector of the monochromated beam ($\lambda = 1.54 \text{ \AA}$) from the skew-grooved monochromator of Ge was analysed with the 333 reflection of Ge. The observed integrated intensities of the 333 reflection (open circles) are given against χ in Fig. 2, where a broken line shows clearly that the E-vector of the incident beam is inclined at 45° to the horizontal plane. The intensity of the beam was about 2×10^5 cps under the conditions of 2.5 GeV, beam current 80 mA and x-ray beam size $0.2 \times 0.2 \text{ mm}^2$.

Summary

Polarization measurements about the SR were done by using the $\chi\phi$ -circle and the analysers of Ge and Si. The linearly and elliptically polarized SR were proved experimentally. The linearly polarized x-rays with the known E-vector inclined at given angle to the horizontal plane are useful for some diffraction experiments and x-ray optics.^{4,5,6)}

The authors would like to thank Photon

Factory — Precision X-Ray Optics Group for their support.

References

- 1) M. Hart and A. R. D. Rodrigues: *Philos. Mag.* **43**(1981)321.
- 2) M. Sauvage, C. Malgrange and J. F. Petroff: *J. Appl. Crystallogr.* **16**(1983)14.
- 3) M. Brunel, G. Patrat, F. de Bergevin, F. Rousseaux and M. Lemonnier: *Acta Crystallogr.* **A39**(1983)84.
- 4) S. Annaka, K. Kohra and M. Ando: *Jpn. J. Appl. Phys.* **20**(1981)L463.
- 5) S. Annaka: *J. Phys. Soc. Jpn.* **51**(1982)1927.
- 6) O. Brümmer, Ch. Eisenschmidt and H. R. Höche: *Z. Naturforsch.* **a37**(1982)524.

MEASUREMENT OF X-RAY REFRACTIVE INDEX BY MULTIPLE REFLECTION DIFFRACTOMETER

H.Kato, T.Ogawa, S.Hattori, M.Kawata, Y.Kobayashi, K.Umezawa, T.Ishikawa* and K.Ishida

Department of Physics, Faculty of Science and Technology, Science University of Tokyo, Noda-shi, Chiba 278

*KEK. National Laboratory for High Energy Physics, Oho-machi, Tsukuba-gun, Ibaraki 305

Introduction

The precise measurement of refractive index of X-ray has been carried out in order to obtain the dispersion relation of X-ray. On this subject, several experiments employing the interferometric method have already been reported.^{1)~3)} Using SOR, Bonse and Materlick⁴⁾ measured X-ray refractive index throughout the whole range of wavelength including K absorption edge of Ni. In the present experiment, we have made direct measurement of the angle of deflection of a beam diffracted through a prismatic specimen⁵⁾ by the multiple reflection diffractometer.⁶⁾ The specimens used are LiF and KCl single crystals having right angle formed by cleavage surfaces.

Apparatus

The experimental arrangement, as shown in Fig.1, is (+,+, -) setting. The first crystal is a Si single crystal with a symmetric 220 reflecting plane, which selects a certain wavelength. The second and the third crystals are Si groove crystals with a symmetric 220 reflecting plane as well. The spatial width of incident beam is restricted by a slit set in front of the first crystal. The beam size is 1x2mm. Another slit (10x10mm) is placed before the second crystal to avoid the undesirable scattered beam. For the wavelength used in this experiment, the beam is reflected three times between the parallel groove of the second crystal, and then highly collimated and monochromatized X-ray is produced.

As the movement of each goniometer and counter is remotely controlled by the computer system, the second and the third goniometers hold the accuracy 1" per 100 pulses, and the goniometer for a specimen crystal, which is placed between them, 0.72" per 1 pulse.

Source and Wavelength

Our experiment was made at the station on the C-15 line for the Precision X-ray Optics. The acceleration voltage was 2.5GeV., and the amount of stored current ranged from 120 to 40mA. The wavelength was measured with the Bond method utilizing 333 and 888 reflections of a Si wafer placed on the goniometer of the third crystal, and then determined as 0.773666A.

Measurement and Results

A specimen prism is set between the second and the third crystals, and its position is regulated so that part of the beam will be refracted and the other part can pass straight on. The major rotation axis of the goniometer is adjusted to coincide with an edge of the specimen. We

measured the glancing angle to the specimen surface and the angle of deflection. Then, after rotating the specimen by a finite angle, the same procedures are repeated. The angle of deflection can be known directly from the rocking curve of the third crystal as shown in Fig.2, where θ_i is the incident angle, and, $\Delta\theta_i$, the angle of deflection. The comparison of these results with theoretical values and other measured values is shown in Table 1.

This work has been done under the support of the Photon Factory Precision X-ray Optics Working Group. Here, we would like to express our sense of gratitude.

References

- 1) U.Bonse and H.Hellkötter; Z.Physik 223 (1969) 345
- 2) D.C.Creagh and M.Hart; Phys.Status Solidi 37 (1970)753
- 3) D.C.Creagh; Aust.JPhys. 28(1975)543
- 4) U.Bonse and G.Materlik; Z.Physik B24(1976)189
- 5) K.Ishida and H.Kato; Jpn.J.Appl.Phys. 21 (1982)1109
- 6) U.Bonse and M.Hart; Appl.Phys.Lett. 7(1965)238
- 7) Z.Bornea; J.Phys.Soc.Japan 21 (1966) 961

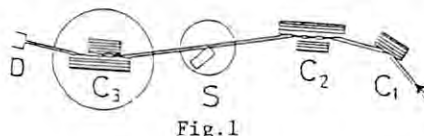


Fig.1

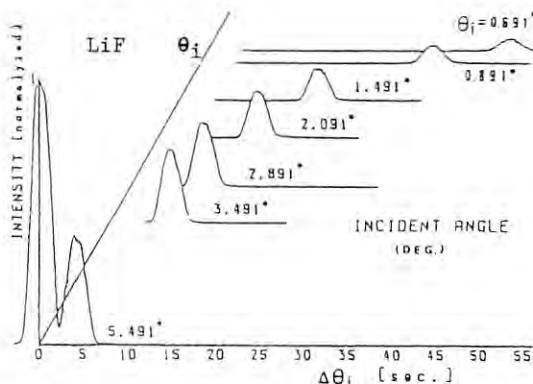


Fig.2

λ (A)	Sample	$\delta \cdot 10^9$ (Exp) ($n=1-\delta$)	Error	$\delta \cdot 10^9$ (Theo)	ϵ' (Exp)	ϵ'' (Honl)
0.709265	LiF	(1.663+0.003)	0.2%	1.6572	(0.04+0.02)	0.02
(Mo K α_1)	KCl	(1.34 +0.02)	1.3%	1.3133	(0.73+0.36)	0.140
0.77366	LiF	(1.975+0.005)	0.3%	1.972	(0.018+0.030)	0.025
Present Exp.)	KCl	(1.59 +0.01)	0.6%	1.562	(0.69 +0.23)	0.163

Table 1

PRECISION LATTICE PARAMETER MEASUREMENT SYSTEM ON THE BASIS OF THE TRIPLE-CRYSTAL ARRANGEMENT APPLIED TO THE BOND METHOD

Kiyomasa Sugii, Tetsuya Ishikawa*, Kan Nakayama**, Hidetoshi Takaoka, Seishi Kikutā**, and Photon Factory-Precision X-ray Optics Working Group
 Musashino Electrical Communication Laboratory, Nippon Telegraph and Telephone Public Corporation, Musashino-shi, Tokyo 180.*National Laboratory for High Energy Physics, Oho-machi, Tsukuba-gun, Ibaraki 305.**National Research Laboratory of Metrology, Sakuramura, Umezono, Niihari-gun, Ibaraki 305.**University of Tokyo, Bunkyo-ku, Tokyo 113.

Precision lattice parameter measurement system has been constructed on the basis of the triple-crystal arrangement applied to the Bond method. In the preliminary experiment in February 1983, it was confirmed that lattice parameters could be obtained with accuracy less than 10 ppm, in spite of the facts that no special temperature control was done in a hutch and Bragg angles were restricted to low values around 20° because of the present status of KEK-SR(horizontal polarization).

The Bond method is the best to measure absolute lattice parameters of materials¹⁾. Figure 1 shows the setup, which was installed in the hutch located downstream of BL15. The wavelength of the probe beam was determined as 1.4607 Å by using an Si(111) wafer with a well-calibrated lattice parameter as the third crystal. The accuracy of the Bond method is limited by ambiguity in Bragg angle determination mainly due to wavelength dispersion. Three key points which played important roles to improve the accuracy in our system are given as follows. The first is development of a computer-controlled multi-axis diffractometer by which an absolute angular-position of the rotation stage mounting the specimen can be read by an encoder with 1 resolution. The second is application of the triple-crystal arrangement of (+++) to the Bond method. In this arrangement, the wavelength dispersion can be neglected²⁾: for example, when Si(111) and Si(220) were used as the first and second crystals as shown in figure 1, angular and wavelength distributions of a probe beam incident on the third crystal were about 5 and 8x10⁻³, respectively. The third is high intensity of the KEK-SR operating at 2.5 GeV and 100 mA in average. The x-ray intensity at the Bragg condition in this system was about 10⁷ photons/mm²s, which was two order larger than that for a conventional source. Such a strong intensity makes it very easy not only to search out a reflection peak quickly but also to take a rocking curve without intensity fluctuation, resulting in high accuracy of the Bragg angle determination.

Figure 2 shows reproducibility in angular-position of the stage corresponding to the Bragg angle(center value of FWHM). It was confirmed that stability of the system was good enough to perform the precision measurement.

Figure 3 shows a relationship between the lattice parameter and carrier concentration for Si-doped GaAs. The lattice parameter decreases with the carrier concentration; Si concentrations measured by the SIMS are also indicated. It is well-known that etch pit density also decreases with increasing the doping level in the Si-doped GaAs. The same relation between the lattice parameter, carrier concentration, and etch pit

density was found in the case of Zn- and S-doped InP³⁾

Further improvement in the accuracy will be possible when a vertical wiggler is in operation; the vertical polarization SR from it makes it possible to use any Bragg angle with the polarization factor of unity.

REFERENCES

- 1) W.L.Bond: Acta Cryst., 13(1960)814.
- 2) M.Renninger: Acta Cryst., 8(1955)597.
- 3) K.Sugii, H.Koizumi, and E.Kubota: J.Electro. Mater., 12(1983)701.

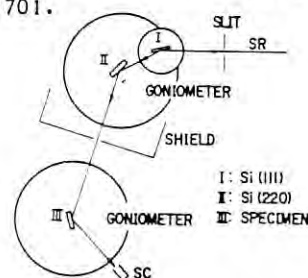


Figure 1. The precision lattice parameter measurement system.

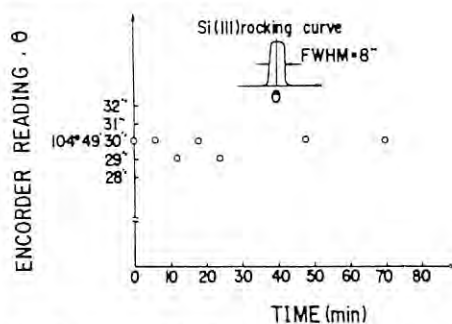


Figure 2. Reproducibility in the stage angular-position which corresponds to the Bragg angle.

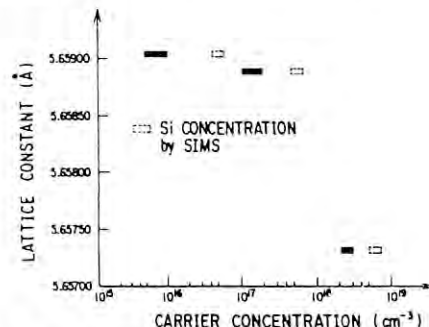


Figure 3. The relationship between the lattice parameter and carrier concentration for Si-doped GaAs.

A NEW TYPE OF UNDULATOR MAKING USE OF STANDING MICROWAVES

T. Shintake, K. Huke, J. Tanaka, I. Sato and I. Kumabe*

National Laboratory for High Energy Physics
Oho-machi, Tsukuba-gun. Ibaraki-ken, 305, Japan

* Department of Nuclear Engineering, Faculty of Engineering,
Kyushu University, Fukuoka, 812, Japan

Introduction

A new type of undulator (named MICROWAVE UNDULATOR) which uses standing microwaves for the periodic undulator fields has been operated at the Photon Factory electron linac.^{1,2} The undulator has the period of 5.5 cm, the equivalent magnetic field of 0.45 kG and the K-parameter of 0.24. The undulator was set into the beam line of the electron linac, and the visible undulator radiation was observed.

Experimental and results

The undulator cavity is a long rectangular cavity with ridges as shown in Fig. 1. The pulsed microwave width of 4 μ sec and the power of 300 kW, is fed into the cavity through the rectangular waveguide and the coupling hole. The electron beam is periodically deflected by the transverse electric and magnetic fields of the standing microwaves and radiates the undulator radiations as illustrated in Fig. 2. The peak electric and magnetic field strength is 12.8 MV/m and 412 Gauss, which is equivalent to the undulator field of 450 Gauss. The wavelength of the microwave is 10.5 cm, and the undulator period is nearly equal to the half wavelength of the microwave, i.e., 5.5 cm. The K-parameter is 0.24, and the number of the periods is 20.

The undulator cavity was installed in the Photon Factory electron linac as shown in Fig. 3. The electron beam is transported into the undulator by the bending magnets, and the energy spread of the electron beam is defined within 0.5% FWHM by the collimator. The undulator radiation was observed by a TV-camera and its spectrum was measured by a monochromator and a photomultiplier.

The photographs of the undulator radiation are shown in Fig. 4. When the microwave power is switched off, the normal synchrotron radiations from the bending magnets are observed as Fig. 4(a). When the microwave power is fed into the cavity, the ring shaped undulator radiation comes out between the synchrotron radiations as Fig. 4(b). The spectrum of the undulator radiation was measured, the wavelength and the intensity agreed with the theoretical values.^{1,2}

References

- 1) T. Shintake, K. Huke, J. Tanaka, I. Sato and I. Kumabe, Jap. J. Appl. Phys. 21 (1982) L602.
- 2) T. Shintake, K. Huke, J. Tanaka, I. Sato and I. Kumabe, Jap. J. Appl. Phys. 22 (1983) 844.

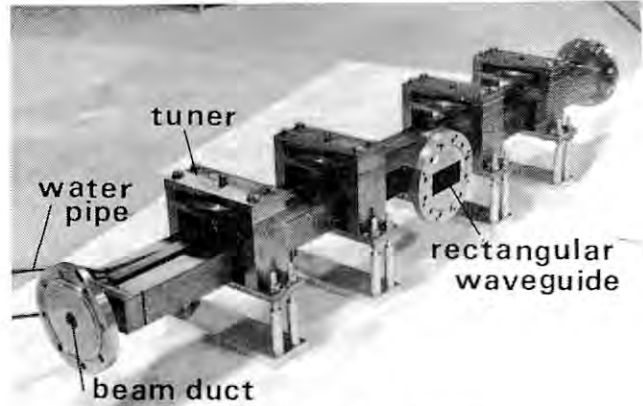


Fig. 1 Undulator cavity.

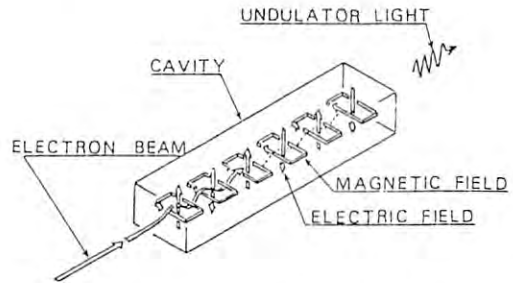


Fig. 2 Operating mechanism.

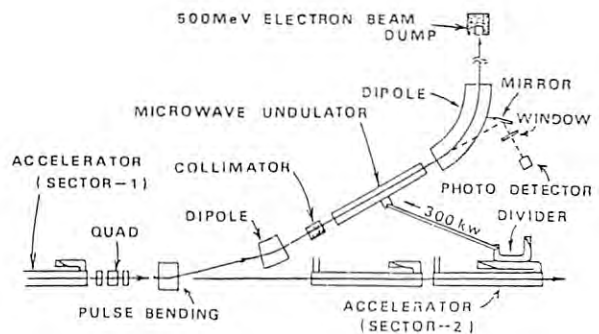
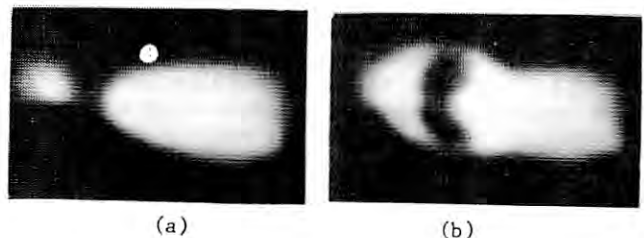


Fig. 3 Experimental set up.



(a)

(b)

Fig. 4 Photographs of the undulator radiation.

VII. ACTIVE PROPOSALS

Experimental proposals submitted by users are reviewed by "Program Assessment Committee" (PAC) of which members are listed in Table VII.1. Assignment of a beam-time to the proposal accepted by PAC will be made according to the decision of the director through the endorsement of Advisory Council of the Photon Fac-

tory. Users belonging to private industries can also apply for beam time by paying charge. Assignment of beam-time in this category is given a lower priority, but a review of PAC is not required.

In July 1983, 67 proposals are accepted by PAC and active. 15 proposals for charged beam-time assignment have been received.

Table VII.1 Members of Program Assessment Committee.

Dr. Jun-ichi Chikawa	Broadcasting Science Research Lab.	Japan Broadcasting Corporation
Prof. Sadao Hoshino	Institute for Solid State Physics	Univ. of Tokyo
Prof. Kazuo Huke	Photon Factory	National Lab. for High Energy Physics
Prof. Yoichi Iitaka	Faculty of Pharmaceutical Sciences	Univ. of Tokyo
Prof. Takehiko Ishii	Institute for Solid State Physics	Univ. of Tokyo
Prof. Tadao Kasuya	Faculty of Science	Tohoku Univ.
Prof. Norio Kato	Faculty of Engineering	Nagoya Univ.
Prof. Haruo Kuroda	Faculty of Sciences	Univ. of Tokyo
Prof. Masatoshi Nakamura	Department of Physics	Univ. of Tsukuba
Prof. Shigefumi Okada	Faculty of Medicine	Univ. of Tokyo
Prof. Fumio Oosawa	Faculty of Engineering Science	Osaka Univ.
Prof. Taizo Sasaki	Photon Factory	National Lab. for High Energy Physics
Prof. Ikuzo Tanaka	Faculty of Science	Tokyo Institute of Technology
Prof. Jiro Tanaka	Photon Factory	National Lab. for High Energy Physics
Prof. Yutaka Toyozawa	Institute for Solid State Physics	Univ. of Tokyo

LIST OF PROPOSALS ACCEPTED BY PROGRAM ASSESSMENT COMMITTEE

<u>Proposal Number</u>	<u>Spokesperson</u>	<u>Title</u>
83-002	M. Hida School of Engineering Okayama Univ.	EXAFS Study on the Premelting Phenomena of Gallium
83-004	M. Hida School of Engineering Okayama Univ.	EXAFS Study on the Lattice Relaxation of Ni Ultra Fine Particles
83-005	T. Murata Kyoto Univ. of Education	Local Lattice Structure in Solid Solutions of Alkali Halides
83-006	H. Terauchi Faculty of Science Kwansei Gakuin Univ.	Studies on the Local Structures near Structural Phase Transitions
83-007	M. Maeda Faculty of Science Okayama Univ.	EXAFS Study on Local Structure of Liquid GeSe System
83-009	O. Yamada Faculty of Science Okayama Univ.	Studies on the Local Structure of the Phase Transition in Invar Alloys
83-010	Y. Tsu Reserch Institute of Mineral Dressing and Metallurgy Tohoku Univ.	Study of the Pre-Melting of Metals
83-011	H. Sugi School of Medicine Teikyo Univ.	Time-Resolved X-Ray Diffraction of Contracting Skeletal Muscle
83-012	T. Ueki Faculty of Engineering Science Osaka Univ.	Dynamic Behaviour of Biopolymers Studied by Small-Angle Scattering
83-013	M. Sano College of General Education Nagoya Univ.	The Structures of Metal Ions in Non-Aqueous Media
83-014	S. Iida Faculty of Science Kwansei Gakuin Univ.	Phase Transition in $TiCl_3$
83-015	H. Kuroda Faculty of Sciences Univ. of Tokyo	EXAFS and XANES Studies of Chemically Fixed Mo and Cr Catalysts
83-016	H. Kuroda Faculty of Sciences Univ. of Tokyo	XANES of Metal Carbonyl Molecules
83-017	H. Kuroda Faculty of Sciences Univ. of Tokyo	EXAFS and XANES Studies of Metal-Halide-Doped Polyacetylenes

<u>Proposal number</u>	<u>Spokesperson</u>	<u>Title</u>
83-018	H. Kuroda Faculty of Sciences Univ. of Tokyo	XANES of Highly-Conductive Mixed-Valence Organic Charge-Transfer Salts, (TMTSF) ₂ X and Related Materials
83-019	H. Kuroda Faculty of Sciences Univ. of Tokyo	Surface Structures of SMSI Catalysts
83-020	K. Tamaru Faculty of Sciences Univ. of Tokyo	Research on the Surface Structure of the Supported Metal Catalysts, which Produce Oxygenated Compounds from CO and H ₂ under Mild Conditions
83-021	T. Ohnishi Res. Lab. of Resources Utilization Tokyo Insititute of Technology	EXAFS Study on the Structure of Catalysis for Photodecomposition of Water
83-022	H. Sano Faculty of Science Tokyo Metropolitan Univ.	XANES Studies of Mixed-Valency and Abnormal Valency in the Complexes of Ferrocene Derivatives
83-023	H. Kuroda Faculty of Sciences Univ. of Tokyo	Surface Structures of Supported Nickel Cluster Catalysts
83-024	H. Kuroda Faculty of Sciences Univ. of Tokyo	XAS Studies on BiMetallic Ph-Co Carbonyl-derived Catalysts
83-025	Y. Sasaki Faculty of Sciences Univ. of Tokyo	EXAFS Study on the Structure of Heteropolymolybdates in Solution
83-26	Y. Ichikawa Institute of Space and Astronautical Science	Electron Correlation Effects in Photoionization Processes of Atoms and Molecules
83-027	A. Itoh College of Arts & Sciences Univ. of Tokyo	Study on the Biological Effect on Monochromatic Soft X-rays Using Synchrotron Radiation
83-028	Y. Fujii Faculty of Engineering Science Osaka Univ.	Synchrotron Radiation X-Ray Scattering Study of Non Equilibrium Systems
83-029	T. Hamanaka Faculty of Engineering Science Osaka Univ.	Structural Study of Visual Cell Membrane by X-Ray Diffraction
83-030	K. Wakabayashi Faculty of Engineering Science Osaka Univ.	X-ray Diffraction Studies of Structural Change of Muscle Filaments in Connection
83-031	S. Kagoshima College of Arts & Sciences Univ. of Tokyo	Structural Study by X-ray Diffraction at Low Temperature

<u>Proposal Number</u>	<u>Spokesperson</u>	<u>Title</u>
83-032	S. Kagoshima College of Arts & Sciences Univ. of Tokyo	Dynamical Study of Structural Fluctuation by X-ray Diffraction at Low Temperature
83-033	N. Sakabe Faculty of Science Nagoya Univ.	Crystallographic Studies of Molecular Biology by Film Methods
83-034	Y. Fujii Faculty of Engineering Science Osaka Univ.	Synchrotron Radiation X-Ray Scattering Study of Staging Transition of K-GIC
83-035	M. Tokonami Faculty of Sciences Univ. of Tokyo	Accurate Determination of Crystal Structures by Using Monochromated Synchrotron Radiation
83-036	S. Kikuta Faculty of Engineering Tokyo Univ.	Experiments on High Precision X-Ray Diffraction
83-037	S. Akimoto Institute for Solid State Physics Univ. of Tokyo	X-Ray Diffraction Experiments under High Pressure
83-038	H. Baba Faculty of Science Osaka Univ.	A Study on Nuclear Excitation by Electron Transition with Synchrotron Radiation
83-041	J. Harada Faculty of Engineering Nagoya Univ.	Study of Short Range Ordering in Ternary Alloys
83-043	Y. Goushi Faculty of Engineering Univ. of Tokyo	Ultra Trace Elements Analysis by Synchrotron Radiation XRF
83-043	F. Marumo Research Laboratory of Engineering Materials Tokyo Institute of Technology	X-Ray Scattering Study on Amorphous and Crystalline Powder Materials
83-044	F. Marumo Research Laboratory of Engineering Materials Tokyo Institute of Technology	Small Angle X-Ray Scattering Experiments Using SSD
83-045	F. Tokunaga Faculty of Science Tohoku Univ.	Localization of Physiologically Active Tyrosine Residues in Purple Membrane and Their Localization Change on Absorption of Light
83-046	T. Iijima Faculty of Science Gakushuin Univ.	Charge Density Studies of Gaseous Molecules by X-Ray Scattering
83-047	Y. Takeuchi Faculty of Sciences Univ. of Tokyo	EXAFS Study of Heulandite (Zeolite)

<u>Proposal Number</u>	<u>Spokesperson</u>	<u>Title</u>
83-048	M. Taniguchi Faculty of Science Nagoya Univ.	Time-Resolved X-Ray Diffraction Studies of TMV and Their Protein Assemblies
83-049	Y. Iidaka Faculty of Pharmaceutical Science Univ. of Tokyo	Structure Analysis of Macromolecular Proteins and Others
83-050	H. Kuroda Faculty of Sciences Univ. of Tokyo	Structural Studies of Polyacetylene Films Doped with Bromine and Iodine
83-051	T. Iizuka School of Medicine Keio Univ.	EXAFS of Hemoprotein-Analysis of Thermal Spin Equilibrium
83-052	T. Ohta Photon Factory National Laboratory for High Energy Physics	Surface EXAFS Studies with the Soft X-Ray Two Crystal Monochromator
83-053	T. Matsushita Photon Factory National Laboratory for High Energy Physics	Development of Dispersive X-Ray Absorption Spectrometer for Time-Resolved Experiments
83-054	A. Higashi Faculty of Engineering Hokkaido Univ.	Studies of Dynamical Behaviour of Lattice Defects in Ice by Rapid X-Ray Topography
83-055	Y. Morioka Univ. of Tsukuba	The Study of Photodissociation of Gases
83-056	Y. Iguchi Univ. of Tsukuba	NEXAFS and Subgiant Resonances of Soft X-Ray $M_{4,5}$ Absorption Spectra
83-057	S. Ikeda Faculty of Science Osaka Univ.	Influences of Various Ligands on Jahn-Teller Effect of Copper Complexes in Solution
83-058	S. Ikeda Faculty of Science Osaka Univ.	Determination of the Structure of Polynuclear Molybdate Complexes in Weakly Acidic Solutions by Means of EXAFS
83-059	N. Kamijo Government Industrial Research Institute, Osaka	EXAFS Study of Phase Transition in $PbZrO_3$ Crystal
83-060	N. Kamijo Government Industrial Research Institute, Osaka	EXAFS Study of Fluorites (Super Ionic Compounds)
83-061	M. Yanagihara Photon Factory National Laboratory for High Energy Physics	Soft X-Ray Reflection from Mirror Surfaces

<u>Proposal Number</u>	<u>Spokesperson</u>	<u>Title</u>
83-062	H. Aritome Faculty of Engineering Science Osaka Univ.	Fabrication of Transmission Gratings for Soft X-Ray Spectroscopy
83-063	S. Nakai Faculty of Engineering Utsunomiya Univ.	Study of the L Absorption Near-Edge Fine Structure of the Transition-Metal Sulfides, Oxides and Hydrides
83-063	T. Namioka Research Institute for Scientific Measurements Tohoku Univ.	Precise Measurements of Atomic and Molecular Spectra in the Photoionization Region
83-065	K. Namikawa Institute for Solid State Physics Univ. of Tokyo	An Examination of the X-Ray Magnetic Bragg Reflexion and its Application to the Fundamental Magnetism
83-066	E. Takenaka Faculty of Medicine Univ. of Tokyo	Studies on Applications of SOR to Radio Diagnosis and Radio Therapy
83-067	T. Hanyu Faculty of Science Tokyo Metropolitan Univ.	Inner Shell Excitation Spectra of Alkaline Earth and Rare Earth Metals
83-068	T. Tomiki Faculty of Science Ryukyu Univ.	The VUV Spectra of Y_2O_3 Single Crystals
83-069	Y. Hatano Faculty of Science Tokyo Institute of Technology	Extreme-UV Spectroscopy and Reaction Dynamics of Highly Excited Atoms and Molecules
83-070	J. Chikawa Technical Research Laboratories Japan Broadcasting Corporation	High Speed X-Ray Topography
83-071	K. Hasegawa Faculty of Engineering Univ. of Tokyo	Test of Integral Type Position- Sensitive Detector and its Application for Small Angle Scattering Experiments
83-072	T. Sasaki Photon Factory National Laboratory for High Energy Physics	Development of Synchrotron Radiation Instrumentation
83-074	Y. Chikaura Faculty of Engineering Kyushu Institute of Technology	Synchrotron Radiation Scattering Radiography
83-075	H. Inoue National Institute of Agrobiological Resources	Time Course of the Reconstitution of Tobacco Mosaic Virus Induced by a Temperature Jump

<u>Proposal Number</u>	<u>Spokesperson</u>	<u>Title</u>
83-076	R. Itoh Faculty of Engineering Univ. of Tokyo	EXAFS Studies on III-V Compound Semiconductor Alloys
83-077	H. Fukutani Institute of Physics Tsukuba Univ.	Piezo-Optical Study of Alkali- and Alkaline Earth-Halides in the VUV Region
83-078	M. Kinoshita The Institute for Solid State Physics Univ. of Tokyo	EXAFS and XANES in Organometallic Polymers Showing Magnetic Orders
83-079	T. Ohta Photon Factory KEK	SEXAFS Studies on the Initial Oxidation of Ni Single Crystal Surfaces
83-080	S. Sato Photon Factory KEK	Extreme Ultraviolet Reflectance Spectra of $\text{La}_x \text{Ce}_{1-x} \text{Al}_2$ Alloys
83-081	K. Koto Institute of Scientific and Industrial Research Osaka Univ.	Crystal Chemistry of Olivine in the $\text{Mg}_2\text{SiO}_4 - \text{Fe}_2\text{SiO}_4$ System by EXAFS
83-082	S. Suzuki Faculty of Science Tohoku Univ.	UPS Measurements on Liquid Metals
83-083	Y. Sasaki Faculty of Sciences Univ. of Tokyo	EXAFS Experiments of Poly (Carbon Diselenide)
83-084	S. Yoshida Faculty of Engineering Kyoto Univ.	Relation between Structures Based on the EXAFS Analysis and Catalytic Activity of Supported- FeCl_3 Catalysts
83-085	H. Kuroda Faculty of Sciences Univ. of Tokyo	Surface Structure of Fe-Mn, Fe-Ru Bimetal-Cluster Catalysts
83-086	T. Mitsui Faculty of Engineering Science Osaka Univ.	Diffraction Study of Muscle Contraction and Photocycle of the Purple of Purple Membrane by Correlation Method
83-087	S. Aoki Institute of Applied Physics Tsukuba Univ.	Soft X-ray Microscopy Using X-Ray Resist
83-090	T. Wakabayashi Faculty of Sciences Univ. of Tokyo	Supramolecular Structure of Chromatin
83-091	T. Wakabayashi Faculty of Sciences Univ. of Tokyo	Structural Study of Molecular Mechanism of Muscle Construction

<u>Proposal Number</u>	<u>Spokesperson</u>	<u>Title</u>
83-092	S. Ikeda Faculty of Science Osaka Univ.	Studies on the Structure of Complexes of Cr(II), Cr(III) in Solution
83-093	S. Ikeda Faculty of Science Osaka Univ.	Studies on the Structure of Chelate Complexes Complexes in Organic Solvents and Mixed Solvents
83-094	S. Ikeda Faculty of Science Osaka Univ.	EXAFS Spectroscopic Studies of Molybdophosphate Containing 2r(IV) in Aqueous Solution
83-095	H. Kihara Faculty of Medicine Jichi Medical School	Time-Resolved Study of Protein Assembly by X-Ray Scattering Methods
83-096	T. Yoshiyama Kyoto Sangyo Univ.	Local Structure Analysis on the Martensitic Transformation in β -CuZn
83-097	F. Marumo Research Laboratory of Engineering Materials Tokyo Institute of Technology	A Crystal Chemical Study on Minor Metal Elements in Cadomium Apatites
83-098	T. Suzuki Faculty of Engineering Yamanashi Univ.	Structural Analyses of MoO_3 , CrO_3 and ZnO in HCONH_2 with EXAFS Measurements
83-099	I. Shibuya Research Reactor Institute Kyoto Univ.	X-Ray Diffraction Study of 2-Dimensional Phase Transition in the Purple Membrane (Fractionated from Halobacterium Halobium)
83-100	E. Taniguchi Faculty of Science Nagoya Univ.	X-Ray Diffraction from Single Cryxstals of Muscle Proteins
83-101	H. Endo Faculty of Science Kyoto Univ.	The Local Structure in Amorphous Se-Te Mixtures

LIST OF PROPOSALS ACCEPTED FOR CHARGED BEAM TIME ASSIGNMENT

<u>Proposal Number</u>	<u>Spokesperson</u>	<u>Title</u>
83-Y01	M. Murata Murata Mfg. Co. Ltd.	Studies on Energy Dependence of Photon Detection of Ceramic Secondary Electron Multiplier
83-Y02	H. Oka LSI Laboratory Mitsubishi Elec. Corp.	Experiments of Fine-Line Patterning by SR
83-Y03	H. Oka LSI Laboratory Mitsubishi Elec. Corp.	Characterization of Process Induced Defects
83-Y04	T. Kimura Central Research Laboratory Hitachi Ltd.	Fundamental Study of X-Ray Lithography
83-Y06	S. Hattori Musashino Electrical Communication Laboratory Nippon Telegraph and Telephone Public Corporation	Evaluation of Perfectness of Crystalline Materials using High Speed X-Ray Topography
83-Y07	S. Hattori Musashino Electrical Communication Laboratory Nippon Telegraph and Telephone Public Corporation	Photoemission Studies of Pb-Alloys, GaAs and Optical Fibers
83-Y08	S. Hattori Musashino Electrical Communication Laboratory Nippon Telegraph and Telephone Public Corporation	EXAFS Investigations of Superconductor, Semiconductor and Glass Materials
83-Y10	H. Kajiyama Hitachi Research Laboratory Hitachi Ltd.	EXAFS of dispersed Metal Catalysts
83-Y11	S. Takayama Resin Research Laboratory Mitsubishi Petroleum Chemistry, Co. Ltd.	Analysis of the Structure of Ziegler Catalysts by EXAFS
83-Y12	K. Susa Central Research Laboratory Hitachi Ltd.	EXAFS Measurement of SiO ₂ -GeO ₂
83-Y13	H. Ando Hitachi Research Laboratory Hitachi Ltd.	EXAFS of Dispersed Metal Catalysts
83-Y14	T. Yamamoto Central Research Laboratory Idemitsu Kosan, Co. Ltd.	The EXAFS Measurement of Supported Iron Catalysts
83-Y15	M. Morimoto Toyota Central Research & Development Labs., Inc.	EXAFS Measurements of Inorganic Si-Y and Si-Zn Specimens

VIII. USER'S LIST

547 users have been registered during the period from April 1982 to September 1983. Among them, 371 researchers are from 50 universities, 140 from national laboratories, and 36 from 10 private industries.

<u>Institution</u> Name	Proposal No.	<u>Institution</u> Name	Proposal No.
<u>Agency of Industrial Science and Technology</u>		<u>The Jikei University School of Medicine</u>	
Y. Kanazawa	35	M. Konishi	30
A. Kawate	42	S. Kurihara	30
Y. Kobayashi	42	Y. Umazume	30
K. Nakayama	36	<u>Josai University</u>	
K. Tsukimura	35, 49	Y. Ito	26
<u>Chubu Institute of Technology</u>		<u>Kagawa Nutrition College</u>	
T. Izumi	72	S. Tachiya	13
<u>Dokkyo University School of Medicine</u>		<u>Keio University</u>	
H. Hyodo	66	K. Hiramatsu	66
<u>Gakushuin University</u>		T. Iizuka	51, 53
K. Arakawa	43, 46	Y. Ishimura	51
C. J. Cui	70	R. Makino	51
T. Iijima	43, 46	K. Sakaguchi	51
T. Mitsuhashi	43, 46	<u>Korea University</u>	
T. Mizoguchi	44	H. T. Kim	36
K. Nishikawa	43, 46	<u>Kwansei Gakuin University</u>	
T. Ogawa	70	S. Iida	2, 4, 6, 7, 10, 14, 31, 32, 41, 59
M. Taguchi	43, 46	T. Minato	6, 14, 31, 32, 41
<u>Gunma University</u>		Y. Nishihata	6, 14, 31, 32, 41
I. Nagakura		H. Terauchi	2, 4, 7, 10, 14, 31, 32, 41, 59, 60
H. Sugawara		<u>Kyoto Industrial University</u>	
<u>Hiroshima University</u>		T. Yoshiyama	5
H. Fujiwara	37	<u>Kyoto University</u>	
Y. Komura	35	Y. Hiragi	12
K. Kurada	37	H. Miyaji	12
M. Nomura	37	T. Nakayama	12
T. Ohba	35	K. Tanizawa	12
<u>Hokkaido University</u>		H. Urakawa	12
S. Amakai	54	H. Utsumi	27
K. Goto	54	T. Yoshimura	12
T. Hondo	54	<u>Kyoto University of Education</u>	
Y. Izumi	12	T. Murata	
K. Katsuta	54	<u>Kyushu Institute of Technology</u>	
Y. Miyake	12	Y. Chikaura	65
Y. Mori	54	H. Kii	65
N. Mouri	31, 37	<u>Kyushu University</u>	
H. Takahashi	31	H. Akiyama	44
K. Yasuda	12	H. Fujii	44
<u>International Christian University</u>		M. Hidaka	44
K. Takakura	27	A. Higashi	54
<u>Jichi Medical School</u>		C. Kajiyama	44
H. Kihara	12	K. Konishi	66
S. Saigo	51	S. Maeda	44

<u>Institution</u> Name	Proposal No.	<u>Institution</u> Name	Proposal No.
<u>Meisei University</u>		<u>Osaka University</u>	
T. Nagata	26	T. Akai	37
		T. Arata	30
<u>Mie University</u>		H. Baba	38
I. Fujishiro	37	S. Emura	35
		S. Fujii	33
<u>Nagoya University</u>		Y. Fujii	28, 34
Y. Ban	31, 41	A. Fujishima	30
K. Gohara	70	Y. Fujita	42
J. Harada	35, 41	T. Fukumoto	57, 58
S. Hashiba	31, 41	T. Hamanaka	30
Y. Kashihara	41	N. Hamaya	28, 37
N. Kashiwakura	41, 31	S. Harada	49
N. Kato	70	T. Hayashi	30
Y. Kawai	41	S. Ikeda	52, 57, 58
Y. Kimura	13	Y. Inoko	12
T. Maruo	13	Y. Ito	35
Y. Masuda	13	K. Kanou	42
Y. Muroga	12	K. Kishi	52
K. Ohshima	41	H. Konishi	28
K. Sakabe	33	K. Kotou	35, 43, 60
N. Sakabe	33, 49	S. Kou	28
M. Sakata	31, 32, 41	M. Kusunoki	33
M. Sano	13	N. Matsubayashi	57, 58
K. Sasaki	33	T. Mitsui	12, 30
M. Senoo	37	S. Monju	52, 57, 58
M. Shimada	41	H. Mukaïdo	34
M. Taniguchi	30, 48	K. Murase	28
T. Taniguchi	48	Ka. Murata	37
H. Yamadera	13	Ko. Murata	57, 58
S. Yamamoto	37	H. Nakayama	30
T. Yamane	33, 49	S. Nishizawa	30
T. Yoshiyama	31, 41	Y. Noda	28
Y. H. Li	70	N. Ogawa	57, 58
N. Wada	4	K. Oka	12
		A. Onodera	37
<u>Nihon University</u>		T. Oonishi	28, 34
K. Kurita	30	M. Sato	12
H. Tagawa	12	T. Saito	38
K. Terashima	12	A. Shinohara	38
		H. Sumiya	37
<u>Okayama University</u>		M. Takahashi	57, 58
M. Hida	2, 4~7, 9, 10, 14, 60	N. Tanaka	12
K. Kamon	9	K. Tomita	33
Y. Kuroda	4	T. Ueki	12
H. Maeda	2, 4~7, 9, 10, 14, 59, 60	W. Utsumi	37
M. Mimura	9	K. Wakabayashi	30, 48
T. Morimoto	4	I. Watanabe	2, 10, 57~59
I. Nakai	9	Y. Yabuhara	57, 58
H. Tokuhara	9	Y. Yamada	28
O. Yamada	9	T. Yanagida	30
L. W. Li	9	N. Yasuoka	33
		A. Yokoyama	38
<u>Osaka Electro-Communication University</u>		<u>Rikkyo University</u>	
K. Taniguchi	13, 38, 42, 52	J. Amagasa	27
<u>Osaka Medical College</u>		K. Hieda	27
M. Matsushima	33	I. Maeda	27

<u>Institution</u> Name	Proposal No.	<u>Institution</u> Name	Proposal No.
<u>The Saitama Institute of Technology</u>		F. Tokunaga	12, 45
T. Fukamachi	31, 43	A. Tomizuka	37
M. Yoshizawa	31, 43	Y. Tsu	2, 4, 10
<u>Saitama Medical School</u>		K. Ueda	64
K. Nishimura	66	S. Watanabe	10
<u>Science University of Tokyo</u>		Y. Watanabe	41
S. Hattori	36, 70	<u>Tokai University</u>	
K. Ishida	36, 70	Y. Furusawa	27
H. Katoh	36, 70	H. Maezawa	27
M. Kawada	36, 70	K. Suzuki	27
Y. Kobayashi	36, 70	<u>Tokyo Institute of Technology</u>	
T. Ogawa	36, 70	S. Arai	69
K. Umezawa	36, 70	K. Domen	21
<u>Shibaura Institute of Technology</u>		T. Fujii	49
M. Yoshino	26	T. Fukano	11
<u>Shinshu University</u>		H. Hashizume	11
M. Nagura	12	Y. Hatano	69
M. Takizawa	66	C. D. Yin	43
<u>Shizuoka University</u>		S. Ito	43
T. Ishidate	31	H. Koizumi	69
K. Yamamoto	31	K. Kozutsumi	43
<u>Sophia University</u>		A. Kudo	21
T. Suzuki	36	S. Gong	70
<u>Suzuka College of Technology</u>		F. Marumo	43
Y. Tamura	11	I. Minato	11
<u>Teikyo University</u>		N. Miyata	43
J. Egawa	66	H. Morikawa	43
T. Kobayashi	11	M. Morita	69
H. Sugi	11	S. Nagakura	70
T. Tameyasu	11	H. Naruse	43
H. Tanaka	11	O. Nittono	70
T. Tsuchiya	11	N. Oda	27
<u>Tohoku University</u>		T. Ogawa	70
T. Fujimura	37	U. Ohhashi	49
S. Hashimoto	35, 41	T. Ohnishi	21
M. Hirai	45	H. Ohtaki	43
O. Hisatomi	12, 45	M. Okuno	43
H. Iwasaki	37, 41	Y. Sasada	49
K. Iwata	45	K. Shimizu	49
M. Kataoka	42	K. Shinsaka	69
T. Kikegawa	37	H. Suzuki	69
S. Kono	52	S. Suzuki	70
J. Murakami	26	Y. Tamura	43
T. Namioka	64	K. Tanaka	49
N. Niimura	28	Y. Tanaka	69
H. Onose	41	M. Toriumi	69
T. Sagawa	52	M. Ukai	69
N. Sato	12, 45	T. Yamaguchi	43
Y. Sato	26	T. Yoshimi	69
S. Suzuki		<u>Tokyo Metropolitan University</u>	
T. Takahashi	52	K. Asada	67
		T. Hanyu	67
		I. Ikemoto	17, 18
		H. Ishii	67
		M. Iwai	22
		I. Kamata	67
		S. Nakajima	22

<u>Institution</u>		<u>Institution</u>	
Name	Proposal No.	Name	Proposal No.
H. Ohkuma	67	N. Kosugi	15~25, 57, 58
H. Sano	22	Y. Kudoh	35, 47
K. Sato	22	H. Kuroda	15~25, 50, 51, 57, 58
K. Shinohara	27	U. Lee	25
Y. Watanabe	22	H. Majima	27
S. Yamaguchi	67	K. Mochiki	11, 49, 71
<u>Tokyo University of Agriculture and Technology</u>		Y. Murata	52
T. Arikawa	26	S. Naitou	20
<u>Tokyo University of Mercantile Marine</u>		K. Nakanishi	35
S. Annaka	36	S. Nakatani	36
<u>Tottori University</u>		K. Namikawa	52, 65
K. Fukayama	33	Y. Nihei	42
T. Tsukihara	33, 49	F. Nishi	35
<u>Toyama University</u>		K. Ogata	35
Y. Sugita	70	K. Ohsumi	35
<u>Toyohashi University of Technology</u>		S. Okada	27
E. Asada	42	M. Owari	42
<u>Toyota Technological Institute</u>		T. Ozawa	35
Y. Kamiya	48	T. Sakamaki	35, 49
<u>The University of Electro-Communications</u>		K. Sakurai	42
S. Hasegawa	66	Y. Sasaki	25
<u>The University of Tokyo</u>		H. Sawada	35
Y. Abe	35	H. Sekiyama	52
K. Akimoto	36	I. Shirotani	37
S. Akimoto	37	K. Sugiyama	35, 43, 47
K. Asakura	15~25, 50, 51, 57, 58	J. Suzaki	37
H. Daimon	52	M. Suzuki	72
C. Ekawa	20	T. Suzuki	37
S. Fukushima	42	Y. Suzuki	
E. F. Granzer	36	T. Tagai	35, 49
Y. Goushi	42	T. Takahashi	36
N. Haga	35	I. Takayama	36
K. Hasegawa	11, 49, 71, 72	H. Takeda	35
Y. Hosono		K. Takemura	31, 37
S. Hosoya	51, 65	E. Takenaka	66
A. Iida	42	Y. Takeuchi	35, 43
Y. Iidaka	49	M. Takezawa	44
H. Imoto	25	T. Tamegai	31, 32
S. Ino	52	M. Tani	31, 32
H. Ishii	15~25, 50, 51, 57, 58	A. Tatara	27
T. Ishii		M. Tokonami	35, 37, 43
A. Ito	27	A. Tomioka	72
T. Ito	27	H. Tomozawa	31, 32
S. Kagoshima	31, 32	S. Toudou	31
Y. Kanai	31, 32	K. Tsujii	31, 32, 37
J. Kawai	42	K. Tsutsumi	31, 32
K. Kikuchi	18	M. Utsumi	49, 71
S. Kikuta	36	T. Wakabayashi	72
M. Koike	49, 71	H. Watanabe	35
G. Kobayashi		T. Yagi	37
K. Kondo	36	H. Yamaguchi	27
M. Konno	31	T. Yamanaka	35, 43
		T. Yokoyama	15~25, 57, 58
		A. Yoshinaga	42
		<u>The University of Tsukuba</u>	
		T. Akahori	55
		M. Akisada	66
		S. Aoki	42
		T. Erata	32

<u>Institution</u> Name	Proposal No.
H. Fukutani	68
T. Hayaishi	55
H. Hirai	35
K. Hyodo	66
Y. Iguchi	56
K. Kakefuda	35
M. Kimata	35
H. Kishino	66
K. Kobayashi	27
K. Matsumoto	66
Y. Morioka	55
H. Nagasawa	32
I. Nakai	35
K. Naito	67
M. Nakamura	55, 64
R. Nishitani	28, 34
M. Ohmasa	35, 43
M. Onoda	32
J. Ryuta	35
Y. Saita	66
S. Saito	35
H. Shirakawa	17, 50
H. Suematsu	28, 34
S. Sueno	35
K. Tabata	37
T. Takahashi	37
K. Takano	37
Y. Uno	34
M. Wakatsuki	37
M. Watanabe	55
N. Yamada	35
H. Yurimoto	35

University of the Ryukyus

Y. Tanahara	68
T. Tomiki	68

Korea University

H. Kim	36
--------	----

Utsunomiya University

M. Kitamura	63
S. Nakai	63
K. Ogata	63
M. Ohashi	63
C. Sugiyura	63

Yamanashi University

K. Ishigaki	43
M. Miyake	43

Yokohama National University

T. Fujikawa	50
J. Iizuka	52
Y. Iwasawa	15, 19
K. Morohashi	52
S. Usami	52

State University of New York

C. T. Prewitt	
---------------	--

<u>Institution</u> Name	Proposal No.
----------------------------	--------------

The University of Hamburg

B. Sonntag	26, 72
------------	--------

Electrotechnical Laboratory

T. Ishiguro	42, 50, 72
H. Oyanagi	42, 50, 51, 72
Y. Okada	42
M. Tokumoto	32, 50
H. Unoki	31, 42

Government Industrial Research Institute Osaka

N. Kamijo	2, 4, 7, 10, 14, 59, 60
-----------	-------------------------

Geological Survey of Japan

Y. Kanazawa	35
K. Tsukimura	35, 49

Institute for Molecular Science

K. Hayakawa	43
K. Kimura	4
K. Suzuki	43
K. Touji	43
Y. Udagawa	43

Institute for Plant Virus Research

H. Inoue	12
Y. Sano	12

The Institute of Physical and Chemical Research

T. Furuno	12
M. Ito	53
T. Ito	49

The Institute of Space and Astronautical Science

Y. Ichikawa	26
-------------	----

Japan Broadcasting Corporation (NHK)

J. Chikawa	70
F. Sato	70
T. Sunada	70

National Cancer Center Research Institute

N. Munakata	27
-------------	----

National Chemical Laboratory for Industry

A. Kawase	42
Y. Kobayashi	42

National Institute for Research in Inorganic Materials

O. Fukunaga	37
H. Kamida	37
I. Kawada	35
T. Nagashima	37
H. Nakazawa	35
A. Nukui	35, 43
F. Okamura	35
O. Shimomura	37
K. Takahashi	43
N. Yamaoka	37
K. Yukino	43

<u>Institution</u> Name	Proposal No.	<u>Institution</u> Name	Proposal No.
<u>National Institute of Genetics</u>		H. Namatsu	
T. Kada	27	M. Ojima	
Y. Sadaie	27	I. Okada	
<u>National Institute of Radiological Sciences</u>		H. Okamoto	
M. Endo	66	M. Okamura	
T. Inuma	66	K. Saito	
H. Ohara	27	Y. Saito	
T. Yamada	27	Y. Sakakibara	
<u>National Research Institute for Metals</u>		M. Sekimoto	
H. Kuwamura	37	T. Shigematsu	
<u>National Research Laboratory of Metrology</u>		K. Shikano	
K. Nakayama	36	S. Shinoyama	
M. Tanaka	36	K. Sugi	
<u>Nippon Telegraph and Telephone Public Corporation</u>		A. Sugita	
H. Akiyama		K. Sukegawa	
K. Deguchi		M. Suzuki	
H. Hanabusa		Y. Tajima	
K. Harada		H. Takaoka	
S. Hattori		N. Takeuchi	
T. Hayasaka		T. Tamamura	
Y. Hibino		H. Tanaka	
T. Higashino		T. Tanaka	
M. Hikita		A. Une	
Y. Hirota		T. Urisu	
N. Honma		Y. Utsugi	
Y. Honma		K. Wada	
T. Horiuchi		M. Wada	
S. Iiyama		S. Yabumoto	
K. Ikeda		E. Yamaguchi	
M. Iki		H. Yonezawa	
N. Inoue		A. Yoshikawa	
Y. Ishii		H. Yoshiwara	
K. Kajiyama			
M. Kanai		<u>Fuji Photo Film Co., Ltd.</u>	
T. Kaneko		M. Takano	66
M. Kato			
T. Kawamura		<u>Hamamatsu Photonics K.K.</u>	
H. Kinoshita		A. Sawaki	
T. Kitayama		T. Yamashita	
K. Kobayashi			
O. Kogure		<u>Hitachi Ltd.</u>	
H. Koizumi		K. Hayakawa	70
K. Komatsu		H. Kajiyama	
K. Kudo		T. Kimura	
S. Kurosawa		A. Kishimoto	
H. Kyuragi		T. Minemura	
S. Maeyama		H. Mochiji	
S. Maruyama		H. Obayashi	
M. Minakata		M. Sakurai	42
K. Minowa		K. Usami	42
S. Miyazawa			
K. Miyoshi		<u>Idemitsu Kosan K.K.</u>	
K. Murase		Y. Akai	
J. Nakano		N. Ishikawa	
S. Nakayama		T. Mibuchi	
		Y. Takeshita	
		T. Takyu	
		<u>Mitsubishi Electric Corporation</u>	
		M. Inuishi	

<u>Institution</u>		Proposal No.
Name		
T. Kawazu		
H. Koyama		
Y. Masuko		
T. Matsukawa		
Y. Suzuki		
K. Tsukamoto		
A. Yamazaki		
N. Yoshioka		
<u>Mitsubishi Yuka K.K.</u>		
S. Takayama		
T. Usami		
<u>Murata Mfg. Co., Ltd.</u>		
M. Murata		42
H. Yamamoto		
<u>Rigaku Corporation</u>		
S. Igarashi		
K. Kumagai		
<u>Sagami Chemical Research Center</u>		
T. Fukushima		23, 24
M. Ichikawa		23, 24
<u>Toyota Central Research & Development</u>		
<u>Labs., Inc.</u>		
Y. Fukushima		
T. Okamoto		
<u>Photon Factory (KEK)</u>		
Y. Amemiya		11,12,29,30,45,48,75,86, 89,90,91,95
M. Ando		31,32,36,38,62,65,70,72, 74,87,88,89
T. Ishikawa		36
K. Ito		26,55,64,69
N. Kamiya		33
H. Kato		67,68,72,77,82
H. Kawata		70,87
K. Kohra		36,51
T. Koide		61,77,80
H. Maezawa		26,56,61,63,64,72
T. Matsushita		12,28,31,32,34,36,41, 42,51,53,72,88,89
T. Miyahara		61,67,68,72,77,80,82
T. Nakajima		30,31,65,88,89
M. Niwano		80
T. Ohta		52,79
S. Sasaki		
T. Sasaki		26,56,61,64,72
S. Sato		61,77,80
Y. Satow		35,41,49
Y. Shidara		77,80
P. Spieker		36,65,74
P.M. Stefan		52
A. Yagishita		26,55,64,69,72
M. Yanagihara		26,56,61,63,80,87

IX. PUBLICATIONS RELATED TO AND BASED ON WORK AT THE PHOTON FACTORY

1975

Kohra, K. and Huke, K. (1975) On Photon Factory Project (in Japanese), Butsuri, 30, No.8.

1977

Kamada, S., Kamiya, Y. and Kihara, M. (1977) Lattice Design of KEK Photon Factory Storage Ring, KEK Report, KEK-77-16.

Kamada, S. and Kihara, M. (1977) Lattice Design of KEK Photon Factory Storage Ring, KEK Report, KEK-77-16.

Takata, K. (1977) Note on the RF System of the 2.5 GeV Electron Storage Ring for the Photon Factory Project, KEK Report, KEK-77-15.

1978

Ando, M. and Ohta, T. (ed) (1978), Proc. the Meeting on the Planning of the Photon Factory Accelerators, Tsukuba, October 25, 1977, KEK Report KEK-77-26 (in Japanese).

Hashizume, H., Mase, K., Amemiya, Y., and Kohra, K. (1978) A System for Kinetic X-Ray Diffraction Using a Position Sensitive Counter, Nucl. Instr. Meth., 152, 199.

Kamiya, Y. (1978) PF-Ring Lattice Parameters with Wiggler, KEK Report, KEK-78-1.

Kamiya, Y. (1978) Closed Orbit Distortion Due to Synchrotron Radiation in an Electron Storage Ring of KEK Photon Factory, KEK Report, KEK-78-6.

Kamiya, Y. (1978) Dispersion and Betatron Functions in Non-Linear Lattice -Computational Method-, KEK Report, KEK-78-17.

Kihara, M. (1978) Bending Magnet of Photon Factory Storage Ring, KEK Internal Report, KEK-ACCELERATOR-77-2.

Kohra, K., Ando, M., Matsushita, T., and Hashizume, H. (1978) Design of High Resolution X-Ray Optical System Using Dynamical Diffraction for Synchrotron Radiation, Nucl. Instr. Meth., 152, 161.

Mathewson, A.G., Horikoshi, G., and Mizuno, H. (1978) Some Note on the Photoelectron Induced Gas Desorption Problems in the Photon Factory and TRISTAN, KEK Report, KEK-78-9.

Ohta, T. (1978) Synchrotron Radiation Photoelectron Spectroscopy (in Japanese), Kagaku-no-ryoiki, 32, 786.

Takata, K. (1978) RF Parameters of the PF Storage Ring, KEK Internal Report, KEK-ACCELERATOR-78-1.

Takata, K. (1978) Beam Loading Effects during Injection Processes in an Electron Storage Ring, KEK Report, KEK-78-4.

Takayama, K. and Kihara, M. (1978) KEK PF Storage Ring Injection, KEK Report, KEK-77-23.

1979

Araki, A., Igarashi, T., Kamiya, Y., and Kihara, M. (1979) Magnetic Field Data on the Ring Bend Magnet of Photon Factory Storage Ring, KEK Internal Report, KEK-ACCELERATOR-79-3.

Batchelor, K. (1979) Note on the Proposed R.F. Parameters for the Photon Factory, KEK Report, KEK-79-26.

Batchelor, K. and Kamiya, Y. (1979) R.F. Cavity Design for the Photon Factory, KEK Report, KEK-79-25.

Fukuda, S., Tanaka, J., Sato, I., and Anami, S. (1979) Bunch Monitors for S-Band Electron Linac (in Japanese), KEK Report, KEK-79-24P.

Kamada, S., Kamiya, Y. and Kihara, M. (1979) Lattice of Photon Factory Storage Ring, IEEE Trans. Nucl. Sci. NS-26, 384B.

Kamiya, Y. (1979) Computational Method for the Dispersion, Betatron Functions and C.O.D. in Non-Linear Lattice, IEEE Trans. Nucl. Sci., NS-26, 3821.

Katsura, T. and Shibata, S. (1979) Beam Position Monitor for the Photon Factory Storage Ring, KEK Report, KEK-79-27.

Kobayakawa, H., Takata, K., and Toyama, I. (1979) Performance Tests of Crowbar Circuit for Klystron Protection, KEK Report, KEK-79-4.

Matsumoto, H., Tanaka, J., Sato, I., Arai, S., Yamaguchi, N., Iino, Y., and Kato, S. (1979) Characteristics of the Door-Knob Type Coupler for an Electron Linear Accelerator, KEK Report, KEK-ACCELERATOR-79-5.

Ohta, T. (1979) SOR and Photon Factory (in Japanese), Kagaku to kogyo, 32, 318.

Takata, K. (1979) Longitudinal Coupled-Bunch Instability due to a Multi-Cell Accelerating Structure, KEK Report, KEK-79-6.

Takata, K., et al. (1979) Performance Tests of Crowbar Circuit for Klystron protection, KEK Report, KEK-79-4P.

Washio, M., Fukuda, S., Tanaka, J., Sato, I., Anami, S., Tabata, Y., Kobayashi, H., Katsumura, Y., Ueda, T., and Tagawa, S. (1979) Bunch Monitors for S-Band Electron Linac (in Japanese), KEK Report, KEK-79-24.

Wilson, P.B. (1979) Ring Impedance and Stored Current for the Photon Factory, KEK Report, KEK-79-28.

1980

Annaka, S., Suzuki, T., and Onoue, K. (1980) Polarization States of Dynamically Diffracted X-Ray Beams, *Acta Crystallogr.* A36, 151-152.

Enomoto, A., Matsumoto, H., Nakahara, K., Sato, I., Tanaka, J., Hosono, Y., Hasegawa, K., Saito, K., Muto, M., Konno, M., and Oyamada, M. (1980) Cavity Resonator-Type Beam Position Monitor (in Japanese), *kakuriken kenkyo-hokoku, Tohoku Univ.*, 13, No.2.

Hasegawa, K., Mochiki, K., and Sekiguchi, A. (1980) Integral Type Position-Sensitive Chamber with Multiplexer Readout System (in Japanese), *Hoshasen*, 7, 3.

Horikoshi, G. and Kobayashi, M. (1980) On the Gas Desorption (in Japanese), *Shinkuu*, 23, 476.

Huke, K. (1980) 2.5 GeV Electron Storage Ring Construction at KEK-PF, *Nucl. Instr. Meth.*, 177, 1.

Huke, K. and Yamakawa, T. (1980) Design of a Vertical Wiggler with Superconducting Coils, *Nucl. Instr. Meth.*, 177, 153.

Kamiya, Y. (1980) Computational Method for the Astral Survey and the Effect of Measurement Errors on the Closed Orbit Distortion, KEK Report, KEK-80-3.

Kamiya, Y. and Kihara, M. (1980) Limitation on Beam Size in the Photon Factory Storage Ring, *Nucl. Instr. Meth.*, 177, 65.

Kitamura, H. (1980) On the Spectral and Polarization Characteristics of an Undulator, *Nucl. Instr. Meth.*, 177, 235.

Kitamura, H. (1980) Polarization of Undulator Radiation, *Jpn. J. Appl. Phys.* 19, L185.

Kobayashi, M., Horikoshi, G., and Mizuno, H. (1980) ESR Vacuum System for the Photon Factory, *Nucl. Instr. Meth.*, 177, 111.

Kohra, K. and Ando, M. (1980) Some Fundamental Studies on X-Ray Optical Systems Using Dynamical Diffraction for Synchrotron Radiation, *Nucl. Instr. Meth.*, 177, 117.

Kohra, K., Tanaka, J., Huke, K., and Sasaki, T. (1980) Present Status of Photon Factory (in Japanese), *Ouyou-butsumuri*, 49, 1066.

Lesmond, C. (1980) Magnetic System Design Computer Program Users Notes, KEK Internal Report, KEK-80-15P.

Lesmond, C. (1980) Design of the Magnetic System of the 6 Tesla Vertical Wiggler, KEK Report, KEK-80-17P.

Matsushita, T. and Kaminaga, U. (1980) A Systematic Method of Estimating the Performance of X-Ray Optical Systems for Synchrotron Radiation. I. Description of Various Optical Elements in Position-Angle Space for Ideally Monochromatic X-Rays, *J. Appl. Cryst.* 13, 465.

Matsushita, T. and Kaminaga, U. (1980) A Systematic Method of Estimating the Performance of X-Ray Optical Systems for Synchrotron Radiation. II. Treatment in Position-Angle-Wavelength Space, *Appl. Cryst.* 13, 472.

Mitra, A.K. (1980) Automatic Gain Amplifier at 500 MHz, KEK Internal Report, KEK-80-4.

Nakagawa, H., Shibata, S., Hiramatsu, S., Uchino, K., and Takashima, T. (1980) Beam-Loss Monitoring System with Free-Air Ionization Chamber, *Nucl. Instr. Meth.*, 174, 401.

Ohta, T. (1980) Synchrotron Radiation Facility of Stanford and the Photon Factory in Japan (in Japanese), *Hyomen kagaku*, 1, 79.

Sato, I. (1980) Accelerator Structure and Beam Transport System for the KEK Photon Factory Injector, *Nucl. Instr. Meth.* 177, 91.

Sato, S. (1980) Characteristics of Acoustic Delay Line (in Japanese), *UVSOR-4*, 37.

Sugawara, H., Sato, S., Miyahara, T., Kakizaki, A., Morioka, Y., Nakakura, Y., Iguchi, Y., Ando, M., Ohta, T., and Aoki, S. (1980) Extreme Ultraviolet Mirrors for Synchrotron Radiation, Activity Report of Synchrotron Radiation Laboratory, ISSP, Univ. of Tokyo, 67.

Takata, K. (1980) Current Limitations due to RF Parameters in the Photon Factory Storage Ring, *Nucl. Instr. Meth.*, 177 75.

Tanaka, J. (1980) Construction of the Photon Factory 2.5 GeV Injector Electron Linac, *Nucl. Instr. Meth.*, 177, 101.

Yamazaki, Y., Takata, K., and Tokumoto, S. (1980) Measurement of the Longitudinal and Transverse Coupling Impedances of the Higher-Order Modes of the Re-Entrant Accelerating Cavities, KEK Report, KEK-80-8.

1981

Annaka, S., Kohra, K., and Ando, M. (1981) Rotation of the Electric Vector of the Polarized X-Rays by Diffraction in Crystals, Jpn. J. Appl. Phys., 20, L463-L466.

Hasegawa, K., Mochiki, K., and Sekiguchi, A. (1981) Integral Type Position-Sensitive Proportional Chamber with Multiplexer Readout System, IEEE Trans. Nucl. Sci. NS-28 3660.

Hashizume, H., Wakabayashi, K., Hamanaka, T., Wakabayashi, T., Amemiya, Y., Matsushita, T., Ueki, T., Hiragi, Y., Izumi, Y., and Tagawa, H. (1981) Design of a Diffractometer for Small-Angle Scattering (the Muscle Diffractometer) at Photon Factory (in Japanese), KEK Internal Report, KEK-81-11P.

Horikoshi, G. and Kobayashi, M. (1981) A Simple Understanding of a Net Outgassing Rate as a Function of Pumping Speed, J. Vac. Sci. Technol., 18, 1009.

Kanaya, N. (1981) A Digital All-Pass Transfer Function with All Possible Coefficient Combinations, IEEE Trans. Circuits and Systems, CAS-28, 12.

Katsura, T., Nakagawa, H., and Shibata, S. (1981) Beam Diagnostic Instrumentation in the Photon Factory Storage Ring, IEEE Nucl. Sci., 28, 2353.

Katsura, T., Nakagawa, H., and Shibata, S. (1981) Test of VUV Beam Position Monitor, Activity Report of Synchrotron Radiation Laboratory, ISSP, Univ. of Tokyo, 135.

Kitamura, H. (1981) New Synchrotron Radiation Source (in Japanese), Butsuri, 36, 279.

Kobashi, S., Mochiki, K., Hasegawa, K., Sekiguchi, A., Hashizume, H., and Yoshioka, Y. (1981) A High-Speed Signal Processor Using a Digital Divider for Position Sensitive Proportional Counters, Adv. in X-Ray Analysis, 24, 173.

Kobayashi, M., Tuzi, Y., and Terada, K. (1981) Performance of a Simplified Directional Detector for Gas Molecules, J. Vac. Sci. Technol., 18 1013.

Matsushita, T. and Phizackerley, P. (1981) A Fast X-Ray Absorption Spectrometer for Use with Synchrotron Radiation, Jpn. J. Appl. Phys., 20, 2223.

Mochiki, K., Hasegawa, K., Sekiguchi, A., and Yoshioka, Y. (1981) Integral Type, Position-Sensitive Proportional Chamber with Multiplexer Readout System for X-Ray Diffraction Experiments, Adv. in X-Ray Analysis, 24, 155.

Ohta, T. (1981) SEXAFS (in Japanese), Nippon kinzoku gakkai Ho, 20, 570.

Ohta, T., et al. (1981) Computer Simulation of the Heating Effect on Mirrors by Synchrotron Radiation, KEK Report, KEK-81-10P.

Oyanagi, H. and Ohta, T. (1981) Application of EXAFS to Surface Science (in Japanese), Hyomen gakkai, 2, 57.

Takeuchi, Y., Iitaka, Y., and Kohra, K. (ed) (1981) Progress in Instrumentations for Crystal-Structure Studies with Synchrotron Radiation (in Japanese), KEK Internal Report, KEK-81-4P.

Taniguchi, K., Oka, K., Yamaki, N., and Ikeda, S. (1981) X-Ray Spectrometer for EXAFS Using a Position Sensitive Detector, Advances in X-Ray Analysis, 24, 177-182.

Yamada, T. (1981) Application of Synchrotron Radiation to the Biological Studies (in Japanese), J. Atom. Energy Soc. Japan, 23, 898-903.

Yamada, T. L(1981) Biomedical Application of Synchrotron Radiation: An Overview (in Japanese), Isotope News, 330, 2-5.

Yamazaki, Y., Takata, K., and Tokumoto, S. (1981) Damping Test of the High-Order Modes of the Re-Entrant Accelerating Cavity, IEEE Trans. Nucl. Sci. NS-28, 2915.

1982

Annaka, S. (1982) Elliptically Polarized X-Rays List Produced by the σ and π Components of Linearly Polarized X-Rays in the Laue Case Dynamical Diffraction, J. Phys. Soc. Jpn. 61, 1927-1931.

Ando, M., et al. (1982) The First Synchrotron Radiation Experiments at the Photon Factory (June-July, 1982) (in Japanese), J. Crystallogr. Soc. Japan, 24, 427.

Kitamura, H., Yamakawa, T., Sato, S., Mikuni, A., Maezawa, H., and Sasaki, T., et al. (1982) Observation of Undulator Radiation, I. Operation Studies and Visual Observation, *Jpn. J. Appl. Phys.*, 21, 1728-1731; KEK Preprint 82-12.

Nagakura, I. (1982) On the Beryllium Window for Synchrotron Radiation (in Japanese) KEK Report, KEK-81-17.

Shintake, T., Huke, K., Tanaka, J., Sato, I., and Kumabe, I. (1982) Microwave Undulator, *Jpn. J. Appl. Phys.*, 21, L601-L603.

Yamada, T. (1982) Synchrotron Radiation and Radiation Biology (in Japanese), *Radiol. Sci.* 24, 181-186.

Yokoi, K., Ozeki, T., Watanabe, I., and Ikeda, S. (1982) Polarographic Study of Mo(VI) in Aqueous Sulfuric Acid Solutions, *J. Electroanal. Chem.*, 132, 191-199.

Yokoi, K., Ozeki, T., Watanabe, I., and Ikeda, S. (1982) Polarographic Study of Mo(VI) in 0.1-5M Sulfuric Acid Solutions, *J. Electroanal. Chem.*, 133, 73-78.

1983

Akimoto, K., Ishikawa, T., Takahashi, T., and Kikuta, S., (1983) Structure Analysis of the $\text{NiSi}_2/(111)\text{Si}$ Interface by the X-ray Standing Wave Method, *Jpn. J. Appl. Phys.*, 22, No.12 (in press).

Amemiya, Y., Wakabayashi, K., Hamanaka, T., Wakabayashi, T., Matsushita, T., and Hashizume, H. (1983) Design of a Small-Angle X-Ray Diffractometer Using Synchrotron Radiation at the Photon Factory, *Nucl. Inst. Meth.*, 208, 471-477.

Ando, M. (1983) Utilization of Synchrotron Radiation at the Photon Factory (in Japanese), *kagaku to kogyo*, 36, 485-486.

Asami, A., Kihara, M., Ando, M., Ohta, T., and Matsushita, T. (1983) Present Status of Photon Factory (II) (in Japanese), *J. At. Energy Soc. Japan*, 25, 172-178.

Hasegawa, K. and Mochiki, K. (1983) Integral Type Position-Sensitive Proportional Chamber (in Japanese), *J. Crystallogr. Soc. Japan*, 24, 289.

Huke, K., Kajiura, K., Kamiya, Y., Kanaya, N., Katsura, T., Kihara, M., Kitamura, H., Kobayakawa, H., Kobayashi, M., Koide, T., Pak, C.O., Sato, S., Shibata, S., Yamakawa, T., and Yamazaki Y. (1983) Photon Factory: Status of Storage Ring, *IEEE Trans. Nucl. Sci.*, NS-36.

Iitaka, Y., Hasegawa, K., Koike, M., Mochiki, K., Hashizume, H., and Ogawa, T. (1983) A High Counting Rate MWPC with Multiple Delay-Line Readout (in Japanese), *J. Crystallogr. Soc. Japan*, 24, 284.

Ito, T., Okada, S., Kada, T., Hieda, K., Kobayashi, K. and Ito, A. (1983) Irradiation System of Monochromatic Vacuum-UV Radiation Using Synchrotron Radiation (in Japanese), *J. Radiat. Res.*, (in press).

Kamiya, Y. (1983) On Some Properties of Longitudinal and Transverse Coupled-Bunch Instabilities, KEK Report, KEK-82-15.

Kamiya, Y. and Kihara, M. (1983) On the Design Guideline for the Low Emittance Synchrotron Radiation Source, KEK Report, KEK-83-6.

Katsura, T., Nakagawa, H., and Shibata, S. (1983) Beam Monitors in the Transport Line of the Photon Factory Storage Ring, KEK Report, KEK 82-14A.

Katsura, T., Nakagawa, H., and Shibata, S. (1983) Beam Position Measurement in the Photon Factory Storage Ring, *IEEE Trans. Nucl. Sci.*, NS-30, No. 3.

Kihara, M., et al. (1983) Results on Accelerator Studies of the Photon Factory Storage Ring, KEK Report, KEK-83-5.

Kobayakawa, H., Yamazaki, Y., and Kamiya, Y. (1983) Measurement of Damping Time and Frequency of Coherent Synchrotron Oscillation in the PF Storage Ring, KEK Report, KEK-83-8.

Kobayakawa, H. and Yamazaki, Y. (1983) Tuner Control System for the PF Cavity, KEK Report, KEK-83-9.

Kobayashi, K., Hieda, K., Maezawa, H., Ito, T., Ito, A., Yamada, T., and Ando, M. (1983) Monochromatic X-Ray Irradiation System Using Synchrotron Radiation for Radiation Biology Study (in Japanese), *J. Radiat. Res.*, (in press).

Kohra, K. and Sasaki, T. (1983) Present Status of the Photon Factory, *Nucl. Instr. Meth.*, 208, 23-30.

Maezawa, H., Mikuni, A., Kitamura, H., Sasaki, T., et al. (1983) Observation of Undulator Radiation, II. Absolute Measurements in Extreme Ultraviolet, KEK Preprint 82-13; *Nucl. Instr. Meth.*, 208 151.

- Namioka, T., Noda, H., Goto, K., and Katayama, T. (1983) Design Studies of Mirror-Grating Systems for Use with an Electron Storage Ring Source at the Photon Factory, Nucl. Instr. Meth., 208, 215.
- Oyanagi, H. and Ohta, T. (1983) Application of Synchrotron Radiation to EXAFS and SEXAFS (in Japanese), Shinku, 26, 219.
- Photon Factory Storage Ring Group (1983) Photon Factory: Status of Storage Ring, IEEE Trans. Nucl. Sci., NS-30, No.3.
- Sato, S., Koide, T., Morioka, Y., Ishii, T., Sugawara, H., and Morioka, I. (1983) Front Ends for the Photon Factory Beam Lines, Nucl. Instr. Meth., 208, 31.
- Sato, S. and Nagakura, I. (1983) Development of Beryllium Windows for Synchrotron Radiation (in Japanese), J. Cryst. Soc. Japan, 24, 274.
- Shinohara, K. (1983) Photon Activation Therapy (in Japanese), News Tokyo Metropol. Inst. Med. Sci., 77, 1.
- Shintake, T., Huke, K., Tanaka, J., Sato, I., and Kumabe, I. (1983) Development of Microwave Undulator, Jpn. J. Appl. Phys., 1, 22, 844-851.
- SOR Working Groups in Biophysics (1983) Studies in Biophysics Using Synchrotron Radiations (in Japanese), Biophysics, 23, 46-50.
- Spieker, P. and Ando, M. (1983) A Diffractometer for X-Ray Interferometry, Nucl. Instr. Meth., 208, 609-611.
- Wakabayashi, K., Hamanaka, T., Hashizume, H., Wakabayashi, T., Amemiya, Y., and Matsushita, T. (1983) X-Ray Optics for the Muscle Diffractometer Using Synchrotron Radiation, In X-Ray Instrumentation for Photon Factory, eds. Hosoya, Iitaka and Hashizume, KEK and Reidel Pub. Co., Tokyo, (in press).
- Yamada, T. (1983) Photon Factory in Operation (in Japanese), Radiat. Biol. Res. Commun., 18, 84.
- Yamazaki, Y., Kihara, M., and Kobayakawa, H. (1983) Partially Filled Multi-Bunch Mode Operation of the Photon Factory Electron Storage Ring and Cure of the Vertical Instability, KEK Report, KEK-83-17.
- Yamazaki, Y., Kobayakawa, H., Kamiya, Y., and Kihara, M. (1983) A Transverse Coupled Bunch Instability Observed in the KEK-PF Electron Storage Ring, KEK Report, KEK-83-3.
- Yamazaki, Y., Kobayakawa, H., Kamiya, Y., and Kihara, M. (1983) A Longitudinal Coupled Bunch Oscillation Observed in the KEK-PF Electron Storage Ring, KEK Report, KEK-83-7.

PROCEEDINGS

1978

Enomoto, A., Matsumoto, H., Sato, I., and Tanaka, J. (1978) Some Improvement of rf Measurement System on Electron Linear Accelerator, Proc. of the 2nd Symp. on Acc. Sci. and Tech., 23-25.

Matsumoto, H., Tanaka, J., Arai, S., Iino, Y., Yamaguchi, N., and Kato, S. (1978) Phase Characteristics of Accelerator Guide with the Coupler, Proc. of the 2nd Symp. on Acc. Sci. and Tech., 23-25.

1979

Sasaki, T. and Ito, T. (1979) Synchrotron Radiation as a light Source for Radiation Research, Proc. 6th Intern. Congr. Rad. Res., Tokyo, 999-1003.

1980

Horikoshi, G., Narushima, K., and Kobayashi, M. (1980) Performance of a Cryo-Surface with a Honeycomb Like Structure as a Cryopump, Proc. 8th Intern. Vac. Congr. II, 308.

Katsura, T. and Shibata, S. (1980) Beam Position Monitor for the PF Storage Ring and Its Calibration System, Proc. of the 3rd Symp. on Acc. Sci. and Tech., 165.

Shibata, S., Katsura, T., Kudo, H., and Shoji, S. (1980) Beam Current Transformer with DC to 500 Hz, Proceedings of the 3rd Symposium on Accelerator Science and Technology, Research Center for Nuclear Physics, 149.

Tanaka, J., Huke, K., Kihara, M., Kobayashi, M., Sato, S., Shibata, S., Takata, K., and Yamakawa, T. (1980) Design and Status of Photon Factory, Proc. 11th Intern. Conf. High Energy Acc., Geneva.

Tanaka, J. (1980) Status of the Photon Factory 2.5 GeV Linac, Proc. 3rd Symp. Acc. Sci. Tech., 27-29.

Tanaka, J., Sato, I., Anami, S., Fukuda, S., Matsumoto, H., Tabata, Y., Kobayashi, H., Tagawa, S., and Washio, M. (1980) Single Bunch Acceleration and Detection in S-Band Electron Linear Accelerator (1980) Proc. 1979 Linear Acc. Conf., Montank, KEK Preprint, KEK-79-25.

1981

Anami, S., Tanaka, J., Fukuda, S., Shidara, T., Saito, Y., Bissonnette, R., and Honma, H. (1981) The rf System of the Photon Factory Injector Linac, Proc. 1981 Linear Acc. Conf., Santa Fe, 177.

Asami, A., Ohsawa, S., Enomoto, A., Matsumoto, H., Sato, I., Tanaka, J., Kobayashi, H., Mashiko, K. (1981) PF Linac Injector (in Japanese), Proc. 6th Meeting Linac, SAPPORO, 59.

Tanaka, J., Sato, I., Asami, A., Matsumoto, H., Osawa, S., Enomoto, A., and Saito, Y. (1981) Construction Progress of the Photon Factory 2.5 GeV Electron Linac, Proc. 1981 Linear Acc. Conf., Santa Fe, KEK Preprint, KEK-81-20.

1982

Asami, A., Ohsawa, S., Tanaka, J. (1982) Beam Characteristics of PF Linac Injection System, Proc. 4th Symp. Acc. Sci. Tech., RIKEN, 125.

Katsura, T., Nakagawa, H., and Shibata, S. (1982) Beam Position Monitoring in the Photon Factory Storage Ring, Proc. of the 4th Symp. on Acc. Sci. and Tech.

Maizawa, H., Mikuni, A., Kitamura, H., Sasaki, T., et al. (1982) Absolute Measurement of Undulator Radiation Spectra (K-Value Dependence of Brightness), Proc. Conf. Acc. Sci. Tech., Wako, 169-170.

Ohsawa, S., Asami, A., and Tanaka, J. (1982) Beam Bunching in the PF Linac Injector (in Japanese), Proc. 7th Meeting Linac, KEK, 32.

Saito, Y., Otake, Y., Anami, S., Fukuda, S., Shidara, T., Honma, H., Nakao, K., and Tanaka, J. (1982) The Phasing System in the PF Linac, Proc. 4th Symp. Acc. Sci. Tech., I.C.P.R.

Sasaki, T. and Kohra, K. (1982) Synchrotron Radiation Research at the Photon Factory, Proc. 4th Conf. Acc. Sci. Tech., Wako, 3-6.

Tanaka, J. (1982) Initial Operation of the Photon Factory 2.5 GeV Electron Linac, Proc. 4th Symp. Acc. Sci. Tech., I.C.P.R., 29.

1983

Abe, I., Nakahara, K., Urano, T., Otake, Y., Enomoto, A., Sato, I., Ooe, A., and Ujihara, Y. (1983) Intelligent Power Supply Controller (in Japanese) Proc. 7th Meeting Linear Acc., KEK-82-14, 196.

Asami, A. and Osawa, S. (1983) Present Status and Beam Characteristics of PF Linac Injector (in Japanese) Proc. 7th Meeting Linear Acc., KEK-82-14, 151.

Enomoto, A., Matsumoto, H., Sato, I., Takeda, K., Yamaguchi, N., Iino, Y., and Taki, H. (1983) Energy Gain of PF 2.5 GeV Linac (in Japanese), Proc. 7th Meeting linear Acc., KEK-82-14, 61.

- Enomoto, A., Matsumoto, H., Sato, I., Takeda, K., Yamaguchi, N., Kato, S., Tsuchiya, S., and Kamouchi, U. (1983) PF 2.5 GeV Accelerator and Waveguide Characteristics (in Japanese), Proc. 7th Meeting Linear Acc., KEK-82-14, 165.
- Enomoto, A., Takeda, K., Matsumoto, H., Sato, I., Abe, I., Otake, Y., Urano, T., Nakahara, K., Asami, A., and Katsura, T. (1983) Focusing System of the PF 2.5 GeV Linac and Its Operation (in Japanese) Proc. 7th Meeting Linear Acc., KEK-82-14, 64.
- Hirayama, H. and Ban, S. (1983) PF Linac Radiation Shielding (in Japanese), Proc. 7th Meeting Linear Acc., KEK-82-14, 238.
- Iino, Y., Ando, S., Fujiwara, S., Takahashi, K., Sato, I., and Matsumoto, H. (1983) PF 2.5 GeV Linac Accelerator Tube Fabrication (in Japanese), Proc. 7th Meeting linear Acc., KEK-82-14, 52.
- Iino, Y., Asaba, H., Fujiwara, S., Tagawa, Y., Igarashi, H., Matsumoto, H., and Sato, I. (1983) PF 2.5 GeV Linac Accelerator Unit Assembly and Alignment (in Japanese), Proc. 7th Meeting linear Acc., KEK-82-14, 56.
- Nakagawa, H., Shibata, S., Katsura, T., Enomoto, A., and Sato, I. (1983) Beam Loss Monitoring System for 2.5 GeV Electron Linac (in Japanese) Proc. 7th Meeting Linear Acc., KEK-82-14, 209.
- Ohsawa, S., Anami, S., Shidara, T., Ozaki, T., and Asami, A. (1983) Beam Characteristics of PF Linac Injector (II), Proc. 8th Meeting Linac, Nihon Univ., 95.
- Otake, Y., Urano, T., Abe, I., and Nakahara, K. (1983) Main Control Console of the PF Electron Linac (in Japanese), Proc. 7th Meeting Linear Acc., KEK-82-14, 203.
- Saito, Y., Anami, S., Fukuda, S., Shidara, T., Honma, H., Nakao, K., and Tanaka, J. (1983) The Phasing in PF Linear (in Japanese), Proc. 7th Meeting Linear Acc., KEK-82-14, 185.
- Sato, I., Matsumoto, H., Enomoto, A., Takeda, K., Iino, Y., Taki, K., and Ando, K. (1983) Alignment System for a Long Beam Line of the PF 2.5 GeV Linac (in Japanese), Proc. 7th Meeting Linear Acc., KEK-82-14, 170.
- Shidara, T., Anami, S., Fukuda, S., Saito, Y., Honma, H., Nakao, K., and Tanaka, J. (1983) Present Status of the rf Source of the PF Injector Linac (in Japanese), Proc. 7th Meeting Linear Acc., KEK-82-14, 71.
- Takeda, K., Sato, I., Matsumoto, H., Enomoto, A., Nakahara, K., Urano, T., and Saito, T. (1983) Vacuum System of the PF 2.5 GeV Linac (in Japanese), Proc. 7th Meeting Linear Acc., KEK-82-14, 173.
- Tanaka, J. (1983) Photon Factory 2.5 GeV Electron Linac (in Japanese), Proc. 7th Meeting Linear Acc., KEK-82-14, 47.
- Tsuchiya, S., Iino, Y., Yamaguchi, N., Sato, I., Matsumoto, H., and Tanaka, J. (1983) Manufacturing of Precise Waveguide Components in PF Linac (in Japanese), Proc. 7th Meeting Linear Acc., KEK-82-14, 168.
- Tuzi, Y. and Kobayashi, M. (1983) Directional Detectors for Gas Molecules and Their Applications to the Direct Measurement of Gases Released from Surfaces, Proc. 9th Intern. Vac. Congr.
- Urano, T., Otake, Y., Abe, I., and Nakahara, K. (1983) The Operation of PF Injector through a Minicomputer Network (in Japanese), Proc. 7th Meeting Linear Acc., KEK-82-14, 76.
- Watanabe, M., Okuno, A., and Matsumoto, H. (1983) Properties of SiC Ceramics and Application for Microwave Absorber (in Japanese), Proc. 7th Meeting Linear Acc., KEK-82-14, 179.

